# THÈSE POUR OBTENIR LE GRADE DE DOCTEUR DE L'INSTITUT AGRO MONTPELLIER ET DE L'UNIVERSITE DE MONTPELLIER

En Biologie, Interactions, Diversité Adaptative des Plantes

École doctorale GAIA – Biodiversité, Agriculture, Alimentation, Environnement, Terre, Eau Portée par

l'Unité de recherche INRAE-LEPSE et l'Institut ARVALIS

Predicting the performance of maize varieties in contrasting environmental conditions by combining phenomics, genomic prediction and crop modelling

Prédiction de la performance de variétés de maïs en conditions environnementales contrastées par combinaison de phénomique, prédiction génomique et modèle de culture

# Présentée par Jugurta BOUIDGHAGHEN Le 11 décembre 2023

Sous la direction de François TARDIEU co-encadrée par Claude WELCKER et Matthieu BOGARD

# Devant le jury composé de

Nicolas LANGLADE, Directeur de Recherche, INRAE Toulouse

Scott CHAPMAN, Professor, University of Queensland

Rapporteur

Fabienne HENRIOT, Head of Maize Breeding Scientific Support, Limagrain

Jacques DAVID, Professeur, Institut Agro Montpellier

Examinateur

Maeva BAUMONT, Ingénieur de Recherche, ARVALIS

Sophie BOUCHET, Chargée de Recherche, INRAE Clermont-Ferrand

Examinatrice







# **ABSTRACT**

Progresses of high-throughput phenotyping, genomic prediction and modelling may jointly provide novel tools for breeding schemes and variety recommendation to farmers, in a context of climate change and water scarcity. Integration of these approaches requires new methods that tackle genotype x environment interactions and evaluate the comparative advantages of varieties in contrasting environmental scenarios. In this thesis, we developed and evaluated a new approach for predicting maize leaf area and grain number across multiple environments, which combined genomic prediction models, novel phenomics methods and a crop model (Sirius Maize). The latter can simulate, based on explicit physiological processes, yield and other traits for multiple genotypes in a large range of environmental conditions, provided that genotype-specific parameters are estimated for many hybrids and fed to the model. We tested our approach by using three panels of maize hybrids: a diversity panel, a panel that captures the genetic progress and a panel of recent hybrids, with 246, 56 and 86 hybrids, respectively. Genotype-specific traits were measured in indoor or field experiments, related to plant phenology, architecture, leaf growth, responses to soil or air water status, and maximum grain number. We first showed that traits measured indoor can translate to the field, either directly or via the use of a model. Then, we showed that they can be successfully estimated, for a larger number of hybrids, via genomic prediction. Finally, we converted these traits into genotype-specific parameters, either via explicit equations or via scaling. Appreciable prediction accuracies were achieved by the crop model for leaf area index and grain number of studied hybrids, simulated in 9 and 21 experiments, respectively, with contrasting environmental conditions. In the thesis, we discuss the relevance of each of these steps, needed for integrating the knowledge from genetics, ecophysiological models and phenomics. We also identify areas to improve the approach and its prediction accuracy and for further applications in a plant breeding or variety recommendation context.

Key words: crop model Sirius Maize, genomic prediction, phenomics, genotype by environment interaction, yield, leaf area index, climate change.

# **RÉSUMÉ**

Les progrès du phénotypage à haut débit, de la prédiction génomique et de la modélisation fournissent potentiellement aux sélectionneurs et aux chercheurs de nouvelles méthodes pour l'amélioration et pour l'évaluation variétale, dans un contexte de changement climatique et de réduction des intrants. L'intégration de ces données dans l'objectif d'une amélioration durable des rendements nécessite le développement de nouvelles méthodes qui considèrent les interactions génotype x environnement et évaluent les avantages comparatifs de nombreuses variétés dans des scénarios environnementaux contrastés. Dans cette thèse, nous avons développé et testé une nouvelle approche prédictive de l'indice foliaire et du nombre de grains dans des scénarios environnementaux variés. Cette approche combine des modèles de prédiction génomique, des méthodes phénomiques développées récemment et un modèle de culture (Sirius Maize). Celui-ci permet de simuler, à partir de processus physiologiques explicites, le rendement et d'autres caractères pour différents génotypes dans une large gamme environnementale, à condition que des paramètres spécifiques à chaque hybride soient estimés et fournis au modèle. Nous avons testé cette approche avec trois panels d'hybrides de maïs : un panel de diversité, un panel qui capture le progrès génétique et un panel d'hybrides récents, comprenant 246, 56 86 hybrides, respectivement. Les caractères génotype-dépendant utilisés pour la paramétrisation du modèle de culture ont été mesurés dans des expériences en plateforme de phénotypage sous serre ou au champ. Ils caractérisent la phénologie, l'architecture, la croissance foliaire, les réponses aux états hydriques du sol ou de l'air, et le nombre de grains maximal de chaque hybride. Nous avons d'abord montré que des caractères mesurés en plateforme de phénotypage sous serre permettent de prévoir les mêmes caractères au champ, soit directement soit via l'utilisation de modèles. Nous avons ensuite montré que ces caractères en plateforme peuvent être estimés, pour un plus grand nombre d'hybrides, au moyen de modèles de prédiction génomique. Enfin, nous avons estimé les paramètres génotype-dépendants du modèle à partir des caractères mesurés, soit au travers d'équations explicites soit par mise à l'échelle. La simulation de l'indice foliaire et du nombre de grains a été satisfaisante, dans 9 et 21 essais au champ, respectivement, en conditions environnementales contrastées. Dans la thèse, nous discutons de la validité de chacune de ces étapes, nécessaires à l'intégration des connaissances issues de la génétique, des modèles écophysiologiques et de la phénomique. Nous identifions également des pistes permettant d'améliorer l'approche et sa qualité prédictive, ainsi que des applications potentielles dans un contexte d'amélioration ou de recommandation variétale.

Mots clés : modèle de culture Sirius Maïs, prédiction génomique, phénomique, interaction génotype-environnement, rendement, indice foliaire, changement climatique.

# REMERCIEMENTS

Cette thèse est le fruit d'un travail auquel ont contribué plusieurs personnes. Je tiens à les remercier ici.

Tout d'abord j'aimerais remercier François, mon directeur de thèse et Claude, mon coencadrant au LEPSE, pour l'énergie qu'ils ont investie dans ce travail. Merci à vous François de m'avoir permis de prendre du recul sur mes analyses et d'avoir su m'accompagner dans la hiérarchisation de mes idées et mes travaux. Promis, je ferai encore plus d'efforts sur la structuration de mes écrits. Merci aussi d'avoir su me faire confiance tout en m'aidant à gérer les moments difficiles. Claude, merci pour tout ce temps consacré au design, à l'animation et la coordination des multiples essais au champ et de l'expérimentation à PhenoArch! J'ai particulièrement apprécié notre déplacement ensemble à PhenoField. À tous les deux, merci de m'avoir fait confiance dès le début et de m'avoir embarqué dans ce projet partenarial avec ARVALIS, l'entreprise qui a été la première à m'accueillir en stage depuis mon arrivée en France en 2016 et qui m'a fait découvrir le monde professionnel et agricole. Je pense avoir eu beaucoup de chance en participant à un projet avec des collaborations entre monde académique et recherche privée d'aussi bonne qualité, mais également avec une dynamique et une bienveillance permanente. Grâce à vous, j'ai pu interagir avec différentes personnes et à différents niveaux du projet et j'ai le sentiment d'avoir énormément appris à votre contact!

Je voulais ensuite remercier chaleureusement Matthieu, mon co-encadrant d'ARVALIS, qui m'a aussi toujours fait confiance sur ce projet de thèse. Merci d'avoir été à l'écoute de mes difficultés et source de propositions pour y remédier. Merci d'avoir donné de ta personne pour porter ces sacs de semences de maïs et les répartir dans cette panoplie de pochettes à poster! Merci pour ces moments sympathiques partagés ensemble lors de nos déplacements à Boigneville ou Montardon. Merci à toi et mes encadrants du LEPSE d'avoir veillé à ma participation à des formations et séminaires chez ARVALIS ou ailleurs. Merci enfin de m'avoir soutenu pour continuer mes travaux de recherche chez ARVALIS après la thèse!

Je souhaite aussi remercier toutes les autres personnes qui ont contribué directement ou indirectement aux travaux de ma thèse, qui sont toujours au LEPSE ou qui l'ont quitté. Merci d'abord à Emilie, Santiago et Italo qui ont réalisé une bonne partie des analyses sur le panel de diversité DROPS-Amaizing et qui m'ont transmis généreusement des conseils pratiques et des scripts R pour mes travaux. Merci également à Nadir, qui lui a effectué une bonne partie des analyses sur le panel progrès génétique et sur les données INVITE maïs. Merci beaucoup aussi à Nathalie L. et Théophile pour leur aide sur la collecte, le nettoyage ou les analyses des données européennes INVITE maïs. Merci à Lucille, Loïc, Pierrick, Boris et Pierre pour leurs participations précieuses au développement du modèle Sirius Maize. Merci à Llorenç, Maëlle, Romane, Benoît S., Maïlys, Alexis, Renaud et Christian F. pour leurs participations techniques ou scientifiques à l'expérimentation PhenoArch. Merci enfin à Randy pour ses conseils sur la partie génétique de l'article publié en thèse.

Je voulais ensuite remercier toutes les personnes d'ARVALIS qui ont été impliquées dans la préparation, l'animation ou la conduite des essais au champ en France. Je remercie d'abord Nathalie M. qui a veillé à avoir les semences des variétés du panel d'hybrides récents et a participé au montage du réseau d'essais de la thèse. Merci à Katia B. qui y a aussi participé et a supervisé avec son équipe les plateformes de phénotypage au champ. Merci à Jean-Pierre C. également pour sa veille à la réalisation des essais de la thèse. Merci beaucoup aux équipes régionales qui ont géré et conduit les essais du panel, notamment : Yves P., Stacy B., Pauline R., Didier L., Florence B., Lucile P., Céline H., Bastien C., Thomas J., Antoine P., Manuel H., Laura D., Clémence A., Monica OV., Céline D., Benjamin B. et Lonni N. Merci aussi à mes collègues du labo génomique Faharidine M., Caroline L. et Adriane R. qui ont aidé aux préparations liées au génotypage du panel.

D'autre part, j'aimerais également remercier les équipes des instituts partenaires du projet INVITE qui ont géré et mené les essais maïs en Europe. Merci à Juan H. et l'équipe Agroscope en Suisse, au BSA en Allemagne, Ukzuz en Tchéquie, ILVO en Belgique, AGES en Autriche, Nebih en Hongrie, à Romain C. et son équipe du Diascope et à l'équipe GEVES en France.

Je souhaite aussi remercier les membres de mon comité de thèse. Merci beaucoup à Laurence M. pour son œil avisé sur la partie génétique de ma thèse et ses conseils précieux pour l'article publié. Un grand merci à Boris P. pour son aide et ses conseils sur la partie liée au modèle Sirius. Merci à Patrice This pour son regard neuf sur mon travail.

Merci à tous les Lepsiens pour l'ambiance de travail, les interactions ou les moments conviviaux partagés ensemble... Merci à Italo, Felipe, Justine, Randy, Arnaud, Thierry, Benjamin, Stéphane L., Mathilde, Benoît D., Mariana, Nicolas D., Pierre K., Jonas, Juliana, Xinxin, Bertrand, Aurélien, Olivier, Teiki, Laurine, Mathis, Jiang, Romain B., Myriam, Gaëlle, Alexis, Vincent N., Anaïs, Laëtitia et Christelle.

Un immense merci à ma famille qui m'a soutenu depuis toujours pour aller au bout de mes études. Merci à ma sœur, mon beau-frère et mes neveux qui ont été mon foyer de réconfort et bonheur en France. Merci à mes chers parents en Algérie, qui m'ont toujours aidé dans mes projets et qui m'ont encouragé à faire ce qui me plaît dans la vie. Promis, je passerai plus souvent au bled désormais!

# **TABLE OF CONTENTS**

GLOSSARY OF TERMS AND ABBREVIATIONS	
INTRODUCTION	1
General context	3
Genomic prediction models	5
Phenomics and high-throughput phenotyping	
Crop growth models (CGMs)	
Integration of CGMs and genomic prediction (GP) models	
Elements on maize cropping cycle and growing conditions	14
Overview and outline of the thesis	16
References	19
CHAPTER 1: ROBOTIZED INDOOR PHENOTYPING ALLOWS GENOMIC PREDICTION	ON OF
ADAPTIVE TRAITS IN THE FIELD	25
Introduction	27
Results	30
Traits measured indoor correlated with those in the field, depending on cate	gories
of traits	30
The differences in absolute values of traits between indoor and fields	were
accounted for by environmental conditions	32
Measurements in indoor platforms can be used for genomic prediction	on of
traits	32
Discussion	33
Methods	35
Genetic material	35
Platform experiments	35
Field experiments	36
Correlation analysis between experiments	36
Genotypic data and diversity analyses	37
Genomic prediction models	37
Training and validation schemes of genomic predictions	37
Poforoncos	20

Acknowledgements	40
Supplementary information	41
CHAPTER 2 : ACQUISITION AND ANALYSIS OF EXTENDED	ED FIELD DATA IN
CONTRASTING ENVIRONMENTAL CONDITIONS FOR CROP MOD	EL SIMULATION ON A
SET OF RECENT HYBRIDS	55
Introduction	57
Results and discussion	58
The distribution of environmental conditions and yield in stu-	died experiments was
typical of maize growing area in Europe	58
Five environmental scenarios, based on temperature ar	nd soil water status,
synthesized environmental conditions and accounted for y	ield variations across
experiments	
Estimation of leaf area index and of maximum grain number	per plants, to be used
to test simulation in Chapter 3	63
Material and methods	65
Genetic material	65
Field experiments	65
Yield and environmental conditions in Europe	66
Field traits Analyses	66
Environmental characterization and multi-environment analy	yses67
References	68
Acknowledgements	70
Supplementary information	71
CHAPTER 3 : SIMULATING LEAF AREA INDEX AND GRAIN NUM	IBER FOR PANELS OF
MAIZE HYBRIDS IN CONTRASTING ENVIRONMENTAL CONDITIO	<b>NS</b> 77
Introduction	79
Approach used in the Chapter	
Genotype-dependent parameters	81
Use of the genotypic parameters by Sirius Maize	82
Test of the relevance of simulation results	83

Results and discussion84
I) Simulation of leaf area index (LAI)84
Sirius Maize accounted for both the genotypic and environmental effects on LAI
but with different accuracies depending on environmental scenarios and
considered test84
LAI simulation accuracies remained nearly unchanged when parameters resulted
from genomic prediction87
The genotypic variability of LAI in contrasting environmental conditions depended
on phenology and leaf elongation rate89
II) Simulation of grain number (GN)90
Sirius Maize accounted for both the genotypic and environmental effects on grain
number per unit area90
GN Simulation accuracies decreased but remained appreciable when genotype-
dependent parameters were predicted from genomic information93
The genotypic variability of GN in contrasting environmental conditions depended
on the maximum grain number potential and leaf growth rate96
Methods99
Calculation of genotype-dependent parameters fed to Sirius Maize99
LAI modelling in Sirius Maize99
Grain number modelling in Sirius Maize100
Simulation tests accuracies101
References101
Supplementary information103
GENERAL DISCUSSION AND PERSPECTIVES109
A link between indoor phenotyping and field crop performance111
Estimation of genotype-dependent parameters of CGMs112
A novel GP-assisted CGM method for predicting LAI and grain number in maize113
Further upgrades of the thesis GP-assisted CGM method114
Toward application in breeding or variety recommendation contexts115
References116
ANNEXE EN FRANCAIS

# **GLOSSARY OF TERMS AND ABBREVIATIONS**

TERM	MEANING OR DEFINITION
ALA	Average Leaf inclination Angle
BayesA, BayesB, BayesC, BayesR	Bayesian regression models incorporating mixture priors that mainly differ in their assumptions regarding markers effects and variance distributions
BLUEs	Best Linear Unbiased Estimates : solutions (estimates) associated with the fixed effects of a linear mixed model
BLUPs	Best Linear Unbiased Predictions : solutions (predictions) associated with the random effects of a linear mixed model
CGM	Crop Growth Model
CI	Confidence Interval
CV scheme	Cross-Validation scheme
CV <sub>RMSE</sub>	Coefficient of Variation of RMSE
df	Degrees of freedom
DL	Deep Learning
EC	Environmental Covariates
ETO	Reference crop evapotranspiration
fiPAR	Fraction of intercepted photosynthetically active radiation
FLN	Final Leaf Number
FSA	Frequency of Similar Assignment
G-BLUP	Genomic - Best Linear Unbiased Prediction
GEI, GxE	Genotype-by-Environment Interaction
GN	Grain Number
GP	Genomic Prediction
GS	Genomic Selection
gS <sub>max</sub>	Max stomatal conductance
GWAS	Genome-Wide Association Study

h <sub>g</sub> <sup>2</sup>	Genomic heritability
НТЗР	High-Throughput Plant Phenotyping Platform
НТР	High-Throughput Phenotyping
Indoor PF	Indoor platform
LAI	Leaf area index
LAR	Leaf appearance rate
LASSO	Least Absolute Shrinkage and Selection Operator
LER	Leaf expansion rate
LUE	Light use efficiency
METs	Multi-Environment Trials
PC-BLUP	PCoA axes - Best Linear Unbiased Prediction
PCoA	Principal Coordinate Analysis
PGR	Plant growth rate in biomass
QTL	Quantitative Trait Locus
rh <sub>PAD</sub>	Relative height at 50% of plant leaf area
RIE	Radiation interception efficiency
RMSE	Root-mean-square error
RR-BLUP	Ridge Regression - Best Linear Unbiased Prediction
rrmse	Relative root-mean-square error (same as CV <sub>RMSE</sub> )
SNP	Single Nucleotide Polymorphism
SWP	Soil Water Potential
UAV	Unmanned Aerial Vehicle
VPD	Vapor Pressure Deficit
WD	Water Deficit
WGP	Whole-Genome Prediction
WW	Well-Watered

# **INTRODUCTION**

# TABLE OF CONTENTS

General context	3
Genomic prediction models	
Phenomics and high-throughput phenotyping	
Crop growth models (CGMs)	10
Integration of CGMs and genomic prediction (GP) models	12
Elements on maize cropping cycle and growing conditions	14
Overview and outline of the thesis	16
References	19

### **General context**

World crop production over the last 70 years has increased at an unprecedented rate as a result of sustained yield increases, via breeding and crop management practices (Agnolucci & De Lipsis, 2020). However, recent contributions point at crop yield stagnating, while the demand for agricultural products is rising (Lobell & Gourdji, 2012; Grassini *et al.*, 2013; Ray *et al.*, 2015; Moore & Lobell, 2015; Schauberger *et al.*, 2018). Changing agricultural policy (support to input reduction), natural annual variability of growing seasons and climate change are among the explanations cited for this stagnation or limited growth in yield (Peltonen-Sainio *et al.*, 2009; Brisson *et al.*, 2010; Moore & Lobell, 2015). Indeed, with warming trends and limitations on irrigation and fertilization in several regions, crops are experiencing negative impacts of more frequent heat events, dry episodes, and an increase in evaporative demand (Tester & Langridge, 2010; Lobell *et al.*, 2011; Challinor *et al.*, 2014).

Maize, a major food and feed crop worldwide (2<sup>nd</sup> largest harvested area, Erenstein *et al.*, 2022), is an example of an annual cereal that had a long-term yield high increase trend in farmers' fields, but tending during last two decades to have a much lower yield growth rate and higher inter-annual variability (Moore & Lobell, 2015; Agnolucci & De Lipsis, 2020). In France for instance, the mean grain yield gain was 1.43 q/ha/year from 1951 to 1999 but only 0.35 q/ha/year from early 2000s (Lorgeou *et al.*, 2009, 2019; Fig. 1). In southern and eastern European countries such as Italy and Hungary, yields are stagnating (Ray *et al.*, 2012).

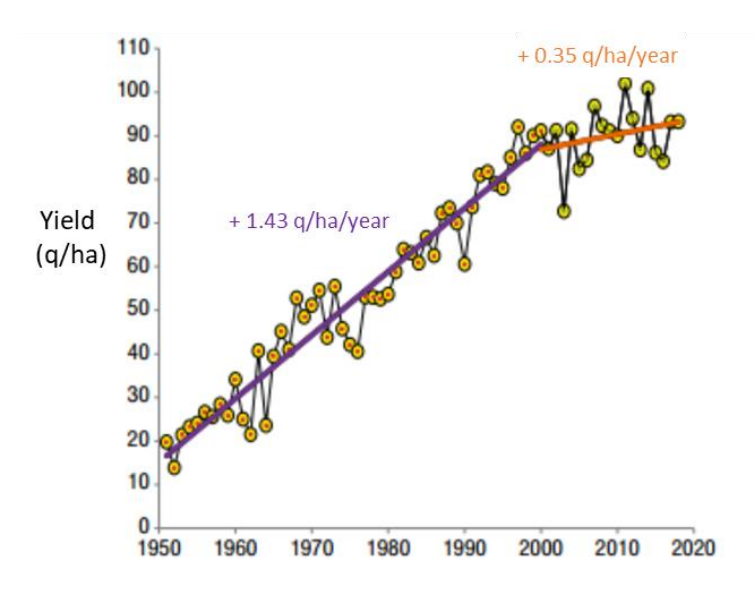


Fig. 1: Maize mean grain yield in France farmers' fields from 1951 to 2018 (Lorgeou et *al.*, 2009, 2019).

Breeding played an important role in maize yield improvement. Starting from the 1930s, maize yield remarkably increased due to the breeding and adoption of hybrid varieties (Duvick, 2001; Fu et al., 2014). Maize breeding contributed to 50–60% of maize yield gains from 1934 to 2004, and the remaining 40–50% were attributed to appropriate field management (Duvick, 2005). The limited yield growth rate or stagnation in farmers' fields during last years were observed despite of the continuous genetic progress in yield of 1.01 q/ha/year, estimated in European growing area with a panel of varieties released from 1950 to 2015 in Welcker et al. (2022). This indicates that the observed limitation or stagnation in annual yield growth in farmers' fields is due more to environmental and crop management effects, along with genotype-by-environment interaction effects that are important especially for quantitative complex traits such as grain yield (Bertin et al., 2010; Malosetti et al., 2013).

The genotype-by-environment interaction (GEI) is the fact that the phenotypic response (e.g. yield trait) to environmental conditions varies for different genotypes beyond what is explained by genotypic and environmental effects, resulting for example in changes of genotypes ranking for the considered trait in different environments (Malosetti *et al.*, 2013). The function describing the phenotypic performance of a genotype in relation to an environmental characterization is called the 'reaction norm' by some authors (Falconer & Mackay, 1996) or 'response curves' by others (Millet et *al.*, 2019). Fig. 2A shows the case where there is no GEI, the genotype and the environment behave additively and the reaction norms are parallel. The remaining plots show different situations in which GEI occurs: divergence (Fig. 2B), convergence (Fig. 2C), and the most critical one, crossover interaction (Fig. 2D). Crossover interactions are the most important for breeders as they imply that the choice of the best genotype is determined by the environment.

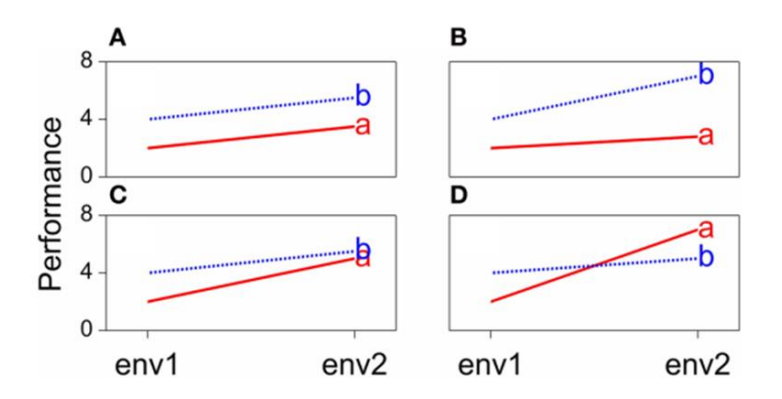


Fig. 2: Genotype-by-environment interaction in terms of changing mean performances across environments: (A) additive model, (B) divergence, (C) convergence, (D) cross-over interaction (Malosetti et *al.* 2013).

GEI can also be regarded in terms of heterogeneity of genetic variance and covariance. As a consequence of GEI, the magnitude of the genetic variance as observed within individual environments will change from one environment to the other, becoming usually lower as stress conditions increase (Malosetti *et al.*, 2013).

Depending on environmental conditions and management practices, environment and GEI effects can prevent varieties from reaching their expected genetic values, and consequently limit yield. The incidence of GEIs and a lack of their understanding results in a reduction in the predictability of trait phenotypes and the realized rates of genetic gain achieved from selection (Cooper *et al.*, 2016). Breeders and other variety testing actors evaluate each year candidate varieties in multi-environment trials (METs). Most varieties are evaluated in a limited number of environments, considered as a combination of year × site × condition (Robert *et al.*, 2020). Consequently, the environments in which the varieties are evaluated can be different from the target environments, because of the significant variation between years (Casadebaig *et al.*, 2016). In addition, only a limited number of varieties are evaluated each year to control the phenotyping costs (Robert *et al.*, 2020). All these constraints are reducing the chance of success as they limit the number of genotypes that can be evaluated in the target environments. Three main tools can help to raise these strong constraints: genomic prediction (GP) models, phenomics and high-throughput phenotyping (HTP), and crop growth models (CGMs).

# **Genomic prediction models**

With the availability of low-cost genotyping, genomic prediction has become an attractive tool to increase the number of genotypes considered for selection and to speed up the breeding cycle (Hickey et al., 2014; Crossa et al., 2014; Cooper et al., 2014; Araus et al., 2018). Genomic prediction (GP) consists in predicting quantitative complex traits of candidate varieties by using all available DNA markers across the genome, usually single nucleotide polymorphism markers (SNPs) (Meuwissen, 2007). In GP, a phenotyped and genotyped calibration (training) set is used to estimate DNA markers additive and non-additive effects. Once the model is calibrated, new candidate varieties can be predicted, as long as their genomic information is available. Several statistical models or machine learning methods have been proposed for genomic prediction using genome-wide SNP markers, including: linear mixed (RR-BLUP, G-

BLUP; Whittaker *et al.*, 2000; VanRaden, 2008; Endelman, 2011; Wang *et al.*, 2018) and Bayesian (LASSO, BayesA, BayesB, BayesC, BayesR; Meuwissen *et al.*, 2001; Wang *et al.*, 2015; Shi *et al.*, 2021; Montesinos López *et al.*, 2022) regression models, gaussian kernel models (Gianola & van Kaam, 2008; Cuevas *et al.*, 2016), random forest and deep learning methods (Montesinos-López *et al.*, 2018; Crossa *et al.*, 2019; Måløy *et al.*, 2021; Wang *et al.*, 2023). These GP models mainly differ in their assumptions regarding markers effects and variance distributions, regarding linearity or nonlinearity of markers effects and their computational complexity. All result in different prediction accuracies depending on trait genetic architecture and heritability, training population size and composition and DNA markers density (Tayeh *et al.*, 2015; Kaler *et al.*, 2022).

Specific GP models were proposed to predict the performance of varieties in different environments, taking the genotype by environment interaction (GEI) into account. Fig. 3 presents a short timeline of the type of statistical and machine learning methods used in GP research in the context of G x E (Crossa *et al.*, 2022).



Fig. 3: History of the main research involving genomic prediction and G x E interaction as reviewed by Crossa et al. (2022). Blue boxes denote studies using only DNA markers or genomic information. Green boxes refer to models in which DNA markers are complemented by stress indices derived from a crop growth model. Purple boxes refer to models in which DNA markers are complemented by the use of environmental covariates (EC), such as micro-climatical variables and soil information.

It was first proposed to adapt the reference GP models to the GEI context by attributing environment specific effects to the markers (Schulz-Streeck *et al.*, 2013; Crossa *et al.*, 2016), or by modeling genetic covariances between environments (Burgueño *et al.*, 2012). In other studies, environmental covariates (EC) were introduced in the GS model (Jarquín *et al.*, 2014; Ly *et al.*, 2018; Millet *et al.*, 2019), which allows predicting the performance of varieties in new environments. Crop growth models (CGM) were sometimes used to adjust the EC estimates to phenological stages, or to derive EC estimating the stress experienced by the plants (Ly *et al.*, 2017; Rincent *et al.*, 2019), instead of directly using pedoclimatic data. Finally, deep learning artificial neural networks (DL) are also being developed for assessing multi-trait, multi-environment genomic prediction (Montesinos-López *et al.*, 2018; Cuevas *et al.*, 2019; Costa-Neto *et al.*, 2021). Overall, GP statistical models integrating environmental covariates or deep-learning models performed the best, with prediction accuracies for yield ranging from 0.50 to 0.85 depending on validation schemes and environment types considered.

# Phenomics and high-throughput phenotyping

Since whole-genome sequencing of many crops has been achieved, genomics and breeding studies have stepped into the big-data and high-throughput era (Li *et al.*, 2021). Hence, acquisition of large-scale phenotypic data (phenomics) became one of the major bottlenecks hindering crop breeding (Houle *et al.*, 2010; Li *et al.*, 2021). Phenotyping applies specific methods and protocols to measure morphological structural traits, physiological functional traits, and component content traits at different spatial scales (cells, tissues, organs, plants, canopy, populations) and at appropriate temporal scales, ranging from minutes to months (Table 1, Fig. 4).

Whole-plant, multi-environment Field multi-environment networks Typical phenotyping platforms High-precision platforms (omic, anatomy, organ) platforms (field or controlled) Level of plant organization Organ Plant or canopy Canopies in a range of environments Omics, 4D organ imaging, Typical methods 4D plant/canopy imaging fluxes, Yield, sensor network, remote fluxes sensors sensing Hydraulics, metabolism, Light interception, water Trade-offs between processes Typical mechanism signalling transfer, whole-plant signalling Ratio biology/other processes Relevance for yield prediction Methods for trans-scale communication Gene editing, plant simulation GWAS, model-assisted dissection

Table 1: Methods for phenotyping at different scales of plant organization (Tardieu et al., 2017).

		Phenotypic traits										
		Mor	Morphological Structural Traits Physiological Functional Traits						Compo	Component Content Traits		
		Plant height	Biomass	Canopy coverage	Lodging	FAPAR	Staygreen/ senescence	Light use efficiency	Diseases/ pests	Chlorophyli content	Nitrogen content	Water
1	RGB Camera											
	Multi/Hyperspectral Camera											
	Thermal Camera											
Sensors for Phenotyping	Photosynthesis Sensor											
Sensor	Fluorescence Sensor											
	Stereo Camera											
1	LiDAR											

Fig. 4: Phenotyping sensors currently available to monitor, quantify, and estimate key morphological structural traits, physiological functional traits and component content traits of plants (Li et al., 2021).

Since early 2010s, a variety of high-throughput plant phenotyping platforms (HT3Ps) have been developed which are now common tools in commercial or research teams (Granier & Vile, 2014; Tardieu *et al.*, 2017; Yang *et al.*, 2020). Li et al. (2021) defines a 'HT3P' as a platform that can collect massive amounts of phenotypic data from hundreds of plants every day with a high degree of automation. HT3P is hence a powerful tool allowing us to monitor and quantify crop growth and production-related phenotypic traits in a non-destructive, fast, and high-throughput manner. The acquired phenomic data can then be valued in genomics-assisted breeding approaches (Rutkoski *et al.*, 2016; Araus *et al.*, 2018; Alahmad *et al.*, 2018; Lopez-Cruz *et al.*, 2020; Guo *et al.*, 2020; Sandhu *et al.*, 2022), along with crop modelling approaches when the measured traits can be linked to crop growth models formalisms

parameters (Araus *et al.*, 2018; Messina *et al.*, 2018; Bustos-Korts *et al.*, 2019; Toda *et al.*, 2020; Lacube *et al.*, 2020).

Various types of indoor and field HT3Ps have been developed (Fig. 5). All phenotyping platforms integrate cameras, supplemental light sources, automatic watering, and weighing devices to automatically collect plant phenotypic data (Li *et al.*, 2021). Available cameras include those capable of capturing RGB, infrared (IR), fluorescence (FLUO), near-infrared (NIR), multispectral or hyperspectral images (Fig. 4). Indoor high-throughput phenotyping (in a growth chamber or greenhouse) entails the precise control of environmental factors and an accurate capture of the plant responses to specific environment conditions. Given the mechanical structure of the platform and movement mode between the sensors and plants, an indoor HT3P can be categorized as either a benchtop-type or a conveyor-type (Fig. 5).

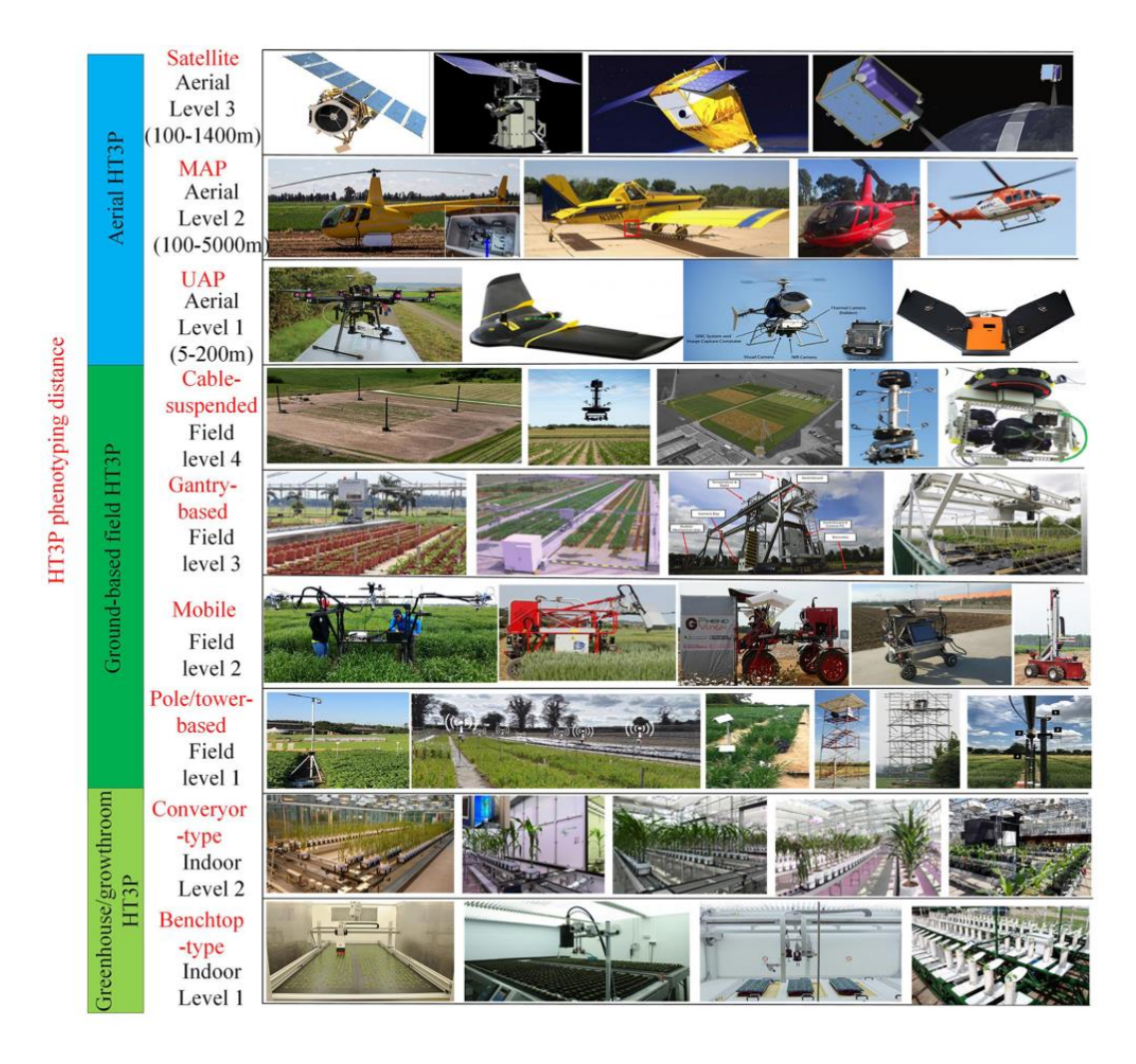


Fig. 5: Examples of high-throughput plant phenotyping platforms (HT3Ps) as reviewed by Li et al., (2021), including HT3Ps in the greenhouse/growth chamber, field ground-based HT3Ps and aerial HT3Ps.

Partial environmental control in indoor platforms limits the unpredictable phenotypic variation caused by the interaction between genotype and natural environment (G×E). Therefore, indoor HT3Ps are widely used to study the response of plants to specific growth conditions, and accurately capture morphological structural, physiological functional or component content traits (Li *et al.*, 2021). Field platforms account only for 18% of HT3Ps worldwide (Yang *et al.*, 2020). They operate at canopy level and are affected by weather, biotic and abiotic stresses, and soil properties, as in farmers' fields. According to their usage scenarios and imaging distance, field HT3Ps can be categorized into ground-based and aerial platforms. Ground-based platforms can be further classified as pole/tower based, mobile, gantry-based, and cable-suspended (Fig. 5). Likewise, aerial platforms can be categorized, as unmanned aerial platforms (UAPs), manned aerial platforms (MAPs) and satellite platforms (Fig. 5).

Each year, the thousands of phenotyping experiments worldwide in environmentally controlled growth facilities or in the field produce large amounts of phenotypic data (Yang *et al.*, 2020). However, the reproducibility of results by different research groups is not always satisfactory because of the unexplained variation of environments (Poorter *et al.*, 2012, 2016). Thus, environmental factors are vital and should receive at least the same amount of attention as the traits that are measured (Tardieu *et al.*, 2017; Yang *et al.*, 2020). Envirotyping, defined as characterizing and quantifying the environmental factors in a high-throughput way, can help to address this issue (Xu, 2016). Integrated with optimized experimental field trials designs, envirotyping, crop modelling and genomics, high-throughput phenotyping can improve the heritability and potential for genetic gain (Araus *et al.*, 2018).

# **Crop growth models (CGMs)**

Crop growth models consist of multiple equations that represent physiological processes of plants and simulate crop development and growth dynamically, given environmental (e.g., air temperature, light and soil water) and management (e.g., sowing date, plant density and fertilizer applications) inputs (Muller & Martre, 2019; Onogi, 2022). CGMs are calibrated using data from controlled environments and field trials, most often by using model inversion. They often use parameters calibrated for each module/process independently using a variety of datasets (Onogi, 2022). Once calibrated, CGMs can predict yield for new (untested)

environments if conditions at these environments are given. When CGMs are calibrated for each genotype, estimates of CGM parameters can differ between genotypes. Differences in parameters are considered as representing the differences in response to environmental conditions among genotypes. However, calibrating the behaviour of genotypes is most often limited to the duration of phenological phases because other parameters are highly interacting, thereby making model inversion nearly impossible. The interconnections and feedback regulations between the CGMs subcomponents and biological processes, generate unexpected global system properties, called emergent properties, which do not appear when the subcomponents are individually considered (Bertin *et al.*, 2010). GxE interactions and some types of non-additive effects on the expressed phenotype are part of these emergent properties in CGMs.

CGMs include, for instance, DSSAT (Decision Support System for Agrotechnology Transfer; Jones *et al.*, 1998) and APSIM (Agricultural Production Systems slMulator; McCown *et al.*, 1996; Hammer *et al.*, 2010; Fig. 6), that model canopy-level processes. Both CGMs use a graphical user interface (GUI) and cover a wide range of crops.

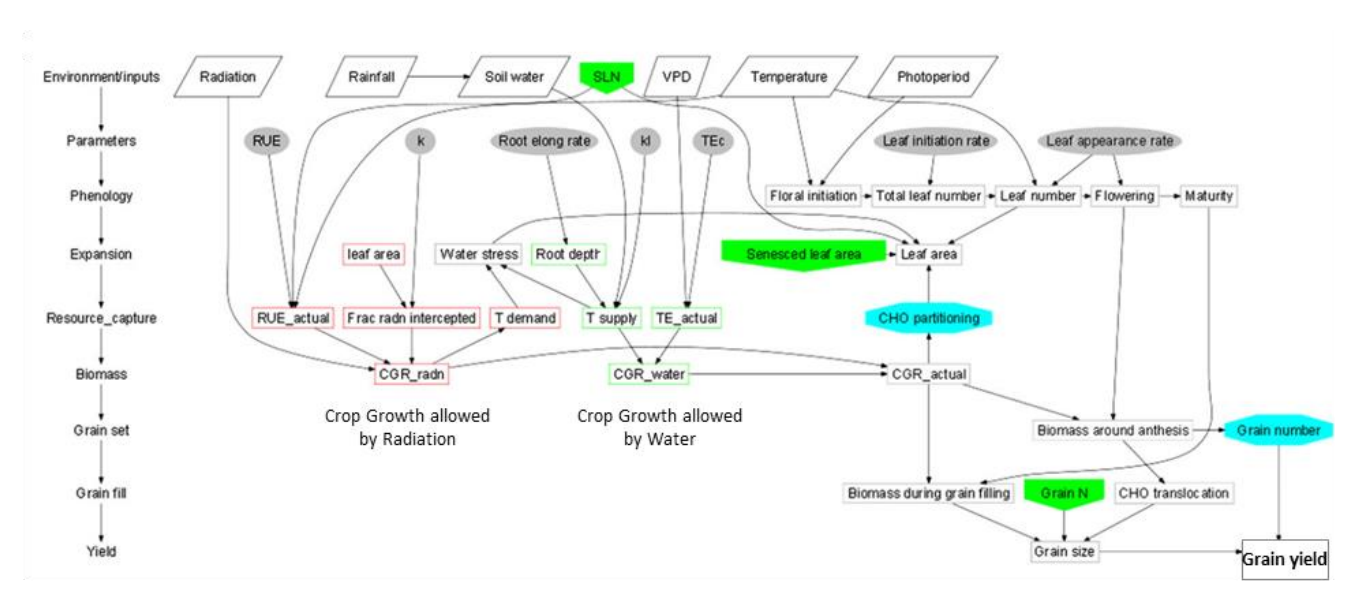


Fig. 6 : Schematic representation of crop growth and development processes interconnection in APSIM (Agricultural Production Systems sIMulator) cereal template (Hammer et al., 2010).

Components of such process-based CGMs are: state variables (X) representing current plant status (e.g., leaf area index, biomass, and developmental stages), rate variables (R) representing rates of change in the state variables, environmental variables (E) representing environmental inputs (e.g., air temperature and light), and parameters characterizing

functional relationships among the variables (X, R and E) (Horie *et al.*, 1992). State variables X then relate to each other, and feedback loops exist among variables. Consequently, process-based CGMs comprise many parameters to be determined. Genotype-dependant parameters of CGMs have various alias, including genetic coefficients, input traits, physiological traits, genotype-specific parameters, and genotypic parameters (Onogi, 2022). A shortcoming of CGMs in a breeding context, is that all necessary input traits have to be measured for all genotypes to be simulated with the CGM. This may prove to be very costly and complex in practice, when done on an industrial scale (i.e., for many populations and repeated yearly).

# Integration of CGMs and genomic prediction (GP) models

Models used to enable genomic prediction are founded on quantitative genetics theory and are statistical representations of a complex biological system (Cooper *et al.*, 2016). Hence, these models do not explicitly take into consideration much of the biology that contributes to GEIs (Hammer *et al.*, 2006). The methodology for GP relies heavily on the creation of suitable training data sets that span the highly combinatorial inference space (genetic combinations in the environments) for the intended applications (Cooper *et al.*, 2016). Fitting the models to the marginal effects across the environments of the training data set to predict marginal performance in the application set is the most common approach; however, the presence of important GEIs in the application set can be challenging. Extensions of GP models discussed before, that rely on the identification of suitable environmental covariates have been developed with success. However, these methods do not explicitly take into consideration the dynamic nature of the biology underlying GEIs.

Recently, Technow et al. (2015) proposed a novel methodology, named CGM-WGP, that outperformed the benchmarked classical GP model (G-BLUP). It was assumed to take into consideration the biology underpinning GEIs through CGM, while avoiding large-scale phenotyping costs by using GP. The CGM-WGP method consisted in combining a simple maize CGM developed by Muchow *et al.* (1990), with a GP Bayesian model for genotype-dependant CGM parameters estimation. The model predicted grain yield as a function of plant density, temperature and solar radiation, as well as four genotype-dependent physiological traits (parameters): total leaf number, area of largest leaf, radiation use efficiency and thermal units to physiological maturity. The tests were performed for a population of inbred lines created

in silico. CGM parameters for new (untested) genotypes were first predicted with GP, then their phenotypes (yield values) in tested or new environments were simulated by running the CGM with the predicted parameters values along with environmental and management inputs. Predictions accuracies obtained with the CGM-WGP method ranged from 0.42 to 0.77 depending on tested prediction schemes, while accuracies ranged from 0.08 to 0.62 with the benchmarked G-BLUP model in the study. The method integrating GP model predictions in a CGM can be generally referred to as GP-assisted CGM (Onogi, 2022; Fig. 7a). Indeed, phenotypes are predicted here by the CGM, and GP aids these predictions. This approach is an extension of gene-based models and QTL mapping on CGM parameters (Hoogenboom *et al.*, 2004; Onogi, 2022). Other early applications of GP-assisted CGM to real data included: Onogi *et al.* (2016) for predicting rice heading dates, Cooper *et al.* (2016) and Messina *et al.* (2018) for predicting maize grain yield, Toda *et al.* (2020) for predicting rice biomass. Finally, a similar GP-assisted CGM method is developed in our thesis study for maize.

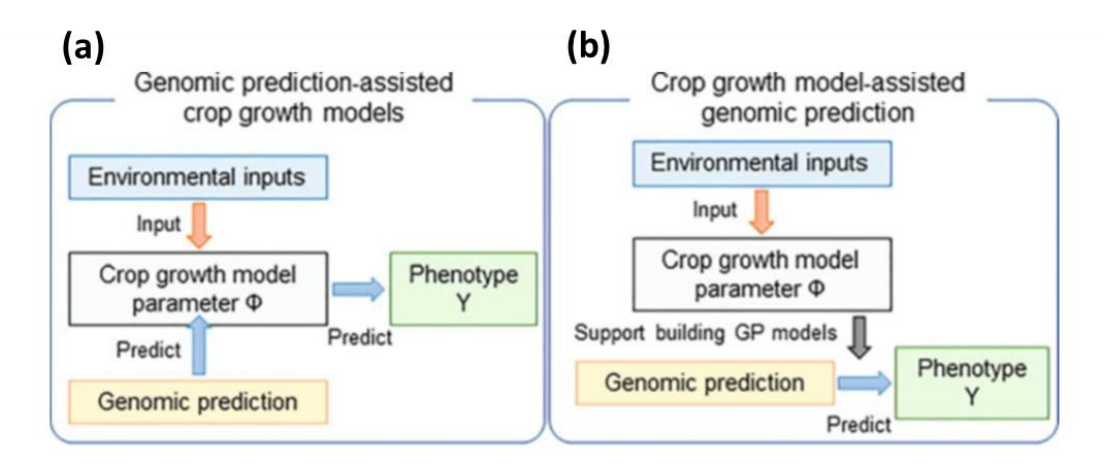


Fig. 7: Genomic prediction-assisted crop growth models (GP-assisted CGMs) and the crop growth model assisted genomic prediction (CGM-assisted GP). In GP-assisted CGMs (a), GP is used to predict parameters of CGM for new genotypes. Phenotypes are then predicted with the CGM. In CGM-assisted GP (b), phenotypes of new genotypes are predicted with GP. CGMs are used to support development of GP models (Onogi, 2022).

Alternatively, CGMs can be used to assist GP models in multiple ways. Such integration can be termed CGM-assisted GP (Onogi, 2022; Fig. 7b). Mainly three approaches have been proposed for that. (i) The first is the use of CGMs to simulate plant growth stages, which are then used for inferring environmental covariates that can affect GxE interactions (Heslot *et al.*, 2014; de los Campos *et al.*, 2020). (ii) The second approach is the use of CGMs to characterize environments (Ly *et al.*, 2017). In the latter study, a CGM model (APSIM) was run to compute

indices of nitrogen nutrition stress for wheat, which were then used to characterize multiple experiments environments. GP was finally conducted by considering the genotype-by-index interactions. (iii) The third approach is the use of CGMs to predict intermediate or indicator traits. In Robert *et al.* (2020), wheat heading dates for new environments were predicted using a CGM, then predicted heading dates were included as covariates in GP mixed models to predict yield. In Bustos-Korts *et al.* (2019), dynamics of biomass and canopy cover for wheat genotypes were simulated using APSIM model, then parametric traits were extracted from these dynamics and used in a multi-trait GP model for predicting grain yield. Similarly, in Jighly *et al.* (2023), a CGM was used to simulate phenology, nitrogen and biomass traits, then these traits were used in a GP model to predict some field performance traits including (yield, grain number and grain protein content).

# Elements on maize cropping cycle and growing conditions

Maize (Zea Mays L.) is a monoecious species of the *Poaceae* family and an annual summer crop in temperate regions. It is usually sown between March and May in Europe, and maize grain is harvested from September to November, depending on varieties maturity groups (duration from sowing to grain complete physiological maturity). Maize is not evenly distributed across Europe. It is concentrated in regions with favourable climate and predominantly grown in rainfed conditions (Webber *et al.*, 2018). When environmental conditions become suboptimal or even dry, as in southern Europe, and when water is available and economical strategies permit it, maize is grown under irrigated conditions. For instance, irrigated maize covered approximately one third of the irrigated cropping area in France in 2022 (Agreste, statistiques agricoles).

The maize cycle is commonly characterized by three main phases, namely (i) the vegetative phase, (ii) the flowering time phase during which reproductive organs rapidly grow and (iii) the grain filling during which the ear grows until maturity (Zhao *et al.*, 2012). The vegetative growth stages extend from sowing to the appearance of tassel (male inflorescence) at the top of the plant (Fig. 8). They include a strictly vegetative period, from sowing to tassel initiation, and a period, from tassel initiation to tasselling (visible tassel), during which vegetative and reproductive growths overlap. The leaves are successively initiated at the shoot apical meristem until the apex becomes reproductive and initiates the tassel. At that stage,

approximately 50 % of the leaves are visible, while the remaining younger leaves are still enclosed in the sheath of the developed older leaves. The female flowering structure, the ear, is usually initiated in axillary buds, 1 to 2 phyllochrons after the tassel. Female flowers are sequentially initiated as floret rings (or cohorts) around a central cob. Successive florets are aligned along rows, the number of which corresponds to the number of florets synchronously initiated in the same ring. Flowers are therefore ranked from ear base to ear apex according to their order of initiation. Each flower includes an ovary with an attached silk (elongated style) and potentially produces one grain if fertilised successfully. The number of fertilisable ovules per ear, i.e. the potential number of grains at pollination, is therefore the product of the number of rows by the number of flowers per row.

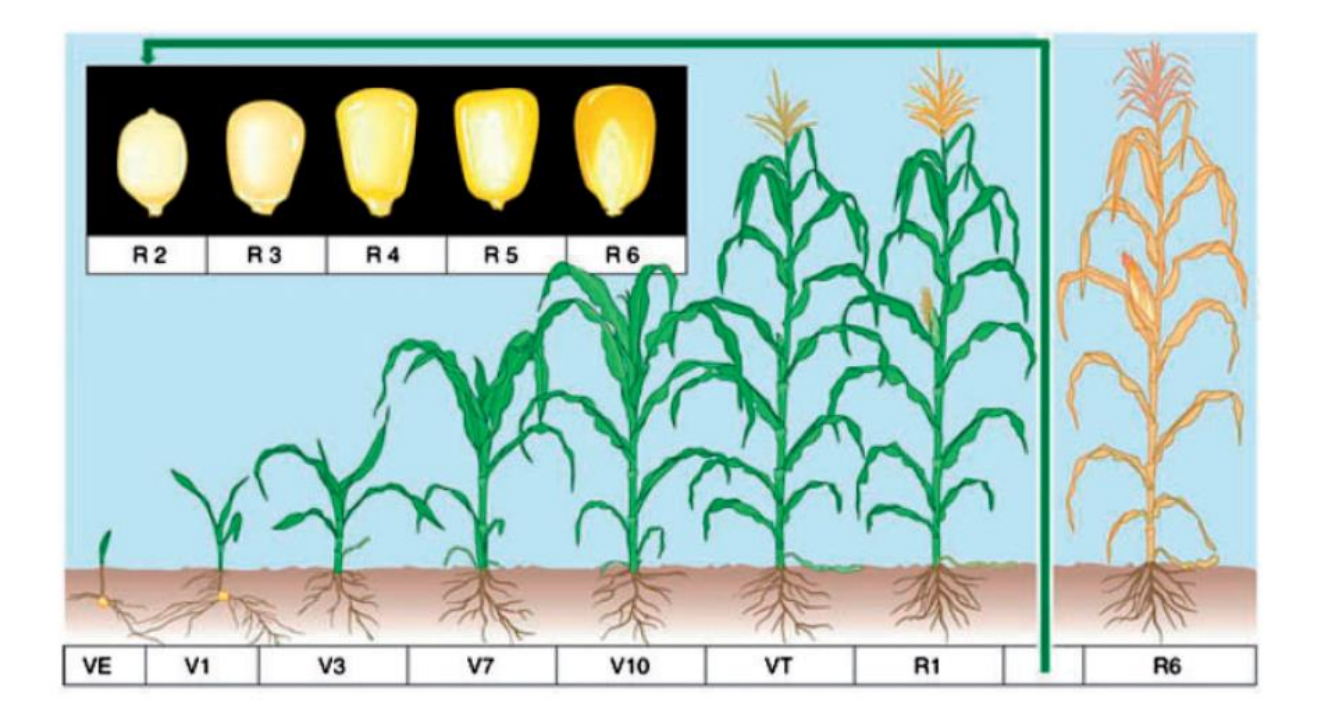


Fig. 8: Different standard growth stages of a maize crop, including vegetative (V) and reproductive (R) stages. The V developmental milestones include: emergence (VE), in which the coleoptile reaches the soil surface and elongates due to its exposure to sunlight; V1, in which the lowermost leaf has a visible leaf collar; V3, in which the plant has three leaf collars, whose growth purely relies on photosynthesis; V7, in which the plant has seven leaf collars and experiences rapid growth; V10, in which the plant equipped with 10 leaf collars has a rapidly-growing stalk and VT, in which the last branch of the tassel is visible. The R developmental milestones include: R1, in which any silk is visible outside the husk; R2, in which kernels are white and resemble a blister in shape; R3, in which kernels are yellow on the outside with a milky white inner fluid; R4, in which starch is dough-like consistency; R5, in which kernels are dented and R6, in which all kernels on the ear have reached maximum dry weight with physiological maturity (Zhao et al. 2012).

Although, strictly speaking, the reproductive stages begin at floral transition, reproductive growth stages are most often considered as beginning with the emergence of the immature tassel about one week before anthesis and female flowering, defined by silk emergence out of the husks (bracts) that enclose the ear (Fig. 8). The rate of silk elongation inside the husks is crucial to ensure male and female synchronous flowering. Pollen is shed for several days from the main axis of the tassel to the base of the lower branches. It is captured by the silk trichomes, small hair-like outgrowths along the silks. Pollen tubes grow through the silk to enter the ovary. During a first period of 8-10 days after fertilisation (lag-phase) tissue differentiation and cell divisions occur in the embryo and endosperm, without noticeable biomass increase. Grain abortion may occur during this period, and the yield component grain number is therefore determined at the end of it (Borrás & Westgate, 2006). It is followed by the period, called grain filling phase, during which starch and proteins are deposited into the reserve tissues of the grain. This period is characterised by a rate and duration of grain filling, which determine the yield component 'individual grain weight'. The physiological maturity, i.e. the date when the grain has reached it maximum dry weight, occurs around eight weeks (50 to 60 days) after pollination. Grains continue to dry until the harvest.

Conditions around flowering time affect the final number of grains by impacting pollination (anthesis, pollen viability), fertilization (silk growth, silk receptivity) and/or ovary/embryo development (ovary or seed abortion) (Oury *et al.*, 2016; Turc & Tardieu, 2018). Individual grain weight depends on conditions during grain filling. Grain weight has usually a lower impact on grain yield that grain number. Hence, maize has a critical period around flowering time, during which it is subjected to abortion due to drought and heat, expected to worsen with climate change (O'Keeffe, 2009).

### Overview and outline of the thesis

The general objective of this thesis is to develop and evaluate a method for predicting yield of a large number of maize varieties across multiple environment, by using the knowledge accumulated for the response of major traits to environmental conditions. To achieve this goal, we combined statistical genomic prediction models, novel phenomic approaches and a crop growth model 'Sirius Maize' (Fig. 9).

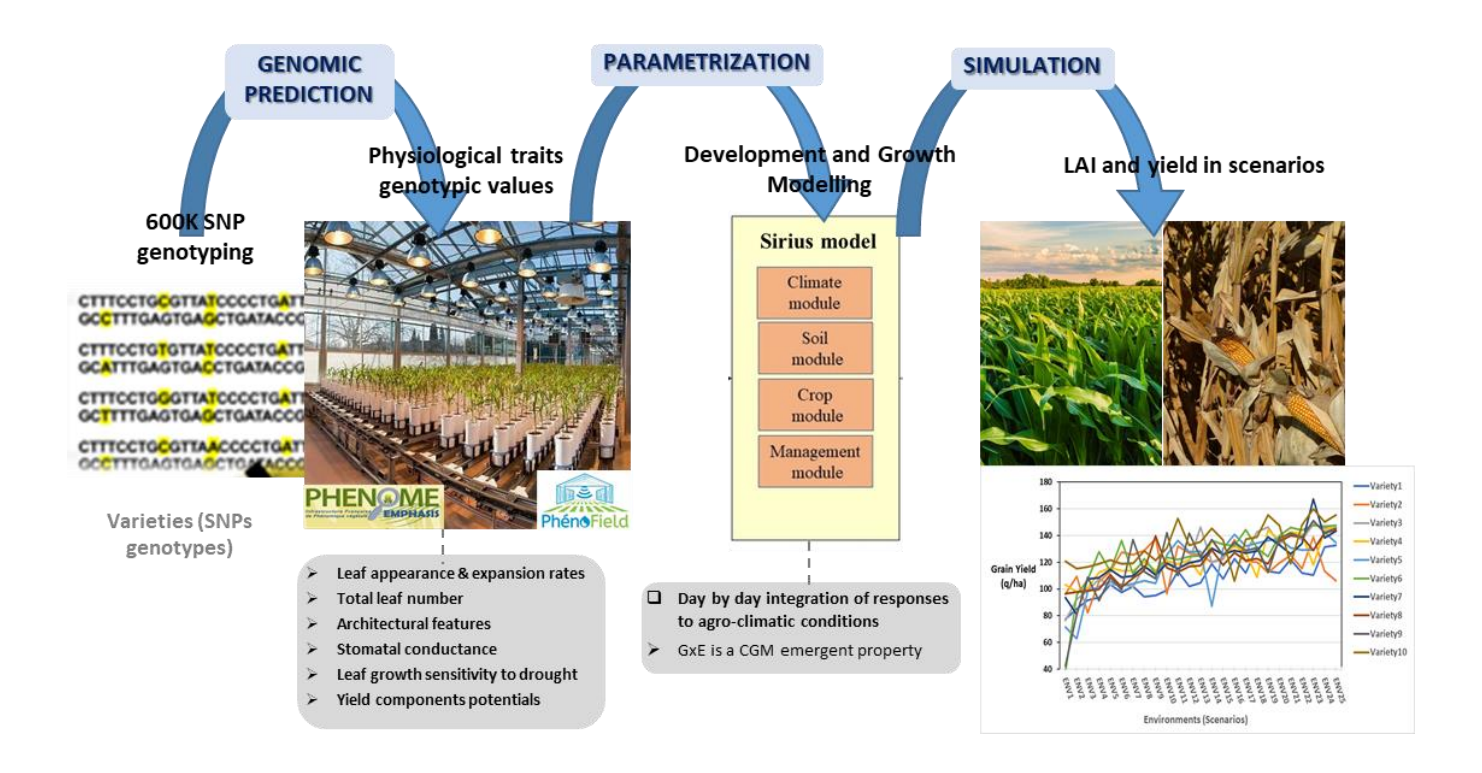


Fig. 9 : Schematic representation of thesis approach combining phenomics, genomic prediction and crop modelling.

This method may result in a new high-throughput tool for simulating performance of hundreds of maize genotypes in hundreds of environments, in the context of either breeding for new varieties or evaluating them for recommendation to farmers. Indeed, this thesis was carried out in partnership with ARVALIS, an applied research organisation for farmers in France, specialised in crops including small grain cereals and maize. Its main mission is to propose effective agronomic solutions in the multiplicity of scenarios. Its includes variety choice and management, along with economic, environmental and sanitary solutions, that are then communicated to farmers, to help them to adapt and face current challenges such as climate change, societal demands and commercial requirements.

The first step in our study is developed in Chapter 1 and published as a research paper in 'Nature Communications', entitled: 'Robotized indoor phenotyping allows genomic prediction of adaptive traits in the field'. Its objective was to analyse traits measured in indoor high-throughput phenotyping platform experiments, which are related to maize development and growth in the field. Three panels of maize hybrids were analysed here (Fig. 10): a 'diversity panel' with 246 hybrids (Millet *et al.*, 2019), a 'genetic progress panel' with a historical series of 56 commercial hybrids (Welcker *et al.*, 2022) and a 'recent hybrids panel' including 86

hybrids marketed from 2008 to 2020 (with most indoor measurements made on 20 contrasting hybrids only, for the latter panel). We showed that genotypic values of traits measured indoor closely correlated with those in the field, either directly or via modelling. We then examined to what extent measurements in indoor platform can serve to train statistical prediction models that estimate genotypic values of traits based on genomic information only.

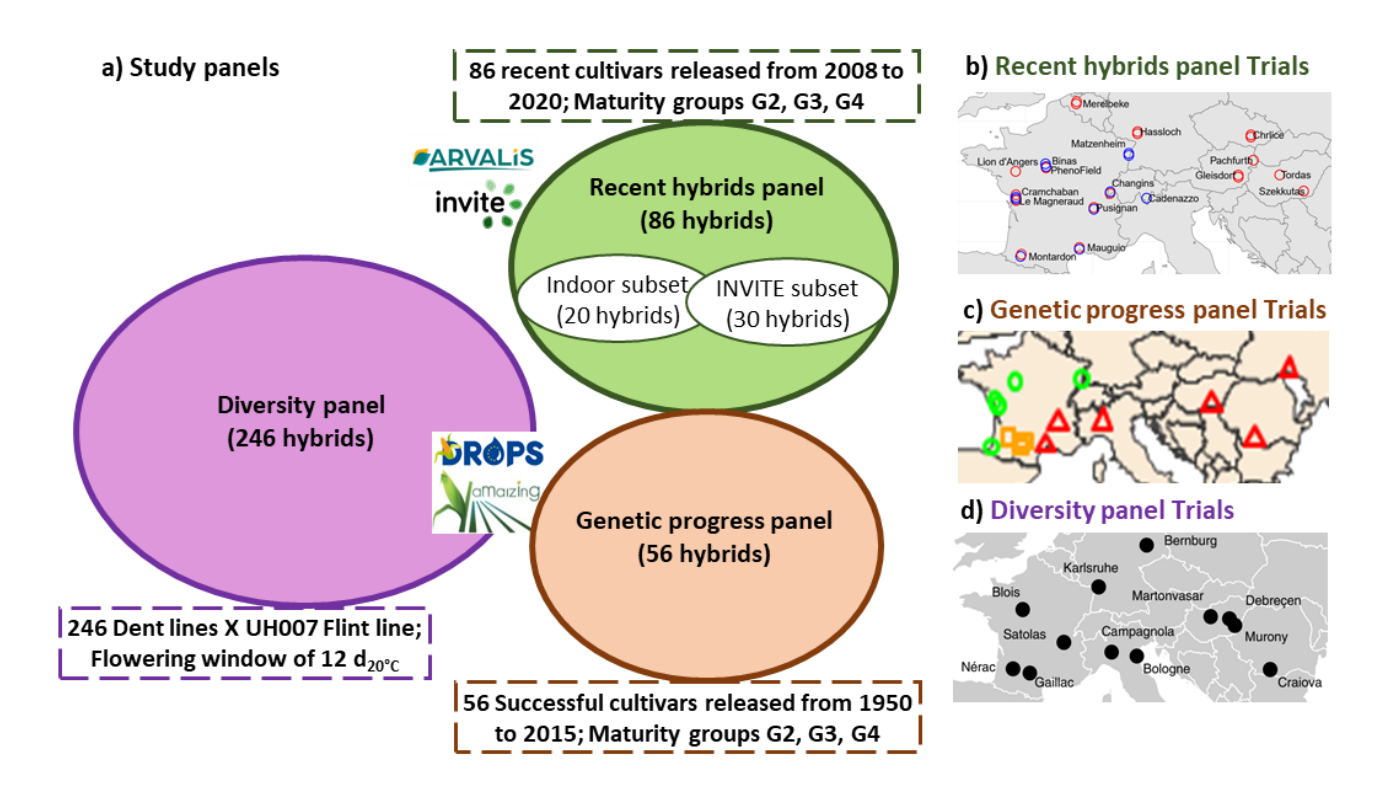


Fig. 10: Diagram of the three studied panels composition (a), and distribution of their field trials networks (b, c & d).

Chapter 2 is entitled: 'Acquisition and analysis of extended field data in contrasting environmental conditions for crop model simulation on a set of recent hybrids'. Its objective was to analyse the dataset collected in a multi-site field experiment for the recent hybrids panel. Indeed, we included here the field data collected in the European project INVITE (https://www.h2020-invite.eu/) on a subset of 30 varieties from the recent hybrids panel. It consisted of 33 experiments, defined as combinations of site x year x watering regime, distributed on a west—east transect for temperature and evaporative demand across Europe in both rainfed and irrigated conditions. We characterized the environmental conditions experienced by plants in each field based on weather and soil water sensors. We estimated environmental indices and scenarios for all experiments. We also calculated a trait that is an

essential genotype-dependent parameter of Sirius Maize model, namely the maximum grain number potential per plant. We also analysed leaf area index in contrasting experiments, which was estimated via drone imaging and inversion of the radiative transfer model 'PROSAIL' (Berger *et al.*, 2018; Blancon *et al.*, 2019). Finally, we estimated genotypic sensitivities of grain number to mean soil water potential and mean daily maximum temperatures during the flowering phase using a linear regression model.

Chapter 3 is entitled: 'Simulating leaf area index and grain number for panels of maize hybrids in contrasting environmental conditions'. Here, we tested the consistency of our approach, which aimed at simulating the performance of hundreds of genotypes in hundreds of environments via combining phenomics, genomic prediction and crop modelling. The specificity of this chapter was to perform simulations based on a crop model whose genotype-dependent parameters originate from traits presented in previous chapters. However, due to time constraints, our study was limited to the first part of maize crop cycle, with running simulations for leaf area index and grain number for tens of varieties in contrasting environmental conditions. We used for that the process-based crop model 'Sirius Maize'.

### References

**Agnolucci P, De Lipsis V. 2020**. Long-run trend in agricultural yield and climatic factors in Europe. *Climatic Change* **159**: 385–405.

Alahmad S, Dinglasan E, Leung KM, Riaz A, Derbal N, Voss-Fels KP, Bassi FM, Christopher J, Hickey LT. 2018. Speed breeding for multiple quantitative traits in durum wheat. *Plant Methods* 14: 36.

**Araus JL, Kefauver SC, Zaman-Allah M, Olsen MS, Cairns JE**. **2018**. Translating High-Throughput Phenotyping into Genetic Gain. *Trends in Plant Science* **23**: 451–466.

**Berger K, Atzberger C, Danner M, D'Urso G, Mauser W, Vuolo F, Hank T. 2018**. Evaluation of the PROSAIL Model Capabilities for Future Hyperspectral Model Environments: A Review Study. *Remote Sensing* **10**: 85.

**Bertin N, Martre P, Génard M, Quilot B, Salon C**. **2010**. Under what circumstances can process-based simulation models link genotype to phenotype for complex traits? Case-study of fruit and grain quality traits. *Journal of Experimental Botany* **61**: 955–967.

Blancon J, Dutartre D, Tixier M-H, Weiss M, Comar A, Praud S, Baret F. 2019. A High-Throughput Model-Assisted Method for Phenotyping Maize Green Leaf Area Index Dynamics Using Unmanned Aerial Vehicle Imagery. *Frontiers in Plant Science* 10.

**Borrás L, Westgate ME**. **2006**. Predicting maize kernel sink capacity early in development. *Field Crops Research* **95**: 223–233.

**Brisson N, Gate P, Gouache D, Charmet G, Oury F-X, Huard F. 2010**. Why are wheat yields stagnating in Europe? A comprehensive data analysis for France. *Field Crops Research* **119**: 201–212.

**Burgueño J, de los Campos G, Weigel K, Crossa J. 2012**. Genomic Prediction of Breeding Values when Modeling Genotype × Environment Interaction using Pedigree and Dense Molecular Markers. *Crop Science* **52**: 707–719.

Bustos-Korts D, Boer MP, Malosetti M, Chapman S, Chenu K, Zheng B, van Eeuwijk FA. 2019. Combining Crop Growth Modeling and Statistical Genetic Modeling to Evaluate Phenotyping Strategies. *Frontiers in Plant Science* 10: 1491.

de los Campos G, Pérez-Rodríguez P, Bogard M, Gouache D, Crossa J. 2020. A data-driven simulation platform to predict cultivars' performances under uncertain weather conditions. *Nature Communications* 11: 4876.

**Casadebaig P, Mestries E, Debaeke P. 2016**. A model-based approach to assist variety evaluation in sunflower crop. *European Journal of Agronomy* **81**: 92–105.

**Challinor AJ, Watson J, Lobell DB, Howden SM, Smith DR, Chhetri N. 2014**. A meta-analysis of crop yield under climate change and adaptation. *Nature Climate Change* **4**: 287–291.

Cooper M, Messina CD, Podlich D, Totir LR, Baumgarten A, Hausmann NJ, Wright D, Graham G. 2014. Predicting the future of plant breeding: complementing empirical evaluation with genetic prediction. *Crop and Pasture Science* 65: 311–336.

**Cooper M, Technow F, Messina C, Gho C, Totir LR**. **2016**. Use of Crop Growth Models with Whole-Genome Prediction: Application to a Maize Multienvironment Trial. *Crop Science* **56**: 2141–2156.

**Costa-Neto G, Fritsche-Neto R, Crossa J. 2021**. Nonlinear kernels, dominance, and envirotyping data increase the accuracy of genome-based prediction in multi-environment trials. *Heredity* **126**: 92–106.

Crossa J, de los Campos G, Maccaferri M, Tuberosa R, Burgueño J, Pérez-Rodríguez P. 2016. Extending the Marker × Environment Interaction Model for Genomic-Enabled Prediction and Genome-Wide Association Analysis in Durum Wheat. *Crop Science* 56: 2193–2209.

Crossa J, Martini JWR, Gianola D, Pérez-Rodríguez P, Jarquin D, Juliana P, Montesinos-López O, Cuevas J. 2019. Deep Kernel and Deep Learning for Genome-Based Prediction of Single Traits in Multienvironment Breeding Trials. *Frontiers in Genetics* 10.

Crossa J, Montesinos-López OA, Pérez-Rodríguez P, Costa-Neto G, Fritsche-Neto R, Ortiz R, Martini JWR, Lillemo M, Montesinos-López A, Jarquin D, et al. 2022. Genome and Environment Based Prediction Models and Methods of Complex Traits Incorporating Genotype x Environment Interaction. In: Ahmadi N, Bartholomé J, eds. Methods in Molecular Biology. Genomic Prediction of Complex Traits: Methods and Protocols. New York, NY: Springer US, 245–283.

Crossa J, Pérez P, Hickey J, Burgueño J, Ornella L, Cerón-Rojas J, Zhang X, Dreisigacker S, Babu R, Li Y, et al. 2014. Genomic prediction in CIMMYT maize and wheat breeding programs. Heredity 112: 48–60.

Cuevas J, Crossa J, Soberanis V, Pérez-Elizalde S, Pérez-Rodríguez P, Campos G de los, Montesinos-López OA, Burgueño J. 2016. Genomic Prediction of Genotype × Environment Interaction Kernel Regression Models. *The Plant Genome* 9: plantgenome2016.03.0024.

Cuevas J, Montesinos-López O, Juliana P, Guzmán C, Pérez-Rodríguez P, González-Bucio J, Burgueño J, Montesinos-López A, Crossa J. 2019. Deep Kernel for Genomic and Near Infrared Predictions in Multi-environment Breeding Trials. *G3 Genes | Genomes | Genetics* 9: 2913–2924.

**Duvick DN**. **2001**. Biotechnology in the 1930s: the development of hybrid maize. *Nature Reviews. Genetics* **2**: 69–74.

**Duvick DN**. **2005**. The Contribution of Breeding to Yield Advances in maize (Zea mays L.). In: Advances in Agronomy. Academic Press, 83–145.

**Endelman JB. 2011.** Ridge Regression and Other Kernels for Genomic Selection with R Package rrBLUP. *The Plant Genome* **4**.

**Erenstein O, Jaleta M, Sonder K, Mottaleb K, Prasanna BM. 2022.** Global maize production, consumption and trade: trends and R&D implications. *Food Security* **14**: 1295–1319.

Falconer DS, Mackay TFC. 1996. Introduction to Quantitative Genetics. Pearson Education.

**Fu D, Xiao M, Hayward A, Fu Y, Liu G, Jiang G, Zhang H. 2014**. Utilization of crop heterosis: a review. *Euphytica* **197**: 161–173.

**Gianola D, van Kaam JBCHM**. **2008**. Reproducing Kernel Hilbert Spaces Regression Methods for Genomic Assisted Prediction of Quantitative Traits. *Genetics* **178**: 2289–2303.

**Granier C, Vile D. 2014**. Phenotyping and beyond: modelling the relationships between traits. *Current Opinion in Plant Biology* **18**: 96–102.

**Grassini P, Eskridge KM, Cassman KG. 2013**. Distinguishing between yield advances and yield plateaus in historical crop production trends. *Nature Communications* **4**: 2918.

**Guo J, Pradhan S, Shahi D, Khan J, Mcbreen J, Bai G, Murphy JP, Babar MA**. **2020**. Increased Prediction Accuracy Using Combined Genomic Information and Physiological Traits in A Soft Wheat Panel Evaluated in Multi-Environments. *Scientific Reports* **10**: 7023.

Hammer G, Cooper M, Tardieu F, Welch S, Walsh B, van Eeuwijk F, Chapman S, Podlich D. 2006. Models for navigating biological complexity in breeding improved crop plants. *Trends in Plant Science* 11: 587–593.

Hammer GL, van Oosterom E, McLean G, Chapman SC, Broad I, Harland P, Muchow RC. 2010. Adapting APSIM to model the physiology and genetics of complex adaptive traits in field crops. *Journal of Experimental Botany* **61**: 2185–2202.

**Heslot N, Akdemir D, Sorrells ME, Jannink J-L. 2014**. Integrating environmental covariates and crop modeling into the genomic selection framework to predict genotype by environment interactions. *Theoretical and Applied Genetics* **127**: 463–480.

Hickey JM, Dreisigacker S, Crossa J, Hearne S, Babu R, Prasanna BM, Grondona M, Zambelli A, Windhausen VS, Mathews K, et al. 2014. Evaluation of genomic selection training population designs and genotyping strategies in plant breeding programs using simulation. *Crop science* 54: 1476–1488.

**Hoogenboom G, White JW, Messina CD**. **2004**. From genome to crop: integration through simulation modeling. *Field Crops Research* **90**: 145–163.

Horie T, Yajima M, Nakagawa H. 1992. Yield forecasting. Agricultural Systems 40: 211–236.

Houle D, et al. 2010. Phenomics: the next challenge. Nature Reviews. Genetics 11: 855-866.

Jarquín D, Crossa J, Lacaze X, Du Cheyron P, Daucourt J, Lorgeou J, Piraux F, Guerreiro L, Pérez P, Calus M, et al. 2014. A reaction norm model for genomic selection using high-dimensional genomic and environmental data. *Theoretical and Applied Genetics* 127: 595–607.

**Jighly A, Thayalakumaran T, O'Leary GJ, Kant S, Panozzo J, Aggarwal R, Hessel D, Forrest KL, Technow F, Tibbits JFG, et al. 2023**. Using genomic prediction with crop growth models enables the prediction of associated traits in wheat. *Journal of Experimental Botany* **74**: 1389–1402.

Jones JW, Tsuji GY, Hoogenboom G, Hunt LA, Thornton PK, Wilkens PW, Imamura DT, Bowen WT, Singh U. 1998. Decision support system for agrotechnology transfer: DSSAT v3. In: Tsuji GY, Hoogenboom G, Thornton PK, eds. Systems Approaches for Sustainable Agricultural Development. Understanding Options for Agricultural Production. Dordrecht: Springer Netherlands, 157–177.

**Kaler AS, Purcell LC, Beissinger T, Gillman JD. 2022.** Genomic prediction models for traits differing in heritability for soybean, rice, and maize. *BMC Plant Biology* **22**: 87.

Lacube S, Manceau L, Welcker C, Millet EJ, Gouesnard B, Palaffre C, Ribaut J-M, Hammer G, Parent B, Tardieu F. 2020. Simulating the effect of flowering time on maize individual leaf area in contrasting environmental scenarios. *Journal of Experimental Botany* 71: 5577–5588.

**Li D, Quan C, Song Z, Li X, Yu G, Li C, Muhammad A**. **2021**. High-Throughput Plant Phenotyping Platform (HT3P) as a Novel Tool for Estimating Agronomic Traits From the Lab to the Field. *Frontiers in Bioengineering and Biotechnology* **8**.

**Lobell DB, Gourdji SM. 2012**. The Influence of Climate Change on Global Crop Productivity. *Plant Physiology* **160**: 1686–1697.

**Lobell DB, Schlenker W, Costa-Roberts J. 2011**. Climate Trends and Global Crop Production Since 1980. *Science* **333**: 616–620.

Lopez-Cruz M, Olson E, Rovere G, Crossa J, Dreisigacker S, Mondal S, Singh R, Campos GDL. 2020. Regularized selection indices for breeding value prediction using hyper-spectral image data. *Scientific Reports* 10: 8195.

**Lorgeou J, Audigeos D, Martin B. 2019**. Progrès génétique de 1986 à 2017 : les apports du renouvellement des variétés. *Perspectives Agricoles*.

**Lorgeou J, Piraux F, Charcosset A, et al. 2009**. Conséquences de l'évolution des conditions climatiques des 20 dernières années sur la production de maïs grain et stratégies d'adaptation. *Colloque 'Changement climatique : conséquences et enseignements pour les grandes cultures et l'élevage'*.

Ly D, Chenu K, Gauffreteau A, Rincent R, Huet S, Gouache D, Martre P, Bordes J, Charmet G. 2017. Nitrogen nutrition index predicted by a crop model improves the genomic prediction of grain number for a bread wheat core collection. *Field Crops Research* 214: 331–340.

Ly D, Huet S, Gauffreteau A, Rincent R, Touzy G, Mini A, Jannink J-L, Cormier F, Paux E, Lafarge S, *et al.* 2018. Whole-genome prediction of reaction norms to environmental stress in bread wheat (Triticum aestivum L.) by genomic random regression. *Field Crops Research* 216: 32–41.

**Malosetti M, Ribaut J-M, van Eeuwijk FA**. **2013**. The statistical analysis of multi-environment data: modeling genotype-by-environment interaction and its genetic basis. *Frontiers in Physiology* **4**.

Måløy H, Windju S, Bergersen S, Alsheikh M, Downing KL. 2021. Multimodal performers for genomic selection and crop yield prediction. *Smart Agricultural Technology* 1: 100017.

McCown RL, Hammer GL, Hargreaves JNG, Holzworth DP, Freebairn DM. 1996. APSIM: a novel software system for model development, model testing and simulation in agricultural systems research. *Agricultural Systems* 50: 255–271.

Messina CD, Technow F, Tang T, Totir R, Gho C, Cooper M. 2018. Leveraging biological insight and environmental variation to improve phenotypic prediction: Integrating crop growth models (CGM) with whole genome prediction (WGP). *European Journal of Agronomy* 100: 151–162.

**Meuwissen Theo**. **2007**. Genomic selection: marker assisted selection on a genome wide scale. *Journal of Animal Breeding and Genetics* **124**: 321–322.

**Meuwissen TH, Hayes BJ, Goddard ME. 2001**. Prediction of total genetic value using genome-wide dense marker maps. *Genetics* **157**: 1819–1829.

Millet EJ, Kruijer W, Coupel-Ledru A, Alvarez Prado S, Cabrera-Bosquet L, Lacube S, Charcosset A, Welcker C, van Eeuwijk F, Tardieu F. 2019. Genomic prediction of maize yield across European environmental conditions. *Nature Genetics* 51: 952–956.

Montesinos López OA, Montesinos López A, Crossa J. 2022. Bayesian Genomic Linear Regression. In: Multivariate Statistical Machine Learning Methods for Genomic Prediction. Springer International Publishing, 171–208.

Montesinos-López A, Montesinos-López OA, Gianola D, Crossa J, Hernández-Suárez CM. 2018. Multienvironment Genomic Prediction of Plant Traits Using Deep Learners With Dense Architecture. *G3 Genes | Genomes | Genetics* 8: 3813–3828.

**Moore FC, Lobell DB**. **2015**. The fingerprint of climate trends on European crop yields. *Proceedings of the National Academy of Sciences* **112**: 2670–2675.

**Muchow RC, Sinclair TR, Bennett JM. 1990**. Temperature and Solar Radiation Effects on Potential Maize Yield across Locations. *Agronomy Journal* **82**: 338–343.

**Muller B, Martre P. 2019.** Plant and crop simulation models: powerful tools to link physiology, genetics, and phenomics. *Journal of Experimental Botany* **70**: 2339–2344.

O'Keeffe K. 2009. Maize growth & development. Orange, N.S.W.: NSW Dept. of Primary Industries.

**Onogi A. 2022.** Integration of Crop Growth Models and Genomic PredictionGenomic predictions (GP). In: Ahmadi N, Bartholomé J, eds. Methods in Molecular Biology. Genomic Prediction of Complex Traits: Methods and Protocols. New York, NY: Springer US, 359–396.

**Onogi A, Watanabe M, Mochizuki T, Hayashi T, Nakagawa H, Hasegawa T, Iwata H**. **2016**. Toward integration of genomic selection with crop modelling: the development of an integrated approach to predicting rice heading dates. *TAG. Theoretical and applied genetics. Theoretische und angewandte Genetik* **129**: 805–817.

**Oury V, Tardieu F, Turc O**. **2016**. Ovary Apical Abortion under Water Deficit Is Caused by Changes in Sequential Development of Ovaries and in Silk Growth Rate in Maize. *Plant Physiology* **171**: 986–996.

**Peltonen-Sainio P, Jauhiainen L, Laurila IP. 2009**. Cereal yield trends in northern European conditions: Changes in yield potential and its realisation. *Field Crops Research* **110**: 85–90.

Poorter H, Fiorani F, Pieruschka R, Wojciechowski T, van der Putten WH, Kleyer M, Schurr U, Postma J. 2016. Pampered inside, pestered outside? Differences and similarities between plants growing in controlled conditions and in the field. *New Phytologist* 212: 838–855.

**Poorter H, Fiorani F, Stitt M, Schurr U, Finck A, Gibon Y, Usadel BR, Munns R, Atkin OK, Tardieu FO,** *et al.* **2012**. The art of growing plants for experimental purposes: a practical guide for the plant biologist. *Functional plant biology: FPB* **39**: 821–838.

**Ray DK, Gerber JS, MacDonald GK, West PC. 2015**. Climate variation explains a third of global crop yield variability. *Nature Communications* **6**: 5989.

Ray DK, Ramankutty N, Mueller ND, West PC, Foley JA. 2012. Recent patterns of crop yield growth and stagnation. *Nature Communications* 3: 1293.

Rincent R, Malosetti M, Ababaei B, Touzy G, Mini A, Bogard M, Martre P, Le Gouis J, van Eeuwijk F. 2019. Using crop growth model stress covariates and AMMI decomposition to better predict genotype-by-environment interactions. *Theoretical and Applied Genetics* 132: 3399–3411.

**Robert P, Le Gouis J, The BreedWheat Consortium, Rincent R. 2020**. Combining Crop Growth Modeling With Trait-Assisted Prediction Improved the Prediction of Genotype by Environment Interactions. *Frontiers in Plant Science* **11**.

Rutkoski J, Poland J, Mondal S, Autrique E, Pérez LG, Crossa J, Reynolds M, Singh R. 2016. Canopy Temperature and Vegetation Indices from High-Throughput Phenotyping Improve Accuracy of Pedigree and Genomic Selection for Grain Yield in Wheat. *G3 Genes | Genomes | Genetics* 6: 2799–2808.

**Sandhu KS, Patil SS, Aoun M, Carter AH**. **2022**. Multi-Trait Multi-Environment Genomic Prediction for End-Use Quality Traits in Winter Wheat. *Frontiers in Genetics* **13**.

Schauberger B, Ben-Ari T, Makowski D, Kato T, Kato H, Ciais P. 2018. Yield trends, variability and stagnation analysis of major crops in France over more than a century. *Scientific Reports* 8: 16865.

Schulz-Streeck T, Ogutu JO, Gordillo A, Karaman Z, Knaak C, Piepho H-P. 2013. Genomic selection allowing for marker-by-environment interaction. *Plant Breeding* 132: 532–538.

Shi S, Li X, Fang L, Liu A, Su G, Zhang Y, Luobu B, Ding X, Zhang S. 2021. Genomic Prediction Using Bayesian Regression Models With Global–Local Prior. *Frontiers in Genetics* 12: 628205.

**Tardieu F, Cabrera-Bosquet L, Pridmore T, Bennett M**. **2017**. Plant Phenomics, From Sensors to Knowledge. *Current Biology* **27**: R770–R783.

**Tayeh N, Klein A, Le Paslier M-C, Jacquin F, Houtin H, Rond C, et al. 2015**. Genomic Prediction in Pea: Effect of Marker Density and Training Population Size and Composition on Prediction Accuracy. *Frontiers in Plant Science* **6**.

**Tester M, Langridge P. 2010**. Breeding technologies to increase crop production in a changing world. *Science (New York, N.Y.)* **327**: 818–822.

Toda Y, Wakatsuki H, Aoike T, Kajiya-Kanegae H, Yamasaki M, Yoshioka T, Ebana K, et al. 2020. Predicting biomass of rice with intermediate traits: Modeling method combining crop growth models and genomic prediction models. *PLOS ONE* **15**: e0233951.

**Turc O, Tardieu F. 2018**. Drought affects abortion of reproductive organs by exacerbating developmentally driven processes via expansive growth and hydraulics. *Journal of Experimental Botany* **69**: 3245–3254.

**VanRaden PM**. **2008**. Efficient Methods to Compute Genomic Predictions. *Journal of Dairy Science* **91**: 4414–4423.

Wang K, Abid MA, Rasheed A, Crossa J, Hearne S, Li H. 2023. DNNGP, a deep neural network-based method for genomic prediction using multi-omics data in plants. *Molecular Plant* 16: 279–293.

Wang T, Chen Y-PP, Goddard ME, Meuwissen TH, Kemper KE, Hayes BJ. 2015. A computationally efficient algorithm for genomic prediction using a Bayesian model. *Genetics Selection Evolution* 47: 34.

Wang J, Zhou Z, Zhang Z, Li H, Liu D, Zhang Q, Bradbury PJ, Buckler ES, Zhang Z. 2018. Expanding the BLUP alphabet for genomic prediction adaptable to the genetic architectures of complex traits. *Heredity* 121: 648–662.

Webber H, Ewert F, Olesen JE, Müller C, Fronzek S, Ruane AC, Bourgault M, Martre P, Ababaei B, Bindi M, et al. 2018. Diverging importance of drought stress for maize and winter wheat in Europe. *Nature Communications* 9: 4249.

Welcker C, Spencer NA, Turc O, Granato I, Chapuis R, Madur D, Beauchene K, Gouesnard B, Draye X, Palaffre C, et al. 2022. Physiological adaptive traits are a potential allele reservoir for maize genetic progress under challenging conditions. *Nature Communications* 13: 3225.

Whittaker JC, Thompson R, Denham MC. 2000. Marker-assisted selection using ridge regression. *Genetical Research* **75**: 249–252.

**Xu Y. 2016**. Envirotyping for deciphering environmental impacts on crop plants. *TAG. Theoretical and applied genetics. Theoretische und angewandte Genetik* **129**: 653–673.

Yang W, Feng H, Zhang X, Zhang J, Doonan JH, Batchelor WD, Xiong L, Yan J. 2020. Crop Phenomics and High-Throughput Phenotyping: Past Decades, Current Challenges, and Future Perspectives. *Molecular Plant* 13: 187–214.

**Zhao X, Tong C, Pang X, Wang Z, Guo Y, Du F, Wu R. 2012**. Functional mapping of ontogeny in flowering plants. *Briefings in Bioinformatics* **13**: 317–328.

## CHAPTER 1: ROBOTIZED INDOOR PHENOTYPING ALLOWS GENOMIC PREDICTION OF ADAPTIVE TRAITS IN THE FIELD

#### **TABLE OF CONTENTS**

Introduction27
Results30
Traits measured indoor correlated with those in the field, depending on categories
of traits30
The differences in absolute values of traits between indoor and fields were
accounted for by environmental conditions32
Measurements in indoor platforms can be used for genomic prediction of
traits32
Discussion33
Methods35
Genetic material35
Platform experiments35
Field experiments36
Correlation analysis between experiments36
Genotypic data and diversity analyses37
Genomic prediction models37
Training and validation schemes of genomic predictions37
References38
Acknowledgements40
Supplementary information 41

#### nature communications



**Article** 

https://doi.org/10.1038/s41467-023-42298-z

## Robotized indoor phenotyping allows genomic prediction of adaptive traits in the field

Received: 30 April 2023

Accepted: 6 October 2023

Published online: 19 October 2023

Check for updates

Jugurta Bouidghaghen <sup>1,2</sup>, Laurence Moreau<sup>3</sup>, Katia Beauchêne<sup>4</sup>, Romain Chapuis<sup>5</sup>, Nathalie Mangel<sup>6</sup>, Llorenç Cabrera-Bosquet<sup>1</sup>, Claude Welcker <sup>1</sup>, Matthieu Bogard <sup>2</sup> & François Tardieu <sup>1</sup>

Breeding for resilience to climate change requires considering adaptive traits such as plant architecture, stomatal conductance and growth, beyond the current selection for yield. Robotized indoor phenotyping allows measuring such traits at high throughput for speed breeding, but is often considered as non-relevant for field conditions. Here, we show that maize adaptive traits can be inferred in different fields, based on genotypic values obtained indoor and on environmental conditions in each considered field. The modelling of environmental effects allows translation from indoor to fields, but also from one field to another field. Furthermore, genotypic values of considered traits match between indoor and field conditions. Genomic prediction results in adequate ranking of genotypes for the tested traits, although with lesser precision for elite varieties presenting reduced phenotypic variability. Hence, it distinguishes genotypes with high or low values for adaptive traits, conferring either spender or conservative strategies for water use under future climates.

Breeding for the improvement of crop resilience is increasingly necessary for the sustainability of cropping systems and for food security in the context of climate change and growing population<sup>1,2</sup>. Most current breeding schemes are based on yield measurement of thousands of genotypes grown under diverse environmental scenarios, assisted by genomic selection that allows yield prediction for many thousands of untested genotypes based on their genomic information<sup>3,4</sup>. In this approach, the measurement of other traits is most often limited to crop cycle duration, which defines the growing areas in which resulting genotypes can be grown, and to traits that may jeopardize the commercialization of selected candidates, such as resistance to diseases or quality performance (e.g. oil content or protein content in rape seed and wheat, respectively)<sup>5</sup>. However, in the context of climate change, other traits that affect

light interception, plant development, transpiration and growth are important for predicting, via statistical or crop models, the suitability of genotypes to future environmental conditions<sup>6-8</sup>. Furthermore, a recent analysis of maize genetic progress suggests that physiological traits involved in plant response to heat and drought, such as leaf growth rate or stomatal conductance, have not been improved over the last 60 years of maize selection<sup>9</sup>. Yield was improved via other traits such as the fine-tuning of phenology and the constitutive increase of grain number, but physiological adaptive traits are still a potential reservoir of interesting alleles for climate change<sup>9</sup>.

The progress of high-throughput phenotyping now allows one to measure physiological traits for hundreds of genotypes. Robotized indoor phenotyping platforms allow estimation, with typical

time definitions of some minutes to one day, of traits that underlie the genetic variability of leaf area and their responses to environmental conditions, e.g. leaf expansion rate, leaf width, phyllochron and leaf number<sup>10-13</sup>. They also allow estimation of traits controlling transpiration, e.g. stomatal conductance<sup>14</sup> and those controlling plant architecture, e.g. the vertical distribution of leaf area and the azimuthal distribution of leaves along the stem, with good heritability<sup>15</sup>. Then, light interception, transpiration, and radiation use efficiency can be simulated in virtual field canopies, which reproduce 3D plants characterized in the indoor platform<sup>15-17</sup>. Field phenotyping also allows measuring leaf area at several dates, for hundreds of genotypes in different fields characterized by measured environmental conditions<sup>18-20</sup>. This can result in the estimation of intercepted light in the same fields and, via model inversion, of leaf area and plant architecture<sup>21-23</sup>.

However, the use in breeding of these physiological and growth-related traits faces the difficulty of their high sensitivity to environmental conditions, resulting in large genotype x environment interactions<sup>24–27</sup>. This difficulty is not limited to the extrapolation of trait values from indoor to field conditions: most of these traits also largely vary between fields depending on environmental conditions, making difficult the prediction of traits in one field from those measured in another field<sup>24,28,29</sup>. The relationship between these traits and yield is also highly depending on environmental scenarios<sup>30,31</sup>. Consequently, physiological adaptive traits have not been considered per se in breeding programs<sup>9,32</sup>.

The recent development of speed breeding in controlled conditions may offer new opportunities for selection strategies involving plant traits. Speed breeding reduces the duration of each generation by setting environmental conditions favouring rapid

development, thereby allowing up to eight generations of selection per year<sup>33,34</sup>. Yield and agronomic traits like disease resistance are predicted based on genomic information at each generation, while a full phenotyping of the most promising genotypes is carried out in the field after some generations<sup>35</sup>. However, this approach also potentially includes, in breeding schemes, other traits measured indoor for training a prediction model used in genomic selection, and phenotyped for selected candidates after a few generations. For instance, in wheat, Watson et al.36 performed speed breeding involving the length of flag leaves and ear length, in addition to yield. Conditions for the use of speed breeding in our case are that physiological adaptive traits translate from indoor conditions to the field, and are accurate enough to make it feasible to implement rapid cycling based on indoor phenotyping and genomic prediction. Three panels of maize hybrids were used to test these conditions (Table 1, Supplementary Table 1): a 'diversity panel' with 246 hybrids<sup>31</sup>, a 'genetic progress panel' with a historical series of 56 commercial hybrids<sup>9</sup> and a 'recent hybrids panel' with 86 commercial hybrids marketed from 2008 to 2020 (most indoor measurements on 20 contrasting hybrids, Supplementary Data 1 and Supplementary Table 2).

In this work, we first show that genotypic values of traits measured indoor closely correlate with those in the field, either directly or via modeling (Table 2). We then show that, although absolute trait values differ if measured indoor or in the field, they still follow common trends in response to environmental conditions, and can be inferred by using an ecophysiological model. Finally, we examine to what extent measurements in indoor platforms can serve to train statistical prediction models that estimate genotypic values of traits based on genomic information only (Table 2).

Table 1 | Summary of variance components and genomic heritability of considered traits

Trait	Unit	Panel	# Hyb	# Rep	Mean value	h <sub>g</sub> <sup>2</sup>	$\sigma_{\!g}^{\;2}$	$\sigma_a^{\ 2}$	$\sigma_{\sf d}^{\;2}$	$\sigma_{\rm e}^{\ 2}$
Leaf appearance rate (LAR)	Leaf/ day <sub>20°C</sub>	Diversity panel	246	11	0.251	0.63	1.4E-04	1.1E-04	3.4E-05	8.1E-05
		Genetic pro- gress panel	56	7	0.265	0.63	1.7E-04	9.2E-05	7.4E-05	9.9E-05
		Recent hybrids panel	50	3	0.262	0.56	4.8E-05	2.5E-05	2.3E-05	3.7E-05
Vegetative phase duration	Days <sub>20 °C</sub>	Diversity panel	246	12	68.22	0.82	4.25	3.66	0.59	0.95
		Genetic pro- gress panel	56	7	63.34	0.71	7.39	5.20	2.19	3.05
		Recent hybrids panel	60	9	65.02	0.68	2.11	1.24	0.86	0.99
rh <sub>PAD</sub> (relative height at 50% of	Unitless	Diversity panel	246	11	0.308	0.74	7.8E-04	6.3E-04	1.4E-04	2.7E-04
leaf area)		Genetic pro- gress panel	56	7	0.279	0.69	1.5E-03	9.9E-04	4.9E-04	6.8E-04
		Recent hybrids panel	20	3	0.360	0.54	1.1E-03	5.3E-04	5.2E-04	9.1E-04
Stomatal conductance (gs <sub>max</sub> )	mmol/m²/s	Diversity panel	246	11	108.4	0.48	57.2	38.4	18.8	61.2
		Genetic pro- gress panel	56	7	119.8	0.53	61.77	31.35	30.42	54.02
		Recent hybrids panel	-	-	-	-	-	-	-	-
Leaf expansion rate (LER)	cm²/day <sub>20 ℃</sub>	Diversity panel	246	11	134.6	0.61	107.6	76.2	31.3	69.0
		Genetic pro- gress panel	56	7	163.9	0.62	343.8	215.0	128.8	211.5
		Recent hybrids panel	20	3	146.9	0.54	221.6	110.0	111.5	185.5
Leaf area index (LAI)	Unitless	Diversity panel	-	-	-	-	-	-	-	-
		Genetic pro- gress panel	56	7	3.65	0.66	0.23	0.15	0.08	0.13
		Recent hybrids panel	-	-	-	-	-	-	-	-

#Hyb, number of hybrids; for the recent hybrids panel, it is defined by the number of hybrids in the considered fields or in the indoor experiment. #Rep, number of independent values calculated for the considered trait.  $h_g^2$ , genomic heritability (narrow-sense, see Methods),  $\sigma_g^2$ , total genetic variance.  $\sigma_a^2$  and  $\sigma_d^2$ , variances explained by additive and dominance relationship matrices<sup>72</sup>, respectively.  $\sigma_e^2$ , residual variance. For estimations per experiment, see Supplementary Table 3.

Table 2 | Summary of correlation and genomic prediction results for each trait

	Method	Method field <sup>b</sup>	Experiment #		Observed genotypic value	c value		Genomic prediction (genotypic means over experiments)	genotypic means	over experime	nts)	
	indoor <sup>a</sup>		ì	2						-		
			5	r (BLUEs correlation) <sup>e</sup>		$r_{ m g}$ (genetic correlation) <sup>d</sup>	Eff	# r (cross- Hyb validation) <sup>f</sup>	Acc (cross- validation) <sup>9</sup>	# $r$ (external Hyb validation) <sup>h</sup>		Acc (external validation)
Leaf appearance rate (LAR)	Time course	Time course	Indoor 2 VS 44 Field 6	4 0.73±0.07		0.69±0.08	0.70±0.08	302 0.58±0.09	0.74±0.06	50 0.53±0.10		0.71±0.08
			Indoor 1 VS 21 Field 3	0.57±0.16		0.43±0.19	0.45±0.19	ı				
			Field 5 VS Field 6 44	4 0.71±0.08		0.65 ± 0.09	0.67±0.09	I				
			Field 1 VS Field 3 26	5 0.49±0.16		0.41 ± 0.17	0.41±0.17	ı				
Vegetative phase	Irrelevant	Recorded	Field 5 VS Field 6 44	4 0.88±0.04		0.77 ± 0.06	0.76 ± 0.07	302 0.84±0.04	0.93±0.02	60 0.71±0.07		0.86 ± 0.04
duration			Field 1 VS Field 3 53	3 0.69 ± 0.07		0.60 ± 0.09	0.62±0.09	ı				
			Field 2 VS Field 3 55	5 0.47±0.11		0.40±0.12	0.41±0.12	ı				
Architecture (rh <sub>PAD</sub> / ALA)	3D imaging	UAV imaging	Indoor 2 VS 56 Field 5	S 0.77±0.06		0.66±0.08	0.66±0.08	302 0.65±0.08	0.75±0.06	20 0.42±0.20		0.57 ± 0.16
			Indoor 1 VS 18 Field 4	0.58±0.17		0.45±0.20	0.44±0.21					
			Indoor 1 VS 18 Field 2	0.60±0.17		0.50 ± 0.19	0.49±0.20	ı				
			Field 4 VS Field 2 18	0.50 ± 0.19		0.41±0.21	$0.41 \pm 0.21$	ı				
Stomatal conductance (gs <sub>max</sub> )	Model inversion	Not measurable at HTP	Indoor –	. 1	1		1	302 0.56±0.09	0.81±0.05	. 1	. 1	
Leaf expansion rate (LER)	Time course		Indoor –	1	-		1	302 0.76±0.06	0.92±0.02	20 0.34±0.21		0.46 ± 0.19
Leaf area index (LAI) Modeling	Modeling	UAV imaging	Indoor 2 VS 51 Field 5_WW	0.64±0.09		0.55±0.10	0.53 ± 0.10	1	I	1	-	
			Indoor 2 VS 51 Field 5_WD	0.44±0.11		0.38±0.12	0.37 ± 0.12	1	1	1	-	

\*\*Method for trait measurement indoor and in field, respectively. HTP, high-throughput phenotyping. \*Correlation between genotypic values (BLUEs) for each couple of experiments. \*Genetic correlation between experiments and trait genomic heritability in model.\*\* \*2.\* \*Efficiency of indirect selection, (case of an indirect phenotypic selection based on trait observed values in a given experiment, indoor or in a field), calculated as the accuracy of indirect selection, divided by the square root of trait genomic heritability in the target field experiment.\*\* \*Correlation between G-BLUP predicted values and measured values in a cross-validation scheme with diversity and genetic progress panels. \*Prediction accuracy of genomic selection, calculated as in 'divided by the square root of trait genomic heritability. \*3. External validation: Correlation between G-BLUP predicted values (with training on diversity and genetic progress panels) and measured values in recent hybrids panel. Prediction accuracy, calculated as in "divided by the square root of trait genomic heritability,\*3. Standard error (SE) estimates?" are shown after the ± symbol. For details, see Supplementary Tables 4 and 5.

#### Results

## Traits measured indoor correlated with those in the field, depending on categories of traits

A genetic approach based on indoor trait measurements requires that the latter are genetically correlated to measurements of the same traits in the field. However, such comparison is not always possible, because robotized indoor phenotyping can measure traits that would be impossible, or very tedious, to measure in the field, such as stomatal conductance or the 3D leaf distribution on the plant stem. Conversely, some traits measured indoor are largely irrelevant to the field, in particular those performed on whole canopies. Hence, comparisons of the genetic variability of trait values obtained indoor and in the field face different levels of difficulty depending on traits. We focused our study on traits that are heritable and have a direct impact on biomass accumulation (Table 1 and Supplementary Table 3). They present contrasting 'phenotypic distances' between indoor and field measurements, thereby causing different degrees of complexity.

Leaf appearance rate (LAR) represents the simplest case, as it is measured with the same protocol indoor and in the field. Its genomic heritability was 0.63 in the diversity and genetic progress panels (Table 1). In the 'recent hybrid panel' (Fig. 1 and Supplementary Tables 2 and 4), correlations between genotypic values indoor and in the field (Fig. 1a and Table 2) were measured either via correlations between BLUEs estimated values or via genetic correlations assessed with a multivariate mixed model<sup>38,39</sup>. As expected<sup>40</sup>, genetic correlations were lower than correlations between BLUEs, but were still

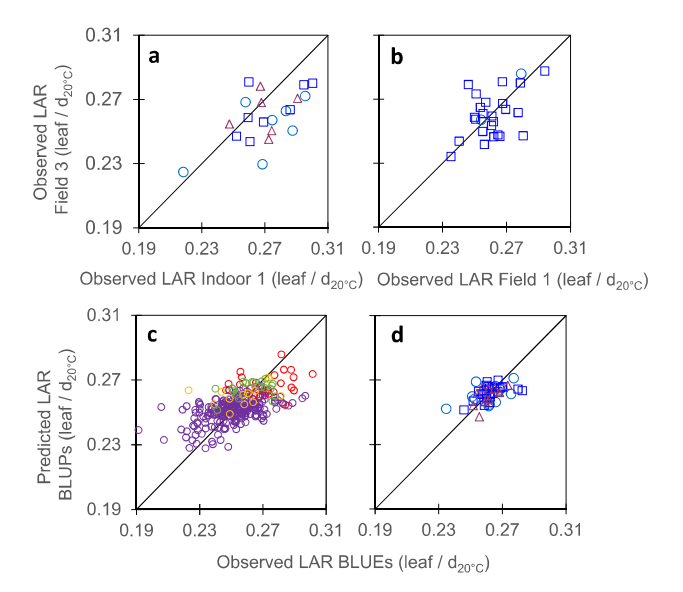


Fig. 1 | Leaf appearance rate (LAR) translated from platform to field, and could be inferred via genomic prediction. a Correlations between genotypic values measured indoor and in a field. b Correlations between one field and another field were similar to those between indoor and a field. c Comparison of observed mean genotypic values and mean predicted values (G-BLUPs) in a 5-fold cross-validation scheme with 10 iterations. d Comparison of observed mean genotypic values and predicted values in the independent dataset, with observed values originating from data of a, b (BLUEs) and G-BLUP model calibration made using dataset of c. In a, b and d light blue circles, mid-early hybrids (G2), dark blue squares, intermediate hybrids (G3), red triangles, mid-late hybrids (G4). In c, purple empty circles, diversity panel; red and yellow empty circles, genetic progress panel, hybrids released before 1980 and 2000, respectively; green empty circles, hybrids released after 2000. In **a**, r = 0.57 (95% CI = 0.19-0.81), n = 21, df = 19, p-value = 0.007,  $CV_{RMSE} = 7.7\%$ . In **b**, r = 0.49 (95% CI = 0.12–0.74), n = 26, df = 24, p-value = 0.011,  $CV_{RMSE} = 5.3\%$ , In **c**, r = 0.58 (95% CI = 0.50–0.65), n = 302, df = 299, p-value < 2.2E-16,  $CV_{RMSE} = 5.2\%$ . In **d**, r = 0.53 (95% CI = 0.30 - 0.71), n = 50, df = 48, p-value = 6.3E-05, CV<sub>RMSE</sub> = 2.8%. Significance of the correlation coefficients was tested using twosided t-test. For spearman correlation of ranks (rho) and other statistics, see Supplementary Tables 4 and 5. Source data are provided as a Source Data file.

significant (p-value < 0.02). In both cases (Table 2), they were slightly higher than those between one field and another field (Fig. 1b; r= 0.57, n= 21, p-value = 0.007 and r= 0.49, n= 26, p-value = 0.011, respectively, for correlations between BLUEs). The latter are considered here as a benchmark for evaluating the quality of translation from indoor to field experiments. Importantly, the ranking of hybrids and their distribution in highest and lowest quartiles were essentially conserved between indoor and field conditions, a necessary condition for breeding (Supplementary Table 4). Furthermore, these correlations and rankings were similar to those between fields for the duration of the vegetative phase, a trait that is commonly measured in breeding programmes (Fig. 2a, b).

Plant architecture is a more difficult case because its measurement relies on different principles in indoor vs field experiments (Fig. 3, Table 2, and Supplementary Tables 2 and 4). The architectural trait considered indoor (rh<sub>PAD</sub>) was derived from 3D reconstructions of individual plants, via the difference in altitude between the top of the plant and the point where half of leaf area is reached, normalized by plant height<sup>15</sup>. This trait is closely related to light interception by a canopy<sup>15</sup> and had high heritability (Table 1). It cannot be measured in the field, where 3D reconstruction of individual plants cannot be

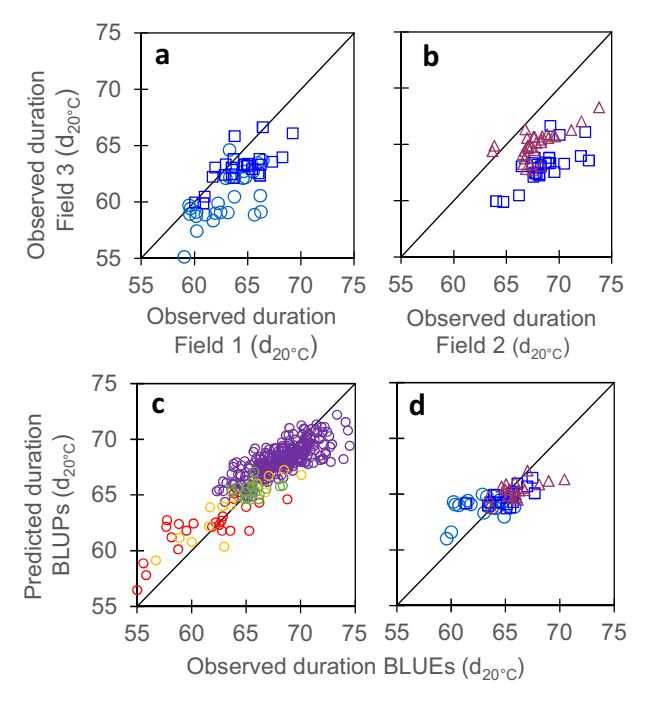
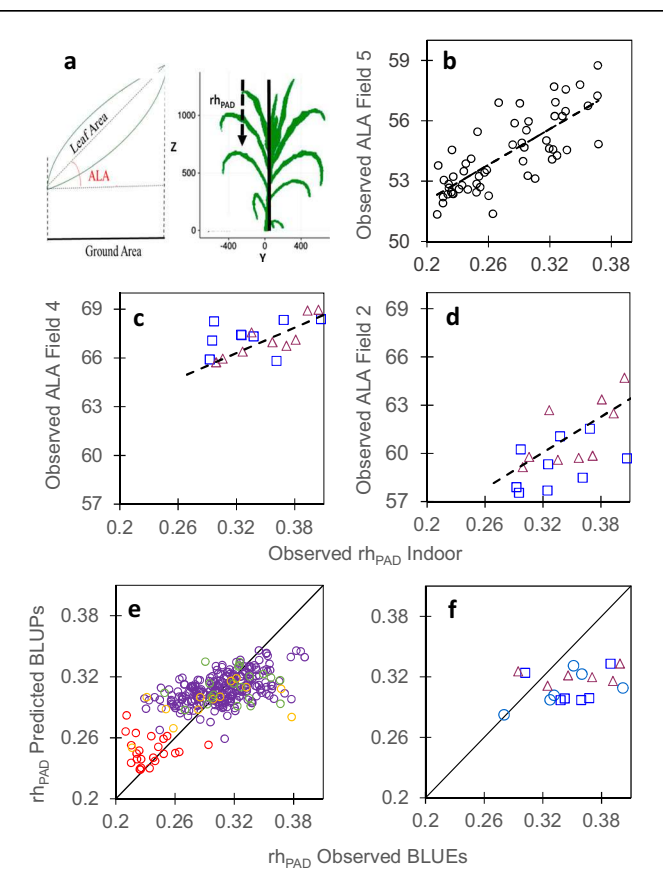


Fig. 2 | The duration of the vegetative phase, a trait measured in most breeding schemes, was not better related between different fields than other traits compared indoor and in the field in Figs. 1-4. a, b Comparison of observed values in 3 field experiments. c Comparison of observed mean genotypic values and mean predicted values (G-BLUPs) in a 5-fold cross-validation scheme with 10 iterations. d Comparison of observed mean genotypic values and predicted values, in the independent dataset. Observed values originated from data of a, b (BLUEs) and G-BLUP model calibration was performed using dataset of  ${\bf c}$ . In  ${\bf a}$ ,  ${\bf b}$  and  ${\bf d}$ , light blue circles, mid-early hybrids (G2), dark blue squares, intermediate hybrids (G3), red triangles, mid-late hybrids (G4). In c, purple empty circles, diversity panel, red and yellow empty circles, genetic progress panel, hybrids released before 1980 and 2000, respectively; green empty circles, hybrids released after 2000. In  $\mathbf{a}$ , r = 0.69(95% CI = 0.52 - 0.81), n = 53, df = 51, p-value = 9.4E-09,  $CV_{RMSE} = 4.4\%$ . In **b**, r = 0.47(95% CI = 0.23–0.65), n = 55, df = 53, p-value = 0.0003,  $CV_{RMSE}$  = 7%, In c, r = 0.84  $(95\% \text{ CI} = 0.81-0.89), n = 302, df = 300, p-value < 2.2E-16, CV_{RMSE} = 2.7\%. In$ **d**, r = 0.71 (95% CI = 0.56–0.82), n = 60, df = 58, p-value = 1.5E-10,  $CV_{RMSE} = 2.5\%$ . Significance of the correlation coefficients was tested using two-sided t-test. For rho and other statistics, see Supplementary Tables 4 and 5. Source data are provided as a source Data file.



Article

Fig. 3 | Plant architecture translated from platform to field, and could be inferred via genomic prediction. a Schematic representation of average leaf inclination angle (ALA) in the field, estimated from UAV images at flowering time, via inversion of the model PROSAIL 42,75 and rhPAD measured indoor as the relative altitude, from the top of the plant, where 50% of leaf area is reached15. **b**, **c** and **d** Correlations between rhPAD (indoor) and ALA (Fields 5, 4 and 2, respectively) for the genetic progress panel (b) and the recent hybrids panel (c, d). e Comparison of observed mean genotypic values and mean predicted values (G-BLUPs) in a 5-fold cross-validation scheme with 10 iterations for  $rh_{PAD}$ . f Comparison of mean genotypic values (BLUEs) and predicted values (G-BLUPs) in the independent dataset. In **b**, **c** and **f**, light blue circles, mid-early hybrids (G2), dark blue squares, intermediate hybrids (G3), red triangles, mid-late hybrids (G4). In **d**, purple empty circles, diversity panel; red and yellow empty circles, genetic progress panel, hybrids released before 1980 and 2000, respectively; green empty circles, hybrids released after 2000. In **b**, r = 0.77 (95% CI = 0.64-0.86), n = 56, df = 54, p-value = 2.85E-12. In **c**, r = 0.58 (95% CI = 0.15–0.82), n = 18, df = 16, p-value = 0.012. In **d**, r = 0.60 (95% CI = 0.18 - 0.83), n = 18, df = 16, p-value = 0.009. In **e**, r = 0.65 (95% CI = 0.59 - 0.72), n = 302, df = 297, p-value < 2.2E-16, CV<sub>RMSE</sub> = 9.4%. In f, r = 0.42 (95% CI = -0.02-0.73), n = 20, df = 18, p-value = 0.06, CV<sub>RMSE</sub> = 15.6%. Significance of the correlation coefficients was tested using two-sided t-test. For rho and other statistics, see Supplementary Tables 4 and 5. Source data are provided as a Source Data file.

performed. Conversely, drone imaging in the field results in the calculation of a related trait, the Average Leaf inclination Angle (ALA), derived from the inversion of the radiative transfer model 'PROSAIL'41,42, which takes into account the deviation of light interception efficiency of a given canopy in relation to a standard canopy having the same leaf area. The genotypic values of ALA measured in the field correlated to those of rh<sub>PAD</sub> measured in a phenotyping platform in an experiment with 56 maize hybrids of the 'genetic progress' panel (Fig. 3b, Field 5, Supplementary Tables 2 and 4). The same applied to 20 hybrids of the 'recent hybrids' panel in two field experiments, with good relationships between rh<sub>PAD</sub> and ALA (Fig. 3c, d), high heritability of both variables (Supplementary Fig. 1) and good conservation of lowest and highest quartiles (Supplementary Table 4). Notably, ALA values and heritability were sensitive to crop phenological stage

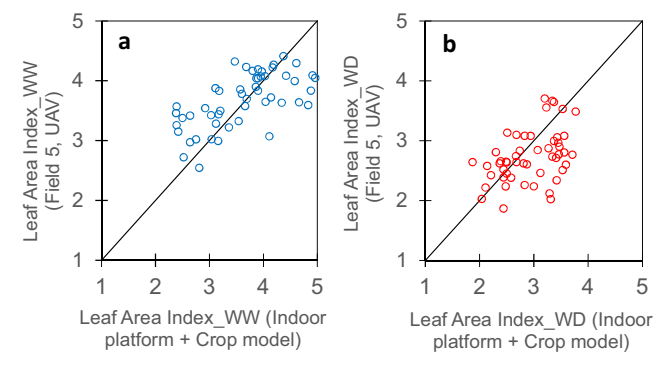


Fig. 4 | Genotypic values of leaf area index (LAI) measured in the field were correlated with values of LAI derived via a crop model taking into account traits measured indoor and environmental data measured in the considered field. a well-watered; b water-deficit. Field values (on y axis) were obtained at flowering time from UAV images via inversion of the model PROSAIL 41, 42. Values on x axis were obtained via the crop model of Lacube et al. 11, fed with measured values of (i) environmental conditions in the same field, (ii) genotypic values measured in the platform for leaf appearance rate (LAR), maximum leaf growth rate (LER), responses of leaf growth rate to vapor pressure deficit (VPD) and soil water potential, and final leaf number per plant. Each point, one genotype. In  $\mathbf{a}$ , r = 0.64 $(95\% \text{ CI} = 0.45 \cdot 0.78)$ , n = 51, df = 49, p-value = 3.6E-07,  $CV_{RMSE} = 15.7\%$ . In **b**, r = 0.44(95% CI = 0.18-0.64), n = 51, df = 49, p-value = 1.3E-03,  $CV_{RMSE} = 19.6\%$ . Significance of the correlation coefficients was tested using two-sided t-test. For rho and other statistics, see Supplementary Table 4. Source data are provided as a Source Data file.

whereas those of rh<sub>PAD</sub> were more stable (Supplementary Fig. 1). Hence, architectural data collected indoor were, in this case, appropriate for characterizing each genotype in models of light interception, whereas ALA measured in the field would be more complex to use in

In the same way, the leaf expansion rate of individual plants (LER) can only be measured indoor, with good heritability (Table 1)<sup>43</sup>. Corresponding measurements in the field are leaf area or leaf dimensions at given dates, so direct comparisons were not possible. However, we show below that the final width and length of maize 8th leaf matched between indoor and field conditions for the diversity panel. Hence, final leaf dimensions potentially allow indirect calculation of LER in the field44.

Leaf area index (LAI), a key feature for light interception and transpiration, is defined for a fraction of field canopy (typically 1 m<sup>2</sup>). Although heritable within a given field, it largely differs between fields in relation to environmental conditions and plant density<sup>45</sup>. It can be measured indoor, but a direct comparison with the field would make no sense because the density and spatial arrangement of plants in indoor experiments make the considered canopy irrelevant to the field<sup>24,46</sup>. Indeed, LAI measured in the field was not correlated to the LAI calculated by considering plant leaf area measured indoor at flowering time, multiplied by the plant density in the corresponding field (Supplementary Fig. 2, r = -0.25, n = 51, p-value = 0.073). This was because environmental conditions and management practices were too different between the greenhouse and the field. Instead, we calculated LAI based on the genotypic values of upstream traits measured indoor (Table 2 and Fig. 4). We compared (i) measured values in the field, obtained via UAV imaging and the inversion of the PROSAIL radiative transfer model<sup>41,42</sup> with (ii) the LAI simulated by a crop model<sup>11</sup>. Model inputs were the genotypic values of four traits measured in indoor platform (LAR, maximum leaf growth rate (LER), responses of leaf growth rate to VPD and soil water potential, and final leaf number), plus plant density and the environmental conditions recorded every hour in the considered field. The correspondence between measured and estimated LAI, tested on the 'genetic progress' panel suggested that this approach is promising in well-watered (WW) condition (r= 0.64, n = 51, p-value = 3.6E-07, Fig. 4a), and even in water-deficit (WD) condition although the indoor platform experiment was performed in WW condition, except for the response of leaf growth rate to soil water potential (r= 0.44, n= 51, p-value = 1.3E-03, Fig. 4b and Supplementary Table 4). Notably, the PROSAIL model inversion allowing LAI estimation in the field always resulted in values lower than 4.5 for all hybrids. When the real LAI was higher, light interception efficiency was close to 100%, so model inversion could not provide LAI values higher than  $4.5^{47}$ .

Finally, stomatal conductance is a difficult case in which traits cannot be directly measured at high throughput, either in the field or in indoor platforms. Its measurement for one leaf requires between 3 and 15 min, depending on the considered device, making high-throughput measurements impossible. However, it can be indirectly estimated at plant level in platform experiments by inversion of the Penman-Monteith equation, based on measurements of individual plant transpiration, leaf area, light, and VPD<sup>14</sup>. Resulting estimations of whole-plant stomatal conductance were well related to leaf stomatal conductance measured via gas exchange, between well-watered and water deficit treatments (Fig. 5a and Supplementary Table 1), but also between genotypes in the well-watered treatment ( $r^2 = 0.54$ ).

Overall, the ranking of genotypes for leaf appearance rate, plant architecture, and LAI were consistent between field and indoor conditions, thereby opening the way for a prediction of values in the field based on platform information (Table 2 and Supplementary Table 4). This could not be tested for stomatal conductance, for which field measurements cannot be performed and indirect measurements via canopy temperature are not precise enough in non-extreme conditions.

## The differences in absolute values of traits between indoor and fields were accounted for by environmental conditions

Beyond the correlations between genotypic values of traits measured indoor and in the field, it is the absolute values of traits, measured in each experiment, that eventually drive the adaptation of studied genotypes to drought and high temperature. For example, a correct estimation of genotype ranking for LAI has a very small impact on light interception if all genotypes have a LAI higher than 4, whereas the same genotype ranking in a range of LAI from 2 to 4 has a large impact<sup>47</sup>. Meta-analyses showed that phenotypic values differ between controlled conditions and field<sup>24</sup>, but they also largely vary from one field to another one<sup>11,24</sup>. Hence, we tested if the difficulty for translating values between two experiments may not be specific to field – platform comparisons, but applies to comparisons between any environment and another one, depending on environmental conditions in each experiment.

This hypothesis was first tested by examining the mean absolute values of maize leaf length and width between field and indoor platforms for the diversity panel in Lacube et al.44. A superficial analysis would suggest that the mean dimensions of leaf 8 largely differed between indoor and field conditions, with a mean leaf length of 115 vs 76 cm, respectively, and a mean leaf width of 6.8 cm vs 7.5 cm, respectively (note the inversion of ranking between the two traits). However, leaf dimensions also largely varied among field experiments, from 6.8 to 10 cm for leaf width and from 68 to 102 cm for leaf length (Fig. 6a, b). We showed earlier that leaf width depends on the amount of light intercepted during the growth of the considered leaf<sup>44</sup>. Accordingly, leaf width in the field was linearly related to the cumulated intercepted light (r = 0.83, n = 64, p-value < 2.2E-16), and the same relationship accounted for the difference between experiments in fields and platform (Fig. 6a). In the same way, the large variability of leaf length, in field and controlled conditions, was accounted for by the vapor pressure deficit (VPD) during leaf growth (Fig. 6b, r = -0.62, n = 44, p-value = 6.2E-06), consistent with studies showing a linear effect of VPD on leaf elongation rate<sup>43</sup>. Hence, leaf width and length did not differ intrinsically between indoor and field conditions: differences were accounted for by the same environmental conditions than those that accounted for differences between one field and another one, and could be calculated via a crop model<sup>11</sup>.

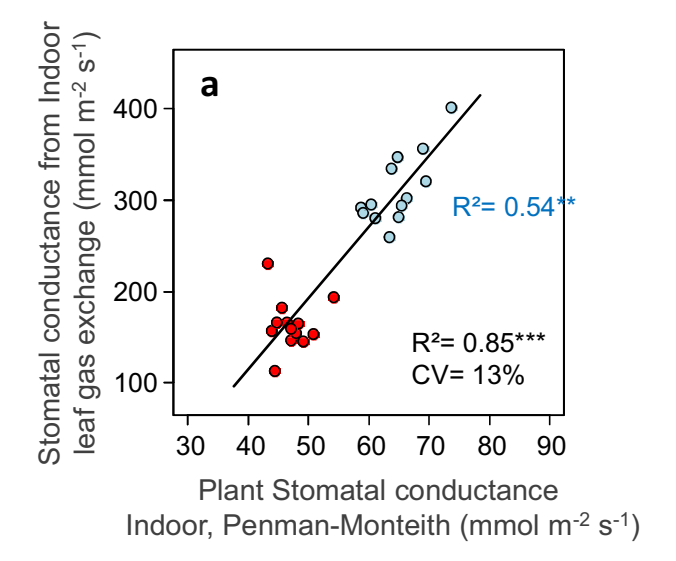
A similar case occurred with temperature-dependent traits, such as the duration of the vegetative phase (Fields 1, 2, and 3, Supplementary Table 2) or leaf appearance rate (Fields 1, 3 and PhenoArch, Supplementary Table 2). When expressed in calendar time, these trait values differed greatly between environments (Supplementary Fig. 3a, b), whereas they were consistent if the effect of temperature was taken into account via a model of thermal time<sup>48,49</sup>. Expressed in this way, measured values were similar between field experiments for the duration of the vegetative phase and for LAR (Figs. 2a, b and 1b, respectively) or between a field experiment and an indoor platform experiment (Fig. 1a), although some differences still existed between experiments (CV<sub>RMSE</sub> = 4.4% and 7% in Fig. 2a, b, CV<sub>RMSE</sub> = 5.3% and 7.7% in Fig. 1a, b). Among possibilities for explaining such differences in duration of the vegetative phase and LAR, the frequency of field visits was three days on average, but slightly differed between experiments.

Overall, values translation from indoor platforms to field, and from one field to another field, could be carried out for a range of traits by taking into account appropriate environmental variables.

#### Measurements in indoor platforms can be used for genomic prediction of traits

High-throughput phenotyping allows characterization of some hundreds of genotypes (at most) whereas many thousands of genotypes are required for breeding<sup>3,4</sup>. In the same way, it would not be feasible to phenotype the offspring at each generation of speed breeding because of the resulting cost and workload<sup>34,36</sup>. Hence, the use of physiological traits in breeding requires one's ability to predict them based on genomic information, as it is the case for yield<sup>50,51</sup>. We have tested this possibility for the traits presented in the former paragraphs. Briefly, we trained a G-BLUP model based on the 246 hybrids of the 'diversity panel' and the 56 hybrids of the 'genetic progress' panel (Supplementary Table 1). This training was performed with the genotypic means (BLUEs over the experiments carried out in Millet et al.31 and Welcker et al.9) of the duration of the vegetative phase, the leaf appearance rate, maximum leaf expansion rate (calculated with two methods based on different assumptions, see "Methods" section), the architectural trait rh<sub>PAD</sub> and stomatal conductance. Predictions were performed using the genomic information at 440 000 polymorphic SNPs. Prediction accuracies and RMSEs were assessed either with a 5-fold cross-validation (CV1) scheme<sup>28</sup> (random sampling of hybrids using a stratification strategy for respecting the proportions of genetic groups, Supplementary Fig. 4), or with an external validation set made of genotypic trait means estimated in the 'recent hybrids panel' (independent experiments, Supplementary Data 1).

Cross-validation provided good quality of prediction for studied traits, assessed either by the correlation (r) between observed BLUEs and predicted G-BLUPs values, or by the prediction accuracy of genomic selection (Acc), calculated by dividing the correlation coefficient (r) by the square root of trait genomic heritability<sup>52,53</sup> (Table 2). This was the case for leaf appearance rate (r = 0.58, n = 302, p-value < 2.2E-16,  $CV_{RMSE} = 5.2\%$  in Fig. 1c), leaf expansion rate (r = 0.76, n = 302, p-value < 2.2E-16, CV<sub>RMSE</sub> = 8.7% in Fig. 7a), rh<sub>PAD</sub> (r = 0.65, n = 302, pvalue < 2.2E-16,  $CV_{RMSE} =$  9.4% in Fig. 3e) and stomatal conductance (r = 0.56, n = 302, p-value < 2.2E-16,  $CV_{RMSE} = 8.4\%$  in Fig. 5b) (Supplementary Table 5). These values are similar but slightly lower than those for the duration of the vegetative phase in our study (r = 0.84, n = 302, p-value < 2.2E-16, CV<sub>RMSE</sub> = 2.7% in Fig. 2c), and for yield or flowering time traits in other studies<sup>51,54-56</sup>. Notably, genomic prediction with G-BLUP model performed similarly for the genotypes originating from the two panels, in spite of the difference in structure and origins of these panels (Supplementary Fig. 5) and the fact that measurements



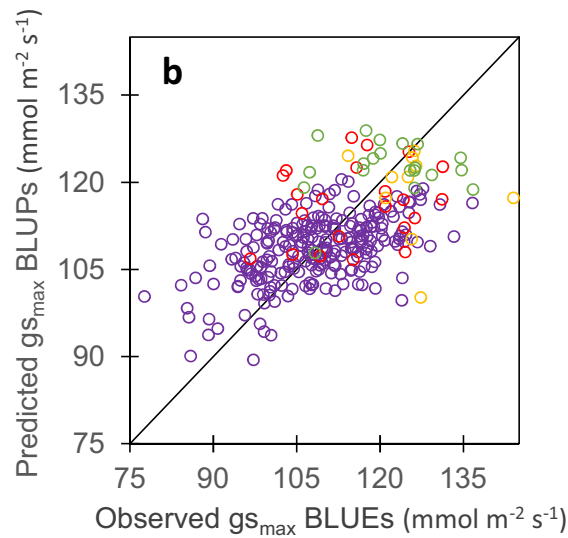


**Fig. 5** | **Stomatal conductance can be measured at plant level in an indoor phenotyping platform and predicted from genomic information.** a Comparison between values obtained at leaf level via gas exchange, and at plant level via inversion of the Penman-Monteith equation  $^{14}$ , in well-watered and water deficit treatments. **b** Comparison of observed mean genotypic values and mean (G-BLUP) predicted values in a 5-fold cross-validation scheme with 10 iterations for plant stomatal conductance. In **a** and **b**, each symbol, one genotype; blue, well-watered; red, water deficit. In **a**, black line, linear regression. In **b**, black line is the 1:1 line. In **a**, r = 0.92 (95% CI = 0.83–0.96), n = 26, df = 24, p-value = 2.4E-11, CV<sub>RMSE</sub> = 13%. In **b**, r = 0.56 (95% CI = 0.47–0.63), n = 302, df = 293, p-value < 2.2E-16, CV<sub>RMSE</sub> = 8.4%. Significance of the correlation coefficients was tested using two-sided t-test. For rho and other statistics, see Supplementary Table 5. Source data are provided as a Source Data file.

were performed in different experiments. Furthermore, when predicting traits with a PC-BLUP model that is used as predictors the genotypes coordinates on the first five axes of SNP PCoA (Principal Coordinate Analysis) of the panels (Supplementary Fig. 5), the prediction quality decreased when considering individual clouds of points corresponding to each panel (Supplementary Fig. 6 and Supplementary Table 6).

The range of G-BLUP predicted values was expectedly smaller, for all tested traits, than that of observed values. This bias is linked to the fact that the narrow-sense heritability estimated using genomic additive and dominance relationships of studied traits was lower than 1 (0.68–0.82, 0.56–0.63, 0.54–0.62, 0.54–0.74, and 0.48–0.53 for the duration of the vegetative phase, LAR, leaf expansion rate,  $rh_{PAD}$  and

stomatal conductance, respectively, Table 1). Hence, the prediction based on genomic information covered a smaller range of values than original data.

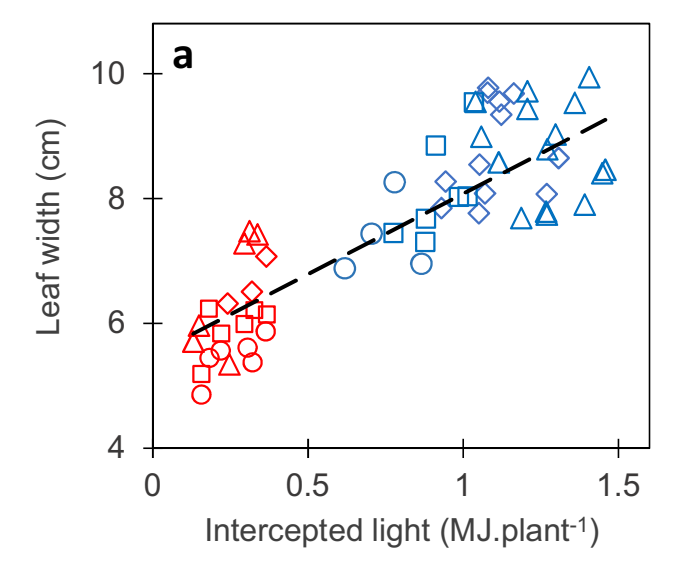
The external validation was a more challenging scheme, where we tried to predict the performance of new genotypes evaluated in new independent experiments. Moreover, the 'recent hybrids panel' used here covered smaller ranges of trait phenotypic values than those in the 'diversity' and 'genetic progress' panels considered jointly. Consequently, the comparison of observed vs G-BLUP predicted values led to lower prediction accuracies than in the case of cross-validation (r ranged between 0.34 and 0.71, Table 2). This applied to traits measured indoor (LAR, Fig. 1d, LER, Fig. 7b and rh<sub>PAD</sub>, Fig. 3f) as well as for the duration of the vegetative phase measured in the field (Fig. 2d and Supplementary Table 5), so this problem was not specific of indoor genomic prediction. The external validation using the simple PC-BLUP model resulted in much lower prediction accuracies than that using the G-BLUP model (Supplementary Fig. 6 and Supplementary Table 6). This suggests that G-BLUP predictions captured genetic effects beyond that explained by population structure.

#### Discussion

Three conditions can be considered as requirements for traits measured indoor to be used in trait-based selection in a context of climate change. Firstly, traits measured indoor should be genetically correlated to those in fields (regardless of absolute values either indoor or in each field), so indoor breeding is relevant to field conditions. Secondly, the absolute value of indoor traits should translate to that in fields with diverse climate scenarios, either directly or via models. Finally, indoor traits need to be predicted with sufficient accuracy from the genomic information of non-phenotyped genotypes.

The traits presented here satisfied the first condition. Close correlations were observed between the genotypic values of traits measured indoor and in multi-site field experiments. This was the case when the considered trait was measured with similar protocols indoor or in the field, for instance leaf appearance rate or the duration of the vegetative phase. It was also the case when the trait was measured with different methods as in the case of plant architecture. Finally, the integrated trait LAI, which is highly dependent on the plant density and environmental conditions in the considered canopy, required a method involving crop modeling. The correlations observed in these three cases between indoor platform and fields are therefore higher (r = 0.57 to 0.77, Table 2) than those reported by Poorter et al.<sup>24</sup> for a set of growth-related traits meta-analysis (median r = 0.51). Two reasons may explain this disparity. (i) Traits considered in Poorter's metaanalysis, namely yield, leaf nitrogen concentration and specific leaf area are more integrated than those studied here (except LAI) and, therefore more prone to high genotype x environment interactions and changes in the ranking of genotypes. (ii) The traits studied here had moderate to high heritabilities over experiments, thereby showing a low residual variance resulting from experimental errors. Furthermore, measuring yield, yield components, or leaf area index in phenotyping platforms is probably not relevant because these traits result from cumulative processes over a long period, during which conditions indoor are very different from those in the field. The methods presented here for comparing indoor and field trait values considerably reduced the genotype x environment interaction (GEI) for such integrated traits. For example, a direct comparison of LAI indoor and in the field resulted in a high GEI, without correlation between them. Conversely, the GEI was largely reduced when upstream traits measured indoor (with a low GEI) were combined, via a crop model, with the management practices and environmental conditions in the considered field<sup>37</sup>.

The second condition, namely that trait values can translate from indoor conditions to a diversity of fields, was fulfilled for the traits reported here if the differences in environmental conditions were



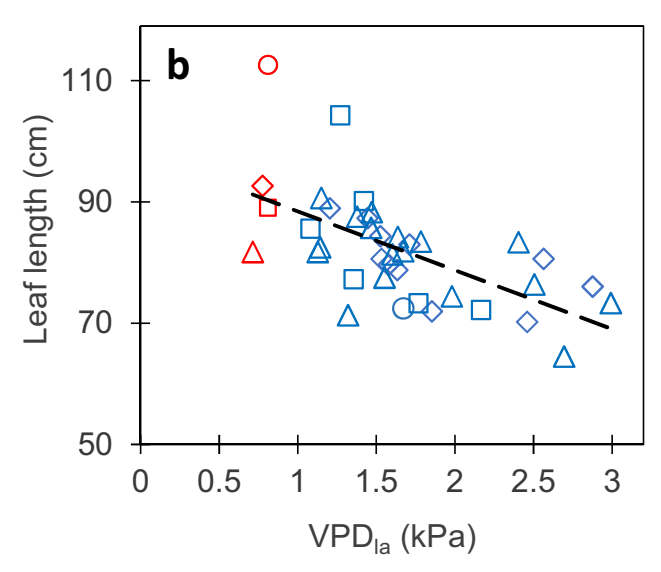


**Fig. 6** | **Leaf width and length responded similarly to environmental conditions in fields and indoor platforms. a** Relationship between leaf width and the cumulated light intercepted by plants during leaf widening. **b** Relationship between leaf length and leaf-to-air vapor pressure deficit (VPD<sub>1a</sub>: mean of maximum daily values) during leaf elongation. Each point, one experiment and leaf rank. Leaf width and length values of four leaf ranks (8–11, circles, squares, diamonds and triangles, respectively) were corrected for leaf rank so equivalent values for leaf 8 are presented<sup>44</sup>. Blue dots: field, red dots: indoor platform. Black lines, linear regressions. In **a**, r = 0.83 (95% Cl = 0.73-0.89), n = 64, df = 62, p-value < 2.2E-16. In **b**, r = -0.62 (95% Cl = -0.78-0.40), n = 44, df = 42, p-value = 6.2E-06. Significance of the correlation coefficients was tested using two-sided t-test. Source data are provided as a Source Data file.

taken into account, thereby dealing with the GEI via a previously reported model<sup>31</sup>.

• Modeling temperature effects allowed consistency between field and platform experiments for leaf appearance rate and the duration of the vegetative phase in this study. This result can be generalized to traits related to the progression of plant development of many species. In particular, germination rate, leaf appearance rate, the reciprocal of the duration of growth of individual leaves and reproductive organs are common to a large range of environments if they are expressed in thermal time<sup>57</sup>. Crop models, based on this result, successfully predict plant phenology in wide ranges of environments<sup>8,30</sup>.

- The amount of intercepted light was also needed for other traits to be consistent between experiments. This was the case here for maize leaf width measured indoor and in several fields. Beyond this particular trait, Monteith showed that biomass accumulation is proportional to the cumulated light intercepted by plants<sup>47</sup>. In particular, we showed that, in a series of experiments with maize, the time course of plant biomass largely differed between experiments but was consistent if expressed as a function of intercepted light<sup>16</sup>. Again, crop models based on intercepted light can predict plant biomass accumulation with reasonable accuracy<sup>30,58</sup>.
- Plant water status was, in addition, necessary to account for differences in traits related to organ expansive growth (expressed in terms of volume or length). Its effect can be predicted from the cell scale<sup>59</sup> to the organ scale<sup>60-62</sup>. Here, this was the case for leaf length in well-irrigated maize fields, as a function of air VPD. Leaf elongation rate is closely related to a combination of soil water potential and VPD in maize, fescue, or barley<sup>60,63</sup>, so our result can probably be extended to other species. Stomatal conductance can also be predicted from a combination of soil water status, evaporative demand, and incident light via functional models involving chemical and hydraulic signals<sup>64</sup>. Crop models that take into account light, soil water content and evaporative demand can predict stomatal conductance and net photosynthesis by simulating physiological processes<sup>65,66</sup>, so photosynthesis in controlled conditions can be extended to a range of field conditions<sup>66</sup>.

Overall, we confirmed that raw phenotypic traits cannot translate directly from indoor platforms to fields, as reviewed in Poorter et al.<sup>24</sup>. However, taking into account specific environmental conditions allowed this translation for the traits presented here, which depend on one or two environmental conditions. Again, more integrated traits such as leaf area index, grain number or grain yield measured in a platform cannot be directly extended to field via simple relationships as presented in former paragraphs. These traits can be predicted in a range of field conditions based on genotype-specific parameters and environmental conditions measured in the considered fields. This was the case here for leaf area index, but was also the case for grain number and grain yield in a multi-site field experiments, based on a mixed model involving genetic parameters and environmental conditions<sup>31</sup>.

The third condition is that traits can be predicted from genomic information. Here, cross-validation based on a large genetic range showed good results (compared to Guo et al.<sup>56</sup>, Yuan et al.<sup>55</sup>, or Toda et al.51), with r ranging from 0.56 to 0.84 for the studied traits (Table 2 and Supplementary Table 5). External validation on the panel of recent hybrid varieties provided less accurate results, but correlations between predicted and observed values still ranged from 0.34 to 0.71 and mostly with significant p-values (from 1.5 E-10 to 0.14) and acceptable CV of errors (from 2.5% to 15.6%) (Supplementary Table 5). By using this panel for external validation, we chose the most challenging case, in which one attempts to use a genomic prediction model, trained with a panel with wide genetic variability, to predict elite genotypes that have a reduced phenotypic variability for studied traits. Hence, our results could not be considered as fully satisfactory if the purpose was to rank elite genotypes (Supplementary Table 5). Conversely, the cross-validation in a wider genetic range suggests that genomic prediction may be used for identifying genotypes with high or low genotypic values for studied traits in breeding populations with higher genetic and phenotypic variabilities. This allows the design of ideotypes with contrasting strategies in relation to water and heat stress, namely 'conservative' ideotypes with low stomatal conductance, leaf growth, leaf appearance rate, for stress-prone areas, vs 'spender' ideotypes with highest values for each of these traits.

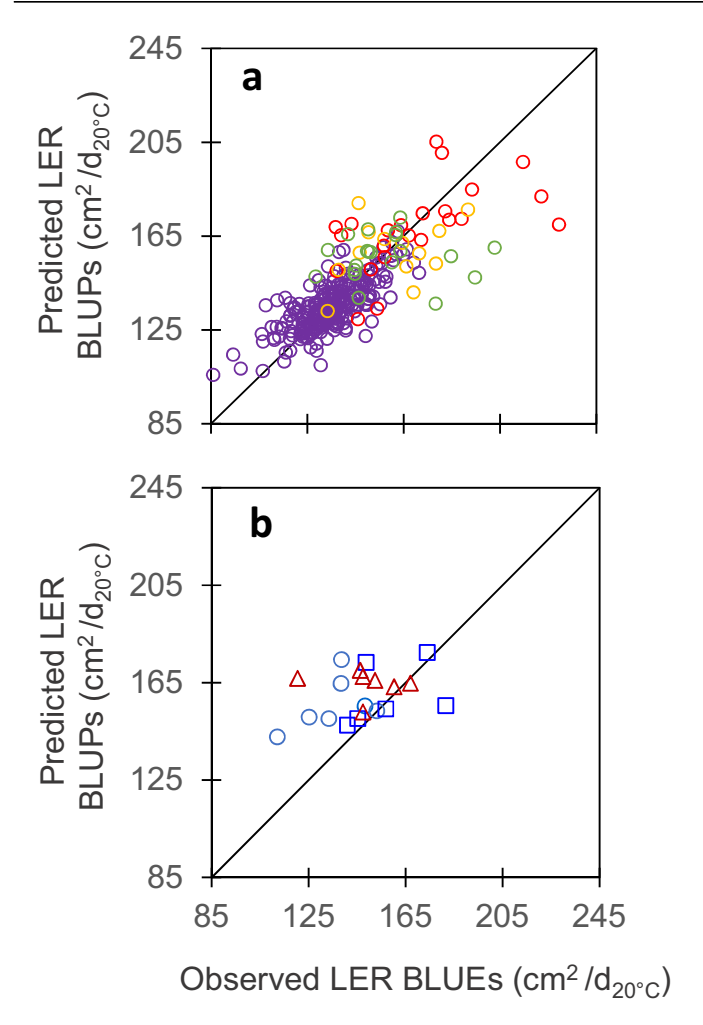


Fig. 7 | Maximum leaf expansion rate (LER) could be predicted from genomic information via cross-validations in panels with large phenotypic variability but predictions were not accurate for the independent dataset, a Comparison of observed mean genotypic values and mean (G-BLUP) predicted values in a 5-fold cross-validation scheme with 10 iterations for plant max leaf expansion rate (LER). b Comparison of observed mean genotypic values and predicted values for the recent hybrids dataset, with G-BLUP model calibration made using dataset of a. LER (Leaf Expansion Rate) was extracted from time courses of leaf area in the platform<sup>14</sup> and determined as the slope of the linear regression between leaf area and thermal time during the period from 24 to 45  $d_{20}$  °C. In **a**, purple empty circles, diversity panel; red and yellow empty circles, genetic progress panel, hybrids released before 1980 and 2000, respectively; green empty circles, hybrids released after 2000. In b, light blue circles, mid-early hybrids (G2), dark blue squares, intermediate hybrids (G3), red triangles, mid-late hybrids (G4). In  $\mathbf{a}$ , r = 0.76 (95%) CI = 0.71-0.82), n = 302, df = 297, p-value < 2.2E-16,  $CV_{RMSE} = 8.7\%$ . In **b**, r = 0.34 (95%) CI = -0.12-0.68), n = 20, df = 18, p-value = 0.14,  $CV_{RMSE} = 14.1\%$ . Significance of the correlation coefficients was tested using two-sided t-test. For rho and other statistics, see Supplementary Table 5. Source data are provided as a Source Data file.

#### **Methods**

#### **Genetic material**

Three panels of maize hybrids were used in this study (Supplementary Table 1). First, a diversity panel included 246 hybrids resulting from the cross of a common flint parent (UH007) with 246 dent lines that maximized the diversity in the dent group while keeping a restricted flowering window<sup>31,67</sup>. This panel involved four genetic groups, namely lodent (39 hybrids), Lancaster (45 hybrids), Stiff-Stalk (55 hybrids), and diverse-dent hybrids (107) consisting in an admixture of the former three groups<sup>67</sup>. Second, a 'genetic progress' panel included 56 highly successful commercial hybrids released on the European market from 1950 to 2015<sup>9</sup>. This panel showed a limited range of maturity classes,

from mid-early (FAO 280) to mid-late (FAO 480), covering the largest growing area in Europe. Finally, a 'recent hybrids' panel included 86 commercial hybrids released from 2008 to 2020, belonging to midearly to mid-late maturity classes (Supplementary Data 1). Yield data in 30 sites x 2 years per hybrid were available at the beginning of this study (ARVALIS, www.varmais.fr).

#### **Platform experiments**

Platform experiments were performed in PhenoArch, an indoor robotized and image-based phenotyping platform that allows precise measurement of plant architecture, plant phenology and growth, transpiration, stomatal conductance and water use efficiency (https:// www6.montpellier.inrae.fr/lepse/Plateformes-de-phenotypage-M3P/ Montpellier-Plant-Phenotyping-Platforms-M3P/PhenoArch)<sup>16</sup> hosted at Montpellier Plant Phenotyping Platforms (M3P). The diversity panel was evaluated in four experiments (in spring 2012, 2013, and 2016, and winter 2013) as described in Prado et al.<sup>14</sup>. Three or two plants per hybrid were grown depending on the experiment (Supplementary Table 1). The 'genetic progress' panel was evaluated in four experiments, with most data used here originating from an experiment with seven replicates per hybrid9. A subset of 20 hybrids of the 'recent hybrids' panel was evaluated in one experiment during winter 2021. with three replicates per hybrid. All experiments followed an alphalattice design, with two levels of soil water content imposed, namely retention capacity (well-watered, soil water potential of -0.05 MPa) and water deficit (soil water potential from -0.3 to -0.6 MPa depending on the experiment). Soil water content in pots was maintained at target values by compensating transpired water three times per day via individual measurements of each plant<sup>16</sup>. Soil water potential was estimated from soil water content based on a water release curve<sup>14</sup>. Air temperature and humidity were measured at six positions in the platform every 15 min. Daily incident photosynthetic photon flux density (PPFD) over each plant within the platform was estimated by combining a 2D map of light transmission, and the outside PPFD measured every 15 min with a sensor placed on the greenhouse roof<sup>16</sup>. The greenhouse temperature was maintained at  $25 \pm 4$  °C during the day and 17 ± 2 °C during the night. Supplemental light was provided either during daytime when external solar radiation was below 300 W m<sup>-2</sup> or to extend the photoperiod by using 400 W HPS Plantastar lamps.

In each experiment, the number of visible leaves of every plant was manually scored weekly during the vegetative phase. Leaf appearance rate (LAR, reciprocal of the phyllochron) was calculated as the slope of the linear relationship between the number of visible leaves and thermal time, during the period from plant emergence to 12-leaf stage. Red-Green-Blue (2056 × 2454) images taken from 13 views (12 side views from 30° rotational difference and one top view) were captured daily for each plant during the night. Plant pixels from each image were segmented from those of the background and used for estimating the whole plant leaf area and fresh biomass<sup>68</sup>. The time courses of leaf area and plant fresh biomass were then fitted individually by using P-spline growth curve models<sup>69</sup>. The architectural trait rh<sub>PAD</sub> was calculated daily from 3D reconstructions of each plant, based on RGB images at PhenoArch platform<sup>15</sup>. rh<sub>PAD</sub> index represented the point in the distribution of leaf area along the stem (from the top of the plant, relative to total plant height) where half of the cumulative leaf area is reached. Whole-plant stomatal conductance was calculated over 4 time-periods per day for 20 days for each hybrid plant in PhenoArch platform, via inversion of the Penman-Monteith equation based on transpiration, plant growth, net radiation and VPD collected in the experiment<sup>14</sup>. Its value under saturating light was estimated for each hybrid by combining coupled values of stomatal conductance and incident light observed in all experiments. The maximum leaf expansion rate (LER) was extracted from time courses of leaf area in the platform and corresponded to the maximum first-

https://doi.org/10.1038/s41467-023-42298-z

order derivative of P-spline fitted growth curves from 24 to 45 days at 20 °C after emergence 69. Because this method provided somewhat unstable results, we also calculated maximum LER as the slope of the linear regression between leaf area and thermal time during the whole period from 24 to 45 days at 20 °C.

Genotypic values (BLUEs) for each trait were estimated by correcting raw traits values for spatial effects, by fitting a mixed model (R package SpATS<sup>70</sup>,), with a fixed term for genotype and random effects for rows and columns as well as a smooth surface defined on row and column coordinates. Broad-sense heritabilities were calculated daily with the same R package, using the same model but with the genotype effect included as a random term. Regarding longitudinal traits, genotypic values at individual time points, t, were obtained from their smoothed time series using a generalized additive model fitted to the spatially adjusted daily measurements,  $\widetilde{y}_{i,k}(t)$ , for each plant k of genotype i:

$$\widetilde{y}_{i,k}(t) = \alpha_i + f_i(t) + \epsilon_{i,k}(t), \epsilon_{i,k}(t) \sim N(0,\sigma^2)$$
 (1)

where  $\alpha_i$  is a genotype-specific intercept,  $f_i$  (t) is a genotype-specific thin plate regression spline function on time, and  $\varepsilon_{i,k}$  (t) is a random error term (R package statgenHTP<sup>69,71</sup>,).

Genomic heritability (narrow-sense,  $h_g^2$ ) was estimated for each trait, panel and experiment with a model considering genomic-based additive and dominance relationship matrices<sup>72</sup>, using the R package "BGLR"<sup>73</sup>.

#### **Field experiments**

The diversity panel was grown in 25 experiments (defined as combinations of site × year × water regime), either rainfed or irrigated, in ten sites in 2012 or 201331. Sites were distributed on a west-east transect for temperature and evaporative demand, across Europe at latitudes from 44° to 49° N. The 'genetic progress' panel was grown in 26 field experiments either rainfed or irrigated, in 16 European sites from 2010 to 2017 spread along the same climatic transect as for experiments with the diversity panel<sup>9</sup>. The 'recent hybrids' panel was grown in four field experiments under irrigated conditions in the same range of latitudes, in 2021 or 2022 in France (Supplementary Table 2). Experiments followed an alpha-lattice design or randomized complete block design (RCBD) and were split by varieties maturity classes (Supplementary Table 2), each with three replicates of four-row plots, 6 m long. The targeted plant density was 9 plants m<sup>-2</sup>. In all experiments, anthesis and silking dates were scored by visiting experiments every third day. The number of appeared leaves was scored every week on ten plants per hybrid during the vegetative phase, and leaf appearance rate was calculated as in indoor experiments (Supplementary Table 2).

The duration of the vegetative phase was defined as the period from plant emergence to anthesis, expressed in thermal time (equivalent days at  $20\,^{\circ}\text{C})^{48}$ . Leaf appearance rate was estimated as in platform experiments.

UAV flights were performed three times in one experiment of the 'genetic progress' panel during the period from plant emergence to flowering, and seven times in two experiments for the 'recent hybrids' panel during the same period (Supplementary Table 2). Quadcopter drone (DJI Phantom 4) were equipped with a DJI multispectral camera with 5.7 mm focal length lens, acquiring 1600×1300 pixel images. They flew at a controlled altitude of 20 m and a constant speed of 2.2 m s<sup>-1</sup> for about 20 min per flight, with images captured at a one-second interval. Flights were performed during clear and cloudless days between 8:00 and 10:00 solar time. An automatic image-processing pipeline was applied by Hiphen, Avignon, France (http://www.hiphenplant.com), following methods presented in Blancon et al.<sup>20</sup>. Environmental variables were recorded every hour in all experiments, including light, air temperature, relative humidity (RH), rainfall and wind speed. Soil water potential was measured every day with

tensiometers at 30 and 60 cm depths with three or two replicates, located in plots sown with a common reference hybrid.

The architectural trait ALA (Average Leaf inclination Angle to the soil level) and Leaf Area Index (LAI) were calculated by inversion of the PROSAIL model 41,74, based on multispectral images of field UAV flights. The PROSAIL model couples the PROSPECT leaf optical properties model with the SAIL canopy bidirectional reflectance model. It links the spectral variation of canopy reflectance, which is mainly related to leaf biochemical contents, with its directional variation, which is primarily related to canopy architecture and soil/vegetation contrast75. This link allows simultaneous estimation of canopy biophysical/structural variables from remote sensing, including ALA and LAI traits42,76.

Leaf area index was also calculated by using a crop model (APSIM model as modified in Lacube et al.<sup>11</sup>) parameterized with the genotypic values (BLUEs) of four traits measured in PhenoArch platform (LAR, maximum leaf growth rate, response of leaf growth rate to VPD and final leaf number), plus the environmental and growing conditions recorded in the considered field.

Spatial corrections, calculations of genotypic values and heritabilities of traits were performed with the same methods as in indoor experiments.

#### Correlation analysis between experiments

Pearson (r) and Spearman (rho) correlation coefficients were calculated to evaluate to which extent the genotypic values (BLUEs) of traits match between experiments, either in one field and another one, or in one field and the indoor platform. Both types of correlations was performed on the hybrids that were common to considered experiments (common hybrids number ranged from 18 to 56, Supplementary Data 1 and Supplementary Table 4). The significance of correlation coefficients was evaluated based on the null hypothesis that there is no correlation between the variables (r or rho = 0). Genetic correlations (rg) between experiments were also assessed, using a multivariate Bayesian Gaussian mixed model, fitted for each couple of experiments (bivariate analysis, Table 2), with MTM R package  $^{38,39}$ . Model fitting was based on 60,000 iterations, after discarding 10,000 cycles for burn-in period and using a thinning rate of 5. Each multivariate model implemented had the form:

$$\mathbf{y}_{i} = \mu_{i} \mathbf{1}_{n} + \mathbf{Z}_{ai} \mathbf{a}_{i} + \mathbf{Z}_{di} \mathbf{d}_{i} + \boldsymbol{\varepsilon}_{i}$$
 (2)

where the subscript i refers to experiments (two experiments analyzed jointly, with trait values measured either indoor and in a field or in two different fields, Table 2),  $y_i$  is the vector of trait values (BLUEs) of n hybrids in the considered couple of experiments,  $\mu_i$  is the overall mean (intercept),  $a_i$  is the vector of random additive genetic effects,  $d_i$  is the vector of random dominance effects and  $\varepsilon_i$  is the vector of random residual effects.  $Z_{ai}$  and  $Z_{di}$  are the incidence matrices for  $a_i$  and  $d_i$ , respectively.

Variance components were calculated assuming:  $a_i \sim \text{MVN}$  (0,  $G_A \otimes V_a$ ) with  $G_A$  as the genomic-based additive relationship matrix described below and  $V_a$  as the additive effects variance–covariance matrix,  $d_i \sim \text{MVN}$  (0,  $G_D \otimes V_d$ ) with  $G_D$  as the genomic-based dominance relationship matrix described below and  $V_d$  as the dominance effects variance–covariance matrix,  $\varepsilon_i \sim \text{MVN}$  (0,  $I \otimes R$ ) where I denotes the identity matrix and R is the residual effects variance–covariance matrix.

Standard errors (SE) of all correlation coefficients were estimated using Bonett and Wright approximations<sup>77</sup>. Additionally, the theoretical accuracy of indirect selection (iAcc), i.e. in case of an indirect phenotypic selection based on observed values in a given experiment (indoor or in a field), was calculated as the genetic correlation between the considered couple of experiments, multiplied by the square root of trait genomic heritability in the reference experiment for selection<sup>52</sup> (Supplementary Table 4). Then, we quantified the efficiency of indirect selection relative to a direct phenotypic selection in the targeted

environment (Eff), by dividing the accuracy of indirect selection by the square root of trait genomic heritability in the target field experiment<sup>52</sup>.

Root mean squared error of estimations (RMSE) and bias showing the discrepancy between experiments genotypic values (BLUEs) were calculated too. We present them as a coefficient of variation of the error (CV  $_{\mbox{\scriptsize RMSE}}$  ) or bias (CV  $_{\mbox{\scriptsize Bias}}$  ), which is the RMSE or bias expressed as a percentage of the mean value. Finally, to appreciate the consistency between experiments of the highest and lowest genotypic values, we evaluated the frequency of similar assignment to the highest or the lowest quartile between experiments for each trait. This consisted of estimating how many hybrids of the highest quartile of one experiment were also present in the highest quartile of the other experiment (Supplementary Table 4). The same was performed for the lowest quartile.

#### Genotypic data and diversity analyses

All panels were genotyped using the 600 K Affymetrix® Axiom® array<sup>78</sup>. Genotypes of the hybrids were either inferred from genotypes of the parental lines (diversity panel) or resulted from the direct genotyping of the hybrids (genetic progress and recent hybrids panels). After quality control, 440,000 polymorphic SNPs were retained for diversity analyses and genomic prediction (excluding SNPs with minor allele frequency lower than 0.05 and/or missing values for more than 20% of hybrids). Missing values were otherwise imputed using BEAGLE v3<sup>79</sup>.

Genotypic data generated were organized as M matrices with N rows and L columns, N and L being the panel size and number of markers, respectively. Genotype of hybrid n at locus (SNP marker) j was coded as 0 (the homozygote for B73 line allele), 1 (the heterozygote) or 2 (the other homozygote). "snpReady" R package<sup>80</sup> was used to estimate observed heterozygosity as

$$H_0 = \frac{1}{I} \sum_{j=1}^{L} (nH_j/N)$$
 (3)

and Nei's index of genetic diversity as

Nei\_GD = 
$$\frac{1}{I} / \sum_{j=1}^{L} (1 - p_j^2 - (1 - p_j)^2)$$
 (4)

with N the number of hybrids,  $nH_{j}$  is the number of heterozygous hybrids at the jth biallelic locus, L is the total number of loci, and p<sub>i</sub> is the frequency of the reference (B73 line allele) at locus j (Supplementary Table 7). Principal Coordinate Analysis (PCoA) was also performed on SNP markers data (Supplementary Fig. 5).

#### **Genomic prediction model**S

Genomic predictions of each trait was performed with a genomic best linear unbiased prediction model (GBLUP-AD), including random additive and dominance effects:

$$\mathbf{y} = \mu \mathbf{1}_n + \mathbf{Z}_a \mathbf{a} + \mathbf{Z}_d \mathbf{d} + \boldsymbol{\varepsilon} \tag{5}$$

where y is the vector of trait genotypic means (BLUEs over experiments) of n hybrids,  $\mu$  is the overall mean (intercept), a is the vector of random additive genetic effects, and is assumed to follow a normal distribution  $\sim$  N (0,  $G_A \sigma_a^2$ ) with  $G_A$  as the genomic-based additive relationship matrix described below and  $\sigma_a^2$  as the additive genetic variance; d is the vector of random dominance effects which follows a normal distribution ~ N  $(0, G_D\sigma_d^2)$  with  $G_D$  as the genomic-based dominance relationship matrix described below and  $\sigma_d^2$  as the dominance genetic variance;  $\epsilon \sim N$  (0,  $l\sigma_{\epsilon}^{\ 2})$  is the vector of random residual effects, where I denotes the identity matrix and  $\sigma_{\epsilon}^{\,2}$  is the residual variance.  $Z_a$  and  $Z_d$  are the incidence matrices for a and d, respectively.

The genomic-based relationship matrices were built as defined in Vitezica et al.  $^{72}$  and González-Diéguez et al.  $^{81}$ . The genomic-based additive relationship matrix (GA), called realized relationship matrix was estimated as

$$G_A = \frac{H_a H_a'}{tr(H_a H_a')/N} \tag{6}$$

https://doi.org/10.1038/s41467-023-42298-z

where  $H_a$  is a rescaled genotype matrix  $H_a = M-P$ , where M is the genotype matrix coded as 0, 1, and 2 for genotypes BB, Bb and bb respectively and with dimensions number of hybrids (N) by number of loci (L); P is the matrix of locus scores  $2p_{j}$ , with  $p_{j}$  being the reference allele frequency of the jth SNP biallelic locus (having alleles B/b); tr is the trace. The genomic-based dominance relationship matrix (G<sub>D</sub>) was estimated as

$$G_D = \frac{H_d H_d'}{tr(H_d H_d')/N}$$
 (7)

where  $\boldsymbol{H}_{\!d}$  is the matrix containing elements  $\boldsymbol{h}_{\!d}$  for each individual and locus equal to:

$$h_{d} = \begin{cases} -2p_{Bb}p_{bb} \left[ p_{BB} + p_{bb} - (p_{BB} - p_{bb})^{2} \right]^{-1} \\ 4p_{BB}p_{bb} \left[ p_{BB} + p_{bb} - (p_{BB} - p_{bb})^{2} \right]^{-1} & \text{for genotypes} \\ BB \\ Bb \\ bb \end{cases}$$

$$-2p_{Bb}p_{BB} \left[ p_{BB} + p_{bb} - (p_{BB} - p_{bb})^{2} \right]^{-1}$$
(8)

where  $p_{BB}$ ,  $p_{Bb}$ , and  $p_{bb}$  are the genotypic frequencies for the genotypes BB, Bb, and bb respectively at the locus.

For moderate heritability physiological traits (LER and gs<sub>max</sub>), in addition to random additive and dominance effects estimated from genomic-based relationship matrices, the genotypes of markers associated to quantitative trait loci (QTLs), previously identified in a genome-wide association study (GWAS) of the diversity panel<sup>14</sup>, were added as fixed effects in prediction models:

$$y = \mu \mathbf{1}_n + X \boldsymbol{\beta} + Z_a \boldsymbol{a} + Z_d \boldsymbol{d} + \boldsymbol{\varepsilon}$$
 (9)

where  $\mathbf{X}$  is an  $n \times I$  marker genotype matrix for n hybrids and I markers associated to trait QTLs and  $\beta$  is the markers fixed effects vector.

To test if G-BLUP model predictions are capturing genetic effects above that explained by population structure, we fitted a simple PC-BLUP model to the same data. In this model, the genotypes coordinates on the first five axes of SNP PCoA of the panels (representing of a cumulative percentage of variance of 35%), were used as predictors. Other genomic prediction models (RR-BLUP, BayesB, BayesC, and BayesR) were also tested but showed no significantly better results than those presented in this paper.

All prediction models were fitted using the Bayesian Generalized Linear Regression (BGLR) R package<sup>73</sup>, based on 60,000 iterations, after discarding 10,000 cycles for burn-in period and using a thinning rate of 5.

#### Training and validation schemes of genomic predictions

Genomic predictions were first evaluated by a 5-fold cross-validation scheme (CV1) repeated 10 times, applied to diversity and genetic progress panels datasets. In CV1, we aimed to measure the ability of the models to predict the performance of hybrids that would not have been evaluated in any of the observed environments<sup>28</sup>. For each iteration, the two panels genotypes were split into 5 subsets, then each subset (one fifth) was predicted using the remaining four fifths as training set. This generated a total of 5 × 10 testing sets. Each training set was sampled randomly but proportionally to 'diversity panel' genetic groups and across years of release of 'genetic progress' hybrids (Supplementary Fig. 4). This sampling method was chosen to maintain

https://doi.org/10.1038/s41467-023-42298-z

a good coverage of the total genetic space covered by the training set<sup>82</sup>. The 'recent hybrids' panel dataset was then considered as an external validation of the prediction models. Here, the 'diversity' and 'genetic progress' panels were used together as training set, and predictions were made for the recent hybrids observed in independent experiments.

Five statistics were calculated to assess the performance of prediction models for each trait: the Pearson (r) and Spearman (rho) correlation coefficients between observed genotypic means (BLUEs over experiments) and predicted values (G-BLUPs), the prediction accuracy of genomic selection (Acc, estimated as the predictive ability (r) divided by the square root of trait genomic heritability<sup>53</sup>), the root mean squared error of predictions (RMSE) showing the discrepancy between predicted and observed values and the coefficient of variation of the error (CV<sub>RMSE</sub>), which is the RMSE expressed as a percentage of mean observed value. For cross-validation scheme, the statistics estimations were performed within each fold and then averaged across folds and iterations. Standard errors (SE) of correlation coefficients were calculated using Bonett and Wright approximations<sup>77</sup>.

#### **Reporting summary**

Further information on research design is available in the Nature Portfolio Reporting Summary linked to this article.

#### Data availability

The data generated in this study have been deposited in the Recherche Data Gouv database [https://recherche.data.gouv.fr/fr]. The datasets for phenotypic and genotypic values for the diversity panel are available at https://doi.org/10.15454/IASSTN. The datasets for phenotypic and genotypic values for the genetic progress panel are available at https://doi.org/10.15454/KLDOGH. The dataset for the 'recent hybrid' panel is available at https://doi.org/10.57745/NZY1KL. Source data are provided with this paper.

#### References

- Tester, M. & Langridge, P. Breeding technologies to increase crop production in a changing world. Science 327, 818–822 (2010).
- 2. McCouch, S. et al. Feeding the future. Nature 499, 23-24 (2013).
- Bassi, F. M., Bentley, A. R., Charmet, G., Ortiz, R. & Crossa, J. Breeding schemes for the implementation of genomic selection in wheat (Triticum spp.). *Plant Sci.* 242, 23–36 (2016).
- Beyene, Y. et al. Application of genomic selection at the early stage of breeding pipeline in tropical maize. Front. Plant Sci. 12, 685488 (2021).
- Krishnappa, G. et al. Integrated genomic selection for rapid improvement of crops. *Genomics* 113, 1070–1086 (2021).
- Lobell, D. B. et al. Greater sensitivity to drought accompanies maize yield increase in the U.S. Midwest. Science 344, 516–519 (2014).
- Challinor, A. J. et al. A meta-analysis of crop yield under climate change and adaptation. *Nat. Clim. Change* 4, 287–291 (2014).
- Parent, B. et al. Maize yields over Europe may increase in spite of climate change, with an appropriate use of the genetic variability of flowering time. *Proc. Natl Acad. Sci.* 115, 10642–10647 (2018).
- Welcker, C. et al. Physiological adaptive traits are a potential allele reservoir for maize genetic progress under challenging conditions. Nat. Commun. 13, 3225 (2022).
- Dignat, G., Welcker, C., Sawkins, M., Ribaut, J. M. & Tardieu, F. The growths of leaves, shoots, roots and reproductive organs partly share their genetic control in maize plants. *Plant Cell Environ.* 36, 1105–1119 (2013).
- 11. Lacube, S. et al. Simulating the effect of flowering time on maize individual leaf area in contrasting environmental scenarios. *J. Exp. Bot.* **71**, 5577–5588 (2020).

- Stuerz, S. & Asch, F. Responses of rice growth to day and night temperature and relative air humidity—leaf elongation and assimilation. *Plants* 10, 134 (2021).
- Langstroff, A., Heuermann, M. C., Stahl, A. & Junker, A. Opportunities and limits of controlled-environment plant phenotyping for climate response traits. Theor. Appl. Genet. 135, 1–16 (2022).
- Prado, S. A. et al. Phenomics allows identification of genomic regions affecting maize stomatal conductance with conditional effects of water deficit and evaporative demand. *Plant Cell Environ*. 41, 314–326 (2018).
- Perez, R. P. A. et al. Changes in the vertical distribution of leaf area enhanced light interception efficiency in maize over generations of selection. *Plant Cell Environ.* 42, 2105–2119 (2019).
- Cabrera-Bosquet, L. et al. High-throughput estimation of incident light, light interception and radiation-use efficiency of thousands of plants in a phenotyping platform. New Phytol. 212, 269–281 (2016).
- Chen, T.-W. et al. Genetic and environmental dissection of biomass accumulation in multi-genotype maize canopies. *J. Exp. Bot.* 70, 2523–2534 (2019).
- Gano, B. et al. Using UAV borne, multi-spectral imaging for the field phenotyping of shoot biomass, leaf area index and height of west african sorghum varieties under two contrasted water conditions. Agronomy 11, 850 (2021).
- 19. Sarkar, S. et al. Aerial high-throughput phenotyping of peanut leaf area index and lateral growth. Sci. Rep. 11, 21661 (2021).
- Blancon, J. et al. A high-throughput model-assisted method for phenotyping maize green leaf area index dynamics using unmanned aerial vehicle imagery. Front. Plant Sci. 10, 685 (2019).
- Baret, F. & Buis, S. Advances in Land Remote Sensing: System, Modeling, Inversion and Application (ed. Liang, S.) 173–201 (Springer Netherlands, 2008).
- 22. Dorigo, W., Richter, R., Baret, F., Bamler, R. & Wagner, W. Enhanced automated canopy characterization from hyperspectral data by a novel two step radiative transfer model inversion approach. *Remote Sens.* **1**, 1139–1170 (2009).
- 23. Fang, H., Baret, F., Plummer, S. & Schaepman-Strub, G. An overview of global Leaf Area Index (LAI): methods, products, validation, and applications. *Rev. Geophys.* **57**, 739–799 (2019).
- 24. Poorter, H. et al. Pampered inside, pestered outside? Differences and similarities between plants growing in controlled conditions and in the field. *New Phytol.* **212**, 838–855 (2016).
- Peirone, L. S., Pereyra Irujo, G. A., Bolton, A., Erreguerena, I. & Aguirrezábal, L. A. N. Assessing the efficiency of phenotyping early traits in a greenhouse automated platform for predicting drought tolerance of soybean in the field. Front. Plant Sci. 9, 587 (2018).
- Cotrozzi, L., Peron, R., Tuinstra, M. R., Mickelbart, M. V. & Couture, J. J. Spectral phenotyping of physiological and anatomical leaf traits related with maize water status. *Plant Physiol.* 184, 1363–1377 (2020).
- 27. Sales, C. R. G. et al. Phenotypic variation in photosynthetic traits in wheat grown under field versus glasshouse conditions. *J. Exp. Bot.* **73**. 3221–3237 (2022).
- de Oliveira, A. A. et al. Genomic prediction applied to multiple traits and environments in second season maize hybrids. *Heredity* 125, 60–72 (2020).
- Fradgley, N. S., Gardner, K., Kerton, M., Swarbreck, S. M. & Bentley,
   A. R. Trade-offs in the genetic control of functional and nutritional quality traits in UK winter wheat. *Heredity* 128, 420–433 (2022).
- 30. Hammer, G. L. et al. Adapting APSIM to model the physiology and genetics of complex adaptive traits in field crops. *J. Exp. Bot.* **61**, 2185–2202 (2010).
- Millet, E. J. et al. Genomic prediction of maize yield across European environmental conditions. Nat. Genet. 51, 952–956 (2019).

- 32. Rose, T. & Kage, H. The contribution of functional traits to the breeding progress of central-european winter wheat under differing crop management intensities. *Front. Plant Sci.* **10**, 1521 (2019).
- 33. Watson, A. et al. Speed breeding is a powerful tool to accelerate crop research and breeding. *Nat. Plants* **4**, 23–29 (2018).
- 34. Alahmad, S. et al. Speed breeding for multiple quantitative traits in durum wheat. *Plant Methods* **14**, 36 (2018).
- 35. Samantara, K. et al. Breeding more crops in less time: a perspective on speed breeding. *Biology (Basel)* 11, 275 (2022).
- Watson, A. et al. Multivariate genomic selection and potential of rapid indirect selection with speed breeding in spring wheat. *Crop Sci.* 59, 1945–1959 (2019).
- Tardieu, F., Simonneau, T. & Muller, B. The physiological basis of drought tolerance in crop plants: a scenario-dependent probabilistic approach. *Annu. Rev. Plant Biol.* 69, 733–759 (2018).
- 38. de los Campos, G. & Grüneberg, A. MTM (Multiple-Trait Model) R package (2016).
- Pérez-Rodríguez, P. & de los Campos, G. Multitrait Bayesian shrinkage and variable selection models with the BGLR-R package. Genetics 222, iyac112 (2022).
- Wisser, R. J. et al. Multivariate analysis of maize disease resistances suggests a pleiotropic genetic basis and implicates a GST gene. *Proc. Natl Acad. Sci. USA* 108, 7339–7344 (2011).
- 41. Casa, R. et al. Estimation of maize canopy properties from remote sensing by inversion of 1-D and 4-D models. *Precis. Agric.* **11**, 319–334 (2010).
- Berger, K. et al. Evaluation of the PROSAIL model capabilities for future hyperspectral model environments: a review study. *Remote Sens.* 10, 85 (2018).
- Welcker, C. et al. A common genetic determinism for sensitivities to soil water deficit and evaporative demand: meta-analysis of quantitative trait loci and introgression lines of maize. *Plant Physiol.* 157, 718–729 (2011).
- Lacube, S. et al. Distinct controls of leaf widening and elongation by light and evaporative demand in maize. *Plant Cell Environ.* 40, 2017–2028 (2017).
- Garriques, S. et al. Intercomparison and sensitivity analysis of Leaf Area Index retrievals from LAI-2000, AccuPAR, and digital hemispherical photography over croplands. *Agric. For. Meteorol.* 148, 1193–1209 (2008).
- Tardieu, F., Cabrera-Bosquet, L., Pridmore, T. & Bennett, M. Plant phenomics, from sensors to knowledge. *Curr. Biol.* 27, R770–R783 (2017).
- Monteith, J. L. Validity of the correlation between intercepted radiation and biomass. Agric. For. Meteorol. 68, 213–220 (1994).
- Parent, B., Turc, O., Gibon, Y., Stitt, M. & Tardieu, F. Modelling temperature-compensated physiological rates, based on the coordination of responses to temperature of developmental processes. J. Exp. Bot. 61, 2057–2069 (2010).
- Kumudini, S. et al. Predicting maize phenology: intercomparison of functions for developmental response to temperature. *Agron. J.* 106, 2087–2097 (2014).
- 50. Cooper, M. et al. Use of crop growth models with whole-genome prediction: application to a maize multienvironment trial. *Crop Sci.* **56**, 2141–2156 (2016).
- 51. Toda, Y. et al. Predicting biomass of rice with intermediate traits: Modeling method combining crop growth models and genomic prediction models. *PLoS ONE* **15**, e0233951 (2020).
- 52. Lopez-Cruz, M. et al. Regularized selection indices for breeding value prediction using hyper-spectral image data. *Sci. Rep.* **10**, 8195 (2020).
- 53. Lorenzana, R. E. & Bernardo, R. Accuracy of genotypic value predictions for marker-based selection in biparental plant populations. *Theor. Appl. Genet.* **120**, 151–161 (2009).

- 54. Ben Hassen, M., Bartholomé, J., Valè, G., Cao, T.-V. & Ahmadi, N. Genomic prediction accounting for genotype by environment interaction offers an effective framework for breeding simultaneously for adaptation to an abiotic stress and performance under normal cropping conditions in rice. G3 Genes|Genomes|Genet. 8, 2319–2332 (2018).
- 55. Yuan, Y. et al. Genome-wide association mapping and genomic prediction analyses reveal the genetic architecture of grain yield and flowering time under drought and heat stress conditions in maize. *Front. Plant Sci.* **9**, 1919 (2019).
- 56. Guo, J. et al. Increased prediction accuracy using combined genomic information and physiological traits in a soft wheat panel evaluated in multi-environments. *Sci. Rep.* **10**, 7023 (2020).
- 57. Parent, B., Vile, D., Violle, C. & Tardieu, F. Towards parsimonious ecophysiological models that bridge ecology and agronomy. *New Phytol.* **210**, 380–382 (2016).
- 58. Martre, P. et al. Multimodel ensembles of wheat growth: many models are better than one. *Glob. Change Biol.* **21**, 911–925 (2015).
- 59. Lockhart, J. A. An analysis of irreversible plant cell elongation. *J. Theor. Biol.* **8**, 264–275 (1965).
- 60. Tardieu, F., Parent, B., Caldeira, C. F. & Welcker, C. Genetic and physiological controls of growth under water deficit. *Plant Physiol.* **164**, 1628–1635 (2014).
- Caldeira, C. F. et al. A hydraulic model is compatible with rapid changes in leaf elongation under fluctuating evaporative demand and soil water status. *Plant Physiol.* 164, 1718–1730 (2014).
- 62. Sharp, R. E. et al. Root growth maintenance during water deficits: physiology to functional genomics\*. *J. Exp. Bot.* **55**, 2343–2351 (2004).
- Schnyder, H. & Nelson, C. J. Diurnal growth of tall fescue leaf blades: i. spatial distribution of growth, deposition of water, and assimilate import in the elongation zone. *Plant Physiol.* 86, 1070–1076 (1988).
- 64. Tardieu, F., Simonneau, T. & Parent, B. Modelling the coordination of the controls of stomatal aperture, transpiration, leaf growth, and abscisic acid: update and extension of the Tardieu-Davies model. *J. Exp. Bot.* **66**, 2227–2237 (2015).
- Farquhar, G. D., von Caemmerer, S. & Berry, J. A. A biochemical model of photosynthetic CO2 assimilation in leaves of C3 species. *Planta* 149, 78–90 (1980).
- Wu, A., Hammer, G. L., Doherty, A., von Caemmerer, S. & Farquhar,
   G. D. Quantifying impacts of enhancing photosynthesis on crop yield. *Nat. Plants* 5, 380–388 (2019).
- 67. Negro, S. S. et al. Genotyping-by-sequencing and SNP-arrays are complementary for detecting quantitative trait loci by tagging different haplotypes in association studies. *BMC Plant Biol.* **19**, 318 (2019).
- 68. Brichet, N. et al. A robot-assisted imaging pipeline for tracking the growths of maize ear and silks in a high-throughput phenotyping platform. *Plant Methods* **13**, 96 (2017).
- 69. Pérez-Valencia, D. M. et al. A two-stage approach for the spatiotemporal analysis of high-throughput phenotyping data. *Sci. Rep.* **12**, 3177 (2022).
- 70. van Eeuwijk, F. A. et al. Modelling strategies for assessing and increasing the effectiveness of new phenotyping techniques in plant breeding. *Plant Sci.* **282**, 23–39 (2019).
- 71. Millet, E. J. et al. statgenHTP: High Throughput Phenotyping (HTP) Data Analysis R package version 1.0.4 (2022).
- 72. Vitezica, Z. G., Legarra, A., Toro, M. A. & Varona, L. Orthogonal estimates of variances for additive, dominance, and epistatic effects in populations. *Genetics* **206**, 1297–1307 (2017).
- Pérez, P. & de los Campos, G. Genome-wide regression and prediction with the BGLR statistical package. Genetics 198, 483–495 (2014).

#### **Article**

- Duan, S.-B. et al. Inversion of the PROSAIL model to estimate leaf area index of maize, potato, and sunflower fields from unmanned aerial vehicle hyperspectral data. *Int. J. Appl. Earth Obs. Geoinf.* 26, 12–20 (2014).
- Jacquemoud, S. et al. PROSPECT + SAIL models: a review of use for vegetation characterization. *Remote Sens. Environ.* 113, S56–S66 (2009).
- Jiao, Q. et al. A random forest algorithm for retrieving canopy chlorophyll content of wheat and soybean trained with prosail simulations using adjusted average leaf angle. *Remote Sens.* 14, 98 (2021).
- 77. Bonett, D. G. & Wright, T. A. Sample size requirements for estimating pearson, kendall and spearman correlations. *Psychometrika* **65**, 23–28 (2000).
- 78. Unterseer, S. et al. A powerful tool for genome analysis in maize: development and evaluation of the high-density 600 k SNP genotyping array. *BMC Genomics* **15**, 823 (2014).
- 79. Browning, B. L., Zhou, Y. & Browning, S. R. A one-penny imputed genome from next-generation reference panels. *Am. J. Hum. Genet.* **103**, 338–348 (2018).
- 80. Granato, I. S. C. et al. snpReady: a tool to assist breeders in genomic analysis. *Mol. Breed.* **38**, 102 (2018).
- 81. González-Diéguez, D. et al. Genomic prediction of hybrid crops allows disentangling dominance and epistasis. *Genetics* **218**, iyab026 (2021).
- 82. Bustos-Korts, D. et al. Combining crop growth modeling and statistical genetic modeling to evaluate phenotyping strategies. *Front. Plant Sci.* **10**, 1491 (2019).

#### **Acknowledgements**

This work was supported by the ANR projects ANR-10-BTBR-01 (Amaizing) and ANR-11-INBS-0012 (Phenome), by an ANRT CIFRE funding 2020/1238, and by INRAE and ARVALIS. Authors are grateful to M. Lis, R. Le Roy, B. Suard, and M. Combes for their technical assistance in the PhenoArch experiment, as well as to key persons from the 2021 and 2022 field experiments at ARVALIS, namely Y. Pousset, P. Raccurt, S. Bourrely, F. Binet, D. Lasserre, L. Pligot, C. Huet, M. Heredia, L. Diez, C. Drillaud, and B. Baron. We are also grateful to I. Granato, N. Abu-Samra Spencer, E. Millet, S. Prado, and C. Fournier for their help with data analysis or advice for R packages.

#### **Author contributions**

J.B., L.M., C.W., M.B., F.T., and M.B. designed research. J.B. performed experiments, supervised by K.B., N.M., C.W., M.B., and F.T. Ll.C.B. and

R.C. performed the experiments. J.B., L.M., C.W., and M.B. performed genomic analyses. J.B., C.W., and F.T. performed phenotypic and modeling analyses. F.T., J.B., C.W., L.M., and M.B. wrote the paper.

#### **Competing interests**

The authors declare no competing interests.

#### **Additional information**

**Supplementary information** The online version contains supplementary material available at https://doi.org/10.1038/s41467-023-42298-z.

**Correspondence** and requests for materials should be addressed to François Tardieu.

**Peer review information** *Nature Communications* thanks Lee Hickey and the other, anonymous, reviewer(s) for their contribution to the peer review of this work. A peer review file is available.

**Reprints and permissions information** is available at http://www.nature.com/reprints

**Publisher's note** Springer Nature remains neutral with regard to jurisdictional claims in published maps and institutional affiliations.

Open Access This article is licensed under a Creative Commons Attribution 4.0 International License, which permits use, sharing, adaptation, distribution and reproduction in any medium or format, as long as you give appropriate credit to the original author(s) and the source, provide a link to the Creative Commons licence, and indicate if changes were made. The images or other third party material in this article are included in the article's Creative Commons licence, unless indicated otherwise in a credit line to the material. If material is not included in the article's Creative Commons licence and your intended use is not permitted by statutory regulation or exceeds the permitted use, you will need to obtain permission directly from the copyright holder. To view a copy of this licence, visit <a href="http://creativecommons.org/licenses/by/4.0/">http://creativecommons.org/licenses/by/4.0/</a>.

© The Author(s) 2023

## Supplementary Table 1. Panels of hybrids and corresponding experiments with analysed traits in this study.

Panel	Hybrid number	Composition 6	Indoor experiments number	Used traits in indoor experiments	Field experiments number	Used traits in field experiments	More info in
Diversity	246	246 dent lines x flint line UH007	4	LAR, LER, gs, rh <sub>PAD</sub> , Leaf dimensions	25	Duration of vegetative phase, Leaf dimensions	https://doi.org/10.1038/s41588- 019-0414-y
Genetic progress	56	Successful hybrids released from 1950 to 2015	4	LAR, LER, gs, rh <sub>PAD</sub> , LER sensitivity to VPD & SWP, Final leaf number	26	Duration of vegetative phase, ALA, LAI	https://doi.org/10.15454/KLD0GH
Recent hybrids	86	Recent hybrids released from 2008 to 2020	1*	LAR, LER, rh <sub>PAD</sub>	4	Duration of vegetative phase, LAR, ALA	https://data.inra.fr/dataset.xhtml? persistentId=doi:10.15454/IASSTN

\*One indoor platform experiment with a subset of 20 recent hybrids. LAR: Leaf Appearance Rate. LER: Leaf Expansion Rate. gs: Stomatal Conductance. rh<sub>PAD</sub>: relative height at 50% of leaf area. Leaf dimensions: length and width. VPD: Vapour-pressure deficit. ALA: Average Leaf inclination Angle. LAI: Leaf Area Index. Detailed information for hybrids and experiments used for the diversity panel and the genetic progress panel are available at the URLs provided in this table.

## Supplementary Table 2. Experiments performed for the 'recent hybrids' panel and Experiments carried out at Field 5, Field 6 & Indoor for 'genetic progress' panel

Panel	Name	Туре	Location	GPS Coord.	Year	Treatment	#	Maturity	Measured traits
	exp.	Field	Matzenheim	48.401, 7.617	2022	ww	Hyb 53	groups G2, G3	LAR, Emergence, Anthesis & Silking dates, Leaf 6 dimensions, Plant density, Final leaf number, Yield & its components
	Field 2	Field	Saint Bonnet de Mure	45.714, 5.046	2022	WW, WD	58	G3, G4	ALA, LAI, fiPAR, Emergence, Anthesis & Silking dates, Plant density, Final leaf number, Yield & its components
Recent hybrids panel	Field 3	Field	Binas	47.919, 1.478	2022	ww	86	G2, G3, G4	LAR, Emergence, Anthesis & Silking dates, Leaf 6 dimensions, Plant density, Final leaf number, Yield & its components
	Field 4	Field	Pusignan	45.741, 5.075	2021	ww	54	G3, G4	ALA, LAI, fiPAR, Emergence, Plant density
	Indoor 1	Indoor Platform	Montpellier	43.618, 3.857	2021	WW, WD	20	G2, G3, G4	Leaf area, Biomass, LAR, LER, Plant architecture variables (rh <sub>PAD</sub> )
	Field 5	Field	Mauguio	43.611, 3.971	2017	WW, WD	56	G2, G3, G4	ALA, LAI, fiPAR, Emergence, Anthesis & Silking dates, Plant density, Final leaf number, Yield & its components
Genetic progress panel	Field 6	Field	Mauguio	43.610, 3.980	2010	WW, WD	44	G2, G3, G4	LAR, Emergence, Anthesis & Silking dates, Plant density, Final leaf number, Yield & its components
	Indoor 2	Indoor Platform	Montpellier	43.618, 3.857	2017	WW, WD	56	G2, G3, G4	Leaf area, Biomass, LAR, LER, gs, Plant architecture variables (rh <sub>PAD</sub> ), LER sensitivity to VPD & SWP, Final leaf number

Name exp.: Experiment name used in the text; Year, year when the experiment was done. Treatment: WW, imposed well-watered (controlled by sensors). WD, imposed water deficit (controlled by sensors)

Supplementary Table 3. Summary of variance components and genomic heritability estimated in the experiments considered in this study

Traits	Unit	Experiments	# Hyb	Mean value	h <sub>g</sub> <sup>2</sup>	$\sigma_g^{\ 2}$	$\sigma_a^{\ 2}$	$\sigma_d^{\ 2}$	$\sigma_e^{\ 2}$
		Indoor 2	44	0.275	0.64	1.9E-04	1.1E-04	8.0E-05	1.1E-04
		Field 6	44	0.281	0.61	7.7E-04	4.3E-04	3.3E-04	4.9E-04
Leaf Appearance	leaf/ day <sub>20°C</sub>	Indoor 1	21	0.271	0.58	2.7E-04	1.4E-04	1.3E-04	2.0E-04
Rate (LAR)	ieai/ day <sub>20°C</sub>	Field 3	26	0.260	0.53	1.5E-04	7.6E-05	7.2E-05	1.3E-04
		Field 5	44	0.287	0.64	4.6E-04	2.8E-04	1.8E-04	2.6E-04
		Field 1	26	0.262	0.53	1.3E-04	6.3E-05	7.1E-05	1.2E-04
		Field 5	44	63.5	0.68	9.52	6.29	3.23	4.57
		Field 6	44	62.6	0.68	11.55	7.77	3.78	5.39
Duration of the vegetative phase	days <sub>20°C</sub>	Field 1	53	63.8	0.62	3.88	1.94	1.94	2.39
		Field 3	55	62.9	0.58	3.23	1.69	1.54	2.37
		Field 2	55	68.2	0.62	3.24	1.60	1.65	1.96
		rh <sub>PAD</sub> Indoor 2	56	0.277	0.69	1.3E-03	9.1E-04	4.4E-04	6.1E-04
rh <sub>PAD</sub> (relative height at 50% of leaf area)	rh <sub>PAD</sub>	ALA Field 5	56	54.33	0.70	2.05	1.38	0.67	0.87
VS	(unitless),	rh <sub>PAD</sub> Indoor 1	18	0.344	0.54	1.1E-03	5.8E-04	5.5E-04	9.5E-04
ALA (Average Leaf inclination Angle)	ALA (°)	ALA Field 4	18	67.24	0.56	0.84	0.43	0.40	0.67
		ALA Field 2	18	60.27	0.57	3.19	1.64	1.55	2.42
Leaf Area Index		LAI Indoor 2 (+Crop model)	51	3.62	0.63	0.34	0.22	0.12	0.20
(LAI)	unitless	LAI Field 5 (UAV)	51	3.67	0.68	0.11	0.07	0.04	0.05

#Hyb, number of hybrids.  $h_g^2$ , genomic heritability.  $\sigma_g^2$ , total genetic variance.  $\sigma_a^2$  and  $\sigma_d^2$ , variances explained by additive and dominance relationship matrices, respectively.  $\sigma_e^2$ , residual variance.

## Supplementary Table 4. Summary of correlation analysis and accuracy results estimated between experiments genotypic values for four traits

Traits	Unit	Experiments	# Hyb	r	rho	Mean value	RMSE	CV <sub>RMSE</sub>	Bias	$CV_Bias$	FSA to the highest quartile	FSA to the lowest quartile	iAcc
		Indoor 2 VS Field 6	44	0.73 ± 0.07	0.68 ± 0.09	0.275	0.025	9.0%	0.006	2.1%	0.63	0.72	0.55 ± 0.11
Leaf Appearance	leaf/ day <sub>20°C</sub>	Indoor 1 VS Field 3	21	0.57 ± 0.16	0.42 ± 0.20	0.259	0.020	7.7%	-0.012	-4.5%	0.60	0.40	0.33 ± 0.21
Rate (LAR)	ieai/ day <sub>20°C</sub>	Field 5 VS Field 6	44	0.71 ± 0.08	0.43 ± 0.13	0.287	0.024	8.4%	-0.006	-2.0%	0.50	0.75	0.52 ± 0.11
		Field 1 VS Field 3	26	0.49 ± 0.16	0.35 ± 0.19	0.260	0.014	5.3%	-0.001	-0.3%	0.50	0.33	0.30 ± 0.19
		Field 5 VS Field 6	44	0.88 ± 0.04	0.91 ± 0.03	63.5	2.2	3.5%	-0.95	-1.5%	0.81	0.72	0.63 ± 0.09
Duration of the vegetative phase	days <sub>20°C</sub>	Field 1 VS Field 3	53	0.69 ± 0.07	0.66 ± 0.09	61.7	2.7	4.4%	-1.94	-3.2%	0.54	0.62	0.47 ± 0.11
		Field 2 VS Field 3	55	0.47 ± 0.11	0.37 ± 0.12	64.1	4.5	7.0%	-4.05	-6.3%	0.60	0.37	0.31 ± 0.12
		rh <sub>PAD</sub> Indoor 2 VS ALA Field 5	56	0.77 ± 0.06	0.77 ± 0.06	0.28					0.71	0.57	0.55 ± 0.10
rh <sub>PAD</sub> (relative height at 50% of leaf area) VS	rh <sub>PAD</sub>	rh <sub>PAD</sub> Indoor 1 VS ALA Field 4	18	0.58 ± 0.17	0.51 ± 0.20	0.34	Irrelev	ant (two comp		t traits	0.60	0.60	0.33 ± 0.23
ALA (Average Leaf inclination Angle)	(unitless), ALA (°)	rh <sub>PAD</sub> Indoor 1 VS ALA Field 2	18	0.60 ± 0.17	0.60 ± 0.18	0.34					0.60	0.60	0.37 ± 0.22
		ALA Field 4 VS ALA Field 2	18	0.50 ± 0.19	0.42 ± 0.22	67.2	7.2	10.7%	-6.97	-10.4%	0.60	0.60	0.31 ± 0.23
Leaf Area Index	itlaaa	LAI Indoor 2 (+Crop model) VS LAI Field 5_WW (UAV)	51	0.64 ± 0.09	0.66 ± 0.09	3.61	0.57	15.7%	0.06	1.7%	0.45	0.61	0.44 ± 0.12
(LAI)	unitless	LAI Indoor 2 (+Crop model) VS LAI Field 5_WD (UAV)	51	0.44 ± 0.11	0.43 ± 0.12	2.74	0.54	19.6%	-0.20	-7.2%	0.33	0.50	0.31 ± 0.13

r, Pearson correlation coefficient. SE r, Standard Error of r. rho, Spearman correlation coefficient. SE rho, Standard Error of rho. e. RMSE, Root Mean Square Error. CV<sub>RMSE</sub>, RMSE Coefficient of Variation. CV<sub>Bias</sub>, Bias Coefficient of Variation. FSA to the highest quartile, Frequency of Similar Assignment to the highest quartile between experiments for each trait. FSA to the lowest quartile, Frequency of Similar Assignment to the lowest quartile between experiments for each trait. iAcc, Theoretical accuracy of indirect selection, i.e. in case of indirect selection based on trait observed values in a given experiment (indoor or in a field), calculated as the genetic correlation between the considered couple of experiments multiplied by the square root of trait genomic heritability in the reference experiment for selection selection (SE) estimates are shown after the ± symbol.

## Supplementary Table 5. Summary of G-BLUP genomic prediction results in cross-validation and external validation schemes

		(		fold Cros		ation gress panels	)			External Recent hy			
Trait	Unit	# Hyb	Mean r	Mean rho	Mean RMSE	Observed mean value	Mean CV <sub>RMSE</sub> (%)	# Hyb	r	rho	RMSE	Observed mean value	CV <sub>RMSE</sub> (%)
Leaf Appearance Rate (LAR)	leaf/ day <sub>20°C</sub>	302	0.58 ± 0.09	0.55 ± 0.10	0.013	0.254	5.2	50	0.53 ± 0.10	0.48 ± 0.12	0.007	0.262	2.8
Duration of the vegetative phase	days <sub>20°C</sub>	302	0.84 ± 0.04	0.81 ± 0.05	1.8	67.3	2.7	60	0.71 ± 0.07	0.68 ± 0.08	1.6	64.6	2.5
rh <sub>PAD</sub> (relative height at 50% of leaf area)	unitless	302	0.65 ± 0.08	0.57 ± 0.10	0.029	0.303	9.4	20	0.42 ± 0.20	0.35 ± 0.22	0.056	0.356	15.6
Stomatal conductance (gs <sub>max</sub> )	mmol/ m²/s	302	0.56 ± 0.09	0.53 ± 0.10	9.30	110.40	8.4			Missi	ng data		
Leaf Expansion Rate (LER)	cm²/ day <sub>20°C</sub>	302	0.76 ± 0.06	0.75 ± 0.06	12.17	140.12	8.7	20	0.34 ± 0.21	0.34 ± 0.22	20.75	146.91	14.1

Mean r, Mean rho, Mean RMSE, Mean  $CV_{RMSE}$ : Pearson & Spearman correlation coefficients, Root Mean Square Error and RMSE Coefficient of Variation, respectively, estimated between G-BLUP predicted values and measured values, averaged across folds and 10 iterations in a cross-validation scheme including diversity and genetic progress panels. r, rho, RMSE,  $CV_{RMSE}$ : Pearson & Spearman correlation coefficients, Root Mean Square Error and RMSE Coefficient of Variation, respectively, estimated between G-BLUP predicted values (with training on diversity and genetic progress panels) and measured values in recent hybrids panel, used as external validation. Standard error (SE) estimates  $^{76}$  are shown after the  $\pm$  symbol.

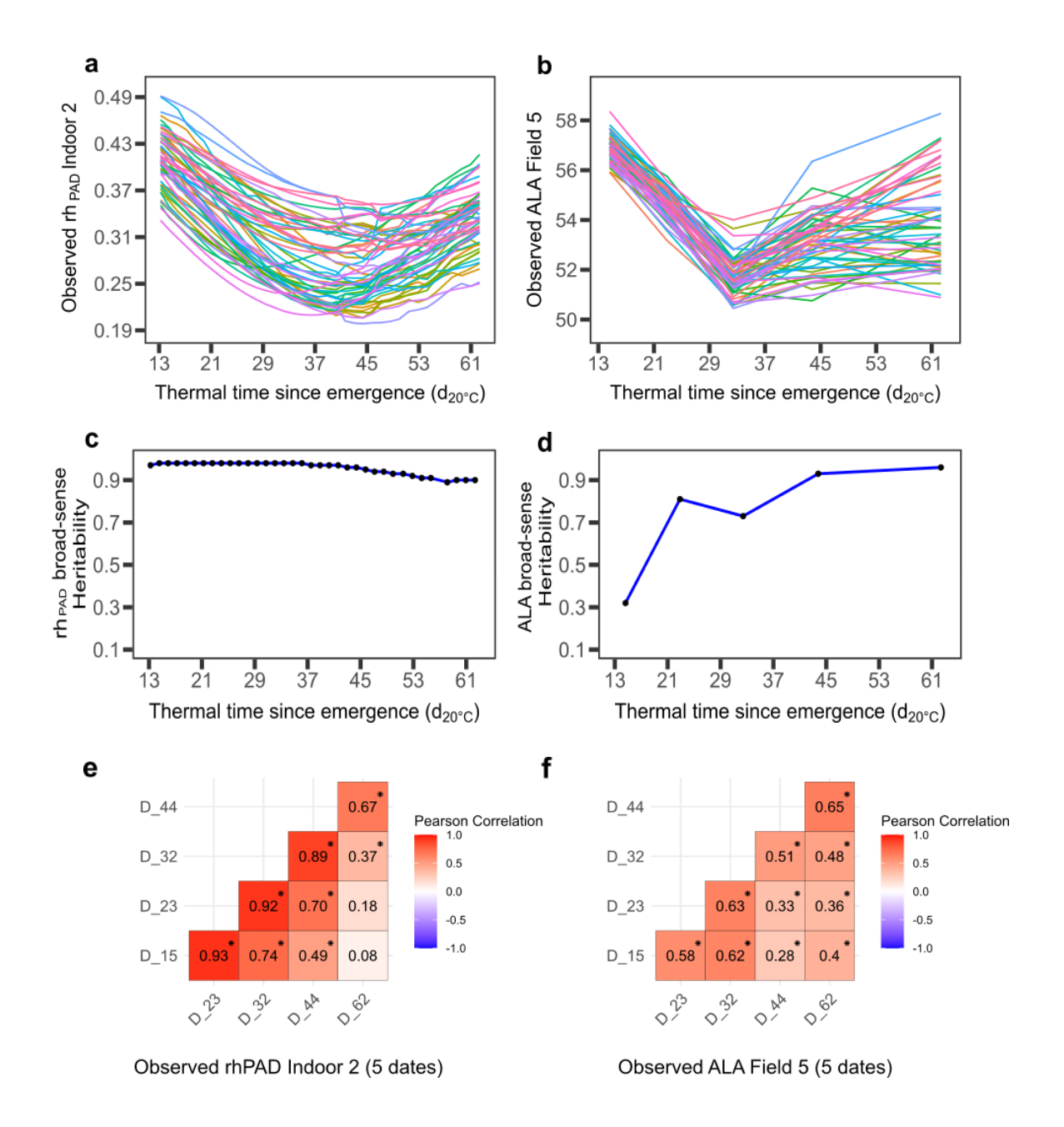
## Supplementary Table 6. Summary of PC-BLUP model prediction results in cross-validation and external validation schemes

<b>-</b>				fold Cros		ation gress panels	)			External Recent hy			
Trait	Unit	# Hyb	Mean r	Mean rho	Mean RMSE	Observed mean value	Mean CV <sub>RMSE</sub> (%)	# Hyb	r	rho	RMSE	Observed mean value	CV <sub>RMSE</sub> (%)
Leaf Appearance Rate (LAR)	leaf/ day <sub>20°C</sub>	302	0.53 ± 0.10	0.50 ± 0.11	0.014	0.254	5.4	50	0.11 ± 0.14	0.16 ± 0.14	0.011	0.262	4.1
Duration of the vegetative phase	days <sub>20°C</sub>	302	0.72 ± 0.06	0.64 ± 0.09	2.3	67.3	3.4	60	0.11 ± 0.13	0.10 ± 0.13	2.7	64.6	4.2
rh <sub>PAD</sub> (relative height at 50% of leaf area)	unitless	302	0.58 ± 0.09	0.45 ± 0.11	0.030	0.303	10.0	20	-0.21 ± 0.09	-0.19 ± 0.11	0.056	0.356	15.7
Stomatal conductance (gs <sub>max</sub> )	mmol/ m²/s	302	0.41 ± 0.11	0.30 ± 0.12	10.09	110.40	9.1			Missi	ng data		
Leaf Expansion Rate (LER)	cm²/ day <sub>20°C</sub>	302	0.61 ± 0.08	0.47 ± 0.11	15.26	140.12	10.9	20	0.25 ± 0.23	0.18 ± 0.24	17.80	146.91	12.1

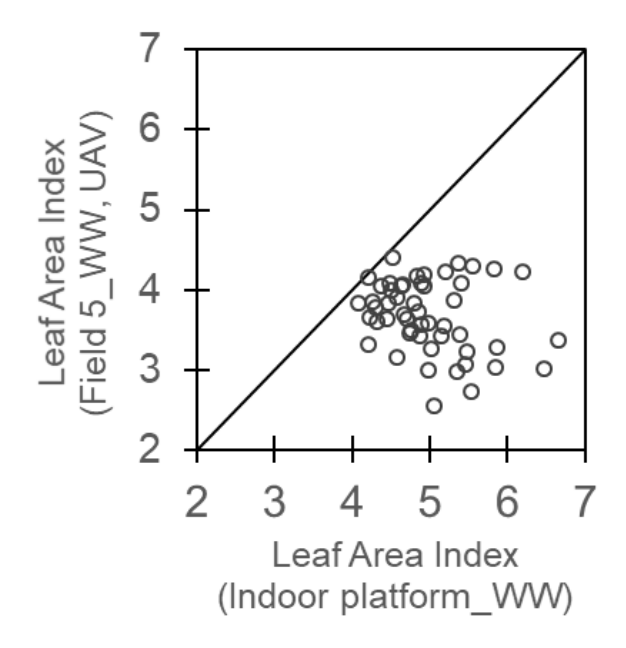
Mean r, Mean rho, Mean RMSE, Mean  $CV_{RMSE}$ : Pearson & Spearman correlation coefficients, Root Mean Square Error and RMSE Coefficient of Variation, respectively, estimated between PC-BLUP predicted values and measured values, averaged across folds and 10 iterations in a cross-validation scheme including diversity and genetic progress panels. r, rho, RMSE,  $CV_{RMSE}$ : Pearson & Spearman correlation coefficients, Root Mean Square Error and RMSE Coefficient of Variation, respectively, estimated between PC-BLUP predicted values (with training on diversity and genetic progress panels) and measured values in recent hybrids panel, used as external validation. Standard error (SE) estimates are shown after the  $\pm$  symbol.

Supplementary Table 7. Diversity analysis of the studied panels using Nei's index of genetic diversity and observed heterozygosity level, based on 440 000 polymorphic SNP markers.

	Nei's Genetic Diversity Index	Observed Heterozygoty
Diversity Panel (246 Parental Dent Lines)	0.45	0.00
Diversity Panel (246 Hybrids : Dent Lines x UH007)	0.31	0.44
Genetic Progress Panel (56 Hybrids)	0.36	0.38
Recent Hybrids Panel (86 Hybrids)	0.31	0.35

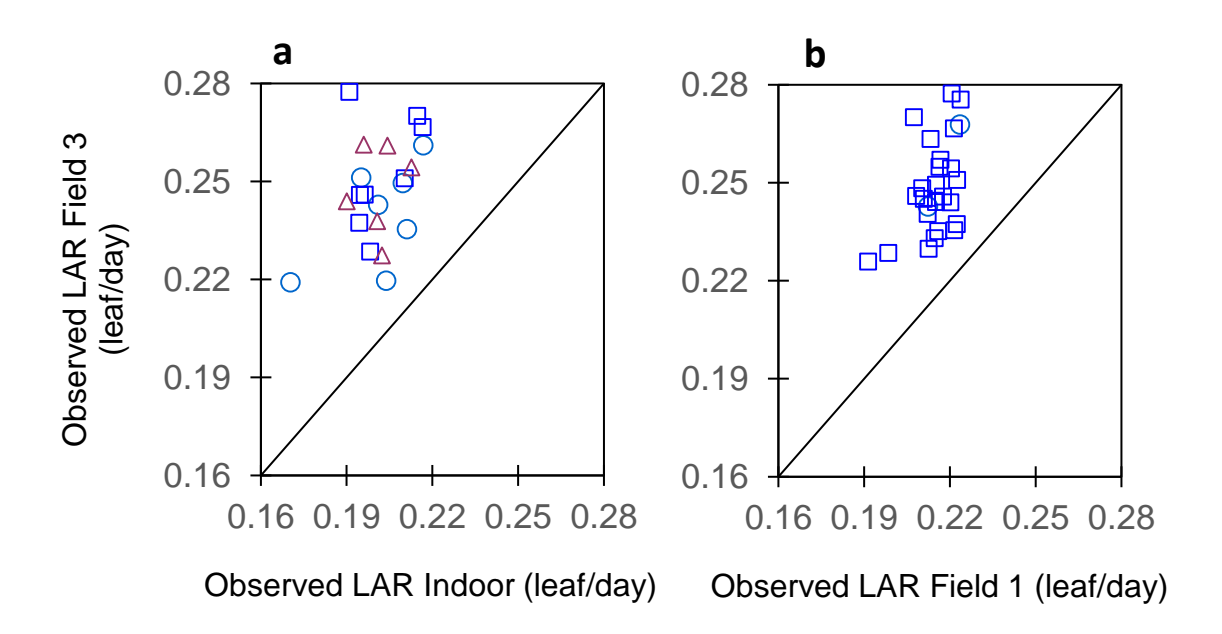


Supplementary Fig. 1. Time courses and broad-sense heritability over time of genotypic values of the architectural traits (rh<sub>PAD</sub> and ALA) and their correlation heat maps for 5 dates. a & b, Time courses of rh<sub>PAD</sub> observed in indoor plarform and ALA observed in the field until flowering. c & d, Broad-sense heritability over thermal time for rh<sub>PAD</sub> and ALA. e & f, Heat map of Pearson correlations between 5 thermal time points for rh<sub>PAD</sub> and ALA trait. rh<sub>PAD</sub>, relative altitude, from the top of the plant, where 50% of leaf area is reached <sup>15</sup>. ALA: average leaf inclination angle estimated from UAV images, via inversion of the model PROSAIL <sup>42,75</sup>. In a & b, lines represent 56 different hybrids. In e & f, statistically significant correlations are shown with an asterisk.

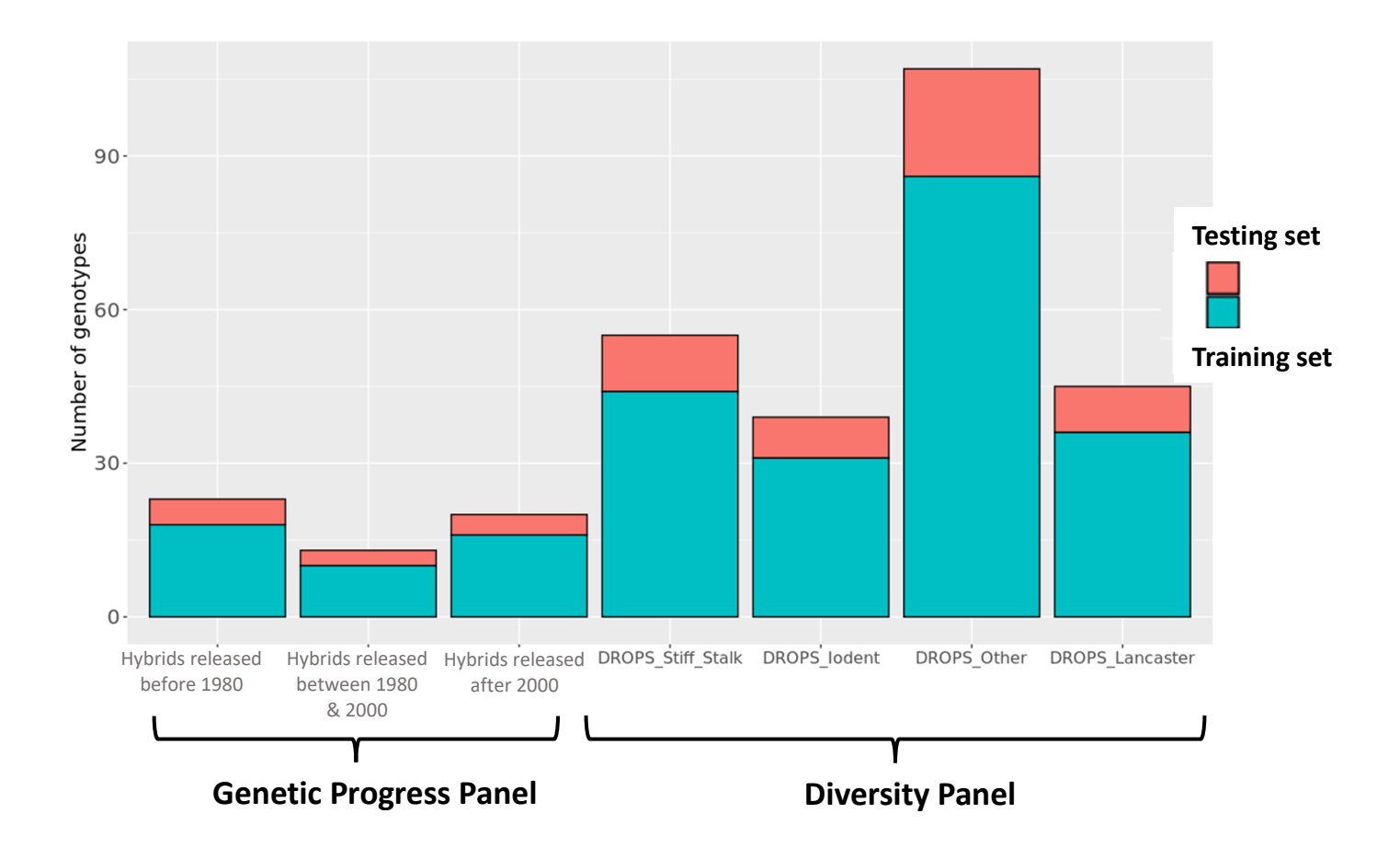


Supplementary Fig. 2. Genotypic values of leaf area index (LAI) measured in the field in well-watered condition were not correlated to LAI values calculated by considering only plant leaf area measured indoor.

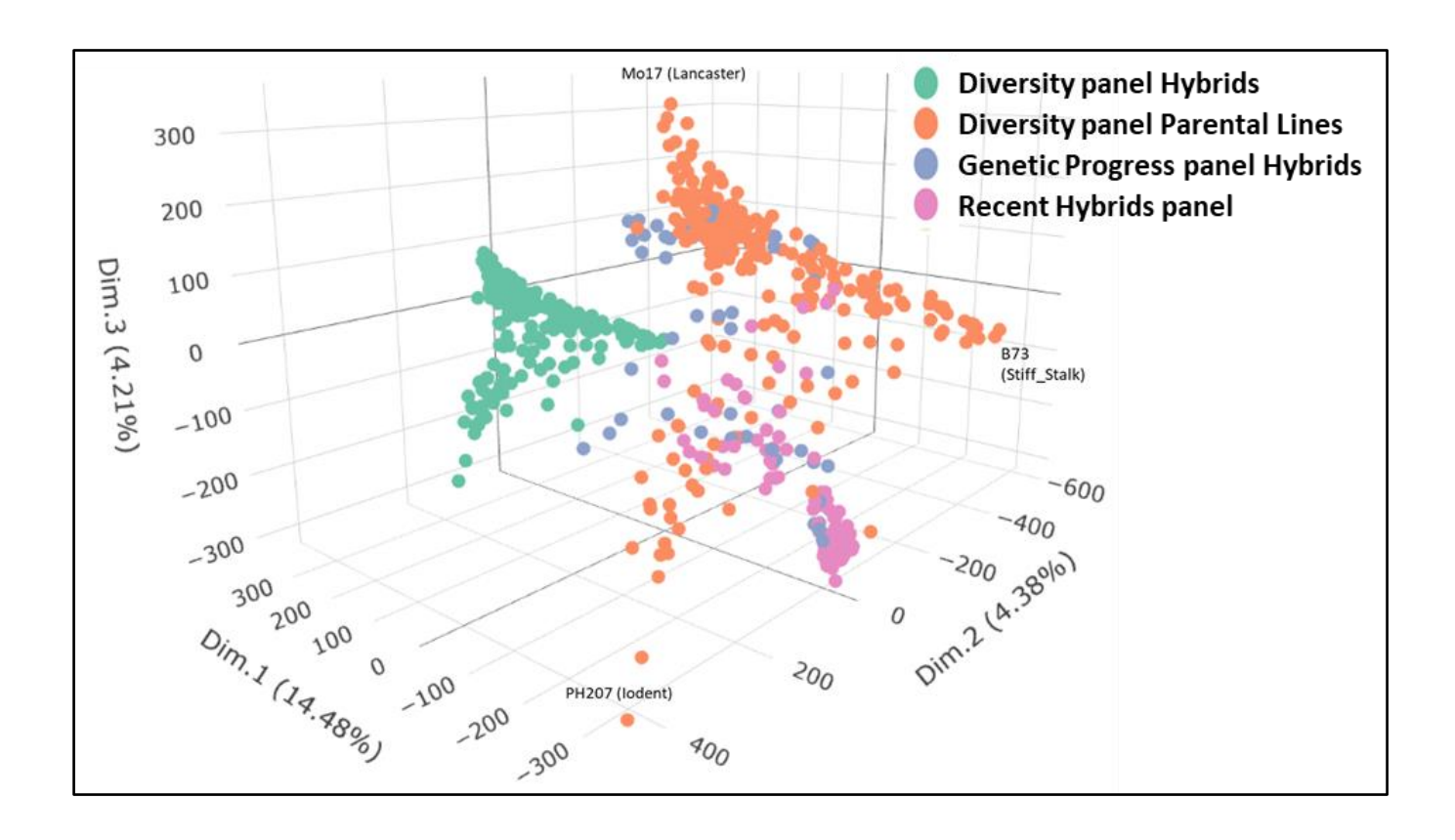
Field values (on y-axis) were obtained at flowering time from UAV images via inversion of the model PROSAIL  $^{41,42}$ . Values on x-axis were calculated as plant leaf area measured indoor at flowering time, multiplied by the plant density in the corresponding field. Each point represents a couple of observed genotypic values for one different hybrid of genetic progress panel. r = -0.25, n=51, p-value = 0.073,  $CV_{RMSF}$  = 30.9%.



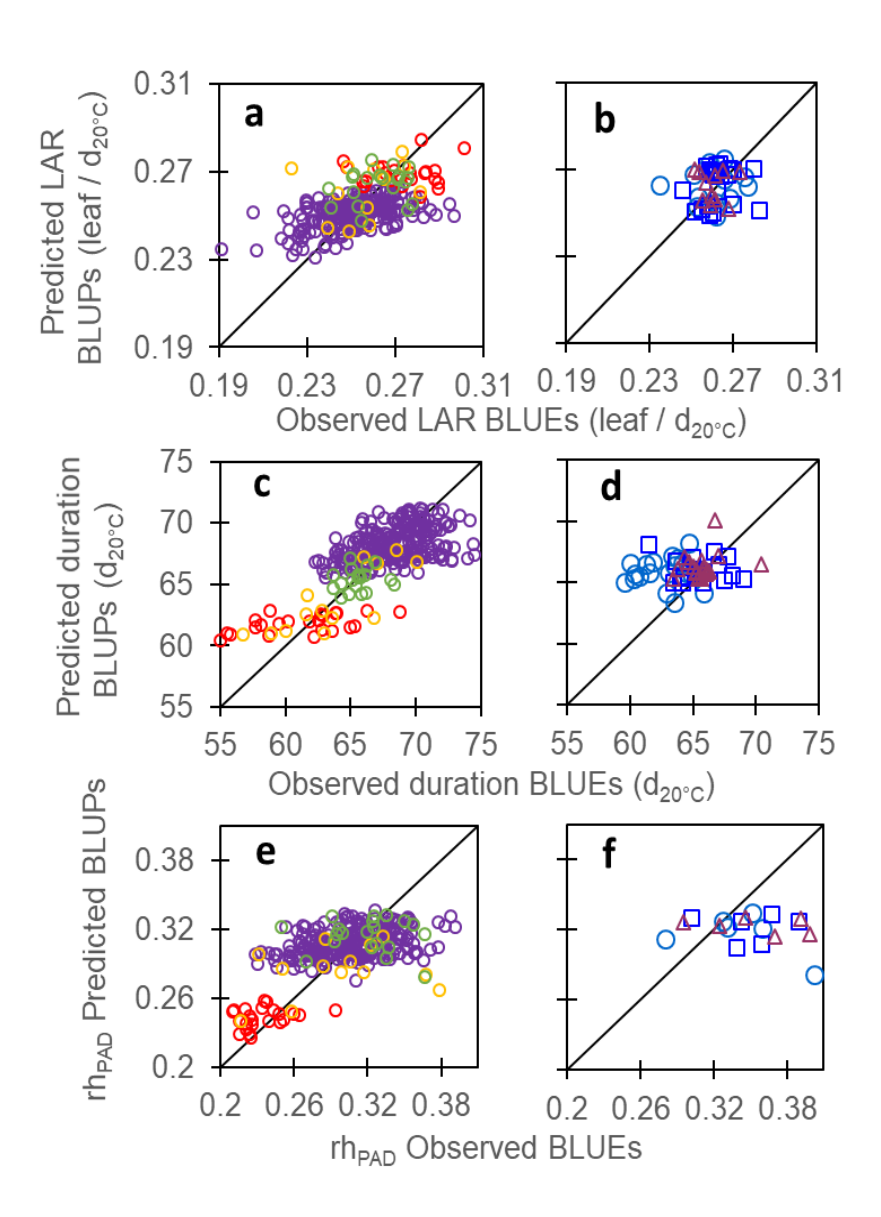
Supplementary Fig. 3. Leaf appearance rate (LAR) when calculated in calendar time had low correlations between genotypic values indoor and a field (a) or from one field to another field (b). Light blue circles, mid-early hybrids (G2), dark blue squares, intermediate hybrids (G3), red triangles, mid-late hybrids (G4). In  $\bf a$ , r=0.40, n=21, p-value = 0.069, CV<sub>RMSE</sub> = 23.8%. In  $\bf b$ , r=0.49, n=26, p-value = 0.0117, CV<sub>RMSE</sub> = 16.91%.



Supplementary Fig. 4. Schematic representation of genomic prediction cross-validation strategy. Each training set was sampled randomly but proportionally to diversity panel genetic groups and across years of release of genetic progress hybrids.

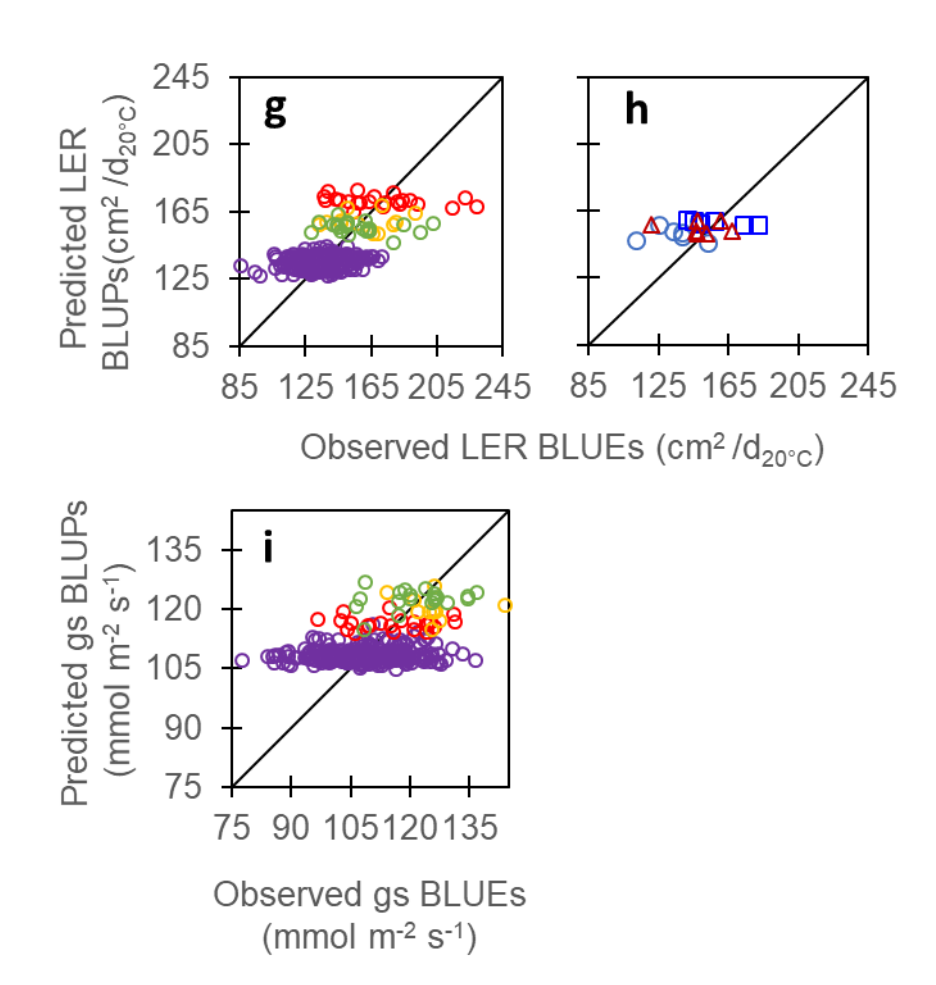


Supplementary Fig. 5. Structure and diversity analysis of the studied panels using a Principal Coordinate Analysis (PCoA) on SNP markers data. The PCoA was based on a set of 440 000 polymorphic SNP markers. The analysis first shows the structuration of the diversity panel parental lines into 4 genetic groups (lodent on the bottom left, Lancaster on the top, Stiff\_Stalk on the bottom right and the other diverse admixed genotypes in the middle). The genetic progress and recent hybrids panels mainly overlap with the lodent and admixed genotypes of diversity panel. The representation of the diversity panel hybrids corresponding to the lines crossed with UH007, highlights the effect of the common parent UH007, which induces a strong genomic relatedness between the diversity panel hybrids and separates them from the other panels following the first PCoA dimension.



Supplementary Fig. 6. The prediction of traits via a PC-BLUP model was less accurate than that with G-BLUP models in Fig. 1cd, 2cd, 3ef, 5b and 7ab for cross-validations (a, c, e, g, i), and lost accuracy for external validation (b, d, f, h). a, c, e, g & i, Comparison of observed mean genotypic values and mean predicted values in a 5-fold CV scheme with 10 iterations, in the 'diversity' and 'genetic progress' panels, for leaf appearance rate (LAR), duration of the vegetative phase,  $\text{rh}_{\text{PAD}}$  trait, LER and  $\text{gs}_{\text{max}}$  trait, respectively. b,~d,~f~&~h,~Comparison of observed mean genotypic values and predicted values in an independent dataset of elite recent hybrids, with model calibration made using dataset of a, c, e & g, respectively. In a, c, e, g & i, purple empty circles, diversity panel; red and yellow empty circles, genetic progress panel, hybrids released before 1980 and 2000, respectively; green empty circles, hybrids released after 2000. In b, d, f & h, light blue circles, mid-early hybrids (G2), dark blue squares, intermediate hybrids (G3), red triangles, mid-late hybrids (G4). In **a**, r = 0.53, n = 302, p-value < 2.2E-16,  $CV_{RMSE} = 5.4\%$ . In **b**, r = 0.11, n = 50, p $value = 0.45, \ CV_{RMSE} = 4.1\%. \ In \ \textbf{c}, \ r = 0.72, \ n = 302, \ p-value < 2.2E-16, \ CV_{RMSE} = 3.4\%. \ In \ \textbf{d}, \ r = 0.72, \ r = 0.72,$ 0.11, n= 60, p-value = 0.39,  $CV_{RMSE}$  = 4.2%. In **e**, r = 0.58, n= 302, p-value < 2.2E-16,  $CV_{RMSE}$  = 10%. In  $\mathbf{f}$ , r = -0.21, n = 20, p-value = 0.37,  $CV_{RMSF} = 15.7\%$ . In  $\mathbf{g}$ , r = 0.61, n = 302, p-value < 2.2E-16,  $CV_{RMSE} = 11\%$ . In **h**, r = 0.25, n = 20, p-value = 0.28,  $CV_{RMSE} = 12\%$ . In **i**, r = 0.41, n = 302, p-value = 0.28,  $CV_{RMSE} = 12\%$ . value = 1.3E-13,  $CV_{RMSE} = 9\%$ .

This figure is continued below.



Supplementary Fig. 6 (continued). The prediction of traits via a PC-BLUP model was less accurate than that with G-BLUP models in Fig. 1cd, 2cd, 3ef, 5b and 7ab for cross-validations (a, c, e, g, i), and lost accuracy for external validation (b, d, f, h). a, c, e, g & i, Comparison of observed mean genotypic values and mean predicted values in a 5-fold CV scheme with 10 iterations, in the 'diversity' and 'genetic progress' panels, for leaf appearance rate (LAR), duration of the vegetative phase,  $\text{rh}_{\text{PAD}}$  trait, LER and  $gs_{\text{max}}$  trait, respectively.  $\textbf{b},\,\textbf{d},\,\textbf{f}\,\,\&\,\,\textbf{h},\,$  Comparison of observed mean genotypic values and predicted values in an independent dataset of elite recent hybrids, with model calibration made using dataset of a, c, e & g, respectively. In a, c, e, g & i, purple empty circles, diversity panel; red and yellow empty circles, genetic progress panel, hybrids released before 1980 and 2000, respectively; green empty circles, hybrids released after 2000. In b, d, f & h, light blue circles, mid-early hybrids (G2), dark blue squares, intermediate hybrids (G3), red triangles, mid-late hybrids (G4). In  $\bf a$ , r = 0.53, n= 302, p-value < 2.2E-16,  $\rm CV_{RMSE}$  = 5.4%. In  $\bf b$ , r = 0.11, n = 50, p-value = 0.45,  $CV_{RMSE} = 4.1\%$ . In **c**, r = 0.72, n = 302, p-value < 2.2E-16,  $CV_{RMSE} = 4.1\%$ . 3.4%. In **d**, r = 0.11, n = 60, p-value = 0.39,  $CV_{RMSE} = 4.2\%$ . In **e**, r = 0.58, n = 302, p-value < 2.2E-16,  $CV_{RMSE} = 10\%$ . In **f**, r = -0.21, n = 20, p-value = 0.37,  $CV_{RMSE} = 15.7\%$ . In **g**, r = 0.61, n = 302, p-value = 0.37,  $CV_{RMSE} = 15.7\%$ .  $value < 2.2E\text{-}16, \ CV_{\text{RMSE}} = 11\%. \ In \ \textbf{h}, \ r = 0.25, \ n = 20, \ p\text{-}value = 0.28, \ CV_{\text{RMSE}} = 12\%. \ In \ \textbf{i}, \ r = 0.41, \ r$ n=302, p-value = 1.3E-13,  $CV_{RMSE} = 9\%$ .

## Supplementary Data 1. Hybrids of the 'recent hybrids' panel and experiments in which each of them was evaluated.

Hybrid	Year of release	Maturity group in France	FAO Index group	Breeder	Field 1	Field 2	Field 3	Field 4	Indoor 1
ARV75	2008	G2 (mid-early)	(280 - 320)	PIONEER	Х		Х		
ARV01	2011	G2 (mid-early)	(280 - 320)	LIMAGRAIN	Χ		Χ		Χ
ARV32	2012	G2 (mid-early)	(280 - 320)	EURALIS	Χ		Χ		
ARV09	2013	G2 (mid-early)	(280 - 320)	BAYER	Χ		Χ		
ARV69	2014	G2 (mid-early)	(280 - 320)	PIONEER	Χ		Χ		Χ
ARV77	2014	G2 (mid-early)	(280 - 320)	LIMAGRAIN	Χ		Χ		
ARV79	2014	G2 (mid-early)	(280 - 320)	RAGT	Χ		Χ		
ARV10	2015	G2 (mid-early)	(280 - 320)	BAYER	X		Χ		
ARV94	2015	G2 (mid-early)	(280 - 320)	BAYER	Χ		Χ		Χ
ARV54	2016	G2 (mid-early)	(280 - 320)	PIONEER	Χ		Χ		
ARV55	2016	G2 (mid-early)	(280 - 320)	PIONEER	Χ		Χ		Χ
ARV11	2017	G2 (mid-early)	(280 - 320)	BAYER	Χ		Χ		
ARV12	2017	G2 (mid-early)	(280 - 320)	BAYER	Χ		Χ		Χ
ARV13	2017	G2 (mid-early)	(280 - 320)	BAYER	Χ		Χ		
ARV14	2017	G2 (mid-early)	(280 - 320)	BAYER	Χ		Χ		
ARV31	2017	G2 (mid-early)	(280 - 320)	EURALIS	Χ		Χ		
ARV36	2017	G2 (mid-early)	(280 - 320)	EURALIS	Χ		Χ		Χ
ARV48	2017	G2 (mid-early)	(280 - 320)	KWS	Χ		Χ		
ARV61	2017	G2 (mid-early)	(280 - 320)	KWS	Χ		Χ		Χ
ARV33	2018	G2 (mid-early)	(280 - 320)	EURALIS	Χ		Χ		
ARV87	2018	G2 (mid-early)	(280 - 320)	SYNGENTA	Χ		Χ		
ARV30	2019	G2 (mid-early)	(280 - 320)	EURALIS	Χ		Χ		
ARV37	2019	G2 (mid-early)	(280 - 320)	RAGT	Χ		Χ		
ARV83	2019	G2 (mid-early)	(280 - 320)	RAGT	Χ		Χ		
ARV15	2020	G2 (mid-early)	(280 - 320)	BAYER	Χ		Χ		
ARV50	2020	G2 (mid-early)	(280 - 320)	KWS	Χ		Χ		
ARV80	2020	G2 (mid-early)	(280 - 320)	RAGT	Χ		Χ		
ARV18	2009	G3 (intermediate)	(320 - 400)	BAYER	Χ	Χ	Χ	Χ	
ARV23	2009	G3 (intermediate)	(320 - 400)	BAYER	Χ	Χ	Χ	Χ	
ARV24	2011	G3 (intermediate)	(320 - 400)	BAYER	Χ	Χ	Χ	Χ	
ARV65	2011	G3 (intermediate)	(320 - 400)	CAUSSADE	Χ	Χ	Χ	Χ	
ARV39	2012	G3 (intermediate)	(320 - 400)	RAGT	Χ	Χ	Χ	Χ	
ARV16	2015	G3 (intermediate)	(320 - 400)	BAYER	Χ	Χ	Χ	Χ	
X47D113_49	2015	G3 (intermediate)	(320 - 400)	BAYER	Χ	Χ	Χ	Χ	
ARV46	2015	G3 (intermediate)	(320 - 400)	CAUSSADE	Χ	Χ	Χ	Χ	
ARV59	2015	G3 (intermediate)	(320 - 400)	PIONEER	Χ	Χ	Χ	Χ	
ARV85	2015	G3 (intermediate)	(320 - 400)	RAGT	Χ	Χ	Χ	Χ	Χ
ARV88	2015	G3 (intermediate)	(320 - 400)	SYNGENTA	Χ	Χ	Χ	Χ	
ARV20	2016	G3 (intermediate)	(320 - 400)	BAYER	X	Χ	Χ	Χ	Χ
ARV22	2016	G3 (intermediate)	(320 - 400)	BAYER	Χ	Χ	Χ	Χ	
ARV28	2016	G3 (intermediate)	(320 - 400)	BAYER	X	Χ	Χ	Χ	Χ
ARV40	2016	G3 (intermediate)	(320 - 400)	BAYER	Χ	Χ	Χ	Χ	
ARV44	2016	G3 (intermediate)	(320 - 400)	BAYER	Χ	Χ	Χ	Χ	
ARV21	2017	G3 (intermediate)	(320 - 400)	BAYER	Χ	Χ	Χ	Χ	

Field 1, Matzenheim. Field 2, St-Bonnet-de-Mure. Field 3, Binas. Field 4, Pusignan. Indoor 1, PhenoArch (Montpellier). See supplementary table 3 for more detail on experiments.

**Supplementary Data 1 (continued)**. Hybrids of the 'recent hybrids' panel and experiments in which each of them was evaluated.

Hybrid	Year of release	Maturity group in	FAO	Breeder	Field 1	Field 2	Field 3	Field 4	Indoor 1
ARV04	2018	France G3 (intermediate)	(320 - 400)	KWS	Х	X	X	X	Х
ARV47	2018	G3 (intermediate)	(320 - 400)	BAYER	X	X	X	X	Α
ARV52	2018	G3 (intermediate)	(320 - 400)	KWS	X	X	X	X	Х
ARV89	2018	G3 (intermediate)	(320 - 400)	SYNGENTA	X	X	X	^	X
ARV91	2018	G3 (intermediate)	(320 - 400)	BAYER	X	X	X	Х	^
ARV90	2019	G3 (intermediate)	(320 - 400)	SYNGENTA	X	X	X	X	
ARV19	2020	G3 (intermediate)	(320 - 400)	BAYER	X	X	X	X	
ARV42	2020	G3 (intermediate)	(320 - 400)	KWS	X	X	X	X	
ARV41	2010	G4 (mid-late)	(400 - 480)	RAGT		X	X	X	
ARV03	2012	G4 (mid-late)	(400 - 480)	KWS		X	X	X	
ARV56	2012	G4 (mid-late)	(400 - 480)	PIONEER		X	X	X	
ARV64	2012	G4 (mid-late)	(400 - 480)	RAGT		X	X	X	
ARV67	2012	G4 (mid-late)	(400 - 480)	PIONEER		X	X	X	
ARV71	2012	G4 (mid-late)	(400 - 480)	PIONEER		X	X	X	
ARV07	2013	G4 (mid-late)	(400 - 480)	LIMAGRAIN		X	X	X	
ARV25	2013	G4 (mid-late)	(400 - 480)	BAYER		X	X	X	
ARV63	2014	G4 (mid-late)	(400 - 480)	MAS_SEEDS		X	X	X	
ARV72	2014	G4 (mid-late)	(400 - 480)	PIONEER		X	X	X	Х
ARV05	2015	G4 (mid-late)	(400 - 480)	RAGT		Х	X	Х	
ARV26	2015	G4 (mid-late)	(400 - 480)	BAYER		X	X	Х	X
X47D113_08	2015	G4 (mid-late)	(400 - 480)	BAYER		X	X	Х	
ARV57	2015	G4 (mid-late)	(400 - 480)	PIONEER		X	X	Х	
ARV60	2015	G4 (mid-late)	(400 - 480)	LIMAGRAIN		X	X	Х	
ARV66	2015	G4 (mid-late)	(400 - 480)	PIONEER		X	X	Х	
ARV82	2015	G4 (mid-late)	(400 - 480)	RAGT		Х	Х	X	
X47D113_12	2015	G4 (mid-late)	(400 - 480)	RAGT		X	X		
ARV08	2016	G4 (mid-late)	(400 - 480)	BAYER		Х	Х	Х	
ARV27	2016	G4 (mid-late)	(400 - 480)	BAYER		Х	Х	Х	Х
ARV34	2016	G4 (mid-late)	(400 - 480)	EURALIS			Χ		Х
ARV06	2017	G4 (mid-late)	(400 - 480)	BAYER		Х	Χ	Χ	X
ARV58	2017	G4 (mid-late)	(400 - 480)	PIONEER		X	Χ	Χ	
ARV73	2017	G4 (mid-late)	(400 - 480)	CAUSSADE		Х	Χ	Χ	X
ARV76	2017	G4 (mid-late)	(400 - 480)	BAYER		Х	Χ	Х	
ARV78	2017	G4 (mid-late)	(400 - 480)	BAYER		X	X	X	
ARV93	2017	G4 (mid-late)	(400 - 480)	RAGT		X	X	X	
ARV51	2018	G4 (mid-late)	(400 - 480)	KWS		X	X	X	
ARV84	2018	G4 (mid-late)	(400 - 480)	RAGT		X	X	X	X
ARV29	2019	G4 (mid-late)	(400 - 480)	BAYER		X	X	X	
ARV35	2019	G4 (mid-late)	(400 - 480)	EURALIS		X	X	Х	
ARV74	2019	G4 (mid-late)	(400 - 480)	BAYER		X	X	Х	
X47D113_09	2020	G4 (mid-late)	(400 - 480)	BAYER		X	X		
X47D113_74	2020	G4 (mid-late)	(400 - 480)	KWS		Х	Х		

Field 1, Matzenheim. Field 2, St-Bonnet-de-Mure. Field 3, Binas. Field 4, Pusignan. Indoor 1, PhenoArch (Montpellier). See supplementary table 3 for more detail on experiments.

# CHAPTER 2: ACQUISITION AND ANALYSIS OF EXTENDED FIELD DATA IN CONTRASTING ENVIRONMENTAL CONDITIONS FOR CROP MODEL SIMULATION ON A SET OF RECENT HYBRIDS

#### **TABLE OF CONTENTS**

Introduction57
Results and discussion58
The distribution of environmental conditions and yield in studied experiments was
typical of maize growing area in Europe58
Five environmental scenarios, based on temperature and soil water status,
synthesized environmental conditions and accounted for yield variations across
experiments61
Estimation of leaf area index and of maximum grain number per plants, to be used
to test simulation in Chapter 363
Material and methods65
Genetic material65
Field experiments65
Yield and environmental conditions in Europe66
Field traits Analyses66
Environmental characterization and multi-environment analyses67
References68
Acknowledgements70
Supplementary information71

#### Introduction

In this chapter, we analysed the dataset collected in a multi-site field experiment for the recent hybrids panel, that will allow us later (chapter 3) to test the consistency of a predictive approach for modelling the genotypic variability of leaf area index (LAI) and grain number (GN). We used the data collected in the European project INVITE (https://www.h2020-invite.eu/), which consisted of 33 experiments, defined as combinations of site x year x watering regime, distributed on a west–east transect for temperature and evaporative demand across Europe. A subset of the 'recent hybrids' panel including 30 varieties (Supplementary Table 1) was evaluated in this extended network, for LAI estimated from UAV imaging data in 7 experiments, and for yield and its components in 32 experiments (Supplementary Table 2).

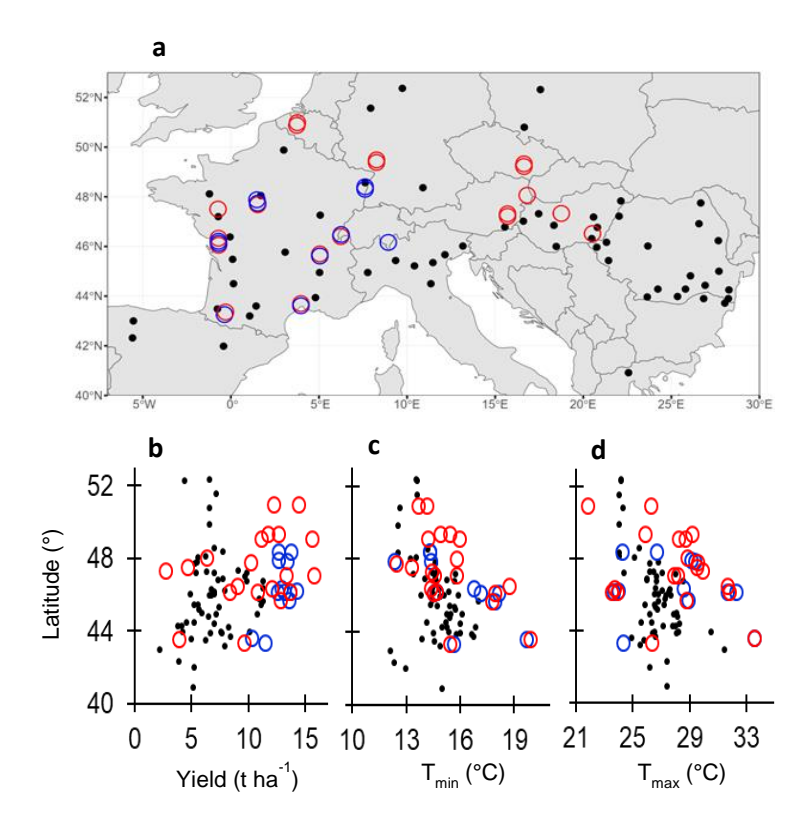
We characterized the environmental conditions experienced by plants in each field based on weather and soil water sensors. We first calculated environmental indices during vegetative, flowering and grain filling phases for a reference hybrid (Millet et al., 2019). We then clustered experiments into five environmental scenarios (Millet et al., 2016) that were used to investigate GEI (genotype-by-environment interaction) variation for grain yield (Y). Finally, we tested the representativeness of tested fields for yield and environment conditions based on a previous simulation study (Parent et al., 2018) performed over 36 years (1975–2010) in 59 locations representative of the European maize growing area and of typical soil types of these regions.

Regarding model parametrization, we first estimated a genotype-dependent parameter used in Sirius-maize, namely the maximum grain number per plant of each studied hybrid. This was estimated in the multi-site experiment by considering grain number in experiments with the highest yield. We also estimated LAI for each hybrid in contrasting experiments in order to test the model across environments. It was calculated via drone imaging and inversion of the PROSAIL model in the studied fields and will be compared in chapter 3 to those simulated by the crop model. Finally, we estimated genotypic sensitivities of grain number to mean soil water potential and mean daily maximum temperatures during the flowering phase using a linear regression model.

#### **Results and discussion**

The distribution of environmental conditions and yield in studied experiments was typical of maize growing area in Europe.

The network of field experiment targeted the range of latitudes 43–51°N which covers a large proportion of the maize growing area in Europe (Fig. 1a, Parent et~al., 2018), and corresponds to the set of 30 commercial hybrids maturity classes (mid-early (FAO 280) to mid-late (FAO 480)). Minimum and maximum temperatures during the flowering phase covered the range of temperatures observed for the European maize growing area over the last 36 years (e.g., maximum temperatures 'maxT\_flo' = 22–34 °C in our experiments vs 24–31 °C for the 59 × 36 studied records in European sites, Fig. 1cd). They tended to be higher, in average, than those measured at the same latitudes in the last 36 years probably a consequence of climate change. Mean soil water potential during the flowering phase 'Psi\_flo' ranged from -0.27 to -0.02 MPa for the reference hybrid (ARV18), representing the range of available water in most agricultural soils as estimated using the equations of van Genuchten (1980). Hence, the recent hybrids panel was studied here in a range of climatic conditions that essentially covered both the current and past climatic conditions in the European maize growing area.



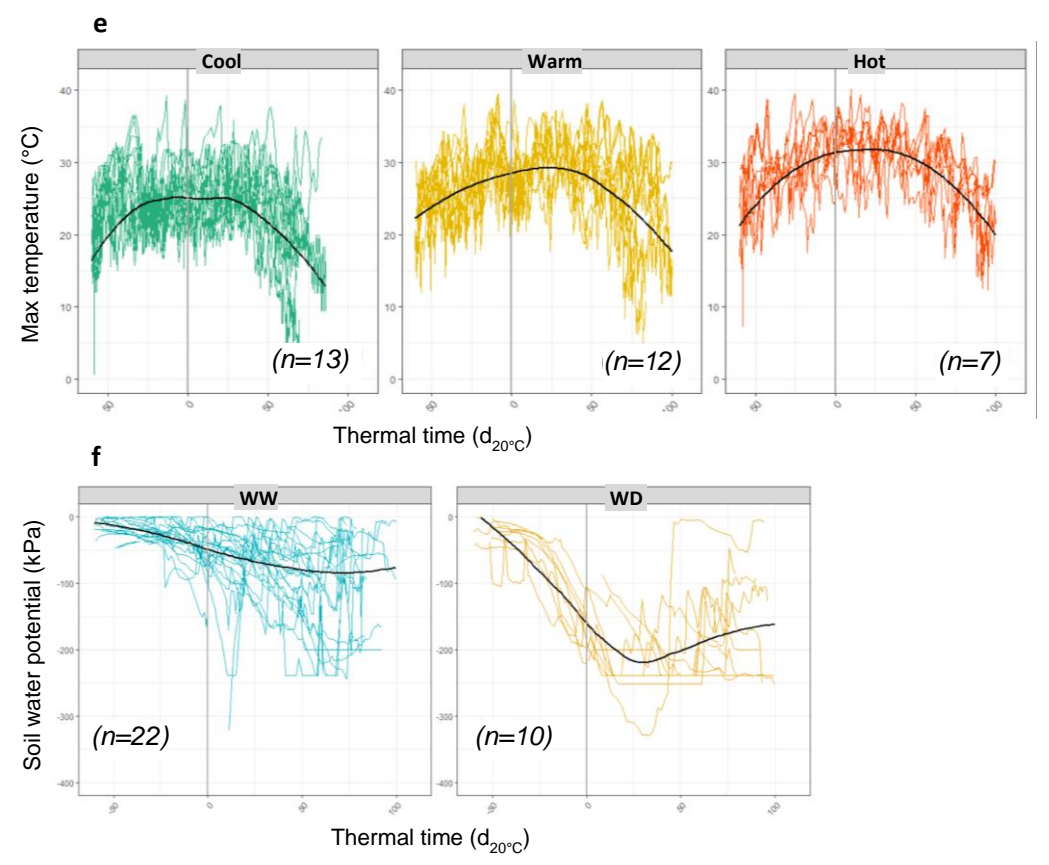


**Fig. 1**: The field experiments covered the latitudes of the maize growing area in Europe, and represented a large part of the variability of yield and environmental conditions. a, Map of field experiments, blue and red circles for irrigated and rainfed experiments, respectively, and black dots for 59 sites distributed over Europe for representation of the maize growing area. **b-d,** Mean yield, mean daily minimum and maximum temperatures during the flowering phase as a function of latitude compared with means for 59 sites over 36 years. **e,** Three temperature scenarios captured a large part of the variability of temperature in the field experiments. Time courses of air temperature in the scenarios cool, warm, and hot. Each line represents one experiment; black lines, mean time course. **f,** Time courses of soil water potential for fields classified as belonging to well-watered (WW) or water deficit (WD) scenarios. Each line represents one experiment. In **e** and **f**, time is centered on flowering time, in equivalent days at 20 °C. n, number of experiments x maturity group.

Yield, grain number per square meter and individual grain weight (weight at 15% moisture content) are presented in Figure 2a, 2b and 2c, respectively, for all experiments. The mean broad-sense heritability observed per experiment was 0.68, 0.78 and 0.83 for yield, grain number and grain weight, respectively. Unsurprisingly, we observed a high correlation between yield and its components (r=0.86 with grain number and 0.60 with individual grain weight, p-value < 2.2e-16). The correlation between grain number and grain weight was expectedly low (r=0.12, p-value=0.001) in spite of the trade-off between them (Fig. 5a-c, Turc & Tardieu, 2018; Fernández *et al.*, 2022). Mean yields in the 32 studied experiments (3–16 t.ha<sup>-1</sup>) covered the range simulated over 36 years (1975–2010) in 59 sites in Europe, with a tendency towards higher yields in experimental than in historical yields (3–12 t.ha<sup>-1</sup>, latitudes

41–53°N, Parent et al., 2018, Fig. 1b). This may be due to the cumulated genetic gain for the tested varieties, released from 2009 to 2020 in relation to the hybrid B73 x UH007 simulated in Fig 1 (0.1 t.ha<sup>-1</sup>.year<sup>-1</sup> genetic gain in Welcker *et al.*, 2022).

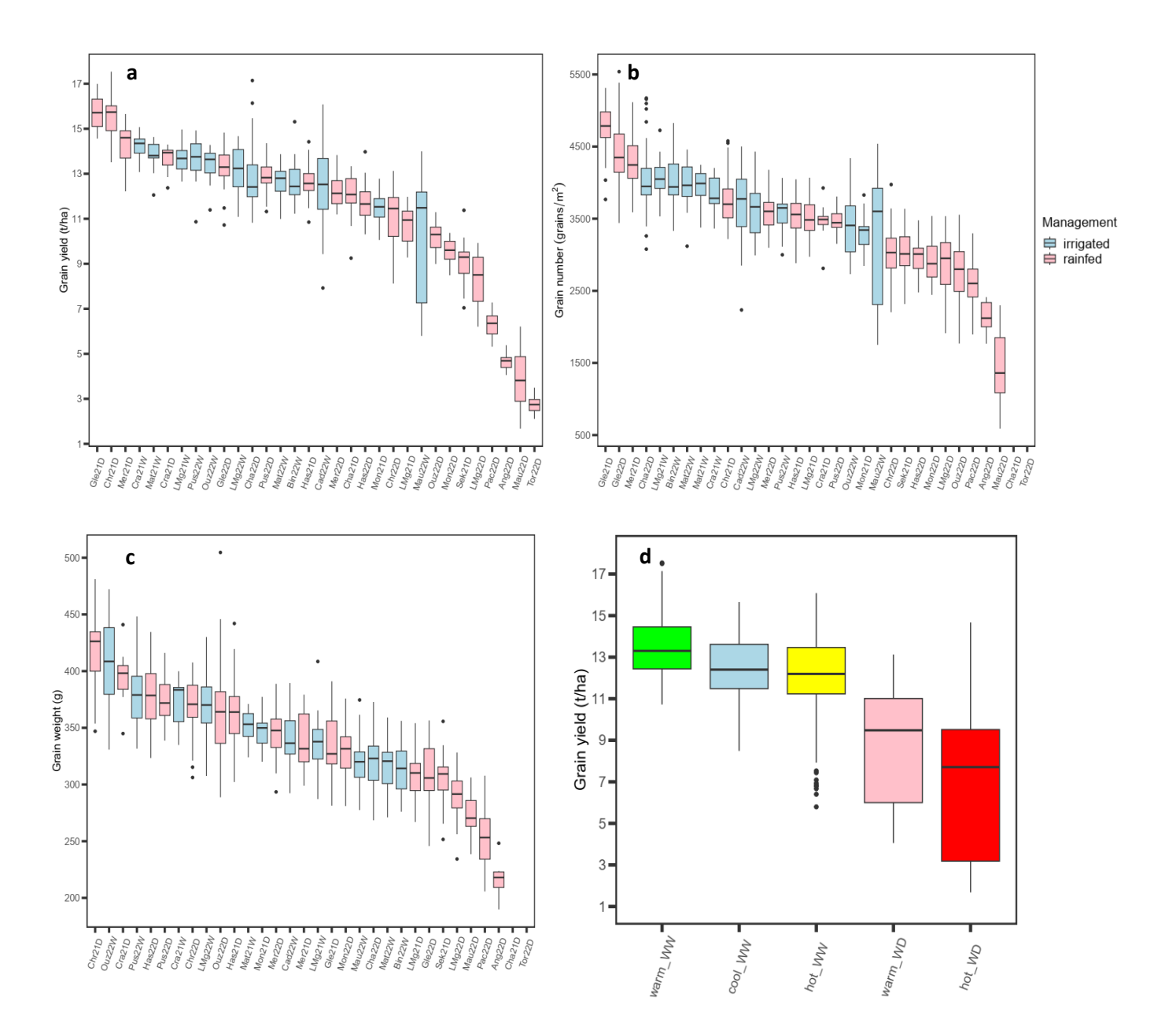
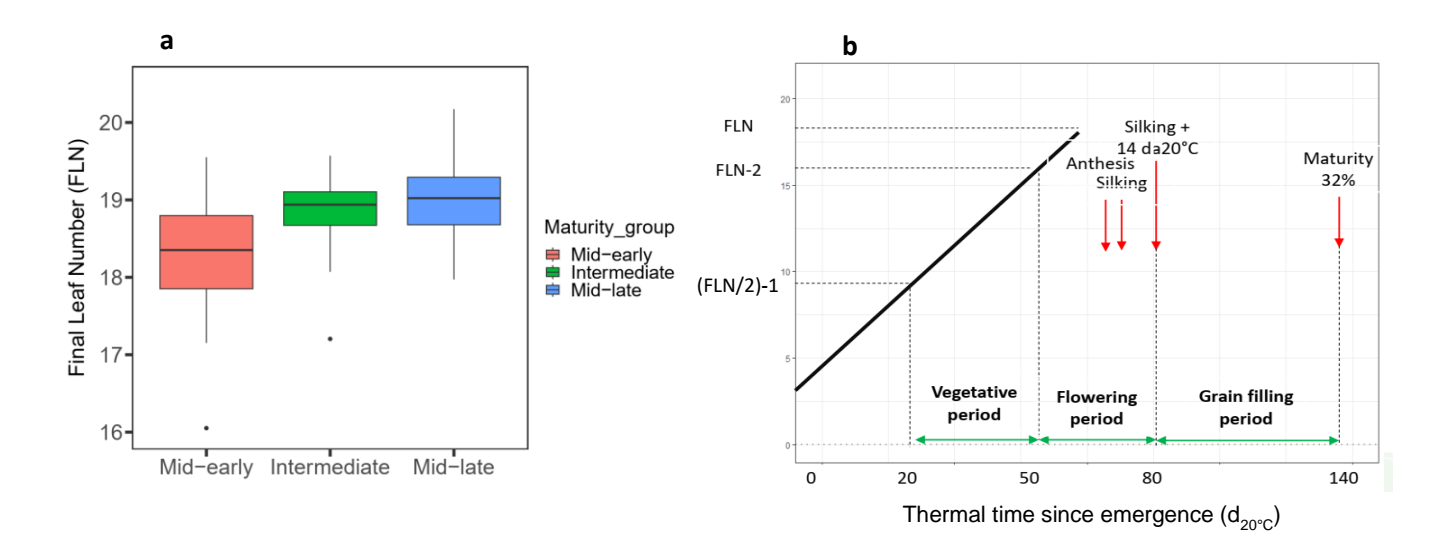


Fig. 2: Grain yield (a, d) and its components (b, grain number; c, individual weight grain x1000) in the 32 harvested field experiments in 2021 and 2022. d, Grain yield in each environmental scenarios identified in Fig. 1. Boxes represent the genotypic variability in each experiment or each scenario (25%, 50% and 75% quantiles). In a, b and c, light blue and pink circles for irrigated and rainfed experiments, respectively.

Five environmental scenarios, based on temperature and soil water status, synthesized environmental conditions and accounted for yield variations across experiments.

To further characterize the environmental conditions sensed by hybrids in each field, we focused on the three phenological phases (vegetative, flowering and grain filling phase) used by Millet et al., (2019), based on the progression of leaf number and maturity for each hybrid (Fig. 3ab). We calculated 36 environmental indices per phenological phase including air temperature, soil water potential, light, air VPD, ETO and rainfall. We then identified two main environmental drivers using a stepwise regression: mean soil water potential (Psi\_flo) and mean of daily maximum temperatures (maxT\_flo) during flowering phase. These were among the predictors in the best regression model for yield with ten explanatory variables (R²=0.65).



**Fig. 3 : The calculation of phenological phases used to estimate environmental indices in a given experiment. a,** The final leaf number (FLN, leaf number per plant at flowering), was estimated as genotypic BLUEs values over three experiments (Bin22W, Mat22W and Pus22W). **b,** The crop cycle was split into three phases based on the FLN of each hybrid, leaf appearance rate and maturity (Millet et al. 2019). These phases were separated by floral transition, silk initiation, end of grain abortion and grain maturity. They occurred at different thermal times for each hybrid.

Experiments were then clustered based on these two indices, calculated for the reference hybrid (ARV18). Five environmental scenarios were identified (Fig. 1ef, Fig. 2d): Warm Wellwatered (mean yield=13.3 t.ha<sup>-1</sup>), Cool Well-watered (mean yield=12.4 t.ha<sup>-1</sup>), Hot Wellwatered (mean yield=11.7 t.ha<sup>-1</sup>), Warm Water-deficit (mean yield=8.7 t.ha<sup>-1</sup>) and Hot Water-deficit (mean yield=7.1 t.ha<sup>-1</sup>). The genotype by environmental scenario interaction represented 35% of the total genotypic variation for grain yield.

We further investigated the GEI in the multi-site experiment using a linear model, where grain number was fitted as a response to Psi\_flo and maxT\_flo during the flowering phase (see Methods). Overall, an appreciable variability was observed for the genotype-dependent sensitivities to the two environmental indices: from -4576 to 3418 grains  $m^{-2}$  MPa $^{-1}$  for  $\beta_1$  (Fig. 4a) and from -99 to 86 grains  $m^{-2}$  °C $^{-1}$  for  $\beta_2$  (Fig. 4b). For example, a decrease in Psi\_flo by 0.15 MPa decreased grain number by 8 to 31% for the least and most sensitive hybrids, respectively; and an increase in maxT\_flo by 6 °C decreased grain number by 1 to 21% for the least and most sensitive hybrids, respectively. These ranges were expectedly lower than those observed in the maize diversity panel of Millet et al. (2019). They may represent genetic parameters for selecting new hybrids in a breeding context.

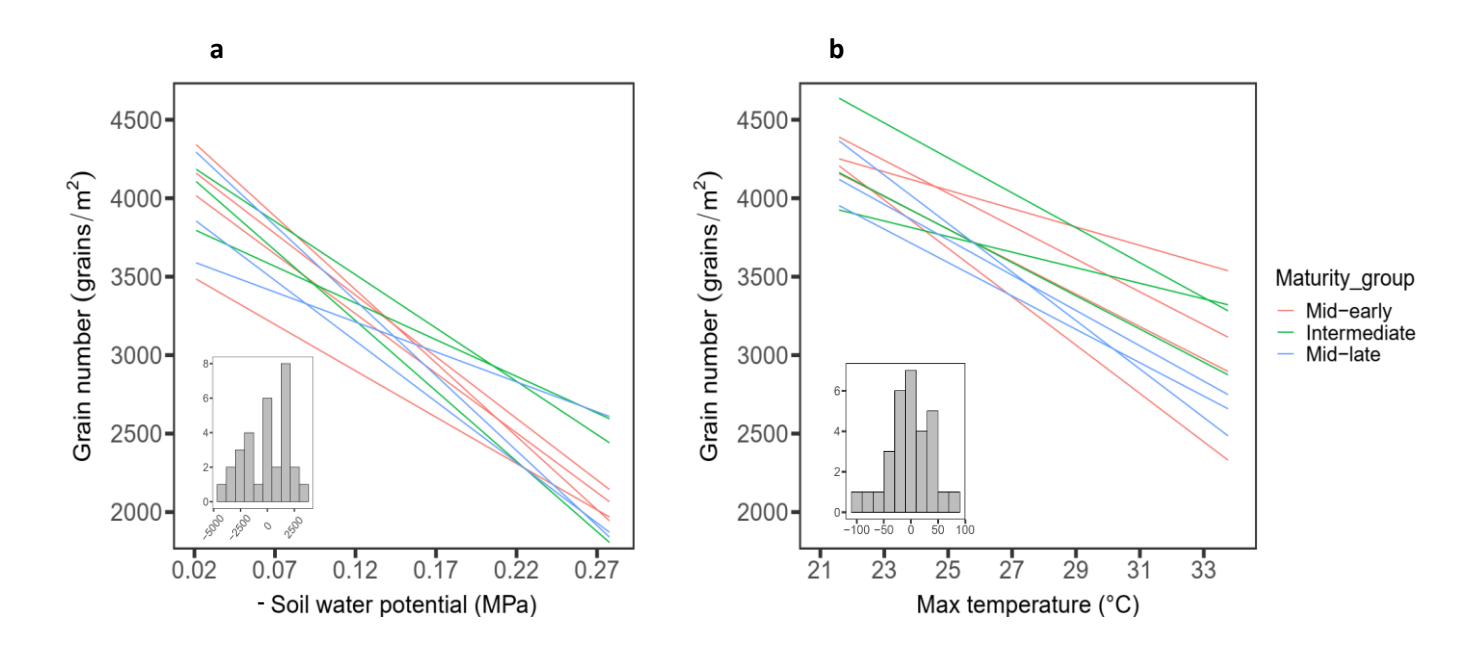


**Fig. 4 : Variability of genotype-specific response of grain number to environmental indices. a,** Grain number as a function of soil water potential averaged during the flowering phase. x-axis in reverse order. **b,** Grain number as a function of daily maximum temperatures averaged during the flowering phase. For better legibility in **a** and **b**, only ten hybrids with different responses are shown, one line per hybrid. The variability of sensitivities from the factorial regression model (equation (3) in methods) across the whole panel is shown in histograms.

# Estimation of leaf area index and of maximum grain number per plants, to be used to test simulation in Chapter 3

The genotypic maximum grain number per plant (GN<sub>max</sub>), is an important genotypic parameter for simulating grain yield in the Sirius maize crop model used in chapter 3. It was calculated as BLUEs values over five high-potential experiments (Gle22D, Cra21W, Mat22W, Bin22W and Cha22D) after correcting for field plant density (Fig. 5a-d). GN<sub>max</sub> values ranged from 422 to 590 grains plant<sup>-1</sup> among studied hybrids. The overall differences between the three maturity classes of hybrids were low (Fig. 5d). This could be due to the fact that irrigation was managed based on phenological stages of one reference intermediate hybrid (ARV18) in irrigated experiments, so irrigation dates were not optimised by maturity group. This penalized latest genotypes, expected to have highest GN<sub>max</sub> otherwise. Furthermore, the standard maturity classification considered for hybrids was determined according to the duration of the whole crop cycle (until physiological maturity) and not according to the vegetative phase duration.

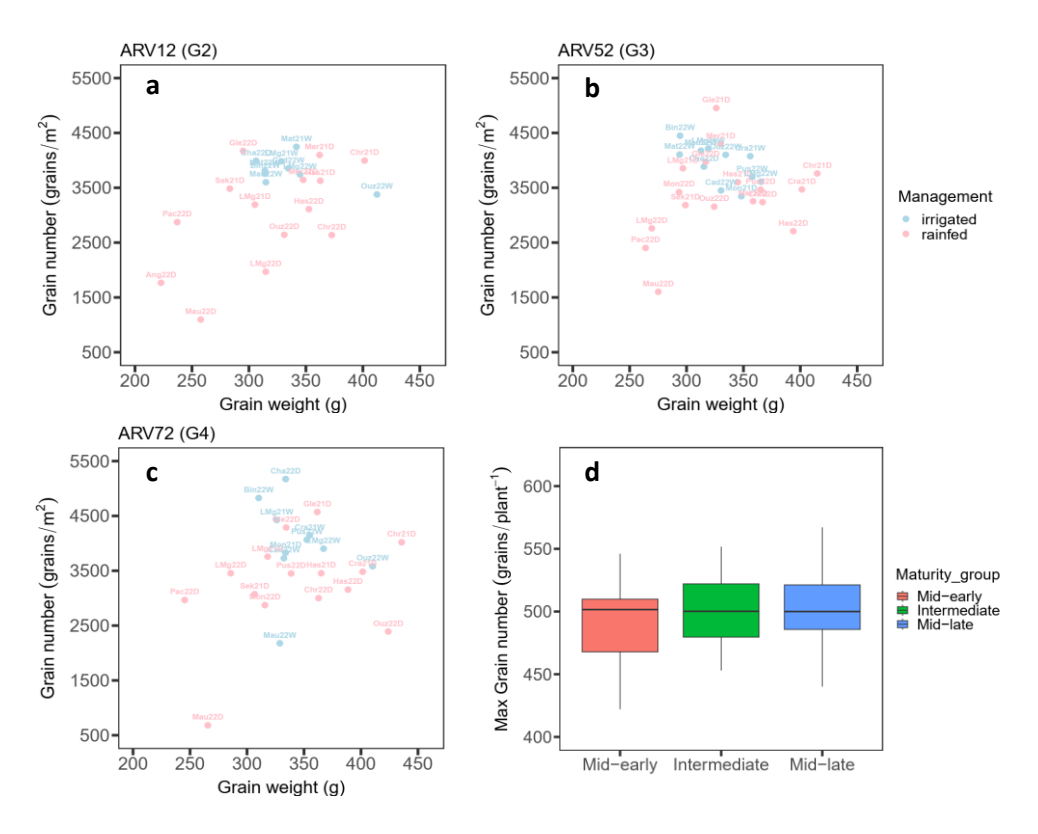


**Fig. 5 : Maximum grain number per hybrid. a-c,** Relationship between grain number per square meter and individual grain weight (x1000) for 3 different hybrids. **d,** GN<sub>max</sub> was calculated after correcting for plant density as BLUEs values over five high-potential experiments having the greatest number of common varieties : Gle22D, Cra21W, Mat22W, Bin22W and Cha22D. In a, b and c, light blue and pink circles for irrigated and rainfed experiments, respectively. In d, different colors for different maturity groups.

Leaf area index (LAI) is a key trait for light interception and transpiration, which largely differs between fields in relation to environmental conditions and plant density (Garriques *et al.*, 2008). We estimated it in this chapter and these estimated values will be compared with simulated values later in chapter 3. LAI was estimated using UAV images, which were analysed by inversion of the PROSAIL radiative transfer model (Casa *et al.*, 2010; Duan *et al.*, 2014; Supplementary Fig. 1). UAV flights were performed three to seven times during the period from plant emergence to flowering in 7 experiments out of the total of 33 field experiments: Mau22W, Mau22D, Ouz22W, Ouz22D, Pus22W, Pus22D and Pus21W (Supplementary Table 2). The broad-sense heritability within experiment and per flying date ranged from 0.20 to 0.90. This could be due to the fact that UAV imaging derived traits are very sensitive to crop phenological stage and weather conditions during flights (Blancon *et al.*, 2019; Zhu *et al.*, 2022). The most relevant and regularly heritable LAI corresponded to flights performed towards the end of the vegetative phase (16-17 leaf stage). They ranged from 0.86 to 4.21, with high overall variability between irrigated and rainfed conditions (Fig. 6), and were appreciably correlated with grain yield (r=0.43, p-value=9E-10).

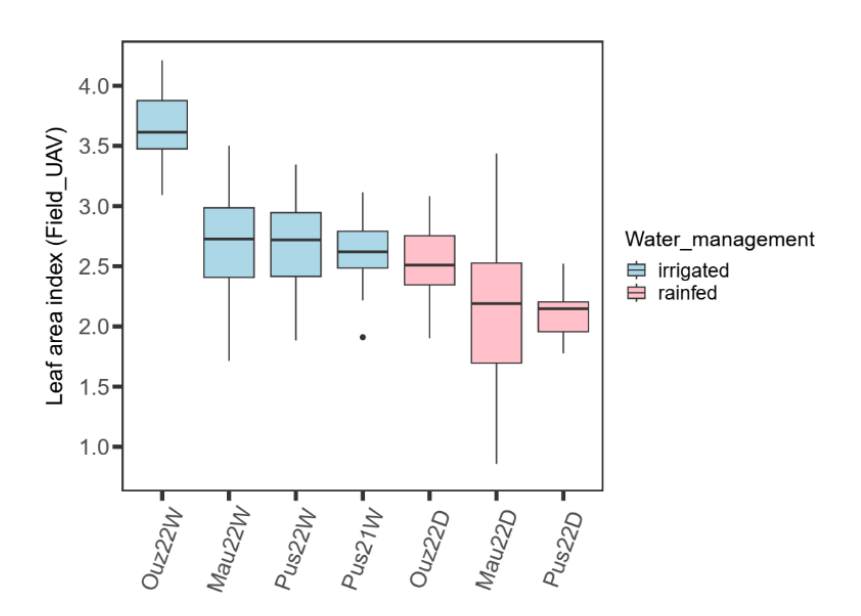


**Fig. 6 : Leaf area index (LAI) in the 7 field experiments, measured via UAV flights.** Boxes represents the genotypic variability in each experiment (25%, 50% and 75% quantiles). LAI was calculated by inversion of the PROSAIL model (Casa et al., 2010; Berger et al., 2018, Supplementary Fig. 1), based on the multispectral images of the 7 experiments UAV flights (16-17 leaf stage). Light blue and pink circles for irrigated and rainfed experiments, respectively.

#### Material and methods, in addition to that in Chapter 1

**Genetic material.** A subset of the 'recent hybrids' panel presented in chapter 1 was designed in the framework of the European project INVITE (https://www.h2020-invite.eu/) and was extensively evaluated in a multi-site field network across Europe. It included 30 commercial hybrids released from 2009 to 2020, belonging to mid-early (G2), intermediate (G3) or midlate (G4) maturity class in France (Supplementary Table 1).

**Field experiments.** In addition to the 4 field experiments presented in chapter 1 for the "recent hybrids" panel, 29 additional experiments (defined as combinations of site x year x watering regime) were carried out in 2021 and 2022, under irrigated or rainfed conditions (Supplementary Table 2). Experiments followed an alpha-lattice design or a randomised complete block design and some of them were split by varieties maturity classes (Supplementary Table 2), each with two or three replicates of four-row plots, 6 m long. The targeted plant density was 8 or 9 plants m<sup>-2</sup>.

In all experiments and hybrids, anthesis and silking dates were scored by visiting experiments every third day. Plots were mechanically harvested, then grain yield was scaled to 15% moisture content after estimation of grain moisture at harvest. 1000 grains weight was measured and used to calculate grain number per square meter from grain yield. One experiment (Pus21W) could not be harvested due to a storm that damaged plants around the flowering stage. The number of appeared leaves was scored on ten plants every week from plant emergence to flowering, for one reference hybrid per maturity class in all experiments, and for all hybrids in three experiments (Bin22W (Field 3), Mat22W (Field 1) and Mau22W, Supplementary Table 2). Leaf appearance rate (LAR) was calculated as the slope of the linear relationship between the number of visible leaves and thermal time (Parent *et al.*, 2010), during the period from plant emergence to the 12-leaf stage. Final leaf number (FLN) corresponded to the total leaf number per plant at flowering.

UAV (drone) flights with a DJI multispectral camera were performed three to seven times during the period from plant emergence to flowering in 7 out of the 33 field experiments: Mau22W and Mau22D in the DiaPHEN INRAE platform; Ouz22W and Ouz22D in the Phenofield ARVALIS platform (Beauchêne *et al.*, 2019); Pus22W, Pus22D (Field 2) and Pus21W (Field 4) in Pusignan ARVALIS station (Supplementary Table 2). An automatic image-processing pipeline

was applied by Hiphen, Avignon, France (http://www.hiphen-plant.com), following methods presented in (Blancon *et al.*, 2019). In addition to ALA trait (Average Leaf inclination Angle to the soil level) presented in chapter 1, leaf area index (LAI) was calculated by inversion of the PROSAIL model (Casa *et al.*, 2010; Duan *et al.*, 2014; Berger *et al.*, 2018) (Supplementary Fig. 1, Supplementary Table 3), based on the multispectral images of the 7 experiments UAV flights.

Environmental variables were recorded daily in all experiments, including light, air temperature, relative humidity (RH), rainfall and wind speed. Meteorological data for some experiments were obtained from the AGRI4CAST database of the JRC (Joint Research Centre) or the INRAE CLIMATIK database. Soil water potential was measured every day with tensiometers at 30 and 60 cm depths with three or two replicates, located in plots sown with a common reference hybrid (ARV18). Soil data (physical and chemical properties) were obtained from the JRC European Soil Commission database and from the FAO Harmonized World Soil database.

Yield and environmental conditions in Europe. We tested the representativeness of the field experiments presented here, compared to the information collected over 36 years in 59 locations representative of the European maize growing area and of typical soil types of these regions (Parent  $et\ al.$ , 2018). Briefly, soil data were obtained from the JRC European Soil Commission database and from the Crop Growth Monitoring System. Meteorological data represented 36 years of daily weather (1975–2010) obtained from the AGRI4CAST database of the JRC or the INRAE CLIMATIK databases. Yields presented in Fig. 1 are mean values simulated over the  $59 \times 36 \times 2$  combinations of location, year and watering regime (Parent et al., 2018). For that, a modified version of the APSIM model was used (Hammer  $et\ al.$ , 2010), parametrized for the B73×UH007 hybrid (Lacube  $et\ al.$ , 2020).

**Field traits Analyses**. Genotypic values (BLUEs) for each trait in each field experiment were estimated by correcting raw traits values for spatial effects, by fitting a mixed model (R package SpATS, van Eeuwijk *et al.*, 2019), with a fixed term for genotype and random effects for rows and columns as well as a smooth surface defined on row and column coordinates. Broad-sense heritabilities were calculated with the same R package, using the same model but with the genotype effect included as a random term. Regarding longitudinal traits (LAI),

genotypic values at individual time points, t, were obtained from their smoothed time series using a generalized additive model fitted to the spatially adjusted daily measurements,  $\tilde{y}_{i,k}(t)$ , for each plant k of genotype i :

$$\tilde{y}_{i,k}(t) = \alpha_i + f_i(t) + \epsilon_{i,k}(t), \quad \epsilon_{i,k}(t) \sim N(0, \sigma^2)$$
 (1)

where  $\alpha_i$  is a genotype-specific intercept,  $f_i$  (t) is a genotype-specific thin plate regression spline function on time, and  $\epsilon_{i,k}$  (t) is a random error term (R package statgenHTP, Millet & al., 2022; Pérez-Valencia *et al.*, 2022).

The genotypic maximum grain number per plant ( $GN_{max}$ ) was calculated after considering field plant density as GN BLUEs values over five high-potential experiments having the greatest number of common varieties : Gle22D, Cra21W, Mat22W, Bin22W and Cha22D.

Environmental characterization and multi-environment analyses. To characterize the above field experiments, we first defined three phenological phases (Millet *et al.*, 2019) (Fig. 3). First, the vegetative phase corresponded to the thermal time period between floral transition (leaf number=(FLN/2)-1), where FLN is final leaf number, and silk initiation (leaf number= FLN-2). Second, the flowering phase elapsed from silk initiation to the end of grain abortion (14 days at 20 °C after silking). Third, the grain-filling phase elapsed from the end of abortion to physiological maturity defined as the date at which grain water content decreases to 0.32 g g-1 matter. 36 environmental indices per phenological phase were then calculated with experiments environmental data including air temperature, soil water potential, light, air VPD, ETO and rainfall (Millet *et al.*, 2016, 2019).

To identify the most important environmental sources of yield variation in the multi-site experiment, an ANOVA-based stepwise regression was performed with the latter indices and variety factor as predictors of yield, using the R package 'olsrr' (Franke, 2010; Hebbali, 2020). Mean soil water potential at 60 cm depth (Psi\_flo) and mean of daily maximum temperatures (maxT\_flo) during the flowering phase for the reference hybrid (ARV18) were used to cluster field experiments into five environmental scenarios (Millet *et al.*, 2016). The three temperature scenarios were : cool (maxT\_flo < 27°C), warm (27°C  $\leq$  maxT\_flo < 30°C) and hot (maxT\_flo  $\geq$  30°C). Soil water conditions resulted in two scenarios : well-watered 'WW' (Psi\_flo  $\geq$  -99 kPa) and water-deficit 'WD' (Psi\_flo  $\leq$  -99 kPa).

To investigate GEI (genotype-by-environment interaction) variation for grain yield (Y) across the experiments grouped into environmental scenarios, we fitted a linear model using the R package 'stats':

$$Y = \mu + G + Scen + G \times Scen + Exp \times Scen + \varepsilon$$
 (2)

where  $\mu$  is the intercept, G is a genotypic main fixed effect, Scen is an environmental scenario main fixed effect, G x Scen is an interaction term fixed effect between genotype and environment scenario, Exp x Scen is a fixed effect representing 'experiments within scenarios' design and  $\epsilon$  is a residual effect.

Finally, we estimated genotypic sensitivities of grain number (GN) to environmental drivers identified above during the flowering phase (Psi\_flo and maxT\_flo). These sensitivities corresponded to regression coefficients obtained after fitting the following linear model:

$$GN_{i,j} = \mu + g_i + Psi_f lo_j + maxT_f lo_j + \beta_{1,i} \times Psi_f lo_{i,j} + \beta_{2,i} \times maxT_f lo_{i,j} + \varepsilon_{i,j}$$
(3)

where  $\mu$  is the intercept,  $g_i$  is a genotypic main fixed effect,  $Psi\_flo_j$  and  $maxT\_flo_j$  are environmental main effects and  $\varepsilon_{i,j}$  is a residual effect;  $\beta_{1,i}$  and  $\beta_{2,i}$  are the genotype-dependent sensitivities to environmental indices Psi\_flo and maxT\_flo, respectively, sensed by the i<sup>th</sup> hybrid in the j<sup>th</sup> experiment.

#### References

Beauchêne K, Leroy F, Fournier A, Huet C, Bonnefoy M, Lorgeou J, de Solan B, Piquemal B, Thomas S, Cohan J-P. 2019. Management and Characterization of Abiotic Stress via PhénoField®, a High-Throughput Field Phenotyping Platform. Frontiers in Plant Science 10.

Berger K, Atzberger C, Danner M, D'Urso G, Mauser W, Vuolo F, Hank T. 2018. Evaluation of the PROSAIL Model Capabilities for Future Hyperspectral Model Environments: A Review Study. *Remote Sensing* 10: 85.

Blancon J, Dutartre D, Tixier M-H, Weiss M, Comar A, Praud S, Baret F. 2019. A High-Throughput Model-Assisted Method for Phenotyping Maize Green Leaf Area Index Dynamics Using Unmanned Aerial Vehicle Imagery. *Frontiers in Plant Science* 10.

Casa R, Baret F, Buis S, Lopez-Lozano R, Pascucci S, Palombo A, Jones HG. 2010. Estimation of maize canopy properties from remote sensing by inversion of 1-D and 4-D models. *Precision Agriculture* 11: 319–334.

**Duan S-B, Li Z-L, Wu H, Tang B-H, Ma L, Zhao E, Li C**. **2014**. Inversion of the PROSAIL model to estimate leaf area index of maize, potato, and sunflower fields from unmanned aerial vehicle hyperspectral data. *International Journal of Applied Earth Observation and Geoinformation* **26**: 12–20.

van Eeuwijk FA, Bustos-Korts D, Millet EJ, Boer MP, Kruijer W, Thompson A, Malosetti M, Iwata H, Quiroz R, Kuppe C, et al. 2019. Modelling strategies for assessing and increasing the effectiveness of new phenotyping techniques in plant breeding. *Plant Science* 282: 23–39.

**Fernández JA, Messina CD, Salinas A, Prasad PVV, Nippert JB, Ciampitti IA. 2022.** Kernel weight contribution to yield genetic gain of maize: a global review and US case studies (S Dreisigacker, Ed.). *Journal of Experimental Botany* **73**: 3597–3609.

**Franke GR. 2010**. Stepwise Regression. In: Wiley International Encyclopedia of Marketing. John Wiley & Sons, Ltd.

**Garriques S, Shabanov NV, Swanson K, Morisette JT, Baret F, Myneni RB. 2008**. Intercomparison and sensitivity analysis of Leaf Area Index retrievals from LAI-2000, AccuPAR, and digital hemispherical photography over croplands. *Agricultural and Forest Meteorology* **148**: 1193–1209.

van Genuchten MTh. 1980. A Closed-form Equation for Predicting the Hydraulic Conductivity of Unsaturated Soils. *Soil Science Society of America Journal* 44: 892–898.

Hammer GL, van Oosterom E, McLean G, Chapman SC, Broad I, Harland P, Muchow RC. 2010. Adapting APSIM to model the physiology and genetics of complex adaptive traits in field crops. *Journal of Experimental Botany* **61**: 2185–2202.

**Hebbali A. 2020**. Introduction to olsrr package. A tool for OLS regression using R. https://cran.r-project.org/web/packages/olsrr/vignettes/intro.html.

Lacube S, Manceau L, Welcker C, Millet EJ, Gouesnard B, Palaffre C, Ribaut J-M, Hammer G, Parent B, Tardieu F. 2020. Simulating the effect of flowering time on maize individual leaf area in contrasting environmental scenarios. *Journal of Experimental Botany* 71: 5577–5588.

**Millet EJ, al. 2022**. statgenHTP: High Throughput Phenotyping (HTP) Data Analysis R package version 1.0.4.

Millet EJ, Kruijer W, Coupel-Ledru A, Alvarez Prado S, Cabrera-Bosquet L, Lacube S, Charcosset A, Welcker C, van Eeuwijk F, Tardieu F. 2019. Genomic prediction of maize yield across European environmental conditions. *Nature Genetics* 51: 952–956.

Millet E, Welcker C, Kruijer W, Negro S, Nicolas S, Praud S, Ranc N, Presterl T, Tuberosa R, Bedo Z, et al. 2016. Genome-wide analysis of yield in Europe: allelic effects as functions of drought and heat scenarios. Plant Physiology: pp.00621.2016.

Parent B, Leclere M, Lacube S, Semenov MA, Welcker C, Martre P, Tardieu F. 2018. Maize yields over Europe may increase in spite of climate change, with an appropriate use of the genetic variability of flowering time. *Proceedings of the National Academy of Sciences* 115: 10642–10647.

**Parent B, Turc O, Gibon Y, Stitt M, Tardieu F. 2010**. Modelling temperature-compensated physiological rates, based on the co-ordination of responses to temperature of developmental processes. *Journal of Experimental Botany* **61**: 2057–2069.

Pérez-Valencia DM, Rodríguez-Álvarez MX, Boer MP, Kronenberg L, Hund A, Cabrera-Bosquet L, Millet EJ, Eeuwijk FA van. 2022. A two-stage approach for the spatio-temporal analysis of high-throughput phenotyping data. *Scientific Reports* 12: 3177.

**Turc O, Tardieu F. 2018**. Drought affects abortion of reproductive organs by exacerbating developmentally driven processes via expansive growth and hydraulics. *Journal of Experimental Botany* **69**: 3245–3254.

Welcker C, Spencer NA, Turc O, Granato I, Chapuis R, Madur D, Beauchene K, Gouesnard B, Draye X, Palaffre C, et al. 2022. Physiological adaptive traits are a potential allele reservoir for maize genetic progress under challenging conditions. *Nature Communications* 13: 3225.

**Zhu W, Rezaei EE, Nouri H, Sun Z, Li J, Yu D, Siebert S**. **2022**. UAV-based indicators of crop growth are robust for distinct water and nutrient management but vary between crop development phases. *Field Crops Research* **284**: 108582.

#### **Acknowledgments**

We are grateful to all INVITE project partners who carried out maize field experiments: ARVALIS (France), GEVES (France), Agroscope (Switzerland), Nebih (Hungary), Ukzuz (Czechia), AGES (Austria), BSA (Germany) and ILVO (Belgium).

We are very grateful to Nathalie Luchaire (GEVES) and Théophile Moreal de Brevans (INRAE) for their contribution to the data management and analysis. We acknowledge Nadir Abu-Samra-Spencer (INRAE) and Juan Herrera (Agroscope) for the supervision of the trials network in Europe. We are also grateful to Katia Beauchêne for the coordination of image-based phenotyping.

## Supplementary table 1. Varieties of the recent hybrids panel, including INVITE subset, and number of field experiments in which they were evaluated.

11.4.22	Year of	NA-t	FAO Index	D I	INVITE	#
Hybrid	release	Maturity group	group	Breeder	subset	Exp
ARV01	2011	G2 (mid-early)	(280 - 320)	LIMAGRAIN	Х	26
ARV12	2017	G2 (mid-early)	(280 - 320)	BAYER	Х	25
ARV31	2017	G2 (mid-early)	(280 - 320)	EURALIS	Х	26
ARV32	2012	G2 (mid-early)	(280 - 320)	EURALIS	Х	26
ARV50	2020	G2 (mid-early)	(280 - 320)	KWS	Х	22
ARV55	2016	G2 (mid-early)	(280 - 320)	PIONEER	Х	23
ARV79	2014	G2 (mid-early)	(280 - 320)	RAGT	Х	26
ARV83	2019	G2 (mid-early)	(280 - 320)	RAGT	Х	26
ARV87	2018	G2 (mid-early)	(280 - 320)	SYNGENTA	Х	26
ARV94	2015	G2 (mid-early)	(280 - 320)	BAYER	Х	16
X47D113_29	2018	G2 (mid-early)	(280 - 320)	SYNGENTA	Х	23
X47D113_95	2020	G2 (mid-early)	(280 - 320)	LIMAGRAIN	Х	23
ARV04	2018	G3 (intermediate)	(320 - 400)	KWS	Х	30
ARV18	2009	G3 (intermediate)	(320 - 400)	BAYER	Х	32
ARV20	2016	G3 (intermediate)	(320 - 400)	BAYER	Х	29
ARV23	2009	G3 (intermediate)	(320 - 400)	BAYER	Х	29
ARV24	2011	G3 (intermediate)	(320 - 400)	BAYER	Х	28
ARV39	2012	G3 (intermediate)	(320 - 400)	RAGT	Х	29
ARV52	2018	G3 (intermediate)	(320 - 400)	KWS	Х	30
ARV85	2015	G3 (intermediate)	(320 - 400)	RAGT	Х	30
ARV89	2018	G3 (intermediate)	(320 - 400)	SYNGENTA	Х	25
ARV25	2013	G4 (mid-late)	(400 - 480)	BAYER	Х	26
ARV27	2016	G4 (mid-late)	(400 - 480)	BAYER	Х	25
ARV60	2015	G4 (mid-late)	(400 - 480)	LIMAGRAIN	Х	26
ARV66	2015	G4 (mid-late)	(400 - 480)	PIONEER	Х	27
ARV72	2014	G4 (mid-late)	(400 - 480)	PIONEER	Х	27
ARV73	2017	G4 (mid-late)	(400 - 480)	CAUSSADE	Х	22
ARV84	2018	G4 (mid-late)	(400 - 480)	RAGT	Х	14
X47D113_09	2020	G4 (mid-late)	(400 - 480)	BAYER	Х	19
X47D113_74	2020	G4 (mid-late)	(400 - 480)	KWS	Х	21
ARV09	2013	G2 (mid-early)	(280 - 320)	BAYER		4
ARV10	2015	G2 (mid-early)	(280 - 320)	BAYER		4
ARV11	2017	G2 (mid-early)	(280 - 320)	BAYER		4
ARV13	2017	G2 (mid-early)	(280 - 320)	BAYER		4
ARV14	2017	G2 (mid-early)	(280 - 320)	BAYER		4
ARV15	2020	G2 (mid-early)	(280 - 320)	BAYER		4
ARV30	2019	G2 (mid-early)	(280 - 320)	EURALIS		4
ARV33	2018	G2 (mid-early)	(280 - 320)	EURALIS		4
ARV37	2019	G2 (mid-early)	(280 - 320)	RAGT		4
ARV48	2017	G2 (mid-early)	(280 - 320)	KWS		4
ARV54	2016	G2 (mid-early)	(280 - 320)	PIONEER		4
ARV61	2017	G2 (mid-early)	(280 - 320)	KWS		4

## Supplementary Table 1 (continued). Varieties of the recent hybrids panel, including INVITE subset, and number of field experiments in which they were evaluated.

	Year of	Year of FAO Index			INVITE	#
Hybrid	release	Maturity group	group	Breeder	subset	Exp
ARV69	2014	G2 (mid-early)	(280 - 320)	PIONEER		4
ARV75	2008	G2 (mid-early)	(280 - 320)	PIONEER		4
ARV77	2014	G2 (mid-early)	(280 - 320)	LIMAGRAIN		4
ARV80	2020	G2 (mid-early)	(280 - 320)	RAGT		4
ARV16	2015	G3 (intermediate)	(320 - 400)	BAYER		7
ARV19	2020	G3 (intermediate)	(320 - 400)	BAYER		7
ARV21	2017	G3 (intermediate)	(320 - 400)	BAYER		7
ARV22	2016	G3 (intermediate)	(320 - 400)	BAYER		7
ARV28	2016	G3 (intermediate)	(320 - 400)	BAYER		8
ARV40	2016	G3 (intermediate)	(320 - 400)	BAYER		7
ARV42	2020	G3 (intermediate)	(320 - 400)	KWS		7
ARV44	2016	G3 (intermediate)	(320 - 400)	BAYER		7
ARV46	2015	G3 (intermediate)	(320 - 400)	CAUSSADE		7
ARV47	2018	G3 (intermediate)	(320 - 400)	BAYER		7
ARV59	2015	G3 (intermediate)	(320 - 400)	PIONEER		7
ARV65	2011	G3 (intermediate)	(320 - 400)	CAUSSADE		7
ARV88	2015	G3 (intermediate)	(320 - 400)	SYNGENTA		7
ARV90	2019	G3 (intermediate)	(320 - 400)	SYNGENTA		7
ARV91	2018	G3 (intermediate)	(320 - 400)	BAYER		7
X47D113_49	2015	G3 (intermediate)	(320 - 400)	BAYER		7
ARV03	2012	G4 (mid-late)	(400 - 480)	KWS		6
ARV05	2015	G4 (mid-late)	(400 - 480)	RAGT		6
ARV06	2017	G4 (mid-late)	(400 - 480)	BAYER		7
ARV07	2013	G4 (mid-late)	(400 - 480)	LIMAGRAIN		5
ARV08	2016	G4 (mid-late)	(400 - 480)	BAYER		6
ARV26	2015	G4 (mid-late)	(400 - 480)	BAYER		7
ARV29	2019	G4 (mid-late)	(400 - 480)	BAYER		6
ARV35	2019	G4 (mid-late)	(400 - 480)	EURALIS		6
ARV41	2010	G4 (mid-late)	(400 - 480)	RAGT		6
ARV51	2018	G4 (mid-late)	(400 - 480)	KWS		6
ARV56	2012	G4 (mid-late)	(400 - 480)	PIONEER		6
ARV57	2015	G4 (mid-late)	(400 - 480)	PIONEER		6
ARV58	2017	G4 (mid-late)	(400 - 480)	PIONEER		6
ARV63	2014	G4 (mid-late)	(400 - 480)	MAS_SEEDS		6
ARV64	2012	G4 (mid-late)	(400 - 480)	RAGT		6
ARV67	2012	G4 (mid-late)	(400 - 480)	PIONEER		6
ARV71	2012	G4 (mid-late)	(400 - 480)	PIONEER		6
ARV74	2019	G4 (mid-late)	(400 - 480)	BAYER		6
ARV76	2017	G4 (mid-late)	(400 - 480)	BAYER		6
ARV78	2017	G4 (mid-late)	(400 - 480)	BAYER		6
ARV82	2015	G4 (mid-late)	(400 - 480)	RAGT		6
ARV93	2017	G4 (mid-late)	(400 - 480)	RAGT		6
X47D113_08	2015	G4 (mid-late)	(400 - 480)	BAYER		6
X47D113_12	2015	G4 (mid-late)	(400 - 480)	RAGT		3

## Supplementary Table 2. Field experiments performed for the entire recent hybrids panel or a subset of it.

Name exp.	Location	GPS Coord.	Year	Country	Institution	Water management	Scenario	Maturity groups	# Hyb	Measured traits
Ang22D	Lion d'Angers	47.573, -0.729	2022	France	ARVALIS	rainfed	Warm_WD	G2	29	Emergence, Anthesis & Silking dates, Plant density, Yield & its components
Bin22W (Field 3)	Binas	47.92, 1.479	2022	France	ARVALIS	irrigated	Warm_WW	G2, G3, G4	86	LAR, Emergence, Anthesis & Silking dates, Leaf 6 dimensions, Plant density, Final leaf number, Yield & its components
Cad22W	Cadenazzo	46.162, 8.934	2022	Switzerland	Agroscope	irrigated	Hot_WW	G2, G3, G4	30	Emergence, Anthesis & Silking dates, Plant density, Yield & its components
Cha21D	Changins	46.399, 6.239	2021	Switzerland	Agroscope	rainfed	Cool_WW	G2, G3, G4	29	Emergence, Anthesis & Silking dates, Plant density, Yield
Cha22D	Changins	46.401, 6.256	2022	Switzerland	Agroscope	irrigated	Warm_WW	G2, G3, G4	30	Emergence, Anthesis & Silking dates, Plant density, Yield & its components
Chr21D	Chrlice	49.125, 16.634	2021	Czechia	Ukzuz	rainfed	Warm_WW	G2, G3, G4	23	Emergence, Anthesis & Silking dates, Plant density, Yield & its components
Chr22D	Chrlice	49.119, 16.632	2022	Czechia	Ukzuz	rainfed	Warm_WD	G2, G3, G4	30	Emergence, Anthesis & Silking dates, Plant density, Yield & its components
Cra21D	Cramchaban	46.2, -0.706	2021	France	ARVALIS	rainfed	Cool_WW	G3, G4	54	Emergence, Anthesis & Silking dates, Plant density, Yield & its components
Cra21W	Cramchaban	46.214, -0.706	2021	France	ARVALIS	irrigated	Cool_WW	G3, G4	54	Emergence, Anthesis & Silking dates, Plant density, Yield & its components
Gle21D	Gleisdorf	47.114, 15.703	2021	Austria	AGES	rainfed	Warm_WW	G2, G3, G4	20	Emergence, Anthesis & Silking dates, Plant density, Yield & its components
Gle22D	Gleisdorf	47.114, 15.703	2022	Austria	AGES	rainfed	Warm_WD	G2, G3, G4	30	Emergence, Anthesis & Silking dates, Plant density, Yield & its components
Has21D	Hassloch	49.385, 8.268	2021	Germany	BSA	rainfed	Cool_WW	G2, G3, G4	28	Emergence, Anthesis & Silking dates, Plant density, Yield & its components
Has22D	Hassloch	49.382, 8.264	2022	Germany	BSA	rainfed	Cool_WW	G2, G3, G4	30	Emergence, Anthesis & Silking dates, Plant density, Yield & its components
LMg21D	Le Magneraud	46.15, -0.695	2021	France	GEVES	rainfed	Cool_WW	G2, G3, G4	30	Emergence, Anthesis & Silking dates, Plant density, Yield & its components
LMg21W	Le Magneraud	46.154, -0.695	2021	France	GEVES	irrigated	Cool_WW	G2, G3, G4	30	Emergence, Anthesis & Silking dates, Plant density, Yield & its components
LMg22D	Le Magneraud	46.153, -0.693	2022	France	GEVES	rainfed	Hot_WD	G2, G3, G4	30	Emergence, Anthesis & Silking dates, Plant density, Yield & its components
LMg22W	Le Magneraud	46.153, -0.694	2022	France	GEVES	irrigated	Hot_WW	G2, G3, G4	30	Emergence, Anthesis & Silking dates, Plant density, Yield & its components

Name exp., Experiment name used in the text; Year, year when the experiment was done.

## Supplementary Table 2 (continued). Field experiments performed for the entire recent hybrids panel or a subset of it.

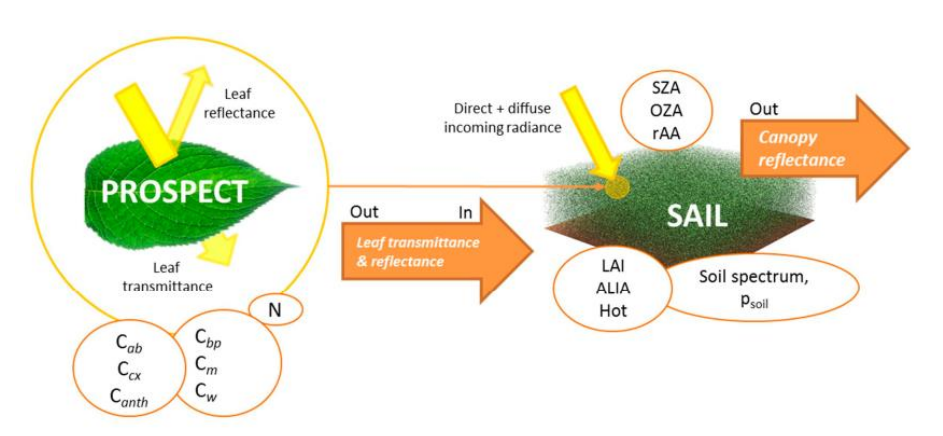
Name exp.	Location	GPS Coord.	Year	Country	Institution	Water management	Scenario	Maturity groups	# Hyb	Measured traits
Mat21W	Matzenheim	48.402, 7.619	2021	France	ARVALIS	rainfed	Cool_WW	G2	26	Emergence, Anthesis & Silking dates, Plant density, Yield & its components LAR, Emergence, Anthesis
Mat22W (Field 1)	Matzenheim	48.401, 7.618	2022	France	ARVALIS	irrigated	Cool_WW	G2, G3	53	& Silking dates, Leaf 6 dimensions, Plant density, Final leaf number, Yield & its components
Mau22D	Mauguio	43.6, 3.973	2022	France	GEVES	rainfed	Hot_WD	G2, G3, G4	30	ALA, LAI, fiPAR, Emergence, Anthesis & Silking dates, Plant density, Yield & its components
Mau22W	Mauguio	43.612, 3.973	2022	France	GEVES	irrigated	Hot_WW	G2, G3, G4	30	LAR, ALA, LAI, fiPAR, Emergence, Anthesis & Silking dates, Plant density, Final leaf number, Yield & its components
Mer21D	Merelbeke	50.975, 3.743	2021	Belgium	ILVO	rainfed	Cool_WW	G2, G3	20	Emergence, Anthesis & Silking dates, Plant density, Yield & its components
Mer22D	Merelbeke	50.983, 3.773	2022	Belgium	ILVO	rainfed	Cool_WW	G2, G3	23	Emergence, Anthesis & Silking dates, Plant density, Yield & its components
Mon21D	Montardon	43.358, -0.36	2021	France	ARVALIS	rainfed	Cool_WW	G3, G4	54	Emergence, Anthesis & Silking dates, Plant density, Yield & its components
Mon22D	Montardon	43.358, -0.36	2022	France	ARVALIS	irrigated	Cool_WD	G3, G4	58	Emergence, Anthesis & Silking dates, Plant density, Yield & its components
Ouz22D	PhenoField	47.8, 1.519	2022	France	ARVALIS	rainfed	Warm_WD	G2, G3, G4	24	ALA, LAI, fiPAR, Emergence, Anthesis & Silking dates, Plant density, Yield & its components
Ouz22W	PhenoField	47.884, 1.519	2022	France	ARVALIS	irrigated	Warm_WW	G2, G3, G4	24	ALA, LAI, fiPAR, Emergence, Anthesis & Silking dates, Plant density, Yield & its components
Pac22D	Pachfurth	48.061, 16.817	2022	Austria	AGES	rainfed	Warm_WD	G2, G3, G4	30	Emergence, Anthesis & Silking dates, Plant density, Yield & its components
Pus21W (Field 4)	Pusignan	45.741, 5.075	2021	France	ARVALIS	irrigated	Cool_WW	G3, G4	54	ALA, LAI, fiPAR, Emergence, Plant density
Pus22D	Saint Bonnet de Mure	45.7, 5.046	2022	France	ARVALIS	rainfed	Warm_WD	G3, G4	20	ALA, LAI, fiPAR, Emergence, Anthesis & Silking dates, Plant density, Yield & its components
Pus22W (Field 2)	Saint Bonnet de Mure	45.714, 5.046	2022	France	ARVALIS	irrigated	Warm_WW	G3, G4	58	ALA, LAI, fiPAR, Emergence, Anthesis & Silking dates, Plant density, Final leaf number, Yield & its components
Sek21D	Szekkutas	46.519, 20.523	2021	Hungary	Nebih	rainfed	Hot_WD	G2, G3, G4	30	Emergence, Anthesis & Silking dates, Plant density, Yield & its components
Tor22D	Tordas	47.329, 18.753	2022	Hungary	Nebih	rainfed	Hot_WD	G2, G3, G4	30	Emergence, Anthesis & Silking dates, Plant density, Yield

Name exp., Experiment name used in the text; Year, year when the experiment was done.

Supplementary Table. 3: Overview of the input parameters of the PROSAIL model, with symbols, units and typical variable ranges published in the literature for five different crops that have been analyzed most often by the studies (Berger et al. 2018).

Parameter	Symbol	Units		Typic	al Ranges for	Crops	
			Maize	Wheat	Rice	Soybean	Sugar Beet
		Leaf Mod	el: (PROSPECT-	·D)			
Leaf structure index	N	Unit less	1.2-1.8	1.0-2.5	1.0-2.0	1.2-2.6	1.0-1.5
Chlorophyll a + b content	C <sub>ab</sub>	(μg/cm <sup>2</sup> )	0-80	0-80	0-80	0-80	20-45
Total carotenoid content	C <sub>cx</sub>	(μg/cm <sup>2</sup> )	1-24	1-24	4–17	-	-
Total anthocyanin content	C <sub>anth</sub>	(μg/cm <sup>2</sup> )	-	-	-	-	-
Brown pigments	C <sub>bp</sub>	Unit less	0-1	0-1	0-1	0-1	0-1
Dry matter content, or leaf mass per area	C <sub>m</sub> /LMA	(g/cm <sup>2</sup> )	0.004-0.0075	0.001-0.02	0.001-0.02	0.001-0.02	0.004-0.007
Equivalent water thickness, or water depth	EWT/C <sub>w</sub>	(cm)	0.01-0.03	0.001-0.05	0.001-0.002	0.001-0.05	0.03-0.08
		Сапору	y Model: (4SAIL)	)			
Leaf area index	LAI	$(m^2/m^2)$	0–7	0-8	0-10	0–7	0–4
Average leaf inclination angle * or: Leaf inclination distribution function **	ALIA LIDF <sub>a/b</sub>	(°) (°)	20–70	20-90	20-80	10–75	20–40
Hot spot parameter	Hot	(m/m)	0.01-0.2	0.01-0.5	0.01-0.1	0.2	0.2-0.4
Soil reflectance	$\rho_{soil}$	(%)					
Soil brightness factor	$\alpha_{soil}$	Unit less		0.5	-1.5 *** or 0-1	****	
		Unit less		23% for a	standard clea	r sky	
		(°)	-				
Viewing (observer) zenith angle	$OZA/\theta_v$	(°)	According	to actual con	ditions during	data/image a	cquisition
Relative azimuth angle between sun and sensor	rAA/ø <sub>SV</sub>	(°)					

<sup>\*</sup> characterizes an ellipsoidal leaf inclination model; \*\* spherical, planophile, erectophile, uniform, extremophile or plagiophile types. LIDF is characterized by LIDFa, which controls the average leaf slope and LIDFb which controls the distribution's bimodality; \*\*\* to be multiplied with single psoil spectrum; \*\*\*\* scaling factor between the two model implemented psoil spectra (wet versus dry).



Supplementary Fig. 1: Calculation of canopy reflectance using the coupled PROSPECT + SAIL models. PROSAIL combines the leaf optical properties model PROSPECT with the turbid medium canopy radiative transfer model SAIL. The models are coupled so that the simulated leaf reflectance and transmittance from PROSPECT are fed into the SAIL model, completed with information about soil optical properties and illumination/observation geometry (Berger et al. 2018). Variable symbols are explained in Supplementary Table 3.

# CHAPTER 3 : SIMULATING LEAF AREA INDEX AND GRAIN NUMBER FOR PANELS OF MAIZE HYBRIDS IN CONTRASTING ENVIRONMENTAL CONDITIONS

This chapter presents the current status of this work, which will still be fine-tuned before submission to a journal, in particular:

- Modelling individual grain weight and grain yield, in addition to leaf area index and grain number presented here
- Optimising the set of genotype-dependent parameters provided to the crop model and their calculations
- Validating the model using more experiments and genotypes

#### **TABLE OF CONTENTS**

Introduction7
Approach used in the Chapter
Genotype-dependent parameters
Use of the genotypic parameters by Sirius Maize
Test of the relevance of simulation results
Results and discussion
I) Simulation of leaf area index (LAI)8
Sirius Maize accounted for both the genotypic and environmental effects on L
but with different accuracies depending on environmental scenarios ar
considered test
LAI simulation accuracies remained nearly unchanged when parameters resulte
from genomic prediction
The genotypic variability of LAI in contrasting environmental conditions depende
on phenology and leaf elongation rate
II) Simulation of grain number (GN)
Sirius Maize accounted for both the genotypic and environmental effects on gra
number per unit area

	GN Simulation accuracies decreased but remained appreciable when	genotype-
	dependent parameters were predicted from genomic information	93
	The genotypic variability of GN in contrasting environmental conditions	depended
	on the maximum grain number potential and leaf growth rate	96
Me	thods	99
	Calculation of genotype-dependent parameters fed to Sirius Maize	99
	LAI modelling in Sirius Maize	99
	Grain number modelling in Sirius Maize	100
	Simulation tests accuracies	101
Ref	erences	101
Sup	pplementary information	103

#### Introduction

In this chapter, we tested the consistency of our predictive approach, which aimed at simulating the performance of hundreds of genotypes via a combination of phenomics, genomic prediction and crop modelling. The specificity of this chapter is to perform simulations based on a crop model whose genotype-dependent parameters originate from traits presented in previous chapters. However, due to time constraints, our study was limited here to the first part of the crop cycle, with the predictions of leaf area index (LAI) and grain number (GN) for tens of varieties in contrasting environmental conditions. Simulations were based on a set of traits, transformed into model parameters, related to (i) plant phenology (leaf appearance rate 'LAR' and final plant leaf number 'FLN'), (ii) plant architecture (rh<sub>PAD</sub>), (iii) leaf growth (max leaf expansion rate 'LER') and (iv) plant responses to environmental conditions (stomatal conductance gs<sub>max</sub>, LER sensitivities to VPD and SWP, Table 1). We also estimated the genotype-dependent maximum plant grain number (GN<sub>max</sub>) based on the dataset presented in Chapter 2. As tested in Chapter 1, the genotypic values of these traits can be estimated via statistical prediction models based on genomic information only.

We used for that the process-based crop model Sirius Maize, which simulates the phenology, the growth and the development of maize plants from sowing to physiological maturity, along with the fluxes of water, nitrogen and carbon in the soil-plant-atmosphere continuum in response to environmental conditions and crop management. Its input data are crop management practices (sowing date, planting density, irrigation dates and amounts, soil fertilisation dates and amounts), micro-meteorological daily data (min and max air temperatures, global radiation, rainfall and air relative humidity) and soil main characteristics of the target simulated field (soil depth; soil water lower, drained upper and saturated limits; soil bulk density and soil organic N content), provided to the model via a specific interface. Genotype-dependent parameters are also provided to the model via an interface. Sirius Maize derives from SiriusQuality2 originally developed for small grain cereals (Jamieson et al., 1998; Martre et al., 2006; Supplementary Fig. 1), but was recently extended to maize. For that, the LEPSE group, in collaboration with Limagrain, adapted original algorithms, used modules developed by Lacube et al. (2020) for the model APSIM (Hammer et al., 2010) and redeveloped the code with the software framework BioMA. The Sirius graphical interface provides tools for complex multi-runs and for parameter optimization.

Table 1 : Summary of measured traits used for estimating genotype-dependent parameters of Sirius Maize.

		Range of t	rait values		Sirius
	Used traits for Sirius parameterization	Genetic progress panel	Recent hybrids panel	Origin	genotypic parameters
PHENOLOGY	1) Leaf Appearance Rate (LAR, leaf/d <sub>20°C</sub> )	0.22 - 0.30	0.23 - 0.29	Indoor PF /Field	phyl <sub>tip</sub> , b <sub>tip</sub> , a <sub>ll1</sub> , b <sub>ll1</sub>
PHENOLOGY	2) Final Leaf Number (FLN)	14 – 20	16 – 20	Indoor PF /Field	N <sub>final</sub> , α <sub>tr</sub> , stopLigul
GROWTH	3) max Leaf Expansion Rate (LER, cm²/d <sub>20°c</sub> )	128 – 230	112 – 182	Indoor PF	LERa
ARCHITECTURE	4) rh <sub>PAD</sub>	0.21 - 0.38	0.29 - 0.43	Indoor PF	KI coeff
	5) Stomatal Conductance (gs <sub>max</sub> , mmol/m²/s)	97 – 144	116 – 125	Indoor PF	LUEpre
RESPONSES TO ENVIRONMENT	6) LER Sensitivity to VPD (mm/d <sub>20°C</sub> /kPa)	-2.051.02	-1.731.38	Indoor PF	LERb
	7) LER Sensitivity to SWP (mm/d <sub>20*C</sub> /MPa)	4.27 - 7.82	5.75 – 6.63	Indoor PF	LERc
MAX YIELD COMPONENTS	8) max Grain number (grains/plant)	256 – 612	422 – 590	Field	GN <sub>max</sub>

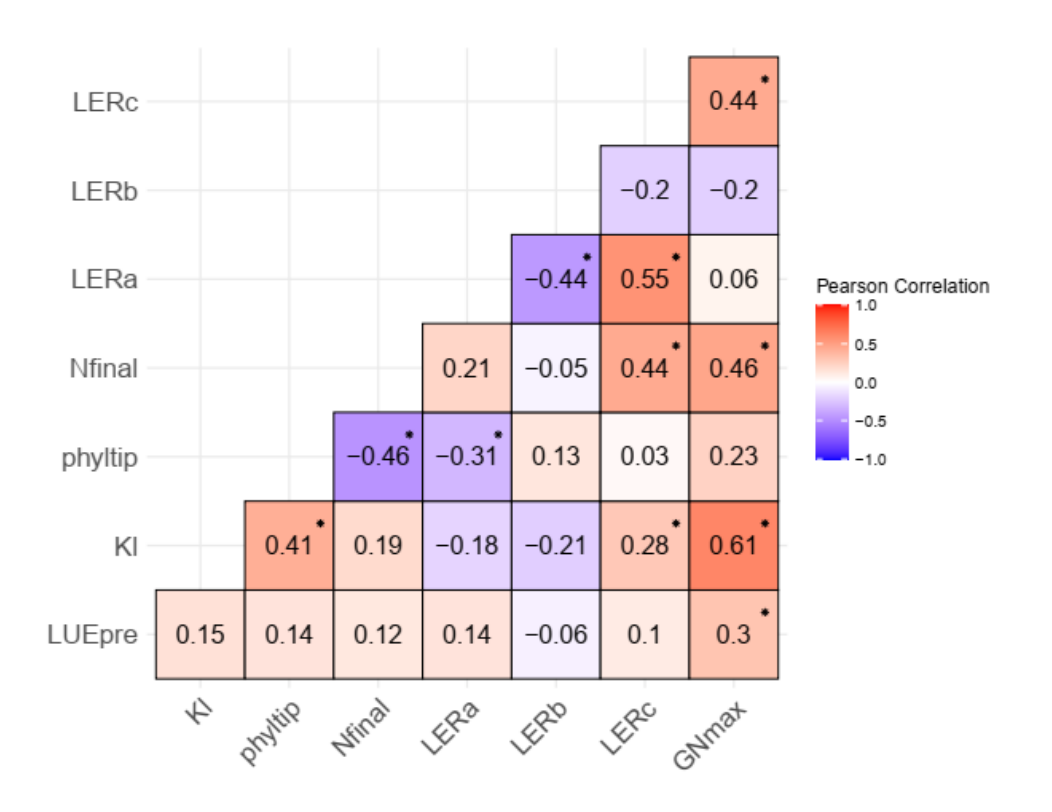


Fig. 1: Correlation heat map for estimated genotype-dependent parameters for the genetic progress panel. Statistically significant correlations are shown with an asterisk.

#### **Approach used in the Chapter**

#### Genotype-dependent parameters.

A set of 13 genotype-dependent parameters that serve to run Sirius maize calculations was derived from the datasets presented in Chapters 1 and 2 (Table 1, Fig. 1, Supplementary Table 1). All parameters not described here were considered as common to all studied genotypes (Lacube et *al.* 2020).

- -Some of these parameters directly derived from measured traits: (i) N<sub>final</sub>, the plant leaf number at flowering time (a trait highly correlated to anthesis date, Parent *et al.*, 2018; Castelletti *et al.*, 2020), (ii) GN<sub>max</sub>, the grain number per plant calculated by considering grain number in fields with best environmental conditions, (iii) LERb, the slope of the linear regression between leaf elongation rate and VPD, estimated in indoor experiments with a time definition of one hour, (iv) LERc, the slope of the linear regression between leaf elongation rate and SWP, estimated in indoor experiments with a time definition of one day (Welcker *et al.*, 2011; Chapuis *et al.*, 2012).
- Other parameters were extracted from traits by using simple equations. Together with traits presented above (N<sub>final</sub>, LERb, LERc), they are used by Sirius Maize to calculate leaf area index (LAI). These parameters are: (i) the genotype-dependent thermal time between the emission and ligulation of two consecutive leaves (phyllochron 'phyl $_{tip}$ ' and ligulochron ' $a_{ll1}$ ', respectively), (ii) genotype-dependent parameters describing the beginning and end of these processes and the shape of their relation to thermal time ( $b_{tip}$ ,  $b_{ll1}$ ,  $\alpha_{tr}$  and stopLigul), (iii) the elongation rate of leaf 6 (LERa), from which the model calculates that of all other leaves. The calculation of these parameters (LERa, phyl $_{tip}$ ,  $b_{tip}$ ,  $a_{ll1}$ ,  $b_{ll1}$ ,  $\alpha_{tr}$  and stopLigul) is detailed in the methods section.
- Finally, two genotype-dependent parameters (kl and LUE) were extracted from traits that are related to them, but cannot be calculated via deterministic equations. These parameters were scaled to the corresponding traits (see Methods). They are used in the model for the Monteith approach of transformation of incident light into biomass:

ΔBiomass (0, t) = 
$$\int_0^t Lx RIEx LUE dt$$
 (1)

Where  $\Delta$ Biomass (0,t) is the accumulation of biomass from times 0 to t, L is the incident light with a time definition (dt) of one day, RIE (radiation interception efficiency) is the ratio of

intercepted to incident light, with the same time definition, and LUE (light use efficiency) is the ratio of biomass accumulation to intercepted light, with the same time definition.

The first parameter used by Sirius Maize is the light extinction coefficient, kl, which affects the shape of the relationship between LAI and RIE.

$$RIE = 1 - e^{-kl \times LAI}$$
 (2)

It was scaled to rh<sub>PAD</sub> plant architecture trait, which largely affects RIE (Perez *et al.*, 2019). Notably, the most recent version of Sirius Wheat (SiriusQuality3) directly involves ALA, as defined in Chapter 1, so the scaling procedure used here will not be necessary any more. This version is not yet implemented in Sirius Maize but will be in the next months.

The second parameter was LUEpre (pre-anthesis LUE), which was scaled to the plant stomatal conductance (gs<sub>max</sub>, presented in Chapter 1). Indeed, LUE is a direct consequence of the ability of the canopy to photosynthesize, itself related to canopy stomatal conductance (Motzo *et al.*, 2013; Wang *et al.*, 2022).

#### Use of the genotypic parameters by Sirius Maize.

Leaf area index was modelled as in Lacube *et al.* (2020), as a result of processes related to plant development and leaf elongation and widening (Supplementary Table 1). The areas of the leaves of each rank on the stem were calculated daily based on the genotype-dependent parameters presented above (see Methods). Importantly, elongation rate of any growing leaf rank was calculated from that of leaf 6 (LERa), leading to a profile of leaf elongation rates, on which the effects of evaporative demand (VPD) and soil water potential (SWP) were applied by taking into account the corresponding genotype-dependent sensitivities (LERb and LERc, respectively). This follows studies showing that leaf elongation rate is primarily impacted by VPD and SWP (Welcker *et al.* 2011; Lacube *et al.* 2017).

Grain number was modelled by taking into account the mean daily plant growth rate in biomass (PGR, g.d<sup>-1</sup>.plant<sup>-1</sup>), estimated during the period from 13 d<sub>20°C</sub> before silking to 22 d<sub>20°C</sub> after it. Indeed, it was shown that straightforward relations are observed between the PGR around flowering time and the grain number per plant (Messina *et al.*, 2019; Larrosa & Borrás, 2022; Supplementary Fig. 2). Grain number was calculated as a logarithmic function of PGR, taking into account the genotype-dependent parameter GN<sub>max</sub>, whereas the parameters

affecting the shape of this function were considered as common to all studied genotypes  $(PGR_{base} \ and \ GN_k, \ see \ methods).$ 

#### Test of the relevance of simulation results.

A first test was performed, where all indoor platform traits used for deriving genotypic parameters were measured for all hybrids (Table 1), based on the BLUEs resulting from four indoor experiments. It was performed on the dataset collected in the genetic progress study (Welcker *et al.*, 2022). This is a near-ideal case for best accuracy, so this first test can be considered as the least stringent one. Indeed, the workload associated with this test is probably not applicable to potential future routine approaches. Simulations were run in 10 field experiments, representing contrasting environmental scenarios for temperature and soil water status, including two experiments where LAI was derived from UAV imaging.

A second test (performed on the recent hybrid panel) considered the case in which three traits/parameters were measured (LAR, FLN and  $GN_{max}$ ), whereas all other traits were obtained via genomic prediction ( $rh_{PAD}$ ,  $gs_{max}$ , LERa, LERb and LERc). Simulations were performed in 17 field experiments, representing contrasting environmental conditions, including seven experiments where LAI was derived from UAV imaging.

The last, most stringent test, was performed by using, in the model, the genomic prediction values of all traits/parameters. The latter were calculated from the cross-validation scheme (CV1) for the genetic progress panel and, for the recent hybrids panel, from the training sets collected with the diversity and genetic progress datasets (see Chapter 1). Simulations were run in the same experiments mentioned before.

Finally, we tested the impact on LAI and GN simulation accuracies of Sirius parameters by running simulations for genetic progress panel in the same experiments as before, but with some parameters fixed to the mean value for all hybrids, while the other parameters were kept as genotype-dependent.

#### **Results and discussion**

Table 2 : Summary of simulation results for LAI and grain number.

	Field	Sirius parameterization with measured genotypic values				Sirius parameterization with predicted genotypic values				
Field Simulated Trait	Experiments Scenario	Genetic progress panel		Recent hybrids panel		Genetic pa	progress nel	Recent hybrids panel		
		r	rrmse	r	rrmse	r	rrmse	r	rrmse	
	Cool_WW	-	-	0.39	24%	-	-	0.39	24%	
	Warm_WW	-	-	0.36	12%	-	-	0.34	12%	
Leaf Area Index (LAI)	Hot_WW	0.64	14%	0.48	16%	0.63	13%	0.49	16%	
(2)	Warm_WD	-	-	0.36	26%	-	-	0.37	26%	
	Hot_WD	0.40	23%	0.21	29%	0.41	25%	0.17	29%	
	Cool_WW	0.85	15%	0.65	14%	0.74	16%	0.31	14%	
	Warm_WW	0.82	16%	0.63	10%	0.73	17%	0.36	12%	
Grain Number	Hot_WW	0.79	15%	0.56	13%	0.72	16%	0.54	13%	
(grains/m²)	Cool_WD	0.71	23%	-	-	0.63	22%	-	-	
	Warm_WD	0.83	41%	0.24	32%	0.74	43%	0.23	32%	
	Hot_WD	0.78	37%	0.36	35%	0.74	40%	0.39	35%	

<sup>#</sup> Pearson correlation coefficient (r) and relative RMSE (rrmse) values shown are mean values obtained within the experiments of each environmental scenario. WW, well-watered. WD, Water-deficit.

#### I) Simulation of leaf area index (LAI)

Sirius Maize accounted for both the genotypic and environmental effects on LAI but with different accuracies depending on environmental scenarios and considered test.

We first tested the model with the genetic progress dataset, in which all genotypic parameters derive from measurements (Table 1). Observed values of LAI were derived from UAV multispectral images at the end of vegetative phase. Tests were performed for two experiments with contrasting soil water status: MAU2017W (hot well-watered (WW) scenario) and MAU2017D (hot water-deficit (WD) scenario). The correlation between observed and simulated LAI values in the hot\_WW experiment 'MAU2017W' was high (r=0.64) with a low relative estimation error (rrmse) of 14% (Fig. 2a, Table 2). The correlation decreased to r=0.40 in the hot\_WD experiment 'MAU2017D', with a higher rrmse of 23%, likely due to an overestimation in LAI simulations here (Fig. 2a, Table 2).

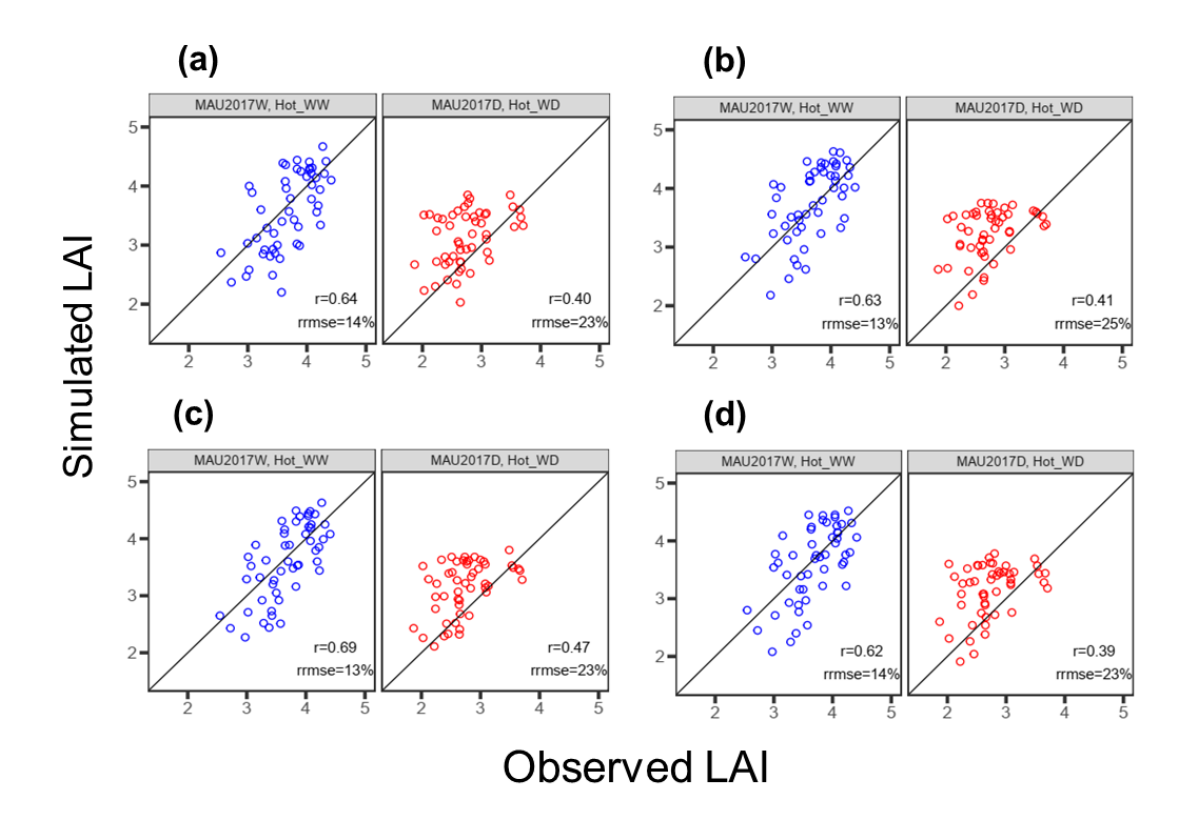


Fig. 2: Simulated LAI for the genetic progress panel, with genotype-dependent parameters derived from measured traits (a, c, d) or genomic prediction (b). a, Simulation results with parameters all derived from measurements. b, Simulation results with parameters all derived from genomic prediction. c, Simulation results with phenology parameters (LAR, FLN) kept as genotype-dependent, and all other parameters fixed to the mean value of the panel. d, Simulation results with all parameters kept as genotype-dependent except leaf elongation rate (LERa), fixed to the mean value of the panel.

We then tested the model with the recent hybrids dataset, in which only some traits used for parameterization were measured (LAR and FLN) while the other genotype-dependent parameters were estimated via genomic prediction. LAI observed values were derived from UAV multispectral images at 16-17 leaf stage, in seven experiments with contrasting environmental conditions: Pus21W (cool\_WW), Pus22W and Ouz22W (warm\_WW), Mau22W (hot\_WW), Pus22D and Ouz22D (warm\_WD) and Mau22D (hot\_WD). Correlations between LAI observed and simulated values ranged from r=0.40 with a low rrmse of 16% on average in well-watered conditions to r=0.31 with a moderate rrmse of 27% on average in water-deficit conditions (Fig. 3).

The overall correlation between LAI observed and simulated values across experiments and environmental scenarios was appreciable in both panels: r=0.61 for genetic progress panel experiments (Supplementary Fig. 3a) and r=0.59 for recent hybrids panel experiments (Supplementary Fig. 4a).

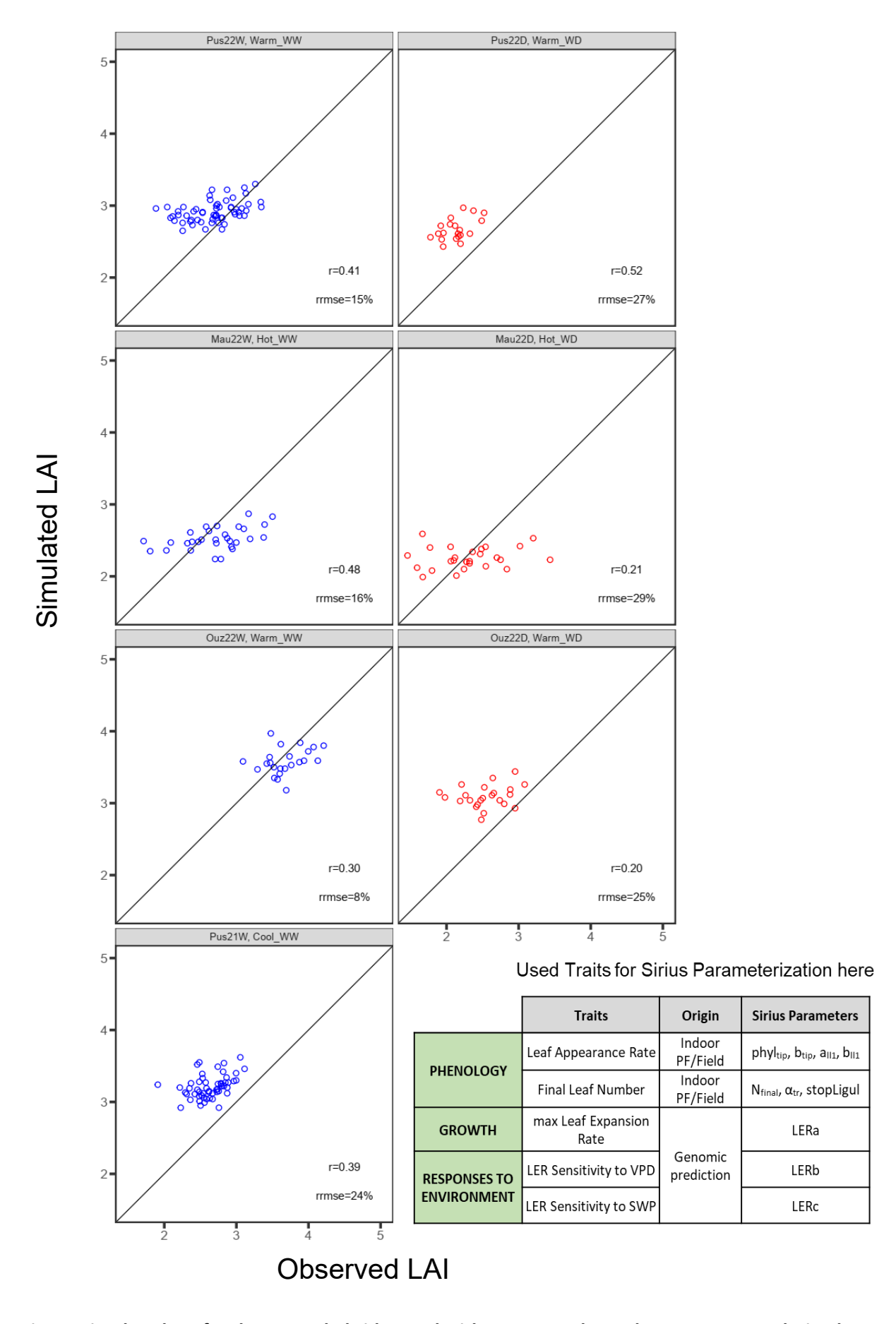


Fig. 3: Simulated LAI for the recent hybrids panel with genotype-dependent parameters derived from measured traits for FLN and LAR, and from genomic prediction for the other parameters.

Altogether, Sirius Maize adequately accounted for genotypic effects variation on LAI in contrasting environmental scenarios, but accuracies were notably lower in water-deficit conditions. This was consistent with Bustos-Korts *et al.* (2019) findings for wheat yield predicted using a multi-trait model in contrasting environment types, where accuracies also significantly decreased in water-deficit conditions. This result can be explained either by lower consistency of estimated values for the traits linked to genotypic responses in water-deficit conditions, or by the well-known complexity of predicting genotype—environment interactions (GEIs) in water limitation conditions (Chenu *et al.*, 2011). GEIs emerge in the case of crop models from the interconnections and feedback regulations between subsystem components and physiological processes of the model (Bertin *et al.*, 2010). Regarding the recent hybrids panel, the expected lower accuracies found were likely due to the lower estimation quality of parameters predicted by genomic prediction, but also to the lower phenotypic variability in this panel as discussed in Chapter 1.

# LAI simulation accuracies remained nearly unchanged when parameters resulted from genomic prediction.

The final test involved parameters estimated by genomic prediction only. For the genetic progress panel, traits genetic values used for parameterization were obtained from the genomic prediction cross-validation scheme CV1 of Chapter 1. The correlations between observed and simulated LAI values for the panel remained similar to those obtained when parameters derived from measurements (Fig. 2b, Table 2). This was the case in both well-watered (r=0.63, rrmse=13%) and water-deficit conditions (r=0.41, rrmse=25%). These results can be explained by the fact that the traits (LAR, FLN) mainly affecting LAI genotypic variability in the panel were highly heritable ( $h_g^2 > 0.60$ ) and could be well predicted via genomic prediction G-BLUP models.

When parameters used in genomic prediction involved different datasets for the training set (diversity and genetic progress panels) and prediction set (recent hybrids panel), correlations between LAI observed and simulated values for the latter panel also remained stable, probably for the same reasons as before (Fig. 4, Table 2). They ranged from r=0.39 with rrmse of 16% on average in well-watered conditions to r=0.30 with rrmse of 27% on average in water-deficit conditions.

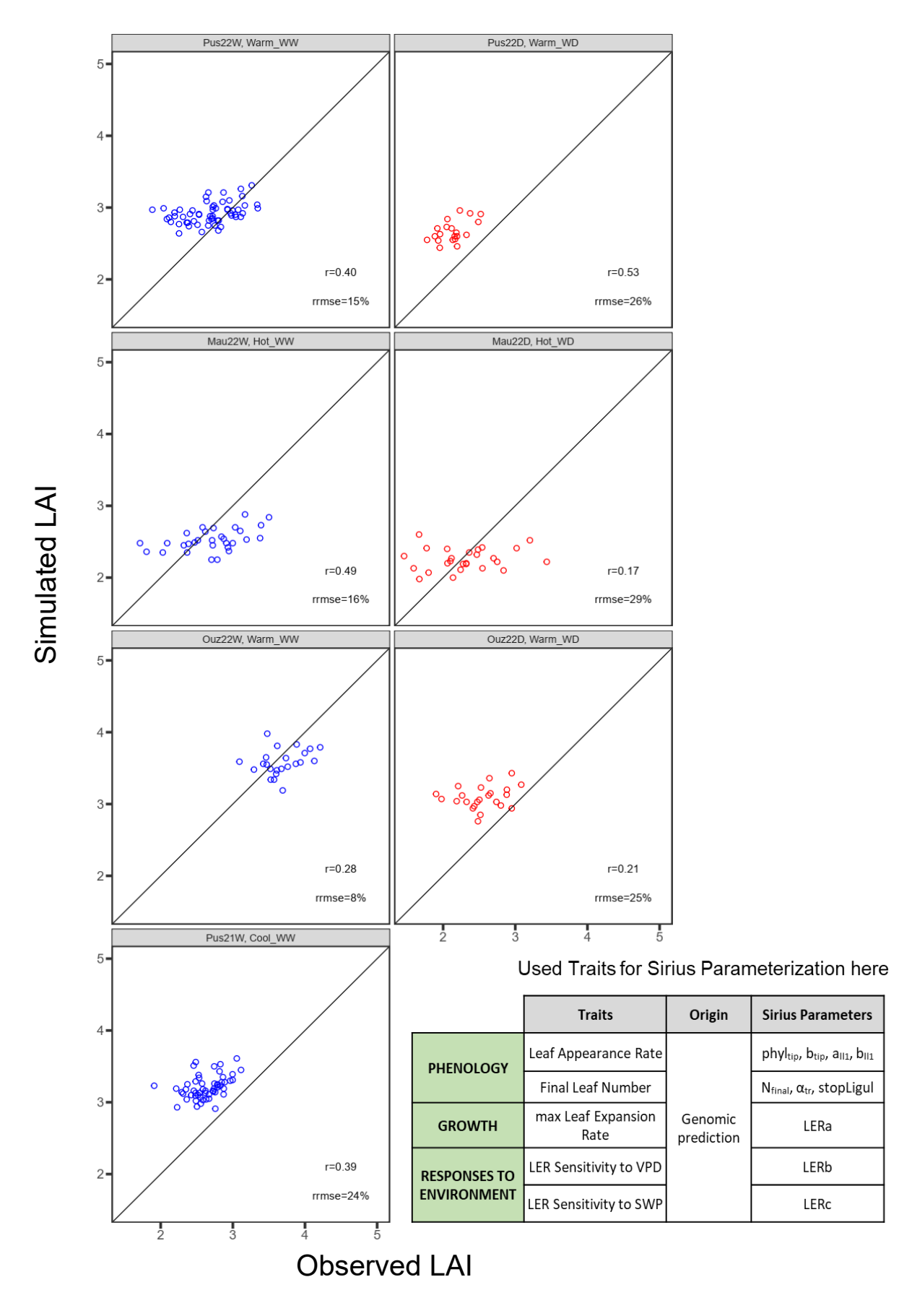


Fig. 4 : Simulated LAI for the recent hybrids panel, with all genotype-dependent parameters estimated via genomic prediction.

# The genotypic variability of LAI in contrasting environmental conditions depended on phenology and leaf elongation rate.

We tested the impact on LAI simulation accuracies of some Sirius parameters by running simulations with some parameters fixed to the mean value for all hybrids, while the other genotype-dependent parameters were kept as they are. This was performed for the genetic progress panel in the same experiments as before.

The first case involved keeping parameters linked to plant phenology (LAR, FLN) (Fig. 2c) as genotype-dependent, whereas all other parameters were set to the mean values of the panel for all genotypes. Here, correlations between LAI simulated and observed values were good in both well-watered (r=0.69, rrmse=13%) and water-deficit conditions (r=0.47, rrmse=23%). This is probably due to the fact that, in the genetic progress panel, the main driver of genotypic differences was the phenology (Welcker *et al.*, 2022). The increase in accuracy compared to simulations where all genotypic parameters were varied between hybrids may be due to some inconsistency between the calculated traits values used for parameterization for few hybrids.

The second case involved varying all genotypic parameters except leaf elongation rate 'LERa' (Fig. 2d). Here, correlations between LAI simulated and observed values decreased slightly in both well-watered (r=0.62) and water-deficit conditions (r=0.39).

Overall, our results suggest that Sirius Maize has the potential for predicting LAI for a large set of genotypes in different environmental conditions. This may potentially result in a high-throughput and low cost method for simulating LAI for hundreds of genotypes in hundreds of environments, if the required genotype-dependent parameters are either measured or predicted from genomic information. However, only some of the measured traits had an appreciable role for the studied panel, essentially those related to phenology, but also leaf elongation rate.

#### II) Simulation of grain number (GN)

Sirius Maize accounted for both the genotypic and environmental effects on grain number per unit area.

As for LAI, we first tested Sirius maize for the case where all genotype-dependent parameters derived from measurements, in the genetic progress panel (Table 1). Tests were performed for nine field experiments in six different sites and three years, with contrasting temperature and soil water status: LEM2017W and VEN2017W (cool\_WW scenario); GAI2017W and NER2013W (warm\_WW scenario); MAU2017W (hot\_WW scenario); VEN2017D (cool\_WD scenario); GAI2017D and LAV2017D (warm\_WD scenario); MAU2010D (hot\_WD scenario). We compared these observed values to those simulated by Sirius maize parameterized with traits measured indoor (LAR, FLN, rh<sub>PAD</sub>, gS<sub>max</sub>, LER and its sensitivities to SWP and VPD) or in the field (GN<sub>max</sub>) (Table 1). The correlations between observed and simulated grain number were high in all scenarios, ranging from r=0.79 to r=0.86 in well-watered conditions with low estimation error (rrmse=15% on average), and ranging from r=0.71 to r=0.87 in water-deficit conditions with a fluctuating estimation error (rrmse=23%–47%) (Fig. 5, Table 2).

We then tested the model with the recent hybrids dataset, in which only some genotype-dependent parameters resulted from measured traits (LAR, FLN and GN<sub>max</sub>), while the other parameters were estimated via genomic prediction. Simulation were run for twelve experiments from ten different sites and two years, presenting contrasting environmental scenarios: Cra21W and Mat22W (cool\_WW); Bin22W, Pus22W and Chr21D (warm \_WW), LMg22W and Cad22W (hot\_WW), Pac22D, Chr22D and Ouz22D (warm\_WD); LMg22D and Sek21D (hot\_WD). (Fig. 6, Table 2). Correlation coefficients between observed and simulated values were moderate to high in well-watered conditions (r=0.31–0.84) with low estimation errors (rrmse=5%–19%), and low to moderate in water-deficit (r=0.11–0.47) with higher and more variable estimation errors (rrmse=18%–49%).

The correlation between observed and simulated values across environmental scenarios was high for the genetic progress dataset (r=0.77, Supplementary Fig. 3b) and lower but still appreciable (r=0.56) for the recent hybrids dataset (Supplementary Fig. 4c).

Used Traits for Sirius Parameterization here

	Traits	Origin	Sirius Parameters
PHENOLOGY	Leaf Appearance Rate	Indoor PF/Field	phyl <sub>tip</sub> , b <sub>tip</sub> , a <sub>II1</sub> , b <sub>II1</sub>
	Final Leaf Number	Field	$N_{final}$ , $\alpha_{tr}$ , stopLigul
GROWTH	max Leaf Expansion Rate	Indoor PF	LERa
ARCHITECTURE	rh <sub>PAD</sub>	Indoor PF	KI coeff
	max Stomatal Conductance	Indoor PF	LUEpre
RESPONSES TO ENVIRONMENT	LER Sensitivity to VPD	Indoor PF	LERb
	LER Sensitivity to SWP	Indoor PF	LERc
MAX YIELD COMPONENTS	max Grain number	Field	GNmax

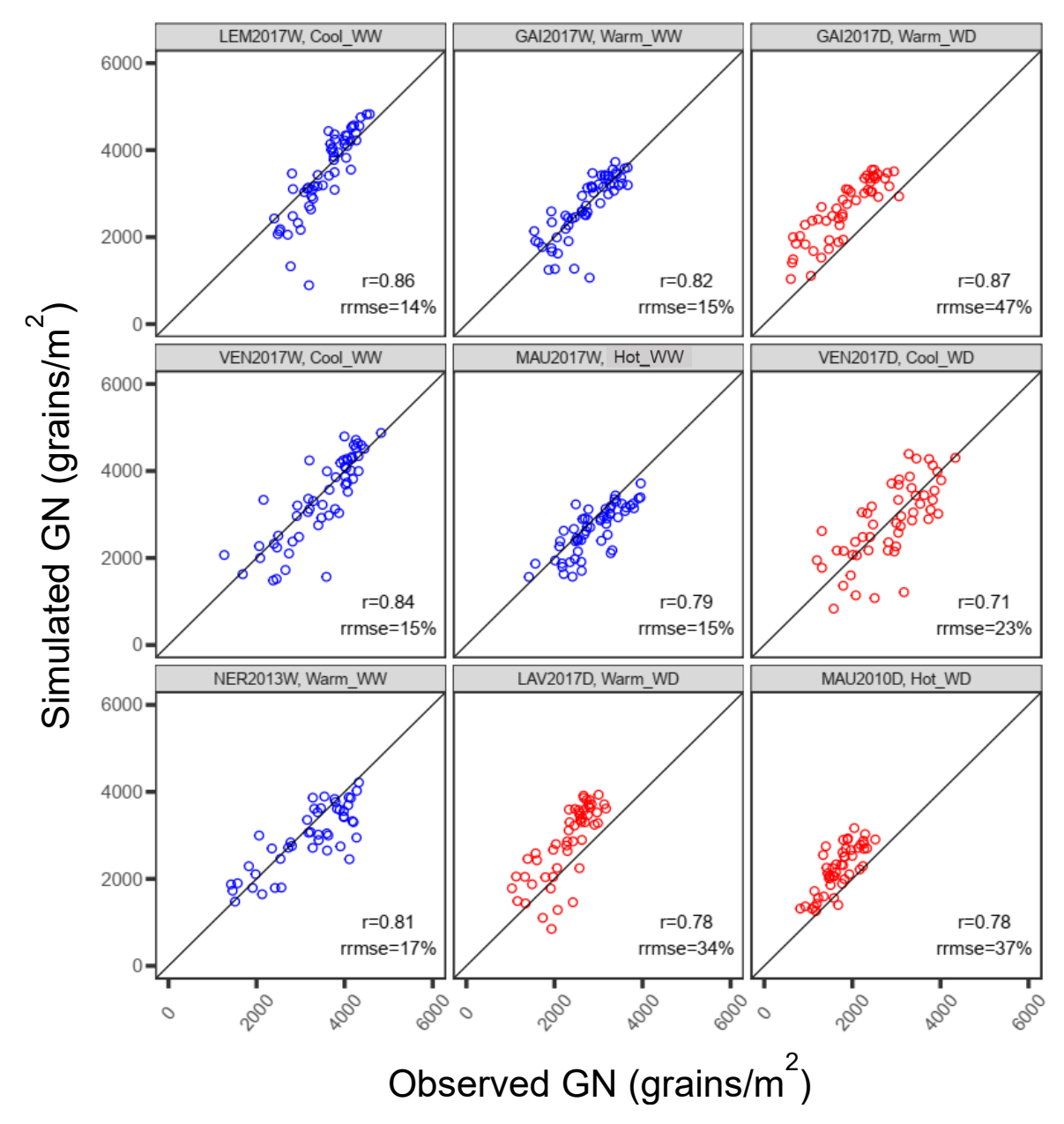


Fig. 5 : Simulated grain number (GN) for the genetic progress panel, with all genotype-dependent parameters derived from measured traits.

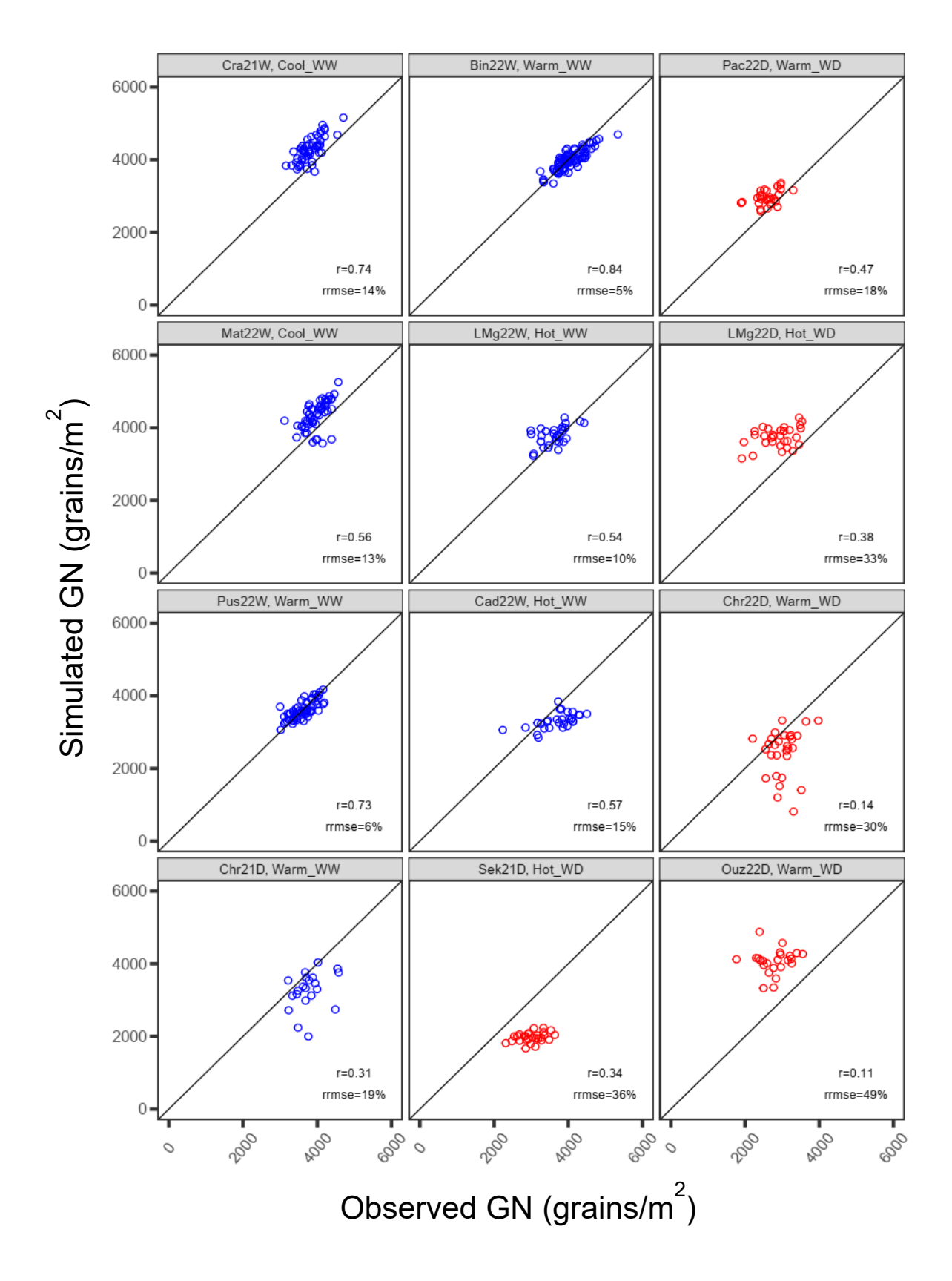


Fig. 6 : Simulated grain number (GN) values for the recent hybrids panel with the genotype-dependent parameters FLN, LAR and  $GN_{max}$  derived from measured traits, and all other genotype dependent parameters estimated via genomic prediction.

Sirius maize therefore accounted for genotypic variations of grain number per unit area in contrasting environmental scenarios, even though accuracies decreased in water-deficit conditions compared to well-watered conditions as in the case of LAI. The genotypic effects and GEI effects on leaf growth and biomass accumulation therefore translated into differences in simulated grain number for the tested genotypes. Interestingly, these simulations, based on our process-based crop model, had similar accuracies as those achieved by other studies based either on another crop growth model (e.g. Toda *et al.*, 2020) or on linear mixed models (e.g. Guo *et al.*, 2020). These two studies for instance, found appreciable prediction accuracies, for genotypes tested in a multi-environment context, when they considered intermediate physiological traits in their modelling approaches for predicting rice biomass and wheat yield, respectively.

### GN Simulation accuracies decreased but remained appreciable when genotype-dependent parameters were predicted from genomic information.

We have run here simulations in which all parameters were estimated by genomic prediction of related traits. The correlations between GN observed and simulated values decreased by 10% on average for the genetic progress panel compared to those when simulations were run with genotype-dependent parameters derived from measurements (Fig. 7, Table 2). This was the case in both well-watered (r=0.68–0.79, rrmse=12%–19%) and water-deficit conditions (r=0.63–0.80, rrmse=22%–51%). These results can be explained by the fact that GN<sub>max</sub> was well predicted via genomic prediction G-BLUP model (r<sub>obs\_pred</sub>=0.85). For comparison, studies using multi-trait or joint regression genomic prediction models for predicting yield showed similar prediction accuracies: in Bustos-Korts *et al.* (2019), r ranged from 0.50 to 0.80 depending on environment types; in Millet *et al.* (2019), r ranged from 0.43 to 0.85 depending on experiments. In Cooper *et al.* (2016) study with a maize GP-assisted CGM method close to our study approach, prediction accuracies ranged from 0.50 to 0.82 depending on prediction environments considered.

When parameters genomic prediction involved the use of different datasets for training set (diversity and genetic progress panels) and prediction set (recent hybrids panel), correlations between observed and simulated values appreciably decreased (-34% on average, r=0.19–0.57) with an increase in estimation errors in well-watered conditions (rrmse=8%–20%, Fig. 8, Table 2). A likely explanation is that GN<sub>max</sub> predicted for recent hybrids was less accurate than in the case of a cross validation reported in the above paragraph (r<sub>obs\_pred</sub>=0.40).

For water-deficit conditions though, correlations remained stable and did not get worse than the case where  $GN_{max}$  and phenology parameters derived from measurements (r=0.10–0.50, rrmse=19%–49%, Fig. 8).

Finally, the overall correlation between observed and simulated values across environmental scenarios remained appreciable for both genetic progress panel experiments (r=0.75, Supplementary Fig. 3c) and recent hybrids panel experiments (r=0.51, Supplementary Fig. 4d).

Used Traits for Sirius Parameterization her							
	Traits	Origin	Sirius Parameters				
PHENOLOGY	Leaf Appearance Rate		phyl <sub>tip</sub> , b <sub>tip</sub> , a <sub>II1</sub> , b <sub>II1</sub>				
PHENOLOGI	Final Leaf Number		N <sub>final</sub> , α <sub>tr</sub> , stopLigul				
GROWTH	max Leaf Expansion Rate		LERa				
ARCHITECTURE	rh <sub>PAD</sub>	Genomic	KI coeff				
	max Stomatal Conductance	prediction	LUEpre				
RESPONSES TO ENVIRONMENT	LER Sensitivity to VPD		LERb				
	LER Sensitivity to SWP		LERc				
MAX YIELD COMPONENTS	max Grain number		GNmax				

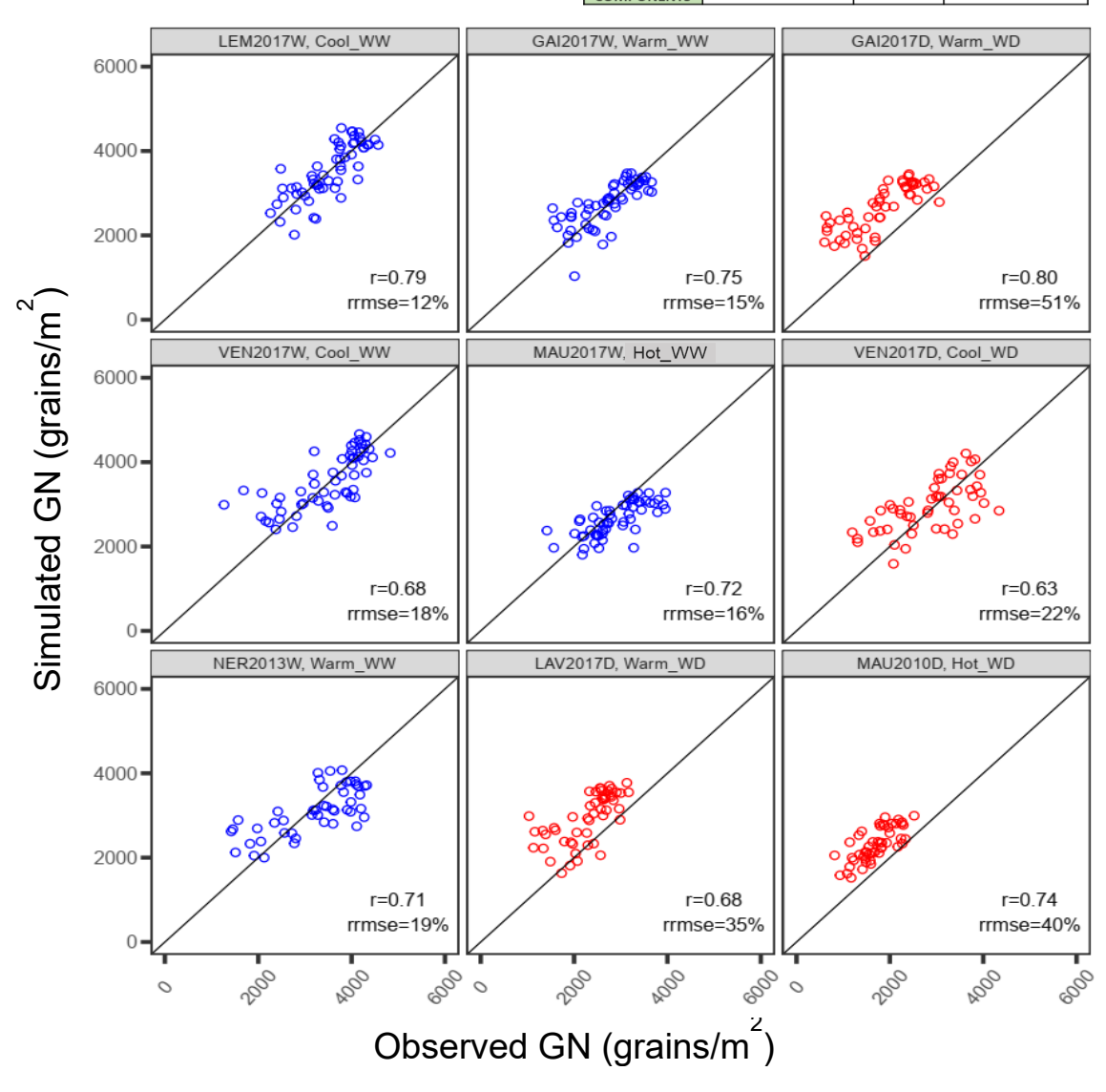


Fig. 7 : Simulated grain number (GN) for the genetic progress panel, with all genotype-dependent parameters derived from genomic prediction.

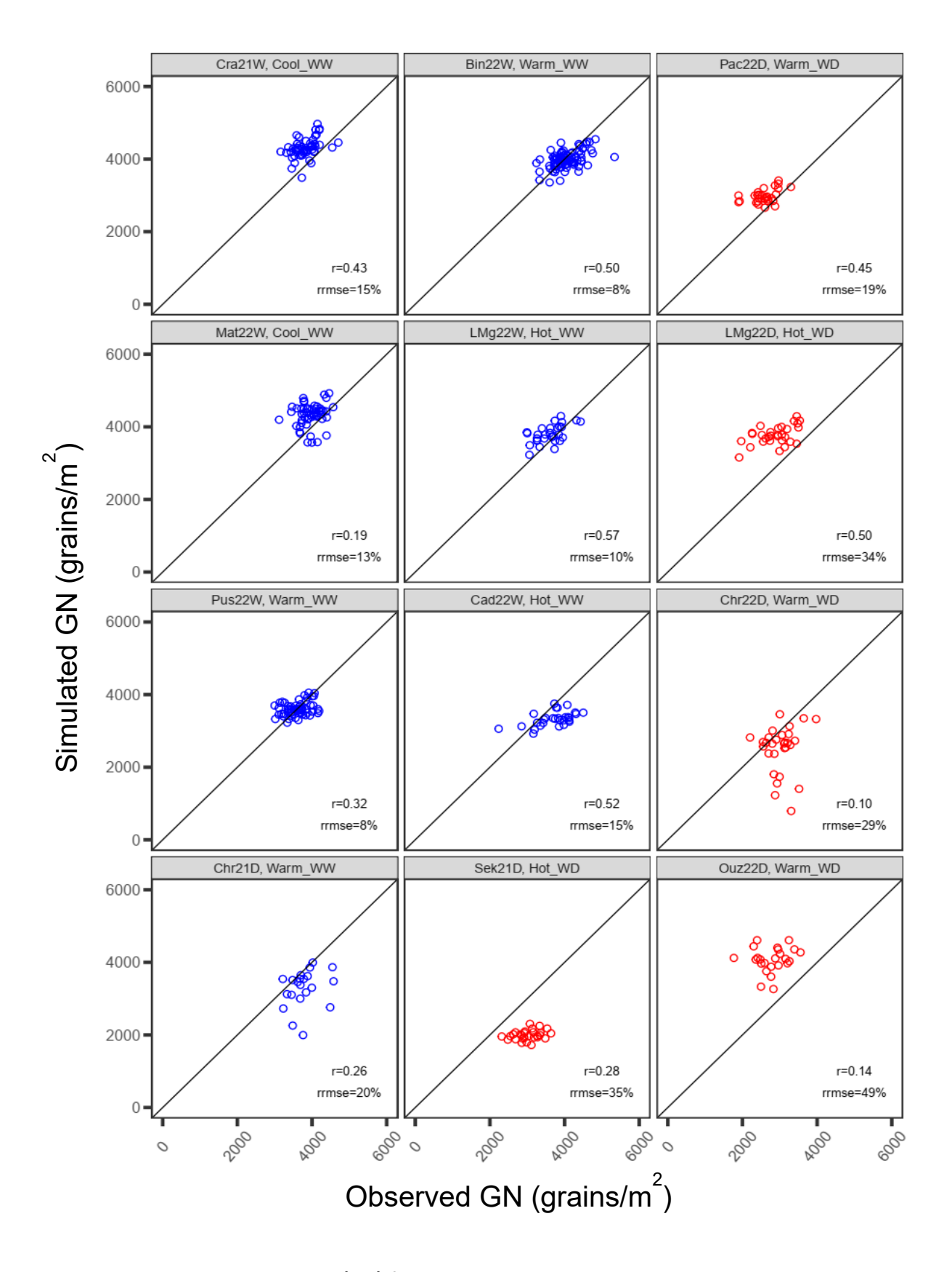


Fig. 8 Simulated grain number (GN) for the recent hybrids panel, with all genotype-dependent parameters derived from genomic prediction.

The genotypic variability of GN in contrasting environmental conditions depended on the maximum grain number potential and leaf growth rate.

We tested the impact on simulation accuracies of some parameters by running simulations for genetic progress panel after fixing certain parameters values.

The first case involved varying all genotypic parameters except  $GN_{max}$  (Fig. 9, Supplementary Fig. 3d). Here, correlations between GN simulated and observed values drastically decreased (-50% on average) in both well-watered (r=0.32–0.55, rrmse=17%–25%) and water-deficit conditions (r=0.15–0.63, rrmse=32%–50%). This confirms the fact that, in the genetic progress panel, maximum grain number was one of the main drivers of the genetic variability of yield (Fig. 1; Welcker *et al.*, 2022).

The second case involved varying all genotypic parameters except leaf elongation rate 'LERa' (Fig. 10, Supplementary Fig. 3e). Here, correlations between simulated and observed values decreased to a much lesser extent than before, but estimation errors for some hybrids notably increased in some experiments (r=0.71–0.88 and rrmse=14%–22% in well-watered conditions, r=0.62–0.87 and rrmse=27%–47% in water-deficit conditions, Fig. 10). This illustrates the fact that simulated grain number is indirectly impacted by leaf growth variability through plant growth rate (PGR).

Overall, as for LAI, our results suggest that Sirius Maize has the potential for predicting grain number yield component for a large set of genotypes in different environmental conditions. This may potentially result in high-throughput and low cost method for simulating grain yield for hundreds of genotypes in hundreds of environments.

#### Used Traits for Sirius Parameterization here

	Traits	Origin	Sirius Parameters
PHENOLOGY	Leaf Appearance Rate	Indoor PF/Field	phyl <sub>tip</sub> , b <sub>tip</sub> , a <sub>II1</sub> , b <sub>II1</sub>
	Final Leaf Number	Field	$N_{\text{final}}$ , $\alpha_{\text{tr}}$ , stopLigul
GROWTH	max Leaf Expansion Rate	Indoor PF	LERa
ARCHITECTURE	rh <sub>PAD</sub>	Indoor PF	KI coeff
RESPONSES TO ENVIRONMENT	max Stomatal Conductance	Indoor PF	LUEpre
	LER Sensitivity to VPD	Indoor PF	LERb
	LER Sensitivity to SWP	Indoor PF	LERc

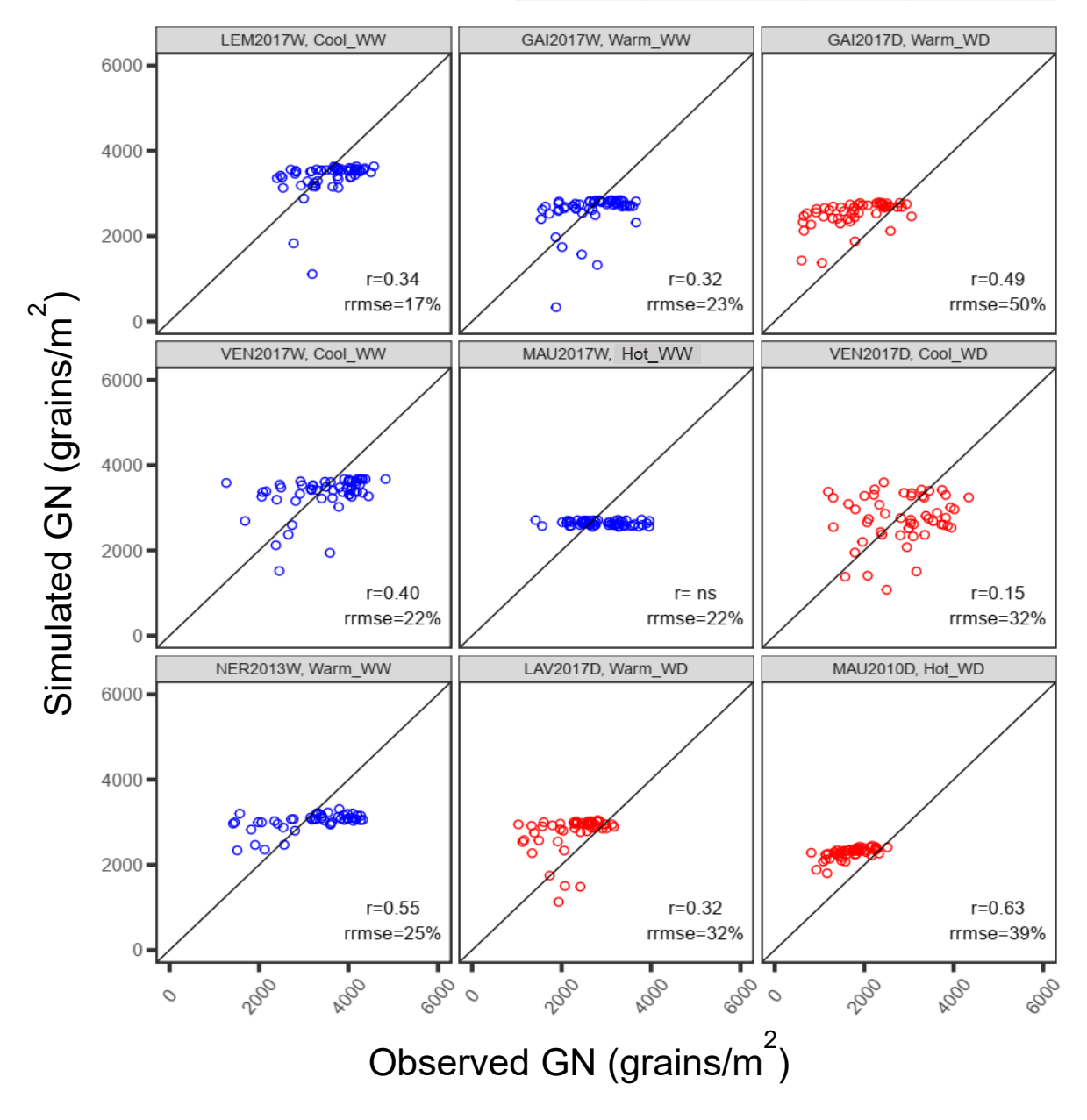


Fig. 9 : Simulated grain number (GN) for the genetic progress panel, with all parameters kept as genotype-dependent, except the maximum grain number per plant,  $GN_{max}$ , fixed to the mean value of the panel.

#### Used Traits for Sirius Parameterization here

	Traits	Origin	Sirius Parameters
PHENOLOGY	Leaf Appearance Rate	Indoor PF/Field	phyl <sub>tip</sub> , b <sub>tip</sub> , a <sub>II1</sub> , b <sub>II1</sub>
	Final Leaf Number	Field	$N_{\text{final}}$ , $\alpha_{\text{tr}}$ , stopLigul
ARCHITECTURE	rh <sub>PAD</sub>	Indoor PF	KI coeff
RESPONSES TO ENVIRONMENT	max Stomatal Conductance	Indoor PF	LUEpre
	LER Sensitivity to VPD	Indoor PF	LERb
	LER Sensitivity to SWP	Indoor PF	LERc
MAX YIELD COMPONENTS	max Grain number	Field	GNmax

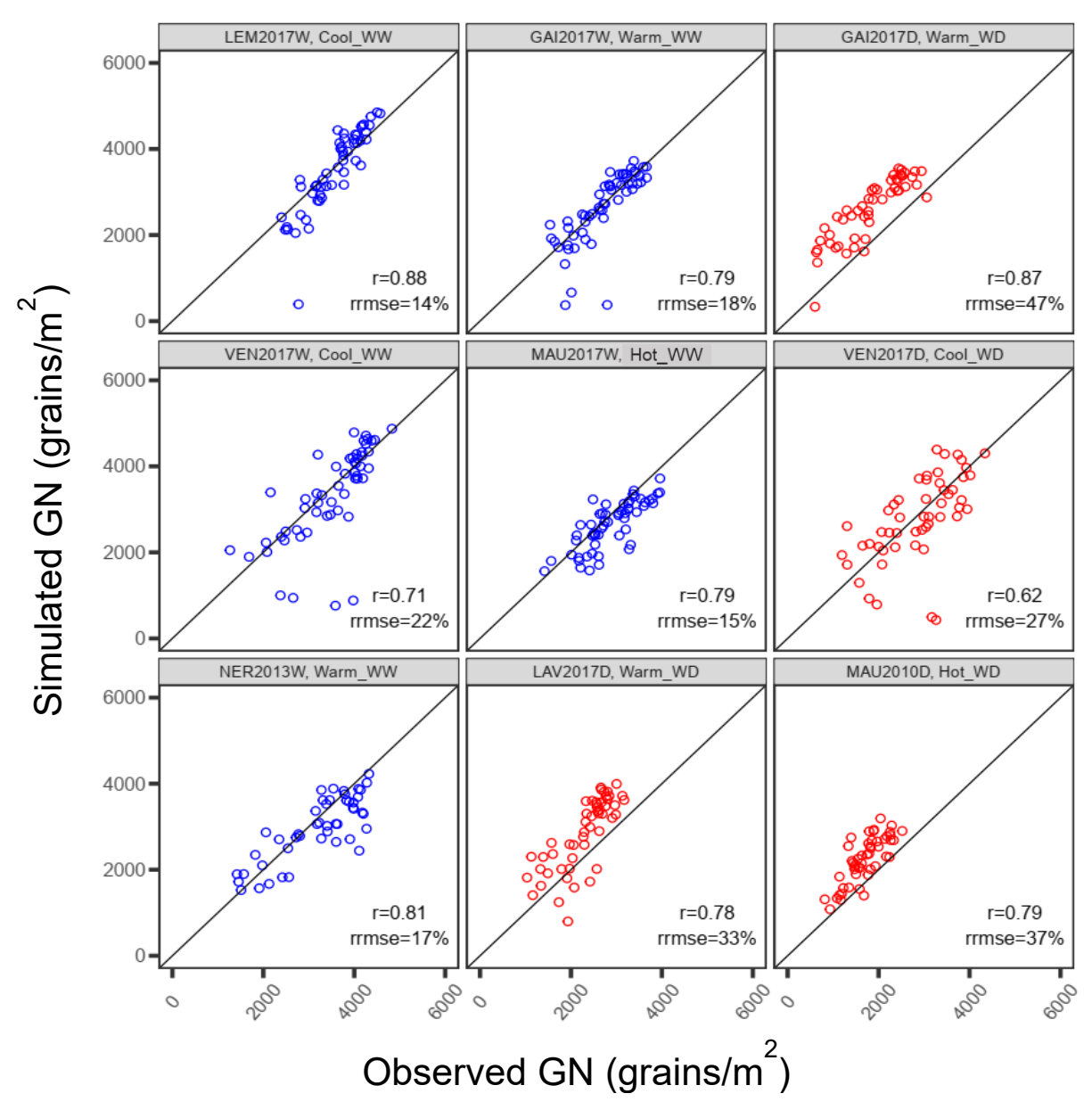


Fig. 10 : Simulated grain number (GN) for the genetic progress panel, with all parameters kept as genotype-dependent except leaf elongation rate (LERa), fixed to the mean value of the panel.

#### Methods

#### Calculation of genotype-dependent parameters fed to Sirius Maize.

Thirteen genotype-dependent parameters were considered in our study (Table 1): phyl<sub>tip</sub>, b<sub>tip</sub>,  $a_{II1}$ ,  $b_{II1}$ ,  $N_{final}$ ,  $\alpha_{tr}$ , stopLigul, LERa, LERb, LERc, kl, LUEpre and  $GN_{max}$ .

The genotype-dependent thermal time between the emission and ligulation of two consecutive leaves derived from LAR (phyllochron 'phyl<sub>tip</sub>'= 1/LAR and ligulochron 'a<sub>II1</sub>'= 1/LAR, respectively). The genotype-dependent parameters describing the beginning and end of these processes and the shape of their relation to thermal time were calculated as follows:  $b_{tip} = phyl_{tip} \ x \ (-1.35) = intercept \ of the regression of thermal time with tip appearance;$   $b_{II1} = a_{II1} - 10 = intercept \ of the regression of thermal time with ligulation;$   $\alpha_{tr} = 3/N_{final} = transition \ between the two linear parts describing leaf ligulation with thermal time relative to <math display="block">N_{final}; \ stopLigul= 3/N_{final} = fraction \ of \ N_{final} \ which \ stops \ growing \ and \ ligulates \ together).$ 

The elongation rate of leaf 6 (LERa) was derived from plant LER (max leaf expansion rate) measured in well-watered indoor experiments, with this empirical regression equation: LERa= LER  $\times$  0.0147 + 4.87. LERb was estimated as the slope of the linear regression between leaf elongation rate and VPD in indoor experiments with a time definition of one hour. LERc was estimated as the slope of the linear regression between leaf elongation rate and SWP in indoor experiments with a time definition of one day.

The parameter kl was scaled to  $rh_{PAD}$  trait, by varying kl maize species reference value from one genotype to the other, by multiplying kl for each genotype by a coefficient equal to the ratio between the genotype  $rh_{PAD}$  value and  $rh_{PAD}$  mean value of the whole studied panel. LUEpre (pre-anthesis LUE) was scaled to plant max stomatal conductance trait ( $gs_{max}$ ), by varying LUEpre maize reference value from one genotype to the other, by multiplying LUEpre for each genotype by a coefficient equal to the ratio between the genotype  $gs_{max}$  value and  $gs_{max}$  mean value of the whole studied panel.

#### LAI modelling in Sirius Maize.

Leaf area index was modelled as in Lacube et al. (2020), as a result of processes related to plant development and leaf elongation and widening. LAI is indeed calculated daily depending on the dimensions (width and length) of different leaf ranks, after estimating their exposed

fraction and considering plant density. Modelling the expansion of individual leaves requires identification of the dates at which leaf elongation and widening begin and end, for each leaf rank. The dates of beginning of leaf elongation were linked to those of leaf tip appearance, and the dates of end of leaf elongation to those of ligule appearance. These dates are estimated for each genotype using the genotypic parameters related to plant phenology described above (Supplementary Table 1).

During the period of leaf elongation, the elongation rate of any growing leaf of the plant is calculated from that of leaf 6 leading to a profile of leaf elongation rate normalized by the maximum rate of leaf 6 (LERa parameter). The distribution of normalized elongation rates along leaf ranks is fitted via a beta function with parameters depending on N<sub>final</sub> (Supplementary Table 1). The effects of evaporative demand (VPD) and soil water potential (SWP) are applied on the normalized leaf elongation rates, along with genotypic sensitivities to VPD (LERb parameter) and to SWP (LERc parameter) (Supplementary Table 1).

The time course of leaf widening is similar to that of elongation but ending before it (Lacube  $et\ al.$ , 2017). The profiles of leaf width are also dependent on leaf rank via a beta function with parameters related to  $N_{final}$  (Supplementary Table 1). The width of individual leaves is calculated as a function of two genotypic parameters: a base width of leaf 6 (W<sub>6</sub>) and a sensitivity to intercepted light ( $r_{RAD}$ ). The latter parameters were fixed for all genotypes in our study because their values were not available for considered panels.

#### **Grain number modelling in Sirius Maize.**

Grain number (GN) was calculated as a logarithmic function of mean plant growth rate 'PGR' around flowering time (Supplementary Fig. 2), taking into account  $GN_{max}$  (maximum grain number per plant), with a minimum PGR (PGR<sub>base</sub>) at which grain number starts to increase; and a parameter of shape (GN<sub>k</sub>), the PGR at which 50% of GN<sub>max</sub> is reached:

$$GN = GN_{max} \times (1 - e^{-GN_k \times (PGR - PGR_{base})})$$
 (3)

 $GN_{max}$  was estimated for each hybrid as described before and the shape parameters  $GN_k$  was kept common to all genotypes.  $PGR_{base}$  parameter was also fixed for all hybrids in our study. Grain number per square meter was calculated by taking into account the corresponding plant density.

#### Simulation tests accuracies.

We assessed Sirius simulation accuracies for LAI measured by inversion of the PROSAIL model (see Chapter 1) and grain number (GN) estimated by dividing grain yield by individual grain weight for each hybrid. We calculated Pearson correlations (r) between observed and simulated values of the traits and root mean squared error of simulations (rmse), expressed as a percentage of mean observed value (rrmse).

#### References

**Bertin N, Martre P, Génard M, Quilot B, Salon C**. **2010**. Under what circumstances can process-based simulation models link genotype to phenotype for complex traits? Case-study of fruit and grain quality traits. *Journal of Experimental Botany* **61**: 955–967.

Bustos-Korts D, Boer MP, Malosetti M, Chapman S, Chenu K, Zheng B, van Eeuwijk FA. 2019. Combining Crop Growth Modeling and Statistical Genetic Modeling to Evaluate Phenotyping Strategies. *Frontiers in Plant Science* 10: 1491.

Castelletti S, Coupel-Ledru A, Granato I, Palaffre C, Cabrera-Bosquet L, Tonelli C, Nicolas SD, Tardieu F, Welcker C, Conti L. 2020. Maize adaptation across temperate climates was obtained via expression of two florigen genes. *PLOS Genetics* 16: e1008882.

**Chapuis R, Delluc C, Debeuf R, Tardieu F, Welcker C**. **2012**. Resiliences to water deficit in a phenotyping platform and in the field: How related are they in maize? *European Journal of Agronomy* **42**: 59–67.

Chenu K, Cooper M, Hammer GL, Mathews KL, Dreccer MF, Chapman SC. 2011. Environment characterization as an aid to wheat improvement: interpreting genotype-environment interactions by modelling water-deficit patterns in North-Eastern Australia. *Journal of Experimental Botany* 62: 1743–1755.

**Cooper M, Technow F, Messina C, Gho C, Totir LR**. **2016**. Use of Crop Growth Models with Whole-Genome Prediction: Application to a Maize Multienvironment Trial. *Crop Science* **56**: 2141–2156.

**Guo J, Pradhan S, Shahi D, Khan J, Mcbreen J, Bai G, Murphy JP, Babar MA**. **2020**. Increased Prediction Accuracy Using Combined Genomic Information and Physiological Traits in A Soft Wheat Panel Evaluated in Multi-Environments. *Scientific Reports* **10**: 7023.

Hammer GL, van Oosterom E, McLean G, Chapman SC, Broad I, Harland P, Muchow RC. 2010. Adapting APSIM to model the physiology and genetics of complex adaptive traits in field crops. *Journal of Experimental Botany* **61**: 2185–2202.

**Jamieson PD, Semenov MA, Brooking IR, Francis GS**. **1998**. Sirius: a mechanistic model of wheat response to environmental variation. *European Journal of Agronomy* **8**: 161–179.

Lacube S, Fournier C, Palaffre C, Millet EJ, Tardieu F, Parent B. 2017. Distinct controls of leaf widening and elongation by light and evaporative demand in maize. *Plant, Cell & Environment* 40: 2017–2028.

Lacube S, Manceau L, Welcker C, Millet EJ, Gouesnard B, Palaffre C, Ribaut J-M, Hammer G, Parent B, Tardieu F. 2020. Simulating the effect of flowering time on maize individual leaf area in contrasting environmental scenarios. *Journal of Experimental Botany* 71: 5577–5588.

**Larrosa FH, Borrás L**. **2022**. Differential Maize Yield Hybrid Responses to Stand Density Are Correlated to Their Response to Radiation Reductions Around Flowering. *Frontiers in Plant Science* **12**.

Martre P, Jamieson PD, Semenov MA, Zyskowski RF, Porter JR, Triboi E. 2006. Modelling protein content and composition in relation to crop nitrogen dynamics for wheat. *European Journal of Agronomy* 25: 138.

Messina CD, Hammer GL, McLean G, Cooper M, Van Oosterom EJ, Tardieu F, Chapman SC, Doherty A, Gho C. 2019. On the dynamic determinants of reproductive failure under drought in maize. *in silico Plants* 1: diz003.

Millet EJ, Kruijer W, Coupel-Ledru A, Alvarez Prado S, Cabrera-Bosquet L, Lacube S, Charcosset A, Welcker C, van Eeuwijk F, Tardieu F. 2019. Genomic prediction of maize yield across European environmental conditions. *Nature Genetics* 51: 952–956.

**Motzo R, Pruneddu G, Giunta F**. **2013**. The role of stomatal conductance for water and radiation use efficiency of durum wheat and triticale in a Mediterranean environment. *European Journal of Agronomy* **44**: 87–97.

Parent B, Leclere M, Lacube S, Semenov MA, Welcker C, Martre P, Tardieu F. 2018. Maize yields over Europe may increase in spite of climate change, with an appropriate use of the genetic variability of flowering time. *Proceedings of the National Academy of Sciences* 115: 10642–10647.

Perez RPA, Fournier C, Cabrera-Bosquet L, Artzet S, Pradal C, Brichet N, Chen T, Chapuis R, Welcker C, Tardieu F. 2019. Changes in the vertical distribution of leaf area enhanced light interception efficiency in maize over generations of selection. *Plant, Cell & Environment* 42: 2105–2119.

Wang Y, Wang Y, Tang Y, Zhu X-G. 2022. Stomata conductance as a goalkeeper for increased photosynthetic efficiency. *Current Opinion in Plant Biology* 70: 102310.

Welcker C, Sadok W, Dignat G, Renault M, Salvi S, Charcosset A, Tardieu F. 2011. A Common Genetic Determinism for Sensitivities to Soil Water Deficit and Evaporative Demand: Meta-Analysis of Quantitative Trait Loci and Introgression Lines of Maize. *Plant Physiology* **157**: 718–729.

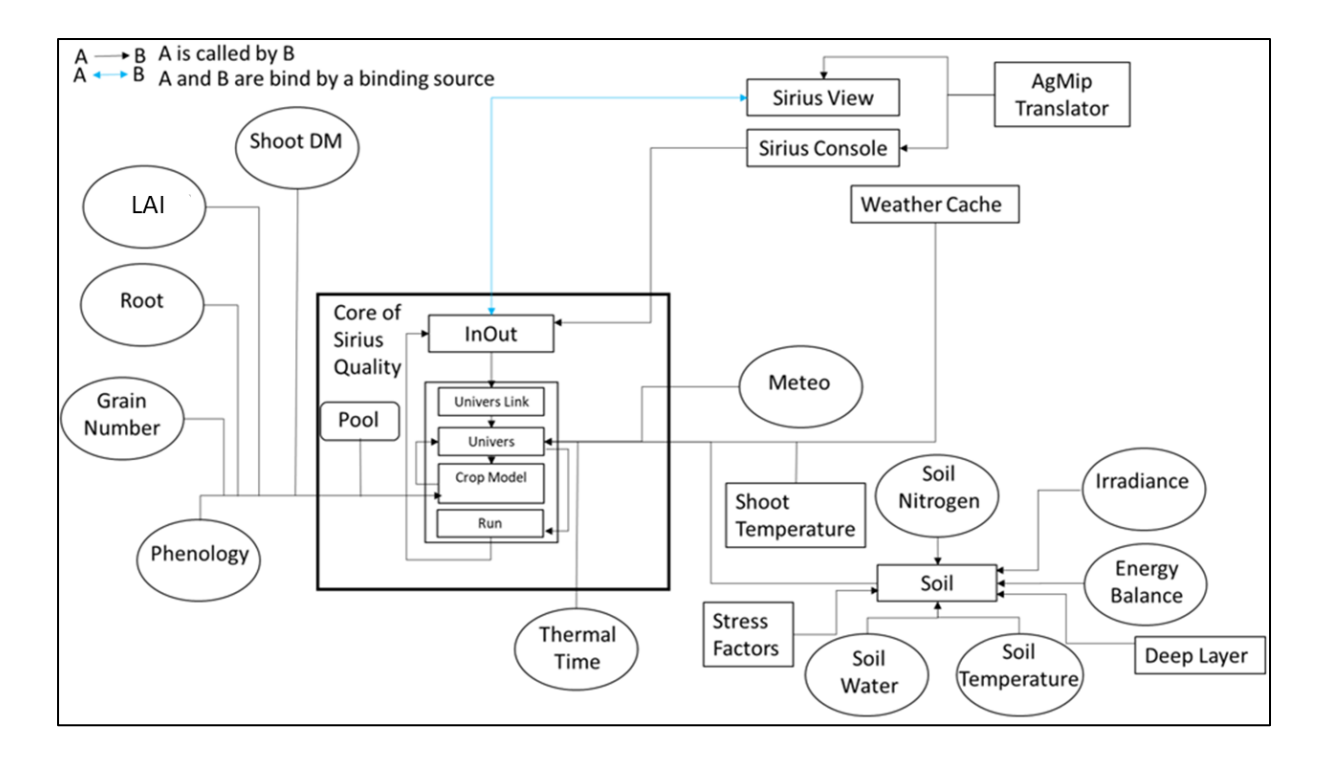
Welcker C, Spencer NA, Turc O, Granato I, Chapuis R, Madur D, Beauchene K, Gouesnard B, Draye X, Palaffre C, et al. 2022. Physiological adaptive traits are a potential allele reservoir for maize genetic progress under challenging conditions. *Nature Communications* 13: 3225.

## **Supplementary Table. 1 :** Synthesis of equations and parameters for phenology and leaf area modeling based on Lacube et al., 2020.

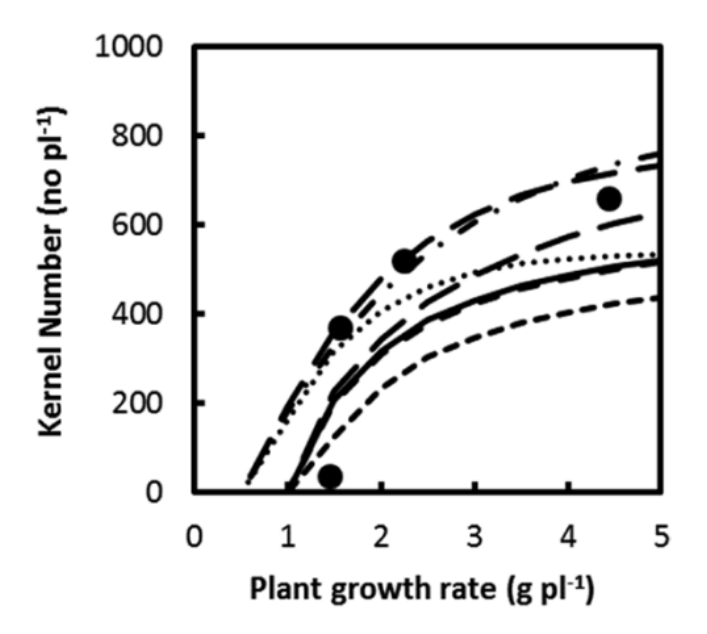
Process	Equation	Parameter	Description	Value
Final leaf number	Measured	N <sub>final</sub>	Maximum number of leaves	Genotypi
Tip appearance	$tt_{\rm tip}$ : thermal time at the	$a_{tip}$	Slope of the regression of thermal time with tip	Genotypi
	appearance of leaf n		appearance (i.e. phyllochron, thermal time	
	Equation 1:		between subsequent leaf tip appearances)	
	$tt_{tip}(n)=a_{tip}\times n+b_{tip}$	$b_{tip}$	Intercept of the regression of thermal time with tip	Genotyp
			appearance	
Beginning of linear	tt <sub>bl</sub> : thermal time at the	$k_{bl}$	Ratio between leaf appearance and linear	0.708
expansion	beginning of elongation		expansion for the last leaves	
	Equation 2:	$N_{bl\_lim}$	Transition between first and last leaves for	6
	If $n \le N_{b \perp lim}$		beginning of leaf linear expansion	
	$tt_{\rm bl}(n) = tt_{\rm tip}(n)$			
	Equation 3:			
	If $n > N_{bl\_lim}$			
	$tt_{bl}(n)=a_{bl}\times n+b_{bl}$			
	a <sub>bl</sub> =k <sub>bl</sub> a <sub>tip</sub>			
	$b_{bl}=b_{tip}+N_{bl\_lim}\times a_{tip}\times (1-k_{bl})$			
Ligule appearance	$tt_{\parallel}$ : thermal time at the	a <sub>∎1</sub>	Slope of the regression of thermal time with	Genotyp
	appearance of ligule		ligulation (i.e. thermal time between subsequent	
	Equation 4:		leaf ligule appearances)	
	If: $n \le \alpha_{II} \times N_{final}$	b <sub>ii1</sub>	Intercept of the regression of thermal time with	Genotyp
	$tt_{\parallel}(n)=a_{\parallel 1}\times n+b_{\parallel 1}$		ligulation	
	Equation 5:	Kbl <sub>II</sub>	Ratio between the two ligulation slopes with	0.454
	If: n>α <sub>II</sub> ×N <sub>final</sub>		thermal time	
	$tt_{\parallel}(n)=a_{\parallel 2}\times n+b_{\parallel 2}$	$\alpha_{\text{II}}$	Transition between the two linear parts describing	0.52
	$a_{\parallel 2}=k_{\parallel}\times a_{\parallel 1}$		leaf ligulation with thermal time relative to $N_{\text{final}}$	
	$b_{112} = b_{111} + a_{111} \times \alpha_{11} \times N_{final} \times (1 - k_{11})$			
End of linear	tt <sub>el</sub> : thermal time at the end of	N <sub>last</sub>	Number of last leaves that finish their expansion at	2
expansion	linear elongation		the same thermal time	
	Equation 6:	a <sub>lag</sub>	Relative thermal time difference per leaf between	5.4
	If $n \le N_{\text{final}} - N_{\text{last}} + 1$		ligulation and end of expansion	
	$tt_{el}(n) = tt_{il}(n) - a_{lag} \times n$			
	Equation 7:			
	If n>N <sub>final</sub> -N <sub>last</sub> +1			
	$tt_{el}(n)=tt_{el}(n-1)$			
Beginning and end of	$tt_{ m beg,w}$ and $tt_{ m end,w}$ : thermal time for	lag <sub>w</sub>	Thermal time lag between ends of leaf elongation	39
widening	beginning and end of widening		and widening	
	Equation 8:			
	$tt_{\text{beg,w}} (n) = tt_{\text{bl}} (n)$			
	Equation 9:			
	tt <sub>end,w</sub> (n)=tt <sub>el</sub> (n)-lag <sub>w</sub>			

## **Supplementary Table. 1 (continued) :** Synthesis of equations and parameters for phenology and leaf area modeling based on Lacube et al., 2020.

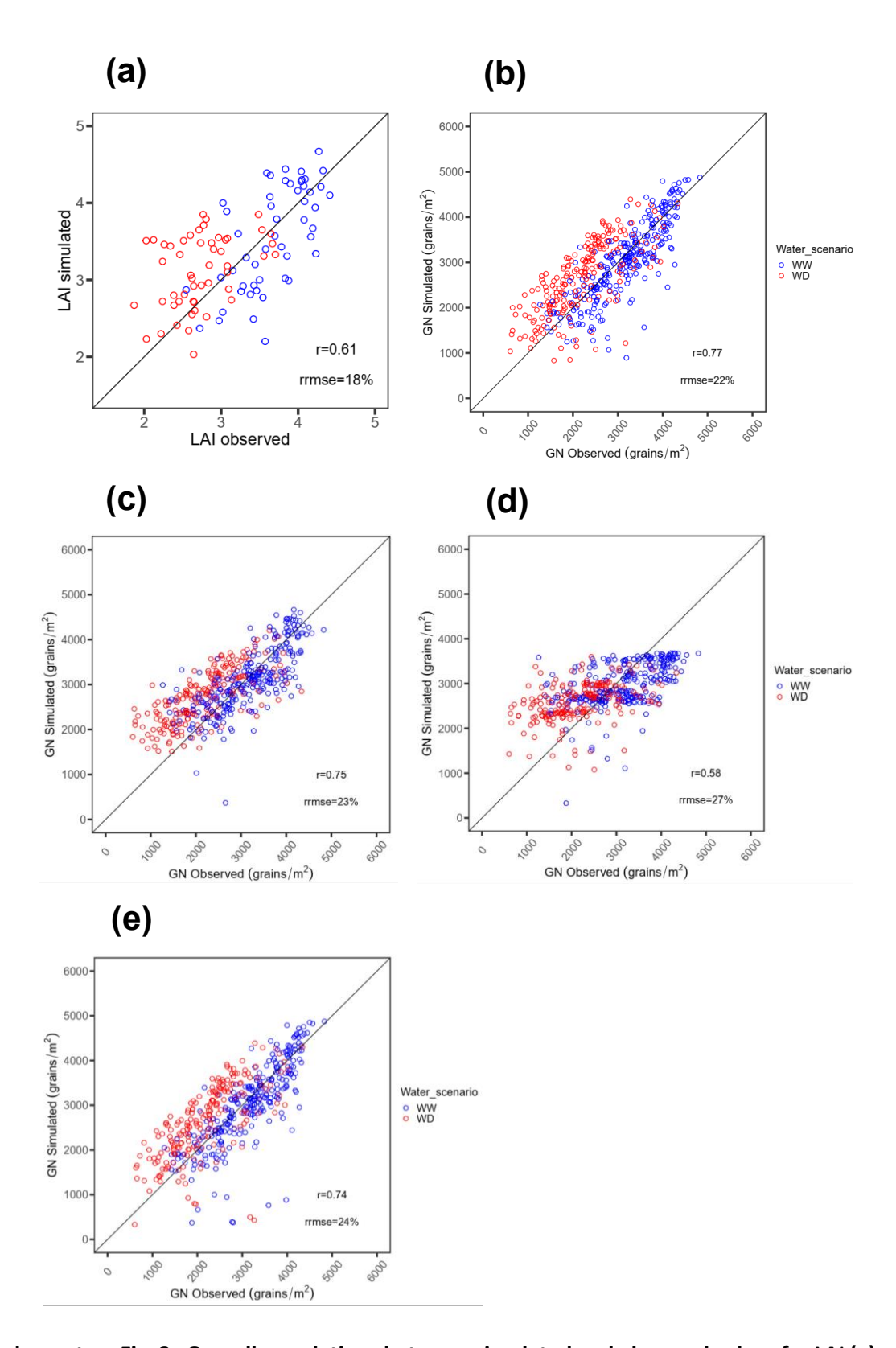
Process	Equation	Parameter	Description	Value
Leaf	L: leaf length	a <sub>6</sub>	Maximum leaf elongation rate of leaf 6	Genotypic
elongation	Equation 10: $L(n,d) = \sum_{emergence}^{d} LER(n)$	b	Sensitivity of leaf elongation rate to vapour pressure deficit	Genotypic
	LER: leaf elongation rate  LER_norm: normalized maximum leaf	С	Sensitivity of leaf elongation rate to soil water deficit	Genotypi
	elongation rate (normalized by maximum rate of leaf 6)  Equation 11: $LER_{norm}(n) = \theta_L * e^{\frac{-(n-\theta_L)^2}{2*G_L^2}}$ $\theta_L = \frac{1}{e^{\frac{-(6-\theta_L)^2}{2*G_L^2}}}$	βL	Coefficient determining the rank of the leaf with maximum growth relative to final leaf number	0.68
	B <sub>L</sub> = $\beta_L$ ×N <sub>final</sub> G <sub>L</sub> = $\sigma_L$ ×N <sub>final</sub> Equation 12:  If $tt_{bl}$ < $tt$ < $tt_{el}$ :  LER( $n$ )=LER <sub>nom</sub> ( $n$ )×( $a_e$ +b VPD+cPSI)× $\Delta tt$ VPD: vapour pressure deficit (kPa)  PSI: soil water potential (MPa) $\Delta tt$ : equivalent thermal time of day d (°C.d) $tt$ : cumulated thermal time at day d (°C.d)	$\sigma_{L}$	Coefficient determining the skewness of the curve or potential leaf growth relative to final leaf number	0.46
Leaf widening	W: leaf width  Equation 13:  W(n,d)=W <sub>base</sub> (n)+RAD <sub>effect</sub> (d)  W <sub>base</sub> : leaf width at intercepted light of 0.15 MJ  RAD <sub>effect</sub> : effect of intercepted light on leaf width		Base value for radiation effect on leaf widening Base leaf width of leaf 6 Sensitivity of leaf widening to intercepted radiation	0.15 Genotypi Genotypi
	Equation 14: $RAD_{effect}(d) = r_{RAD} * (RAD_{i}(d) - RAD_{base})$	$\beta_W$	Coefficient determining the rank of the leaf with maximum base width relative to final leaf number	0.41
	RAD; mean daily plant intercepted radiation from $tt_{\rm beg,w}$ to $tt$ Equation 15:	m $\sigma_{\!\scriptscriptstyle W}$	Coefficient determining the skewness of the curve of base width relative to final leaf number	0.69
	$\begin{aligned} W_{\textit{base}}(n) &= W_6*e^{-(-n$			



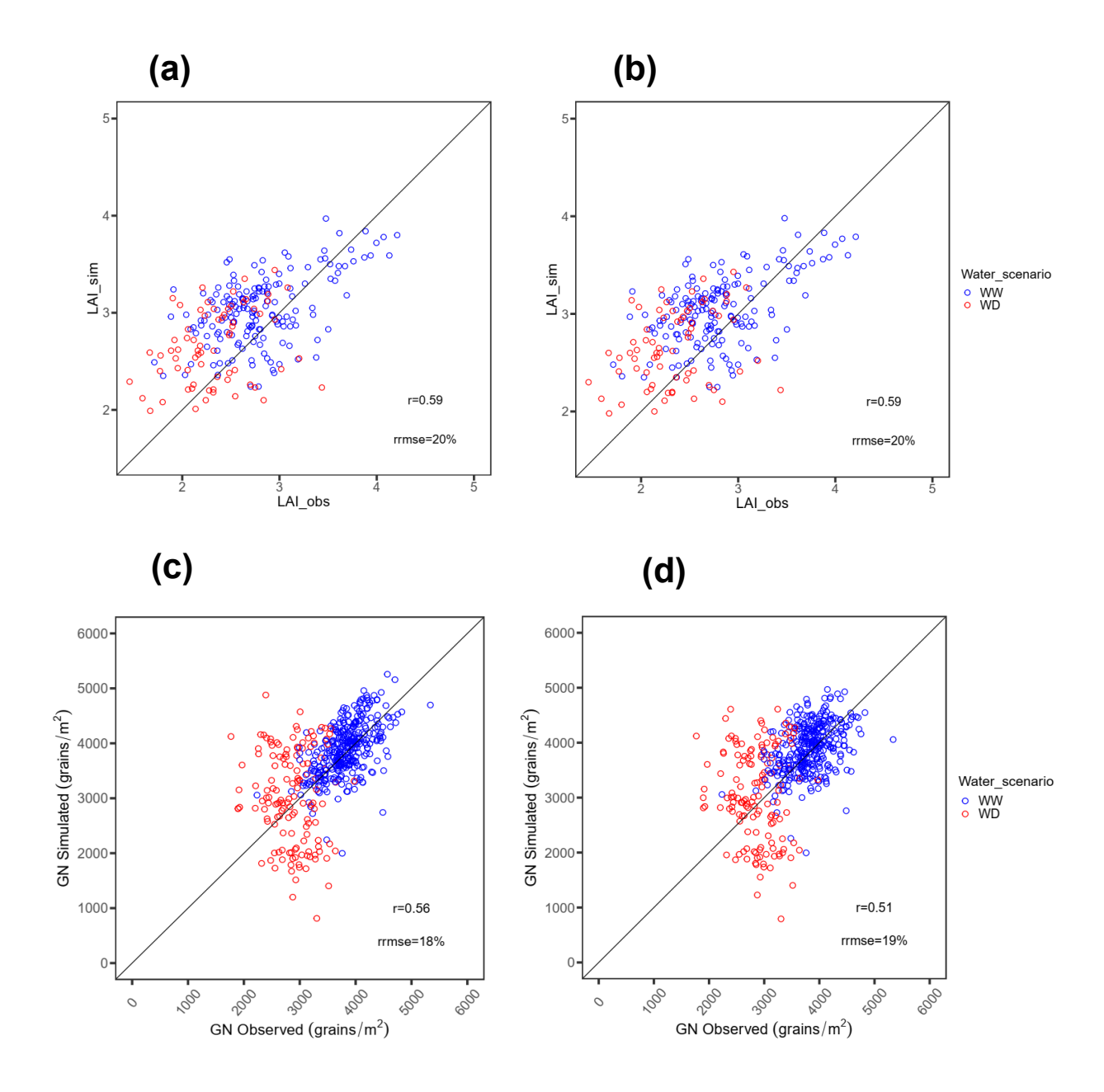
Supplementary Fig. 1: Global overview of the interaction between SiriusQuality2 components. Boxes are regular C# projects, circles are BioMa components and the rounded box is a storage class. The entry points of the diagram are the Sirius View project and the Sirius Console project.



Supplementary Fig. 2 : Simulated association between kernel (grain) number per plant and mean plant growth rate (PGR) over a 20-day period bracketing anthesis (filled circles). Lines correspond to statistical models fitted to experimental data for different hybrids and years (Messina et al. 2019). Correlation calculated between simulated and mean observed kernel number (r = 0.88, n = 4). Observed plant growth rate at which kernel number equals 0 is  $0.74 \pm 0.22$  g per plant.



Supplementary Fig. 3: Overall correlations between simulated and observed values for LAI (a) and grain number (b-f) across genetic progress panel field experiments. In a & b, genotype-dependent parameters derived from measured traits. In c, genotype-dependent parameters derived from genomic prediction. In d, genotype-dependent parameters derived from genotypes measured traits, except maximum grain number  $(GN_{max})$  fixed to the mean value of the panel. In e, genotype-dependent parameters derived from genotypes measured traits, except leaf elongation rate 'LERa' fixed to the mean value of the panel. One dot, one hybrid in one experiment.



Supplementary Fig. 4: Overall correlations between simulated and observed values for LAI (a,b) and grain number (c,d) across recent hybrids panel field experiments. In a & c, the genotype-dependent parameters FLN, LAR and  $GN_{max}$  were derived from measured traits and the other parameters derived from genomic prediction. In **b** & **d**, all genotype-dependent parameters were estimated via genomic prediction. One dot, one hybrid in one experiment.

## **GENERAL DISCUSSION AND PERSPECTIVES**

## **TABLE OF CONTENTS**

A link between indoor phenotyping and field crop performance	111
Estimation of genotype-dependent parameters of CGMs	112
A novel GP-assisted CGM method for predicting LAI and grain number in maize	113
Further upgrades of the thesis GP-assisted CGM method	114
Toward application in breeding or variety recommendation contexts	115
References	116

The main objective of my thesis was to develop and evaluate a new approach for predicting maize varieties complex field traits (LAI and grain yield) across multiple environments. This approach combined statistical genomic prediction models, phenomics methods developed recently and a novel crop growth model (Sirius Maize). The originality of this work was to combine different methods (quantitative genetics, statistics, phenomics and ecophysiology) and to carry out all the necessary steps for developing and testing the approach. These steps included: designing and monitoring indoor and multi-site field experiments; collecting and analysing phenotypic, genotypic and envirotypic datasets; calculating physiological traits; calibrating genomic prediction models; parameterizing the crop growth model and performing several simulation tests

### A link between indoor phenotyping and field crop performance

We provided in this thesis insights for how indoor phenotyping can be linked to crop performance in the field. Indeed, indoor phenotyping allowed us to measure at high throughput structural and adaptive traits related to plant phenology, architecture, leaf growth and its responses to environment. We showed that these traits can be translated in field for hundreds of genotypes if three main conditions are met. Firstly, traits measured indoor should be heritable and genetically correlated to those in fields, regardless of absolute values. This was showed in our study, either when the considered trait was measured with similar protocols indoor and in the field (e.g., LAR), when the trait was measured with different methods (e.g., architecture traits) or when the trait was more complex (e.g., LAI) and required a method involving crop modelling. Secondly, the absolute values of indoor traits should translate to that in fields with diverse environmental scenarios, either directly or via crop models that take into account differences in environmental conditions. Finally, indoor traits need to be predictable with sufficient accuracy from the genomic information of nonphenotyped genotypes. Here, cross-validation based on a large genetic range panels showed good results (with r ranging from 0.56 to 0.84 for the studied traits). These findings open new prospects in speed breeding (Watson et al., 2018, 2019; Alahmad et al., 2018; Samantara et al., 2022), by allowing screening genetic material for high or low values of adaptive traits, conferring either spender or conservative strategies for water use under future climates.

#### **Estimation of genotype-dependent parameters of CGMs**

Using crop growth models simulations for defining ideotypes (optimal combinations of genotypes x environments x management practices), requires a dialogue between CGMs formalisms and phenomic methods for measuring genotype-dependent CGM parameters of hundreds of genotypes in phenotyping facilities (Tardieu et al., 2017; Wang et al., 2019; Lacube et al., 2020). Despite the long history of CGMs, no common good ways exist for choosing genotype-dependent parameters (Onogi, 2022), while CGMs ability to describe phenotypic variations depends on these chosen parameters (Yin et al., 2000; Bannayan et al., 2007). A usual practice to determine genotype-dependent parameters is to adopt knowledge garnered from the published literature. In previously reviewed studies using CGMs, the number of parameters chosen as genotype-dependent ranged from 3 to 12. Another method is to identify parameters that cause large variations in phenotype via sensitivity analyses (Quilot et al., 2005), even though genetic aspects are lacking in this procedure. In our study, we used 8 traits (leaf appearance rate, final leaf number, max leaf expansion rate, rhPAD architecture trait, max stomatal conductance, leaf elongation sensitivity to VPD, leaf elongation sensitivity to SWP and max grain number per plant) to estimate 13 genotypedependent parameters of Sirius Maize model. These were chosen based on literature knowledge about Sirius model processes and for the practical reason of being able to measure them at high-throughput. Some of the traits corresponded directly to Sirius parameters; other parameters were deduced via simple equations or regressions with measured traits and two parameters were scaled to traits.

In GP-assisted CGM methods, two approaches for genomic prediction of parameters can be used: joint or independent (Onogi, 2022). The independent approach is easier to implement, but the joint approach can present the advantage that uncertainty in some CGM parameters estimation can be compensated by using a joint multi-trait GP, especially when GP training data sets are of small size (Onogi, 2020). In our thesis study, we predicted the genotypic parameters independently as they were not all acquired from the same experiments, but a joint approach can be tested later.

## A novel GP-assisted CGM method for predicting leaf area index and grain number in maize

A key consideration for successful application of the GP-assisted CGM methodology is the availability of a suitable CGM that can be used to incorporate the genetic variation of physiological effects and environmental responses for the input traits, that influence the genetic variation of a target simulated trait such as yield (Cooper *et al.*, 2016). Ultimately, the GP-assisted CGM method can only be as good as the CGM used to represent the genetic variation for the target trait. In our study, we benefited from the Sirius Maize CGM derived from SiriusQuality2 (Jamieson *et al.*, 1998; Martre *et al.*, 2006).

Up to now, we were able to parameterize Sirius Maize for tens of varieties and test the consistency of our GP-assisted CGM approach for simulating leaf area index and grain number yield component, in contrasting environmental conditions. Tests were run in different cases assumed to be more or less stringent, including a case where only genomic prediction values of all traits/parameters were used in the CGM. Grain number simulation accuracies for the genetic progress panel, in the latter case, ranged from 0.63 to 0.80 depending on environmental scenarios. These findings were comparable for example with the CGM-assisted GP method results of Bustos-Korts *et al.* (2019), where dynamics of biomass and canopy cover for wheat genotypes were simulated using APSIM, then parametric traits were extracted from these dynamics and used in a multi-trait GP model for predicting grain yield. Prediction accuracies in the latter study ranged from 0.50 to 0.80 depending on environment types. Additionally, as a benchmark, our maize GP-assisted CGM results can be compared to prediction accuracies obtained for the same maize panels, using a joint regression GP model which considers environmental covariates (Millet *et al.*, 2019).

An advantage of the GP-assisted CGM approach is the inclusion of observed intermediate input traits in the CGM, which enables us to consider parameters in the model as representations of plant biology. As suggested by Cooper *et al.* (2016), for approximation, the GP-assisted CGM methodology can be viewed as a special case of a broader neural network approach (Crossa *et al.*, 2019; Costa-Neto *et al.*, 2021) for extending additive GP methods to deal with non-additive effects of the target trait. Both can be represented as a network diagram. In the neural network framework, the intermediate nodes would correspond to the component physiological traits. In the case of the GP-assisted CGM method, the mapping from

SNPs to intermediate nodes to the output trait yield is defined by the CGM instead of arbitrarily derived from the data at hand as in the case of the neural network. An important difference between the neural network and the CGM is that there are functions in the biological network that the neural network method could suppress, while this is not possible in a CGM. The fact that the GP-assisted CGM correctly predicts the mean and the range of the target trait in the simulated environments while parameterized using data from indoor experiments or other field environments, and was sensitive to specified meteorological, soil and management data inputs, shows that the physiological and environmental information is being used by the CGM in the GP-assisted CGM methodology.

Use of GP-assisted CGMs remains though a new approach that needs further development and benchmark to reach its potential for phenotype prediction and ideotyping. Issues to be considered for prediction accuracies levels of the method include: (i) the choice of the CGM; (ii) the choice of the genotype-dependent parameters of the CGM, (iii) the accuracy of the CGM parameters estimation, (iv) the relationships (or similarities) between target and training environments (Onogi, 2022). Moreover, a fundamental assumption for use of CGMs for GEIs analyses is that genotype-dependent parameters are assumed to be constant among environments and differences of phenotypes of a genotype (i.e., reaction norms) are brought about by environmental conditions via the CGMs. However, this assumption does not always hold (Lamsal *et al.*, 2018).

#### Further upgrades of the thesis GP-assisted CGM method

The work that remains to be done includes modelling individual grain weight yield component with Sirius Maize, which is determined during grain filling phase. This would then enable us to simulate grain yield for the same panels and environmental scenarios, as for leaf area index and grain number.

Another upgrade of the model is the use of the parameter PGR<sub>base</sub> in grain number calculation. PGR<sub>base</sub> represents the minimum plant growth rate at which grain number takes values above 0. In the current work, this parameter was fixed for all genotypes, but is expected to vary between genotypes in such a way that the most sensitive hybrids to water deficit for grain number would be those with highest sensitivity of leaf growth to water deficit (Welcker *et al.*, 2011; Turc *et al.*, 2016). This may improve simulation accuracies in water-deficit conditions.

Finally, the set of genotype-dependent parameters provided to the CGM and their calculations will be optimised, after considering more experiments and genotypes (diversity panel).

#### Toward application in breeding or variety recommendation contexts

Our results can be considered as promising and open new possibilities for tackling the genotype by environment interaction and ideotyping, either in a plant breeding or a variety recommendation to farmers context. Indeed, our GP-assisted CGM approach may represent a new high-throughput tool for evaluating in silico the performance of hundreds of maize genotypes in hundreds of environments, given that the required genotype-dependent CGM parameters are either measured or predicted from genomic information.

In commercial maize breeding programs, genomic prediction is now used routinely as an integrated component (Cooper et al., 2014, 2021). Combining GP with a CGM into an integrated prediction method (GP-assisted CGM) presents interesting opportunities to combine crop physiology knowledge and plant breeding to tackle the genetic improvement of complex traits such as grain yield, for multiple or specific target scenarios defined as combinations of environments and management practices (Cooper et al., 2016, 2023). Crop physiology has helped to explain how structural and functional traits variation contribute to long term yield gains and has identified putative sources of traits genetic variation that could be important for further genetic improvement of yield in drought-prone environments and future climates (Welcker et al., 2022; Garcia et al., 2023). Physiologists have advocated the use of such traits for screening genetic material in breeding programs. However, few, if any, have been scaled and routinely adopted by breeders as integrated components of their breeding programs (Cooper et al., 2016). The GP-assisted CGM methodology provides an opportunity to overcome some of the limitations that are associated with developing and applying additional physiological traits screening within a breeding program (Hammer et al., 2006). The cost and effort involved in developing an appropriate CGM for specific breeding program objectives has to be weighed against the importance of GEIs and other sources of non-additive variations of the target trait (Cooper et al., 2016).

For the variety recommendation context, there is an increasing demand from farmers to have access to integrative decision support tools that can help in their decisions regarding cropping and field management practices, including variety choice. This demand is rising especially in

the context of more fluctuating environmental conditions due to climate change, increasing frequency of heat and drought waves, in addition to agriculture policies supporting inputs reduction. As a complement to information produced for farmers based on classical multi-annual trials networks performed by applied research organisms (such as ARVALIS), the GP-assisted CGM in silico method may represent a valuable additional tool for enhancing recommendation to farmers, mainly by testing in silico multiple combinations of varieties, field environmental conditions and management practices.

#### References

Alahmad S, Dinglasan E, Leung KM, Riaz A, Derbal N, Voss-Fels KP, Able JA, Bassi FM, Christopher J, Hickey LT. 2018. Speed breeding for multiple quantitative traits in durum wheat. *Plant Methods* 14: 36.

**Bannayan M, Kobayashi K, Marashi H, Hoogenboom G**. **2007**. Gene-based modelling for rice: an opportunity to enhance the simulation of rice growth and development? *Journal of Theoretical Biology* **249**: 593–605.

Bustos-Korts D, Boer MP, Malosetti M, Chapman S, Chenu K, Zheng B, van Eeuwijk FA. 2019. Combining Crop Growth Modeling and Statistical Genetic Modeling to Evaluate Phenotyping Strategies. *Frontiers in Plant Science* 10: 1491.

Cooper M, Messina CD, Podlich D, Totir LR, Baumgarten A, Hausmann NJ, Wright D, Graham G. 2014. Predicting the future of plant breeding: complementing empirical evaluation with genetic prediction. *Crop and Pasture Science* 65: 311–336.

**Cooper M, Powell O, Gho C, Tang T, Messina C. 2023**. Extending the breeder's equation to take aim at the target population of environments. *Frontiers in Plant Science* **14**: 1129591.

Cooper M, Powell O, Voss-Fels KP, Messina CD, Gho C, Podlich DW, Technow F, Chapman SC, Beveridge CA, Ortiz-Barrientos D, et al. 2021. Modelling selection response in plant-breeding programs using crop models as mechanistic gene-to-phenotype (CGM-G2P) multi-trait link functions. in silico Plants 3: diaa016.

**Cooper M, Technow F, Messina C, Gho C, Totir LR**. **2016**. Use of Crop Growth Models with Whole-Genome Prediction: Application to a Maize Multienvironment Trial. *Crop Science* **56**: 2141–2156.

**Costa-Neto G, Fritsche-Neto R, Crossa J. 2021**. Nonlinear kernels, dominance, and envirotyping data increase the accuracy of genome-based prediction in multi-environment trials. *Heredity* **126**: 92–106.

Crossa J, Martini JWR, Gianola D, Pérez-Rodríguez P, Jarquin D, Juliana P, Montesinos-López O, Cuevas J. 2019. Deep Kernel and Deep Learning for Genome-Based Prediction of Single Traits in Multienvironment Breeding Trials. *Frontiers in Genetics* 10.

Garcia A, Gaju O, Bowerman AF, Buck SA, Evans JR, Furbank RT, Gilliham M, Millar AH, Pogson BJ, Reynolds MP, et al. 2023. Enhancing crop yields through improvements in the efficiency of photosynthesis and respiration. The New Phytologist 237: 60–77.

Hammer G, Cooper M, Tardieu F, Welch S, Walsh B, van Eeuwijk F, Chapman S, Podlich D. 2006. Models for navigating biological complexity in breeding improved crop plants. *Trends in Plant Science* 11: 587–593.

**Jamieson PD, Semenov MA, Brooking IR, Francis GS. 1998.** Sirius: a mechanistic model of wheat response to environmental variation. *European Journal of Agronomy* **8**: 161–179.

Lacube S, Manceau L, Welcker C, Millet EJ, Gouesnard B, Palaffre C, Ribaut J-M, Hammer G, Parent B, Tardieu F. 2020. Simulating the effect of flowering time on maize individual leaf area in contrasting environmental scenarios. *Journal of Experimental Botany* 71: 5577–5588.

**Lamsal A, Welch SM, White JW, Thorp KR, Bello NM**. **2018**. Estimating parametric phenotypes that determine anthesis date in Zea mays: Challenges in combining ecophysiological models with genetics. *PLOS ONE* **13**: e0195841.

Martre P, Jamieson PD, Semenov MA, Zyskowski RF, Porter JR, Triboi E. 2006. Modelling protein content and composition in relation to crop nitrogen dynamics for wheat. *European Journal of Agronomy* 25: 138.

Millet EJ, Kruijer W, Coupel-Ledru A, Alvarez Prado S, Cabrera-Bosquet L, Lacube S, Charcosset A, Welcker C, van Eeuwijk F, Tardieu F. 2019. Genomic prediction of maize yield across European environmental conditions. *Nature Genetics* 51: 952–956.

**Onogi A. 2020**. Connecting mathematical models to genomes: joint estimation of model parameters and genome-wide marker effects on these parameters. *Bioinformatics* **36**: 3169–3176.

**Onogi A. 2022.** Integration of Crop Growth Models and Genomic Prediction (GP). In: Ahmadi N, Bartholomé J, eds. Methods in Molecular Biology. Genomic Prediction of Complex Traits: Methods and Protocols. New York, NY: Springer US, 359–396.

**Quilot B, Génard M, Lescourret F, Kervella J. 2005**. Simulating genotypic variation of fruit quality in an advanced peach×Prunus davidiana cross. *Journal of Experimental Botany* **56**: 3071–3081.

Samantara K, Bohra A, Mohapatra SR, Prihatini R, Asibe F, Singh L, Reyes VP, Tiwari A, et al. 2022. Breeding More Crops in Less Time: A Perspective on Speed Breeding. Biology 11: 275.

**Tardieu F, Cabrera-Bosquet L, Pridmore T, Bennett M**. **2017**. Plant Phenomics, From Sensors to Knowledge. *Current Biology* **27**: R770–R783.

**Turc O, Bouteillé M, Fuad-Hassan A, Welcker C, Tardieu F**. **2016**. The growth of vegetative and reproductive structures (leaves and silks) respond similarly to hydraulic cues in maize. *New Phytologist* **212**: 377–388.

Wang E, Brown HE, Rebetzke GJ, Zhao Z, Zheng B, Chapman SC. 2019. Improving process-based crop models to better capture genotype×environment×management interactions. *Journal of Experimental Botany* **70**: 2389–2401.

Watson A, Ghosh S, Williams MJ, Cuddy WS, Simmonds J, Rey M-D, Asyraf Md Hatta M, et al. 2018. Speed breeding is a powerful tool to accelerate crop research and breeding. *Nature Plants* 4: 23–29.

Watson A, Hickey LT, Christopher J, Rutkoski J, Poland J, Hayes BJ. 2019. Multivariate Genomic Selection and Potential of Rapid Indirect Selection with Speed Breeding in Spring Wheat. *Crop Science* 59: 1945–1959.

Welcker C, Sadok W, Dignat G, Renault M, Salvi S, Charcosset A, Tardieu F. 2011. A Common Genetic Determinism for Sensitivities to Soil Water Deficit and Evaporative Demand: Meta-Analysis of Quantitative Trait Loci and Introgression Lines of Maize. *Plant Physiology* 157: 718–729.

Welcker C, Spencer NA, Turc O, Granato I, Chapuis R, Madur D, Beauchene K, Gouesnard B, et al. 2022. Physiological adaptive traits are a potential allele reservoir for maize genetic progress under challenging conditions. *Nature Communications* 13: 3225.

**Yin X, Kropff MJ, Goudriaan J, Stam P. 2000**. A Model Analysis of Yield Differences among Recombinant Inbred Lines in Barley. *Agronomy Journal* **92**: 114–120.

## **ANNEXE EN FRANÇAIS**

## Thèse de Jugurta BOUIDGHAGHEN (2020-2023):

Prédiction de la performance de variétés de maïs en conditions environnementales contrastées par combinaison de phénomique, prédiction génomique et modèle de culture

## Objectifs de la thèse

L'objectif de la thèse est de développer et d'évaluer une méthode pour prédire le rendement d'un grand nombre de variétés de maïs dans des environnements multiples, en utilisant les connaissances scientifiques accumulées sur la réponse aux conditions environnementales. Pour atteindre cet objectif, nous avons combiné des modèles de prédiction génomique, de nouvelles approches phénomiques et un modèle de culture (Sirius Maize). Cette méthode a, potentiellement, la capacité d'aboutir à un nouvel outil efficace pour simuler la performance de centaines de génotypes de maïs dans des centaines d'environnements, que ce soit dans le contexte de l'amélioration ou l'évaluation variétale pour les agriculteurs. Cette thèse a été réalisée en partenariat avec ARVALIS, un organisme de recherche appliquée pour les agriculteurs en France, spécialisé dans les grandes cultures, dont notamment les céréales à paille et le maïs. Sa mission principale est de proposer des solutions agronomiques efficaces dans une multiplicité des scénarios. Cela inclut le choix variétal et les pratiques culturales, ainsi que des solutions économiques, environnementales et sanitaires, qui sont ensuite communiquées aux agriculteurs, pour les aider à faire face aux défis actuels tels que le changement climatique, les demandes sociétales et les exigences commerciales du marché.

La première étape de notre étude avait pour objectif d'analyser les caractères mesurés lors d'expériences menées en plateforme de phénotypage haut-débit sous serre. Trois panels d'hybrides de maïs ont été analysés pour cela : un "panel de diversité" avec 246 hybrides (Millet et al., 2019), un "panel progrès génétique" composé d'une série historique de 56 hybrides commerciaux (Welcker et al., 2022) et un "panel d'hybrides récents" comprenant 86 hybrides commercialisés entre 2008 et 2020 (la plupart des mesures en plateforme ayant été effectuées sur seulement 20 hybrides contrastés, pour ce dernier panel). Nous avons montré

que les valeurs génotypiques des caractères mesurés en plateforme sous serre étaient corrélées avec les valeurs au champ, soit directement, soit par le biais de modèles écophysiologiques simples. Nous avons ensuite examiné si les mesures des caractères effectuées en plateforme peuvent servir à entraîner des modèles de prédiction qui estiment les valeurs génotypiques des caractères sur la base des informations génomiques (génotypage SNP 600k) uniquement.

L'objectif de l'étape suivante était d'analyser l'ensemble des données collectées dans le cadre d'un réseau d'essais multi-site pour le panel d'hybrides récents. Nous avons inclus ici les données au champ collectées dans le cadre du projet européen INVITE sur un sous-ensemble de 30 variétés du panel d'hybrides récents. Il s'agit de 33 essais, définis comme des combinaisons de site x année x conduite, répartis à travers l'Europe, en conduites pluviales et irriguées. Nous avons caractérisé les conditions environnementales subjes par les plantes dans chaque champ à l'aide de capteurs météorologiques et de capteurs tensiométriques du sol. Nous avons estimé des indices environnementaux et assigné les essais à des scénarios rencontrés en maïsiculture à l'échelle européenne. Nous avons également calculé un caractère qui est un paramètre essentiel du le modèle Sirius Maize, à savoir le nombre maximal de grains par plante de l'hybride considéré. Nous avons aussi analysé l'indice foliaire (LAI) dans des essais contrastés, dérivé d'imagerie par drone et l'inversion du modèle 'PROSAIL' (Berger et al., 2018 ; Blancon et al., 2019). Enfin, nous avons estimé les sensibilités génotypiques du nombre de grains au potentiel hydrique du sol et aux températures maximales pendant la phase de floraison à l'aide d'un modèle de régression linéaire.

L'objectif de la dernière étape était de tester l'efficacité de notre approche, qui vise à simuler la performance de centaines de génotypes dans des centaines d'environnements en combinant la phénomique, la prédiction génomique et la modélisation des cultures. La spécificité ici était de réaliser des simulations basées sur un modèle de culture dont les paramètres génotype-dépendants proviennent des caractères présentés dans les étapes précédentes. Toutefois, par contrainte de temps, notre étude s'est limitée à la première partie du cycle cultural du maïs, avec des simulations effectuées pour l'indice de surface foliaire et le nombre de grains pour des dizaines de variétés dans des conditions environnementales contrastées. Nous avons utilisé pour cela le modèle de culture 'Sirius Maize'.

## Principaux résultats

Les caractères adaptatifs du maïs mesurés en plateforme sous serre peuvent être inférés dans différents champs et prédits par des modèles de prédiction génomique.

Plusieurs caractères ont été analysés dans la thèse, liés à la phénologie (vitesse d'apparition des feuilles et durée de phase végétative), à l'architecture des plantes (rh<sub>PAD</sub>) ou à la croissance foliaire (vitesse d'expansion foliaire, LAI). Des corrélations étroites ont été observées entre les valeurs génotypiques des caractères mesurés en plateforme de phénotypage sous serre et dans des essais multi-sites au champ. C'était le cas lorsque le caractère considéré était mesuré avec des protocoles similaires sous serre et au champ, par exemple la vitesse d'apparition des feuilles ou la durée de la phase végétative. C'était également le cas lorsque le caractère était mesuré à l'aide de méthodes différentes, comme dans le cas de l'architecture des plantes. Enfin, l'indice foliaire, qui dépend fortement de la densité des plantes et des conditions environnementales dans le couvert considéré, a nécessité une méthode impliquant la modélisation de la culture. Les corrélations observées dans ces trois cas entre plateforme sous serre et champs allaient de 0,57 à 0,77.

Les valeurs des caractères ont été transposées des conditions sous serre à une diversité de champs, quand les différences de conditions environnementales ont été prises en compte par le biais d'un modèle. La modélisation des effets de la température a permis par exemple d'assurer la correspondance des valeurs entre les essais au champ et en plateforme sous serre pour la vitesse d'apparition des feuilles et la durée de la phase végétative. La quantité de lumière interceptée était également nécessaire pour que d'autres caractères soient cohérents entre les expériences. C'était le cas ici pour la largeur des feuilles de maïs mesurée en plateforme sous serre et dans plusieurs champs. L'état hydrique de la plante était, en outre, nécessaire dans certains cas pour tenir compte des différences dans les caractères liés à la croissance des organes. C'était le cas ici pour la longueur des feuilles en fonction de la demande évaporative (VPD de l'air). La vitesse d'élongation des feuilles était étroitement liée à une combinaison du potentiel hydrique du sol et du déficit de saturation de l'air.

Enfin, la prédiction génomique menée par validation croisée sur les panels de diversité et progrès génétique ont donné de bons résultats avec des coefficients de corrélation entre

valeurs observées et prédites allant de 0,56 à 0,84 pour les caractères étudiés. La validation externe sur le panel de variétés hybrides récentes a fourni des résultats moins précis, mais les corrélations entre les valeurs prédites et observées étaient toutefois majoritairement significatives, allant de 0,34 à 0,71.

Le modèle 'Sirius Maize', paramétré avec des valeurs de caractères mesurées ou prédites par prédiction génomique, a permis de simuler l'indice foliaire et le nombre de grains avec une bonne qualité prédictive, pour un large nombre d'hybrides dans des conditions environnementales contrastées.

Nous avons testé le modèle 'Sirius Maize' avec les données du panel progrès génétique, pour lequel tous les paramètres génotypiques proviennent de mesures.

Pour l'indice foliaire, les valeurs prédites ont été comparées avec des valeurs dérivées d'images multi-spectrales de drone à la fin de la phase végétative. Les simulations ont été réalisées pour deux essais au champ : MAU2017W (conditions hydriques favorables 'WW') et MAU2017D (déficit hydrique 'WD'). La corrélation entre les valeurs observées et simulées dans l'essai 'MAU2017W' était élevée (r=0,64). La corrélation a diminué à r=0,40 en déficit hydrique, pour l'essai 'MAU2017D', mais elle est restée significative, avec une erreur d'estimation légèrement plus importante.

Pour le nombre de grains par unité de surface, les simulations ont été réalisées pour neuf essais au champ: LEM2017W et VEN2017W (scénario cool\_WW); GAI2017W et NER2013W (scénario warm\_WW); MAU2017W (scénario hot\_WW); VEN2017D (scénario cool\_WD); GAI2017D et LAV2017D (scénario warm\_WD); MAU2010D (scénario hot\_WD). Les corrélations entre le nombre de grains observé et simulé étaient élevées dans tous les scénarios, allant de r=0,79 à r=0,86 dans des conditions hydriques favorables avec une faible erreur d'estimation (rrmse=15% en moyenne), et allant de r=0,71 à r=0,87 dans des conditions de déficit hydrique avec une erreur d'estimation fluctuante (rrmse=23%–47%).

Nous avons aussi testé le modèle de culture lorsque tous ses paramètres génotypedépendants sont estimés par prédiction génomique pour le panel progrès génétique. Les valeurs génétiques des caractères utilisées ici pour la paramétrisation ont été obtenues à partir des schémas de validation croisée évoqués précédemment. Les corrélations entre les valeurs observées et simulées d'indice foliaire pour le panel sont restées similaires à celles obtenues lorsque les paramètres sont dérivés de mesures, aussi bien dans les conditions hydriques favorables (r=0,63) qu'en déficit hydrique (r=0,41). Pour le nombre de grains, les corrélations entre les valeurs observées et simulées ont diminué de 10 % en moyenne pour le panel, par rapport à celles des simulations effectuées avec des valeurs des paramètres génotypiques mesurées. C'était le cas dans les conditions hydriques favorables (r=0,68–0,79, rrmse=12%–19%) et dans les conditions de déficit hydrique (r=0,63–0,80, rrmse=22%–51%).

### Discussion générale et conclusion

L'originalité de cette thèse a été de combiner différentes méthodes (génétique quantitative, statistiques, phénomique et écophysiologie) et de réaliser toutes les étapes nécessaires pour développer et tester une nouvelle approche prédictive des caractères au champ. Ces étapes comprenaient : la conception et le suivi d'expériences en plateforme de phénotypage sous serre et sur plusieurs sites au champ; la collecte et l'analyse d'ensembles de données phénotypiques, génotypiques et environnementales ; le calcul de caractères physiologiques ; la calibration de modèles de prédiction génomique ; le paramétrage de modèle de culture et la réalisation de plusieurs tests de simulation.

# Un lien entre le phénotypage en plateforme sous serre et la performance des cultures au champ.

Dans cette thèse, nous avons montré comment le phénotypage en plateforme sous serre peut permettre d'évaluer la performance des cultures au champ. En effet, le phénotypage sous serre nous a permis de mesurer à haut débit des caractères liés à la phénologie de la plante, à son architecture, à la croissance des feuilles et à ses réponses à l'environnement. Nous avons montré que ces caractères peuvent être inférés au champ pour des centaines de génotypes si trois conditions principales sont remplies. Premièrement, les caractères mesurés en plateforme doivent être génétiquement corrélés à ceux au champ (indépendamment des valeurs absolues), de sorte que la sélection des génotypes en plateforme soit pertinente pour les conditions du champ. Deuxièmement, la valeur absolue des caractères mesurés en plateforme doit correspondre à celle des caractères mesurés au champ dans divers scénarios environnementaux, soit directement, soit par l'intermédiaire de modèles. Enfin, les caractères de plateforme doivent être prédits avec suffisamment de précision à partir des informations génomiques des génotypes non phénotypés. Ces résultats ouvrent de nouvelles perspectives

en matière en sélection rapide (Watson et al., 2018, 2019), en permettant de cribler le matériel génétique pour des valeurs élevées ou faibles de caractères adaptatifs, conférant des stratégies soit dépensières soit conservatrices pour l'utilisation de l'eau sous les futurs climats.

#### Estimation des paramètres génotype-dépendants des modèles de culture.

L'utilisation de modèles de culture pour définir des idéotypes (combinaisons optimales de génotypes x environnements x pratiques culturales) nécessite un dialogue entre les formalismes des modèles de culture et les méthodes phénomiques pour mesurer les paramètres génotype-dépendants de centaines de génotypes dans les plateformes de phénotypage (Tardieu et al., 2017 ; Lacube et al., 2020). Malgré la longue histoire des modèles de culture, il n'existe pas de bonnes méthodes pour choisir les paramètres dépendants du génotype (Onogi, 2022), alors que la capacité de ces modèles à décrire les variations phénotypiques dépend de ces paramètres. Une pratique habituelle pour déterminer les paramètres dépendants du génotype consiste à adopter les connaissances tirées de la littérature. Dans les études publiées utilisant les modèles de culture combinés à la prédiction génomique, le nombre de paramètres choisis comme dépendants du génotype variait de 3 à 12. Une autre méthode consiste à identifier les paramètres qui causent de grandes variations dans le phénotype via des analyses de sensibilité (Quilot et al., 2005), même si les aspects génétiques sont absents dans cette procédure. Dans notre étude, nous avons utilisé huit caractères (la vitesse d'apparition des feuilles, le nombre final de feuilles, la vitesse d'expansion foliaire, un caractère d'architecture rh<sub>PAD</sub>, la conductance stomatique maximale, la sensibilité de l'élongation foliaire au VPD et au potentiel hydrique du sol, et le nombre maximal de grains par plante) pour estimer treize paramètres dépendants du génotype du modèle 'Sirius Maize'.

# Une nouvelle méthode combinant modèle de culture et prédiction génomique pour prédire l'indice foliaire et le nombre de grains chez le maïs.

Une considération essentielle pour une application réussie de la méthodologie développée dans la thèse est la disponibilité d'un modèle de culture approprié, qui peut être utilisé pour incorporer la variabilité génétique de caractères physiologiques clés et la répercuter sur la variation génétique d'un caractère complexe simulé comme le rendement. Dans notre étude,

nous avons bénéficié du modèle de culture 'Sirius Maize' développé au LEPSE à partir de SiriusQuality2 (Jamieson et al., 1998 ; Martre et al., 2006).

Dans cette thèse, nous avons paramétré Sirius Maize pour des dizaines de variétés et testé l'efficacité de notre approche, combinant modèle de culture et prédiction génomique, pour simuler l'indice foliaire et la composante de rendement 'nombre de grains', dans des conditions environnementales contrastées. Les tests ont été effectués dans différents cas plus ou moins stringents, y compris un cas où seules les valeurs de prédiction génomique de tous les caractères/paramètres étaient utilisées dans le modèle de culture. Dans ce dernier cas, les précisions de simulation (r) du nombre de grains pour le panel progrès génétique allaient de 0,63 à 0,80 en fonction des scénarios environnementaux. Ces résultats sont comparables, par exemple, à ceux de l'étude Bustos-Korts et al. (2019), où la dynamique de la biomasse et du couvert végétal pour des génotypes de blé a été simulée à l'aide du modèle de culture 'APSIM', puis des paramètres ont été extraits de ces dynamiques et utilisés dans un modèle de prédiction génomique multi-caractères pour prédire le rendement. Dans cette étude, les précisions de prédiction allaient de 0,50 à 0,80 en fonction des types d'environnement.

Un avantage de l'approche de la thèse est l'inclusion de caractères intermédiaires observés dans un modèle de culture, ce qui nous permet de considérer les paramètres du modèle comme des représentations de la biologie de la plante. Comme le suggèrent Cooper et al. (2016), la méthodologie combinant modèle de culture et prédiction génomique peut être considérée comme un cas particulier d'une approche d'apprentissage profond de type 'réseau de neurones' (Crossa et al., 2019 ; Costa-Neto et al., 2021), qui tient compte des effets non additifs sur le caractère prédit. Dans le cadre du réseau de neurones, les nœuds intermédiaires correspondraient aux caractères physiologiques considérés. Dans le cas de la méthode de la thèse, la correspondance entre les SNPs, les nœuds intermédiaires et le caractère simulé est définie par le modèle de culture, au lieu d'être dérivée arbitrairement des données d'entrainement comme dans le cas du réseau de neurones.

L'utilisation de méthodes combinant modèle de culture et prédiction génomique nécessite encore un développement plus poussé et une évaluation comparative pour atteindre son potentiel en matière de prédiction du phénotypes et d'idéotypage. Les questions à prendre en compte pour améliorer les niveaux de précision de prédiction comprennent : i) le choix du modèle de culture ; ii) le choix des paramètres génotype-dépendants du modèle, iii) la

précision de l'estimation de ces paramètres, iv) les relations (ou similitudes) entre l'environnement cible et l'environnement d'entraînement (Onogi, 2022).

#### Perspectives concernant la méthode de la thèse.

Le travail prévu pour compléter les résultats de la thèse, comprend la modélisation de la composante du rendement 'poids du grain' avec Sirius Maize, qui est déterminée pendant la phase de remplissage chez le maïs. Cela nous permettrait de simuler le rendement en grains pour les mêmes panels et scénarios environnementaux que pour l'indice foliaire et le nombre de grains. Une autre amélioration du modèle sera l'utilisation du paramètre PGR<sub>base</sub> dans le calcul du nombre de grains. Dans le présent travail, ce paramètre a été fixé pour tous les génotypes, mais on s'attend à ce qu'il varie entre les génotypes de telle sorte que les hybrides les plus sensibles au déficit hydrique pour le nombre de grains seraient ceux dont la croissance foliaire est la plus sensible au déficit hydrique aussi (Welcker et al., 2011 ; Turc et al., 2016). Cela pourrait améliorer la précision des simulations dans des conditions de déficit hydrique. Enfin, l'ensemble des paramètres dépendants du génotype fournis au modèle de culture et leurs calculs seront optimisés après avoir pris en compte davantage d'expériences et de génotypes (panel de diversité).

## Vers une application dans des contextes de sélection ou de recommandation variétale.

Dans les programmes de sélection du maïs, la prédiction génomique est désormais couramment utilisée en tant que composante intégrée (Cooper et al., 2014, 2021). La combinaison de la prédiction génomique avec un modèle de culture dans une méthode de prédiction intégrée offre des possibilités intéressantes pour l'amélioration génétique de caractères complexes tels que le rendement en grains, pour des scénarios multiples ou spécifiques définis comme des combinaisons d'environnements et de pratiques culturales. Le coût et les efforts nécessaires à l'établissement d'un modèle de culture approprié pour des objectifs spécifiques d'un programme de sélection doivent être mis en balance avec l'importance des interactions génotype x environnement et d'autres sources de variation non additives du caractère d'intérêt ciblé (Cooper et al., 2016).

En ce qui concerne la recommandation des variétés, les agriculteurs sont de plus en plus nombreux à souhaiter avoir accès à des outils d'aide à la décision qui peuvent les aider à choisir les variétés à cultiver conjointement aux itinéraires techniques. Cette demande augmente surtout dans le contexte de conditions environnementales plus fluctuantes dues au changement climatique, à la fréquence accrue des vagues de chaleur et de sécheresse, ainsi qu'aux politiques agricoles favorisant la réduction des intrants. En complément des informations produites pour les agriculteurs sur la base des réseaux d'essais pluriannuels réalisés par les organismes de recherche appliquée (tels qu'ARVALIS), l'approche de simulation de la thèse peut représenter un outil supplémentaire précieux pour améliorer les recommandations faites aux agriculteurs, principalement en testant in silico de multiples combinaisons de variétés, de conditions environnementales et de pratiques culturales.

### Références

Berger K, Atzberger C, Danner M, D'Urso G, Mauser W, Vuolo F, Hank T. 2018. Evaluation of the PROSAIL Model Capabilities for Future Hyperspectral Model Environments: A Review Study. *Remote Sensing* 10: 85.

Blancon J, Dutartre D, Tixier M-H, Weiss M, Comar A, Praud S, Baret F. 2019. A High-Throughput Model-Assisted Method for Phenotyping Maize Green Leaf Area Index Dynamics Using Unmanned Aerial Vehicle Imagery. *Frontiers in Plant Science* 10.

Bustos-Korts D, Boer MP, Malosetti M, Chapman S, Chenu K, Zheng B, van Eeuwijk FA. 2019. Combining Crop Growth Modeling and Statistical Genetic Modeling to Evaluate Phenotyping Strategies. *Frontiers in Plant Science* 10: 1491.

Cooper M, Messina CD, Podlich D, Totir LR, Baumgarten A, Hausmann NJ, Wright D, Graham G. 2014. Predicting the future of plant breeding: complementing empirical evaluation with genetic prediction. *Crop and Pasture Science* 65: 311–336.

Cooper M, Powell O, Voss-Fels KP, Messina CD, Gho C, Podlich DW, Technow F, Chapman SC, Beveridge CA, Ortiz-Barrientos D, et al. 2021. Modelling selection response in plant-breeding programs using crop models as mechanistic gene-to-phenotype (CGM-G2P) multi-trait link functions. in silico Plants 3: diaa016.

**Cooper M, Technow F, Messina C, Gho C, Totir LR**. **2016**. Use of Crop Growth Models with Whole-Genome Prediction: Application to a Maize Multienvironment Trial. *Crop Science* **56**: 2141–2156.

**Costa-Neto G, Fritsche-Neto R, Crossa J. 2021**. Nonlinear kernels, dominance, and envirotyping data increase the accuracy of genome-based prediction in multi-environment trials. *Heredity* **126**: 92–106.

Crossa J, Martini JWR, Gianola D, Pérez-Rodríguez P, Jarquin D, Juliana P, Montesinos-López O, Cuevas J. 2019. Deep Kernel and Deep Learning for Genome-Based Prediction of Single Traits in Multienvironment Breeding Trials. *Frontiers in Genetics* 10.

Garcia A, Gaju O, Bowerman AF, Buck SA, Evans JR, Furbank RT, Gilliham M, Millar AH, Pogson BJ, Reynolds MP, et al. 2023. Enhancing crop yields through improvements in the efficiency of photosynthesis and respiration. The New Phytologist 237: 60–77.

Hammer G, Cooper M, Tardieu F, Welch S, Walsh B, van Eeuwijk F, Chapman S, Podlich D. 2006. Models for navigating biological complexity in breeding improved crop plants. *Trends in Plant Science* 11: 587–593.

**Jamieson PD, Semenov MA, Brooking IR, Francis GS. 1998.** Sirius: a mechanistic model of wheat response to environmental variation. *European Journal of Agronomy* **8**: 161–179.

Lacube S, Manceau L, Welcker C, Millet EJ, Gouesnard B, Palaffre C, Ribaut J-M, Hammer G, Parent B, Tardieu F. 2020. Simulating the effect of flowering time on maize individual leaf area in contrasting environmental scenarios. *Journal of Experimental Botany* 71: 5577–5588.

Martre P, Jamieson PD, Semenov MA, Zyskowski RF, Porter JR, Triboi E. 2006. Modelling protein content and composition in relation to crop nitrogen dynamics for wheat. *European Journal of Agronomy* 25: 138.

Millet EJ, Kruijer W, Coupel-Ledru A, Alvarez Prado S, Cabrera-Bosquet L, Lacube S, Charcosset A, Welcker C, van Eeuwijk F, Tardieu F. 2019. Genomic prediction of maize yield across European environmental conditions. *Nature Genetics* 51: 952–956.

**Onogi A. 2022.** Integration of Crop Growth Models and Genomic Prediction (GP). In: Ahmadi N, Bartholomé J, eds. Methods in Molecular Biology. Genomic Prediction of Complex Traits: Methods and Protocols. New York, NY: Springer US, 359–396.

**Quilot B, Génard M, Lescourret F, Kervella J. 2005**. Simulating genotypic variation of fruit quality in an advanced peach×Prunus davidiana cross. *Journal of Experimental Botany* **56**: 3071–3081.

**Tardieu F, Cabrera-Bosquet L, Pridmore T, Bennett M**. **2017**. Plant Phenomics, From Sensors to Knowledge. *Current Biology* **27**: R770–R783.

**Turc O, Bouteillé M, Fuad-Hassan A, Welcker C, Tardieu F. 2016**. The growth of vegetative and reproductive structures (leaves and silks) respond similarly to hydraulic cues in maize. *New Phytologist* **212**: 377–388.

Watson A, Ghosh S, Williams MJ, Cuddy WS, Simmonds J, Rey M-D, Asyraf Md Hatta M, Hinchliffe A, Steed A, Reynolds D, et al. 2018. Speed breeding is a powerful tool to accelerate crop research and breeding. *Nature Plants* 4: 23–29.

Watson A, Hickey LT, Christopher J, Rutkoski J, Poland J, Hayes BJ. 2019. Multivariate Genomic Selection and Potential of Rapid Indirect Selection with Speed Breeding in Spring Wheat. *Crop Science* 59: 1945–1959.

Welcker C, Sadok W, Dignat G, Renault M, Salvi S, Charcosset A, Tardieu F. 2011. A Common Genetic Determinism for Sensitivities to Soil Water Deficit and Evaporative Demand: Meta-Analysis of Quantitative Trait Loci and Introgression Lines of Maize. *Plant Physiology* 157: 718–729.

Welcker C, Spencer NA, Turc O, Granato I, Chapuis R, Madur D, Beauchene K, Gouesnard B, Draye X, Palaffre C, et al. 2022. Physiological adaptive traits are a potential allele reservoir for maize genetic progress under challenging conditions. *Nature Communications* 13: 3225.